Flexible Theories
for
Flexible Molecules

Flexible Theories
for
Flexible Molecules

Academisch Proefschrift

ter verkrijging van de graad van doctor aan de Universiteit van Amsterdam op gezag van de Rector Magnificus prof. mr. P. F. van der Heijden ten overstaan van een door het college voor promoties ingestelde commissie, in het openbaar te verdedigen in de Aula der Universiteit op vrijdag 15 maart 2002, te 14.00 uur
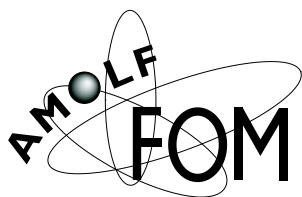
door

Paul Petrus Franciscus Wessels

geboren te Lichtenvoorde

Promotores: prof. dr. B. M. Mulder
prof. dr. D. Frenkel

Faculteit: Natuurwetenschappen, Wiskunde en Informatica

Subject headings: density functional theory / liquid crystals / polymers / phase transitions

CONTENTS

1

INTRODUCTION

A historical and phenomenological introduction is given to the fields of liquid crystals and liquid crystalline polymers. Some terminology and molecular architecture are also discussed. In the last section, we set the work in the thesis in a wider context.

1.1. Liquid Crystals

Many chemical compounds can be in one of three physical states: i.e. the solid, liquid or gaseous phase. The solid phase traditionally refers to the fact that matter does not flow when it is subject to a (small) force. The molecules in a crystalline solid are located on a regular lattice and this order extends beyond many lattice spacings. Gases and liquids do flow but differ in the sense that gases tend to occupy the available volume whereas liquids keep their own volume and gather at the bottom of the container. In both phases, the molecules have no fixed position or orientation and on average there is no order. Upon cooling from a high temperature phase, the usual phase sequence is gas - liquid - solid or, sometimes the liquid is skipped, gas - solid.

Liquid crystalline phases are phases with partial order, and in that sense intermediate between totally ordered crystals and disordered liquids. The first observation of liquid crystals was made by Friedrich Reinitzer, in 1888, reporting that esters of cholesterol had two melting points. In between these melting points, the liquid was birefringent. In the next years, Otto Lehmann described the material as 'flowing crystals', 'crystalline liquids' and 'liquid crystals' (see e.g. Refs. [1, 2]). Other names which are frequently used are mesophases or mesomorphic phases and also refer to the intermediate nature of these phases. Molecules forming these phases are then called mesogens. The most well-known liquid crystalline (LC) phases are the nematic, the smectic [1] and the cholesteric phase.

In the nematic phase, the molecules are oriented with respect to a director $\hat{n}$, but there is no spatial order and therefore, it is still a fluid. In order to form a nematic the molecules need to be fairly anisotropic in shape. An example is given in Fig. 1.1 where rodlike molecules form a calamitic nematic (as opposed to disklike molecules forming a discotic nematic). Opposed to this orientationally ordered fluid phase, we call the orientationally disordered fluid phase the isotropic phase. A nematic phase flows like a fluid but is birefringent similar to a crystal. Usually the capital (roman) letter N is used for the nematic and I for the isotropic phase. The most common nematic phase is

---

[1]These names were given by George Friedel in 1922 and are drawn from Greek; nematic refers to the threadlike defects in these phases and smectic to the soapy appearence it has [3].

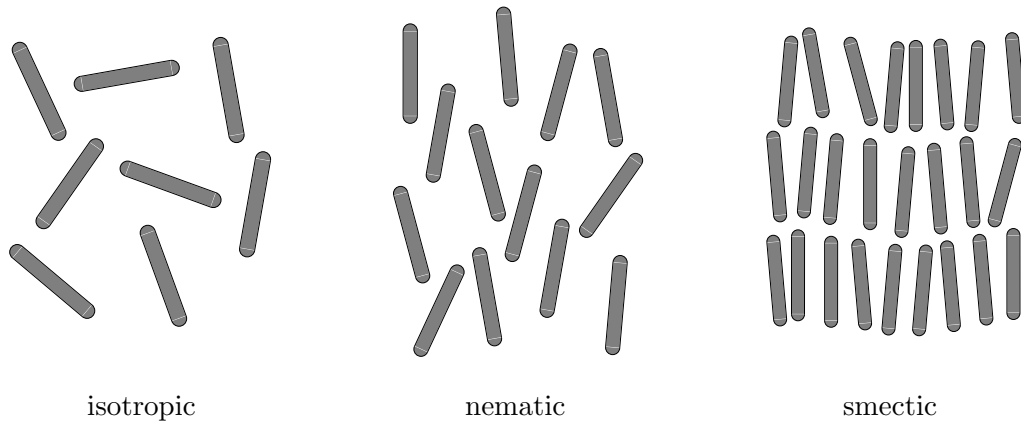isotropic   nematic   smectic

FIGURE 1.1. Liquid crystalline phases for rodlike molecules. On the left the ordinary isotropic liquid. In the middle the nematic phase and on the right the smectic A phase. For simplicity the phases have been drawn in a plane.

symmetric around the director $\hat{n}$ as well as to the interchange $\hat{n} \leftrightarrow -\hat{n}$, and is called the uniaxial nematic. A nematic with orientational order with respect to two different directors is called a biaxial nematic.

The smectic phase consists of layers stacked on top of each other. Within each layer the molecules are spatially disordered but do have orientational ordering. Rodlike molecules can have a smectic phase, as is shown in Fig. 1.1. Also amphiphilic molecules can form such a phase, where the hydrophobic (water-hating) parts form layers, driving out the water to in between these layers where the hydrophylic (water-loving) parts are located. In these systems, one usually speaks of a lamellar phase. There exist many different types of smectic phases due to differences in preferred orientation with respect to the layer normal or ordered bond orientations within the layers. The simplest one, in Fig. 1.1, is called smectic A (SmA) and has the preferred orientation parallel to the layer normal and the layers are two dimensional liquids.

The last LC phase we mention is the cholesteric phase for rodlike molecules (see Fig. 1.2). Locally this phase is like the uniaxial nematic. However, due to a small chiral interaction between the molecules, the rods tend to tilt their long axes a little with respect to each other. This results in a helical director field where the molecules in the planes perpendicular to the helical axis all have the same orientation. The periodicity of this helix is very much larger than the dimensions of the individual molecules. The name cholesterics is due to the fact that this phase was first found in esters of cholesterol.

Most low-molecular weight liquid crystals are thermotropic. This means they show LC phase transitions as a function of temperature. The transition from crystal to liquid crystal is the melting point and the transition from liquid crystal to isotropic liquid is called the clearing point (where the sample becomes optically clear). A typical example is p-octyl-p'-cyanobiphenyl (usually called 8CB) which has both a nematic and a smectic phase (see Fig. 1.3). The '8' in 8CB refers to the length of the (carbon) tail, and correspondingly the versions with other lengths are called 5CB, 6CB etc. A series of such molecules (with increasing tail length) is called a homologous series. Many phase diagrams consist of transition temperatures versus tail lengths. In general, longer tails stabilize the smectic phase and therefore destabilize the nematic. Another interesting
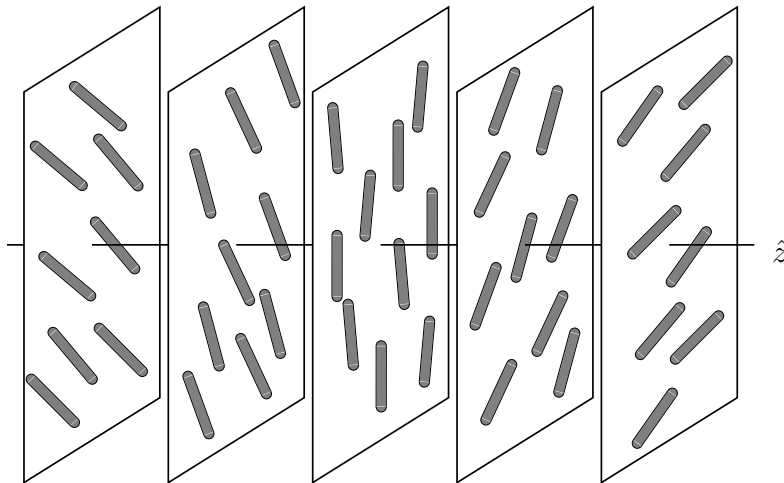
FIGURE 1.2. The cholesteric phase for chiral rodlike molecules. The preferred orientation rotates clockwise when we move in the direction of $\hat{z}$. Within the planes perpendicular to $\hat{z}$, all rods have the same preferred direction. The planes themselves are only drawn as a guide to the eye, so the cholesteric is still a fluid.

property is that homologous series usually show an odd-even effect; i.e. the transition temperatures of the even-numbered tail lengths are on average a bit higher/lower than those of the odd tail lengths. In the phase diagrams this appears as a zigzag curve. Vast amounts of thermotropic liquid crystals were synthesized and characterized by Daniel Vorländer in the beginning of the 20'th century [4].

Another class of liquid crystals is called lyotropic. In lyotropic systems the molecules are in solution and have LC phase transitions as a function of concentration. Suspensions of anisotropic colloids and the already mentioned amphiphilic molecules in water are lyotropic systems. A well-known example of a lyotropic liquid crystal is a concentrated solution of the Tobacco Mosaic Virus (TMV) [5]. TMV particles appear as rods with lengths of 300 nm and diameters of 18 nm and it shows a nematic as well as a smectic phase. These virus particles are extremely monodisperse (unlike synthesized colloids) and serve as an excellent model system as they interact approximately as hard bodies. [2] Solutions of TMV particles were already studied by Bernal et. al. in the 1930's [6]

By far most molecular theories for LC behaviour concern the nematic phase and the isotropic-to-nematic transition. In 1949, Onsager proposed a theory for LC behaviour [7]. He aimed to describe colloidal suspensions like TMV solutions, modelling the colloids as rigid cylinders with hard-body interactions. Using the second virial approximation and approximate solutions, he basically introduced, explored and solved it all in a single paper [7]. Additionally, he showed that this description is exact in the isotropic phase for extremely elongated rods. Another theory was proposed by Flory, who used his lattice model for the case of rigid rods [8] and Maier and Saupe used a mean-field model where the particles interact via a potential proportional to the second Legendre polynomial [9].

---

[2]In fact the interaction potential is a very steep repulsive potential due to screened Coulomb interactions.
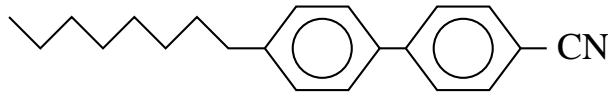
FIGURE 1.3. The molecule 8CB. It has a nematic as well as a smectic phase. The two phenyl rings form the mesogen and the aliphatic chain on the left is the more flexible tail.

Zwanzig used hard rods with 3 discrete orientations [10]. The theories of Onsager and Zwanzig use density as a parameter and could be considered to be of lyotropic nature, where the other ones use temperature and describe therefore thermotropic systems. In many cases this difference is only formal as for instance the Onsager and Maier-Saupe theory give equivalent results when density is identified with 1/Temperature. Most other molecular theories for LC behaviour are extensions of the above.

Computer simulations have become an important tool in the field of liquid crystals. The nematic behaviour in fluids of hard anisotropic particles was studied by Vieillard-Baron [11] and Frenkel and Mulder [12] (see also Ref. [13]). Bolhuis and Frenkel computed the full phase diagram of hard spherocylinders in Ref. [14] (which could be used as a model system for TMV particles). Simulations have also been performed on Maier-Saupelike systems; Lebwohl and Lasher connected the Maier-Saupe rods to a lattice [15] and Luckhurst and coworkers used freely moving rods (see Chap. 3 in Ref. [16]). In ending this section, we mention some literature we used. Books on the physics of (thermotropic) liquid crystals are Refs. [17, 18, 19]. An extensive collection of contributions on the molecular origin of liquid crystals is given in Ref. [16]. Statistical mechanics of liquid crystals is treated in Ref. [20] and hard-particle fluids are the subject of Ref. [13].

1.2. Liquid Crystalline Polymers

Polymers are long molecules consisting of many monomers chemically linked to each other. Polymers are abundant in nature and especially in biological systems. Also, many different ways of synthesis are known and large quantities of polymers are being produced in industry. Their main interest lies in the intrinsic mechanical properties and their possible modification through inclusion of groups with different chemical or physical properties. Cooperation of or competition between such groups gives rise to new phenomena and resultingly, whole new fields of science and industrial applications [21].

LC ordering is believed to play a role in some processes involving biological polymers like DNA and microtubules. Also, the previously mentioned virus particles like TMV can be considered biopolymers and show LC behaviour in concentrated solutions. Contrary to these biopolymers, which are lyotropic, most polymers synthesized in laboratories are thermotropic liquid crystals. These thermotropic polymers exist in roughly three classes; in the first case, the stiff main chains themselves act as liquid crystal formers. The other two use mesogens incorporated in the polymer, connected with more flexible parts called spacers. These polymers come in two flavours, those with mesogens in the main chain and those with side chains containing them. Presently, there are also combinations of the last two.

The first to systematically study the effect of increasing molecule length on the LC phase behaviour was probably Vorländer [4]. In 1923, he synthesized poly(p-benzamide)

and concluded that the melting temperature was too high as the polymer burned before it was reached. In general, linking LC groups (like benzene rings) rigidly together should provide a stable LC phase as the molecules become more and more anisotropic. Indeed, the clearing temperature does increase with increasing molecule length. However, also the melting temperature shoots up for these long rigid polymers. And although generally the melting temperature increases less than the clearing temperature, thus stabilizing the LC phases, still both become very quickly so high that the molecules decompose before they can melt.

One way to get around this is flexibility. The first successfull LC polymers (LCP's) were polypeptides and were investigated in an effort to develop synthetic silk. In 1956, Robinson reported about birefringency in solutions of poly-γ-benzyl-L-glutamate (PBLG) concluding that these were LC phases [22]. PBLG molecules consist of rather stiff main chains, i.e. stiff enough to allow for liquid crystallinity, but flexible enough to be manageable at moderate temperatures. Eventually these investigations led to the development of high-tensile strength fibers like Kevlar [23]. However, the importance of the liquid crystallinity in these systems was not fully recognized until the 1980's.

Other ways of manipulating the molecular architecture to increase the stability of LC phases is by frustrating the crystalline phase, and thus bringing down the melting temperature. Jackson and coworkers synthesized aromatic polyesters which were not periodic along the chain [24]. This random copolymerization proved to be a powerfull way to prevent crystallization and several commercially available polymers use this concept (see in Ref. [1]). Introducing kinks or side groups can also reduce the melting temperature considerably, where usually the LC tendency is not so much affected. Sometimes, the crystalline phase disappears altogether and instead anisotropic glass phases appear.

It was attempted for some time to use flexible polymers and laterally attach the chemical groups responsible for the LC behaviour in low-molecular weight liquid crystals. These first side chain polymers, however, were unsuccessful as the entropic (coillike) tendency of the polymer proved to be stronger than the LC tendency of the side chains. Also, direct linkage of these groups to the polymer sterically frustrated the orientational and spatial freedom these groups need to have. This was solved when the spacer concept was introduced by Finkelmann and coworkers [25]. Instead of direct linkage, they used an aliphatic chain (spacer consisting of CH_2's) to decouple the mesogens from the flexible polymer (backbone). This discovery really boosted the field and later the spacer concept was also used in main chain polymers [26].

If we want to compare low molecular weight LC's and LCP's, there are a few things we should bear in mind. In general, there is a strong reduction in entropy when mesogens are incorporated in polymers. As a result, the same mesogens order stronger when embedded in polymers compared to when they are isolated (e.g. nematic mesogens yield smectic polymers). Another characteristic of polymers is that due to the way of synthesizing (e.g. polymerization reactions), one will always obtain a mixture of polymers with many different lengths. The degree of polydispersity may have quite some effect on the phase diagram. An indication for the degree of polydispersity is given by the ratio M_w/M_n, where M_w is the weight average molecular weight and M_n is the number average molecular weight. In Chap. 3 in Ref. [27] and in Refs. [28, 29, 30, 31], this is discussed using the example of the polyacrylate poly(4-(5-acryloyloxypent-1-yloxyphenyl)-4'-butoyloxybenzoate) (or shorter, PABB-5) (see Fig. 1.4). Fairly monodisperse melts
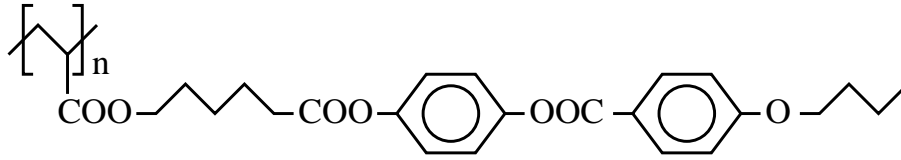
FIGURE 1.4. A monomer of the molecule PABB-5. The square brackets in
the upper left part refer to the fact that here the neighbouring monomers con-
nect. For long polymers (n>100), monodisperse melts of PABB-5 have various
nematic and smectic phases. The phenyl rings form the mesogen, the aliphatic
chain connecting the rings to the polymer is the spacer and the polymer is called
the backbone. Right of the mesogen, there is a small aliphatic tail.

of this polymer ($M_w/M_n \approx 1.2$) show a phase sequence I - N - SmA - RN - SmF, where
RN is a reentrant nematic and SmF is a kind of smectic phase. Wider distributions
($M_w/M_n \approx 2.9$) just show I - N - SmF.

Most molecular theories for LCP's start from the theories for low molecular weight
LC's and then include flexibility. Khokhlov and Semenov use impenetrable wormlike
chains and this yields an excluded volume interaction similar to Onsager's [32, 33].
They derived a new expression for the conformational entropy which includes the flex-
ibility of the molecule. Warner and coworkers use wormlike chains with Maier-Saupe
interactions [34]. Keeping only the leading terms, they are able to calculate radii of
gyration in the nematic phase. There are some more extensions (also to the case of side
chain polymers), but these we will discuss in the appropriate chapters. There are no
simulations of genuinely long LCP's as these systems are too large for the present gener-
ation computers. In ending this section, we mention a paper by Holyst and Oswald [35]
which is a review of some basic models for LCP's. Ref. [2] is a historical review of the
development of LCP systems.

1.3. Flexible Theories for Flexible Molecules

Relatively a lot of work has been done on the nematic ordering in melts of wormlike
chains. Wormlike chains are linear and are completely symmetric along the chain; i.e.
every part of the chain is identical to every other part. This simplicity is the reason why
wormlike chains are an interesting model system. Also, the nematic phase is usually
considered as it is by far the most easy phase to treat theoretically. And moreover,
experimentally, it is a very common phase and phenomena occurring in other LC phases
can often be understood (partially) by first studying the nematic.

However, as we argued earlier, a realistic LC polymer is often not a plain repetition of
some simple monomer. These consist of rigid mesogens connected with flexible spacers
which can again be located in side chains or embedded in the main chain. There are
very little theories explicitly considering these geometries. And the ones which do,
treat these objects on the mean-field level so all possibly important correlations between
the various parts of the molecules are lost. In this thesis, we develop a formalism for
nematic ordering in LCP's, where the explicit geometries are considered and in which
the interactions within the molecules are taken into account exactly.

As we stated at the end of the previous section, Khokhlov and Semenov (KS) have created a formalism for nematic ordering in hard wormlike chains [32, 33]. Their formalism is capable of including correlations within the polymers and they conclude, using a scaling argument, that for long polymers in the nematic the order in the middle is twice as large as at the ends [33]. However, for the rest they mainly considered very long 'semiflexible' chains for which these contributions from within the chain do not show and seem averaged out, like in a mean field treatment (which they are not). Only later, in Ref. [36], Chen solved KS's equations numerically and computed the distribution of order along the wormlike chain.

Kayser and Raveché showed that in the context of Onsager's original model, the nematic solution branches off from the isotropic solution [37]. They were able to construct the nematic solution perturbatively starting from this bifurcation point and showed that it connects to the globally stable solution further away. The strength of this method is that the bifurcation density gives a good indication of the nematic coexistence density and that the bifurcation analysis can be performed analytically. KS have applied a bifurcation analysis for the wormlike chains and mention the result in Ref. [33].

In this thesis, we start from a more fundamental level and consider a chain as being built up of rodlike segments. For these objects, we develop a density functional formalism, with a firm theoretical foundation for the various terms in the functional and the approximations needed. Next, we can define an appropriate limit, which transforms the segmented chains into wormlike chains. This limit can be taken at virtually every point in the analysis and reduces our formalism to that of KS. Apart from the above, we find the segmented chain formalism conceptually easier to start with. The bifurcation analysis of Kayser and Raveché is readily generalized and numerical work becomes more straightforward as the chains are already discrete. This is the subject of Chap. 3.

Most importantly, the segmented chain formalism is generalizable to systems with a more complicated geometry in a straightforward way. This generalization is rather direct because in considering segmented chains, one can write the equations in a coupled way, for every segment seperately. Considering different-sized segments or branched chains boils down to changing only a few of the contributions in these equations in a straightforward fashion. It is in this sense that the theories we are considering are flexible, explaining the title, *flexible theories for flexible molecules*. After the analysis is performed and the results are obtained it is then still possible to apply the wormlike chain limit.

In Chap. 2, we discuss some technical background needed to appreciate this thesis. The rest of the thesis is organized in two parts. In the first part, we consider polymers consisting of only one type of segment and are consequently homogeneous along the chain: hence, homopolymers. Chap. 3 is about chains of cylindrically symmetric or uni-axial segments and in Chap. 4 the segments are biaxial. In the second part, the polymers can be built up from different types of segments and we call them heteropolymers. Also, we include the possibility of branching within the chains. In Chap. 5, we consider very general segmented and possibly branched heteropolymers. Main chain LCP's are the subject of Chap. 6 and side chain LCP's are considered in Chap. 7.

The only liquid crystalline phase, we consider throughout this thesis is the nematic. This is mainly because the theories we use for flexible molecules are tractable in the nematic, and moreover, being the 'first' liquid crystalline phase, bifurcation analysis of

the trivial isotropic solution can be performed. Positionally ordered phases for flexible molecules are notoriously more difficult. Whereas in fluid phases, orientational correlations along the polymer sustain for length scales on the order of the persistence length, in inhomogeneous phases, the spatial correlations usually travel much further. Furthermore, the intuitively useful concept of excluded volume can not be used anymore in inhomogeneous phases.

Most experimental liquid crystalline polymer systems are thermotropic, meaning that they show liquid crystalline phase behaviour as a function of temperaure. In this thesis, all theories are formulated in terms of the density, which would make them lyotropic theories. Although an essential difference in experimental systems, when considering these theories, it is usually a detail. Mean field theories, like that of Maier-Saupe, using the temperature as a control parameter, have the same formal structure as DFT in the Onsager approximation using the density. The density and the inverse of the temperature play similar roles, and often phase diagrams can be qualitatively 'translated' between lyotropic and thermotropic by replacing one with the inverse of the other. However, when other degrees of freedom are also considered, one has to take caution in making this translation. In Chap. 7, this point is addressed in order to compare the nematic behaviour of Onsagerlike side chain LCP's considered in this thesis and Maier-Saupelike side chain LCP's considered elsewhere.

2 Theoretical Background

In this chapter, we give a technical introduction to the fields of thermodynamics and statistical mechanics. The density functional formulation of statistical mechanics is discussed and bifurcation analysis is introduced as a tool to study symmetry-breaking transitions. Finally, we briefly discuss Onsager's model for liquid crystals and introduce the concept of wormlike chains.

2.1. Thermodynamics

2.1.1. General Principles. Thermodynamics is designed in accordance with our experience; it is a phenomenological theory. It is also inherently macroscopic, meaning that it makes no statements on microscopic properties and in turn assumes that there is no explicit appearence of the molecular character of matter. In that sense, it applies to almost everything in the world around us, and is probably the most general physical theory. This generality is, in a way, also its weakness; thermodynamics does not give new fundamental laws, it merely relates properties of matter and sets limits as to what can happen. There is just one catch; thermodynamics describes systems which are in equilibrium. This seems a strong restriction as not many systems in the world around us are in thermodynamic equilibium. Still, the success of thermodynamics as a physical theory justifies the assumption that in practice an operational form of equilibrium can be reached for most systems [38, 39, 40]. The approach, we take here, largely follows Callen [38].

The formulation of thermodynamics starts with a few postulates which are drawn directly from experiments and use the macroscopic character of the considered systems.

(1) A thermodynamic equilibrium state of a system is, macroscopically, completely characterized by the internal energy U, and the other extensive parameters [1] (like the volume V, the mole numbers $N_1, N_2, \cdots, N_r$ of the chemical components, etc.).

(2) The entropy S of a system is a (continuous, differentiable) function of the extensive parameters $S(U, V, N_1, \text{etc.})$, and these extensive parameters assume values that maximize the entropy within the constraints set to the system.

These two postulates are usually called the first and second law of thermodynamics, respectively. Although seemingly simple, their implications are huge and most of thermodynamics can be constructed using these statements. We are now in a position to

---

[1] A thermodynamic parameter is extensive when it scales linearly with the size of the system. Intensive parameters do not scale with the size of the system.

construct the quantities,

$$T = \left(\frac{\partial U}{\partial S}\right)_{V,N_1,\text{etc.}} \quad P = -\left(\frac{\partial U}{\partial V}\right)_{S,N_1,\text{etc.}} \quad \mu_1 = \left(\frac{\partial U}{\partial N_1}\right)_{S,V,\text{etc.}} \quad \text{etc.} \quad\quad (2.1)$$

where T is defined as the temperature, P as the pressure and μ as a chemical potential and these are all intensive. Defined in this way, these quantities agree with our intuitive concepts of temperature and pressure. The role of the internal energy U as a thermodynamic potential is ensured by an additional postulate that $T > 0$ (see again Ref. [38]) and with $U = U(S, V, N_1, \text{etc.})$, Eqs. 2.1 are called equations of state. The two formulations, using either the energy U, or the entropy S, as potential are completely equivalent. However, the energy formulation is the most common and is what we also use. Another important implication of $T > 0$ is that the principle of maximum entropy (2nd law) is equivalent to a principle of minimum energy. The entropy S, as a thermodynamic parameter is extensive as well. Therefore, often the energy of a system is written in terms of that of one mole of a certain compound,

$$\begin{aligned} U(S, V, N_1, N_2, \text{etc.}) &= N_1 U(S/N_1, V/N_1, 1, N_2/N_1, \text{etc.}) \\ &= N_1 u(s, v, x_2, \text{etc.}). \end{aligned}$$

So, the dependence of one extensive parameter can be scaled out, which makes sense as thermodynamics is scale invariant.

2.1.2. Thermodynamic Potentials. In most cases, it is not so natural to characterize a system in terms of extensive parameters. For instance, consider a system with one component, which is in thermal contact with the "outside world" but is for the rest isolated from it. The outside world has a constant temperature T_0, and imposes this through the thermal contact to the system. Then, the thermodynamic state of our system would be determined by the extensive parameters S, V, N, and the additional constraint $T(S, V, N) = T_0$. In such a case, it is easier to use a formulation where T would be a parameter instead of its conjugate extensive parameter S (which is allowed to fluctuate due to the flow of heat). This can be done by taking the Legendre transform of U,

$$F = U - TS. \quad\quad (2.3)$$

Eliminating U and S by using $U = U(S, V, N)$ and $T = \partial U/\partial S$ yields $F = F(T, V, N)$. The new potential F is called the Helmholtz potential and contains the same information as $U(S, V, N)$. Conveniently, the principle of minimum energy translates directly, and the values of any unconstrained internal parameters assume values which minimize the Helmholtz free energy, given $T = T_0$. These Legendre transformations can be performed with respect to other parameters as well, yielding a whole set of thermodynamic potentials and corresponding minimum principles. Each of these potentials has a corresponding system, to which applied, it shows its full advantage. Here we mention only the grand canonical potential,

$$\Xi = U - TS - \mu N, \qu\quad (2.4)$$

with $\Xi = \Xi(T, V, \mu)$. The grand canonical potential is minimized when the system is in thermal contact with the outside world as well as that it can exchange matter with it.

The constraints are: $T = T_0$ and $\mu = \mu_0$. This potential plays a central role in density functional theory (Sec. 2.3).

2.1.3. Stability. In order to investigate the stability of thermodynamic systems, we turn again to the principle of minimum energy. It can be formulated as follows,

$$dU = 0 \quad \text{and} \quad d^2U > 0, \tag{2.5}$$

with $U = U(S, V, N_1, \text{etc.})$. The first condition ensures the energy is an extremum and the second that it is a minimum. Because of the positive curvature in all directions, the energy is said to be a convex function of its external parameters. However, the effect of the Legendre transformation is that the thermodynamic potentials obtain negative curvature with respect to their intensive parameters, i.e. they are concave with respect to them. So, in case of the Helmholtz potential, for a one-component system, this means

$$\left(\frac{\partial^2 F}{\partial T^2}\right)_{V,N} \leq 0 \quad \left(\frac{\partial^2 F}{\partial V^2}\right)_{T,N} \geq 0 \quad \left(\frac{\partial^2 F}{\partial N^2}\right)_{T,V} \geq 0. \tag{2.6}$$

(To not complicate things too much, we do not mention the "combined" stability criterion for V and N here.) In practice, however, when one uses the Helmholtz potential, the system is in thermal contact with the outside world, which has a fixed temperature $T = T_0$. Consequently, we are only concerned with the convexity of the free energy surface in the direction of the extensive parameters.

2.1.4. Phase Transitions. We proceed in considering the one-component system of the previous subsection. One might argue that the two other (external) parameters V, N are also fixed, as there is no mechanical or chemical contact with the outside world. However, it can happen that the free energy surface $F(T_0, V, N)$ becomes locally nonconvex as a function V and N, like for instance in Fig. 2.1. Then, this nonconvexity is cancelled by the system by dividing into two subsystems; this is called phase separation. These subsystems are not separated by any wall, so matter can flow between them, and they can exchange volume. They are characterized by V_1, N_1 and V_2, N_2 respectively, and have both the same temperature T_0 as they are both in thermal contact with the outside world. The incentive for this division is that the new free energy F', which is a sum of that of the two subsystems, is lower than the original one,

$$F'(T_0, V, N) = F(T_0, V_1, N_1) + F(T_0, V_2, N_2) < F(T_0, V, N), \tag{2.7}$$

with of course $N = N_1 + N_2$ and $V = V_1 + V_2$ (with T_0, V, N fixed by the experimenter, there are two free parameters). If we use molar quantities, $f' = F'/N$ and $f_i = F/N_i$ ($i = 1, 2$), and rewrite a little bit,

$$f'(T_0, \rho) = x_1 f_1(T_0, \rho_1) + x_2 f_2(T_0, \rho_2), \tag{2.8}$$

with densities, $\rho = N/V$, $\rho_i = N_i/V_i$ and mole fractions $x_i = N_i/N$. Then, the constraints are $x_1 + x_2 = 1$ and $x_1/\rho_1 + x_2/\rho_2 = 1/\rho$. From Fig. 2.1, it is easy to see that this "linear combination" of two subsystems lowers the total free energy of the system and as such, cancels the nonconvexity of the free energy surface. This construction, presented in Fig. 2.1, is called the common tangent construction or Maxwell construction, and the densities, ρ_1 and ρ_2, are found by solving the following (two) equations

$$\left.\frac{\partial f(T_0, \rho)}{\partial \rho}\right|_{\rho=\rho_1} = \left.\frac{\partial f(T_0, \rho)}{\partial \rho}\right|_{\rho=\rho_2} = \frac{f(T_0, \rho_2) - f(T_0, \rho_1)}{\rho_2 - \rho_1}. \tag{2.9}$$
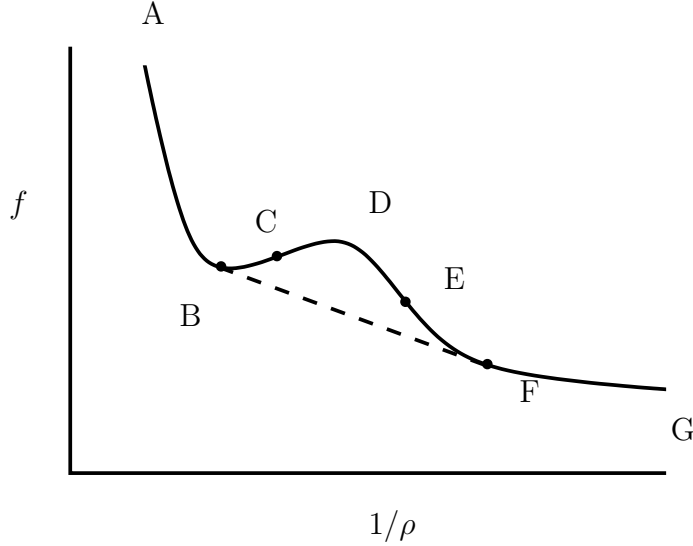
FIGURE 2.1. An example of a nonconvex free energy surface: ABCDEFG. In between B and F, the system will divide into two subsystems in order to make the free energy convex: ABFG (following the dashed curve). The points B and F are the binodal points and C and E are the spinodal points. The dashed line is the common tangent of B and F. The parts AB and FG are globally stable, BC and EF are metastable and CDE is unstable.

Having determined these densities, ρ_1 and ρ_2, x_1 and x_2 can be obtained from the constraints. Locating the common tangents, in this way, is equivalent to imposing that the pressures and the chemical potentials of both subsystems be equal,

$$P(T_0, \rho_1) = P(T_0, \rho_2) \quad \text{and} \quad \mu(T_0, \rho_1) = \mu(T_0, \rho_2), \tag{2.10}$$

which are, in the Helmholtz representation, given by

$$P(T_0, \rho) = -\left(\frac{\partial F}{\partial V}\right)_{T_0, N} = \rho^2 \left(\frac{\partial f}{\partial \rho}\right)_{T_0} \tag{2.11}$$

$$\mu(T_0, \rho) = \left(\frac{\partial F}{\partial N}\right)_{T_0, V} = f(T_0, \rho) + \rho \left(\frac{\partial f}{\partial \rho}\right)_{T_0}. \tag{2.12}$$

These last remarks are of course, physically, more intuitive. The two subsystems do not have any barrier between them, so they can freely exchange matter and volume. Therefore, equal pressures and chemical potentials seem a necessary (and sufficient) condition. As was already stated, it is fully equivalent with constructing the common tangents.

The situation, we have just sketched above, is a very well known scenario for phase separation. The archetype system is the van der Waals fluid which can phase separate into a high-density fluid (liquid) and a low-density fluid (gas). The phase transition is first order as the density has a discontinuous jump at the transition. The densities ρ_1 and ρ_2, of the two coexisting phases are called coexistence or binodal densities. And, as we already saw, between these densities, the "global" convexity of the free energy

surface is lost. However, *locally* the surface can still be convex, $(\partial^2 f/\partial \rho^2)_{T_0} > 0$ (as can be checked from Fig. 2.1). The densities where

$$\left(\frac{\partial^2 f}{\partial \rho^2}\right)_{T_0} = 0, \tag{2.13}$$

are called the spinodal densities, and in between the second derivative is negative. So, between the binodal densities, the phase is globally unstable, but between the spinodal densities, even local stability is lost. Physically, it is usually said that one can overcompress the system, beyond the lower binodal density and still, the system can remain in the original phase. This is because a "critical" fluctuation is needed to drive the phase transition. However, when the spinodal density is approached the critical fluctuation needed goes to zero, and inevitably, phase separation sets in.

Finally, we note that Fig. 2.1) is typical for phase separation where the two phases have the same symmetry (like for instance the gas-liquid coexistence in the van der Waals fluid). If by some means, we would be able to change the temperature of the outside world, we would find that the coexistence region is not constant in size. Increasing the temperature, it would shrink until, at some temperature, it would disappear. Beyond, for higher temperatures, the free energy surface has no nonconvex parts. The point where the coexistence region has "zero size" is called the critical point, characterized by T_c, ρ_c. At the critical point, binodal and spinodal points meet, so $(\partial^2 f/\partial \rho^2)_{T_0}(T_c, \rho_c) = 0$. This is a common feature for phases with the same symmetry. Phases with different symmetry do not have a critical point.

2.2. Statistical Mechanics

2.2.1. General Remarks. Thermodynamics is concerned with macroscopic systems. In equilibrium, these systems can be descibed by only a few parameters, and other thermodynamic quantities can be expressed in terms of these parameters. However, thermodynamics just states that they exist, but does not provide the explicit relations between them. For instance, the equations of state Eqs. 2.1, will surely be different for different chemical substances, but that can not be obtained from thermodynamic theory. These relations have to be measured in experiments, or other ingredients or theories are needed to supply them. From this point of view, it is worthwile to go more "fundamental" and consider the composition of macroscopic systems. Microscopically, all matter is made up of small particles called molecules. Different substances consist of different types of molecules and the macroscopic appearence of a substance results from the collective behavior of a large number of the consisting molecules. If we know the properties of the individual molecules and how they interact, it should, in principle, be possible to connect those to the macroscopic properties of the substance. This bridge between the microscopic and the macroscopic world is formed by statistical mechanics [41, 42, 43].

From a classical-mechanical point of view, the state of a molecule is described by its "coordinates" **q** and the conjugate momentum **p**. The coordinates of a molecule contain the position, and possibly the orientation and even other (internal) degrees of freedom, like for instance for composed molecules, orientations of the independent components. The quantity **p** contains the conjugates of **q** and, therefore, has the same

dimension, which we set to be $3 + d$ (3 for the position coordinates, and d for the rest). Then, the microscopic state, or microstate, of the whole system is described by the collection of coordinates and momenta of all N molecules, $\Gamma_N = \{\mathbf{q}^N, \mathbf{p}^N\}$, with $\mathbf{q}^N = \{\mathbf{q}_1, \mathbf{q}_2, \cdots, \mathbf{q}_N\}$ and $\mathbf{p}^N = \{\mathbf{p}_1, \mathbf{p}_2, \cdots, \mathbf{p}_N\}$. The energy of a particular microstate is equal to the Hamiltonian of the system, $U = \mathcal{H}(\Gamma_N)$. The equations of motion of all particles can be obtained from the Hamiltonian, yielding, in principle, all the past and future of the system. However, it needs no comment that these will be impossible to solve, so we do not proceed.

In case of a single-component system the microstate Γ_N is described by $2(3 + d)N$ parameters, whereas we saw in the previous section, the thermodynamical state is described by 3 parameters (i.e. U, V, N). Inevitably, many microstates correspond to one and the same macroscopic state. This leads to the following assumption, which forms the foundation of (classical) statistical mechanics.

> For a macroscopic system in equilibrium, any microstate satisfying the macroscopic conditions is equally likely.

This is often called the postulate of equal a priori probability. For the closed single-component system (which is called a microcanonical ensemble in statistical physics), the above postulate simply means that all microstates with energy $\mathcal{H}(\Gamma_N) = U$ are equally likely and those with $\mathcal{H}(\Gamma_N) \neq U$ do not occur. The postulate of equal a priori probability implies that the system spends as much time in every accessible microstate. It is therefore likely to find the system in a macroscopic state corresponding to the largest number of microstates. This allows a rather direct connection of the number of accessible microstates to the thermodynamic entropy, and of the above postulate to the second law of thermodynamics. The first law of thermodynamics is taken to be a consequence of conservation of energy on the microscopic scale, following from (quantum) mechanics.

2.2.2. The Canonical Ensemble. In the previous section, we considered a system which was in thermal contact with the outside world and was therefore characterized by parameters T, V, N (in case of only one component). In statistical physics, such a system is called a canonical ensemble. Because of the constant temperature, energy is allowed to fluctuate and in principle all microstates Γ_N contribute to the macroscopic system. However, it can be shown that high-energy microstates are less likely than low-energy ones, and that the probability scales with $\exp[-\mathcal{H}(\Gamma_N)/k_{\mathrm{B}}T]$. The constant k_{B} is called the Boltzmann constant and sets the energy scale. We are now in the position to sum over all possible microstates, weighted with their probability,

$$Q(T, V, N) = \int \frac{d\Gamma_N}{N! h^{(3+d)N}} \exp[-\beta_{\mathrm{B}} \mathcal{H}(\Gamma_N)], \qquad (2.14)$$

with $d\Gamma_N = d\mathbf{q}^N d\mathbf{p}^N = d\mathbf{q}_1 \cdots d\mathbf{q}_N d\mathbf{p}_1 \cdots d\mathbf{p}_N$ and $\beta_{\mathrm{B}} = 1/k_{\mathrm{B}}T$. Q is the canonical partition function. The constant h is introduced in order to make Q dimensionless. Its origin lies in quantum mechanics and it has to be identified with Planck's constant. The factor $1/N!$ is also nonclassical and is due to the indistinguishability of the molecules. The partition function is related to the Helmholtz free energy,

$$F(T, V, N) = -k_{\mathrm{B}}T \log Q(T, V, N), \qquad (2.15)$$

and contains therefore all thermodynamic information of the system. In the canonical ensemble, the partition function Q is the central quantity as it bridges the gap from microstates to macroscopic states. For other ensembles, which characterized by other thermodynamic parameters, similar partition functions can be formulated. It is, however, still a formidable job to do the integration and there are only few (mostly one-dimensional) systems for which it can be performed exactly.

We proceed with a partial evaluation of the canonical partition function. The Hamiltonian can be written as the sum of a kinetic and a potential part,

$$\mathcal{H}(\Gamma_N) = U_{\text{pot}}(\mathbf{q}^N) + U_{\text{kin}}(\mathbf{p}^N). \tag{2.16}$$

The kinetic energy has contributions from the linear momentum of the molecules and possible other modes (like angular momentum). For now, we concentrate on the linear momentum, and the kinetic energy is quadratic its components.

$$U_{\text{kin}} = \sum_{i=1}^{N} \frac{\mathbf{p}_i \cdot \mathbf{p}_i}{2m}. \tag{2.17}$$

Then, every integration over $\mathbf{p}_i$ are 3 Gaussian integrals, yielding a total factor

$$\Lambda^3 = \left(\frac{h}{\sqrt{2\pi m k_{\text{B}} T}} \right)^3, \tag{2.18}$$

in which m is the mass of the molecule. The quantity Λ is the de Broglie thermal wavelength. The kinetic energy contained in the other modes typically contribute similar factors, i.e. for one component of the angular momentum, $\Lambda_\sigma = h/(\sqrt{2\pi I_\sigma k_{\text{B}} T})$ with I_σ a principal moment of inertia, around axis σ (see the appendix in Ref. [13]). Collecting these contributions, we define a quantity $\mathcal{V}_T$ called the thermal volume of the molecule,

$$\mathcal{V}_T = \Lambda^3 \prod_\nu \Lambda_\nu \tag{2.19}$$

where the index ν runs over the d "other" degrees of freedom. Λ has the dimension of length and the Λ_ν are dimensionless. An important thing to realize is that $\mathcal{V}_T$ scales with $T^{-(3+d)/2}$ [2]. Putting this back in Eq. 2.14, we obtain

$$Q(T, V, N) = \frac{1}{N! \mathcal{V}_T^N} \int d\mathbf{q}^N \exp[-\beta_{\text{B}} U_{\text{pot}}(\mathbf{q}^N)]. \tag{2.20}$$

where the integrations over momentum space are all contained in the factor $1/\mathcal{V}_T^N$. Using the Stirling approximation, $\log n! = n \log n - n$ for large n, we write down the free energy by combining Eqs. 2.15 and 2.20,

$$F(T, V, N) = N k_{\text{B}} T \left(\log \left(\rho \mathcal{V}_T \right) - 1 \right) - k_{\text{B}} T \log \int \frac{d\mathbf{q}^N}{V^N} \exp[-\beta_{\text{B}} U_{\text{pot}}(\mathbf{q}^N)], \tag{2.21}$$

with $\rho = N/V$ the number density.

---

[2]Obviously, for molecules with an infinite number of degrees of freedom (like the wormlike chains of Sec. 2.6) this approach breaks down because $d \to \infty$. However, this is only a real problem when one is considering the actual temperature dependence, computing for instance the specific heat. In this thesis, we use a fixed temperature and then we can discard the (constant) term $\log \prod_\nu \Lambda_\nu$.

In ending this subsection, we consider a system of noninteracting (ideal) molecules, $U_{\mathrm{pot}} = 0$. The integral in Eq. 2.20 is trivial, and the partition function becomes

$$Q_{\mathrm{ideal}}(T, V, N) = \frac{w^N V^N}{N! \mathcal{V}_T^N}, \tag{2.22}$$

where $W = wV = \int d\mathbf{q}$. The volume V is due to the spatial integrations and the factor w comes from the integrations over the other degrees of freedom. The "ideal" free energy is

$$F_{\mathrm{ideal}}(T, V, N) = N k_{\mathrm{B}} T \left(\log \left(\rho \mathcal{V}_T / w \right) - 1 \right). \tag{2.23}$$

2.2.3. The Virial Expansion. The central effort in statistical mechanics goes to performing the partition sum Eq. 2.20, for nontrivial interactions, $U_{\mathrm{pot}} \neq$ constant, between the molecules. This can be done analytically only for a few (mainly one dimensional) systems. In all other cases, some kind of approximation or perturbation theory has to be employed. For systems where the density is low, like gases, sometimes an expansion in powers of the density is used where the series is cut off beyond a certain power. This expansion is called the virial expansion and the coefficients are virial coefficients. In this thesis, we are concerned with very elongated molecules. In isotropic fluids of these molecules, it is not so much the density which is low but the virial coefficients which decrease rapidly with increasing order. For these systems, the virial expansion is a convenient starting point for an analysis.

For simplicity, we start by assuming that there is no external field and that possible internal degrees of freedom have all the same energy. In the next section, these can be reimplemented in a natural way. The molecules under consideration interact pair-wise, so the potential energy becomes

$$U_{\mathrm{pot}}(\mathbf{q}^N) = \sum_{i<j} u_{\mathrm{pot}}(\mathbf{q}_i, \mathbf{q}_j), \tag{2.24}$$

where $u_{\mathrm{pot}}(\mathbf{q}, \mathbf{q}')$ is the interaction energy of two molecules with coordinates $\mathbf{q}$ and $\mathbf{q}'$ and the summation runs over all i, j with $1 \leq i < j \leq N$. Next, we define the Mayer function,

$$\phi_{\mathrm{M}}(\mathbf{q}, \mathbf{q}') = \exp[-\beta_{\mathrm{B}} u_{\mathrm{pot}}(\mathbf{q}, \mathbf{q}')] - 1. \tag{2.25}$$

The Mayer function is short ranged as it goes to zero when the molecules are far apart (because u_{pot} vanishes for large distances). From this observation, we consider the expansion of the integrand $\exp[-\beta_{\mathrm{B}} U_{\mathrm{pot}}(\mathbf{q}^N)]$, in Mayer functions,

$$\exp[-\beta_{\mathrm{B}} U_{\mathrm{pot}}(\mathbf{q}^N)] = \prod_{i<j} \left(1 + \phi_{\mathrm{M}}(\mathbf{q}_i, \mathbf{q}_j) \right).$$

$$= 1 + \sum_{i<j} \phi_{\mathrm{M}}(\mathbf{q}_i, \mathbf{q}_j) + \sum_{\substack{i<j; i'<j' \\ (i,j) \neq (i',j')}} \phi_{\mathrm{M}}(\mathbf{q}_i, \mathbf{q}_j) \phi_{\mathrm{M}}(\mathbf{q}_{i'}, \mathbf{q}_{j'}) + \cdots \tag{2.26}$$

Putting this expansion in the free energy Eq. 2.21, and rearranging quite a bit, we obtain what is called the virial expansion of the free energy,

$$F(T, V, N) = N k_{\mathrm{B}} T \left(\log \left(\rho \mathcal{V}_T \right) - 1 + B_2 \rho + \tfrac{1}{2} B_3 \rho^2 + \cdots \right), \tag{2.27}$$

where the series expansion $\log(1 + x) = x - \frac{1}{2}x^2 + \cdots$ is used. The second and third virial coefficients are given by

$$B_2 = -\frac{1}{2Vw^2} \int d\mathbf{q}\,d\mathbf{q}'\,\phi_M(\mathbf{q}, \mathbf{q}'), \tag{2.28}$$

$$B_3 = -\frac{1}{3Vw^3} \int d\mathbf{q}\,d\mathbf{q}'\,d\mathbf{q}''\,\phi_M(\mathbf{q}, \mathbf{q}')\phi_M(\mathbf{q}, \mathbf{q}'')\phi_M(\mathbf{q}', \mathbf{q}''). \tag{2.29}$$

We have not given any more terms in Eq. 2.27 and the corresponding virial coefficients, as they quickly become much more elaborate. Going from Eqs. 2.21 and 2.26 to 2.27, 2.28 and 2.29 is far from trivial and we do not go into this. However, it involves extensive rearranging of the terms and recognizing that many of them are the same. Most integrals can be expressed in terms of a few "irreducible" ones. These irreducible integrals appear in the virial coefficients. The second and the third virial coefficient contain only one integral, but higher order coefficients very quickly contain many more (for instance, the fourth contains 3). Physically, each of the integrals in the nth virial coefficient B_n, corresponds to a contribution of n particles interacting simultaneously in a certain way.

We make a few more remarks on the virial expansion as given in Eqs. 2.27 to 2.29. Every n'th virial coefficient consists of n integrals over $\mathbf{q}$. However, making use of a coordinate transformation, one finds that one of them is trivial, yielding a factor wV. This factor V then cancels with the factor $1/V$ in front of every coefficient. Consequently, every virial coefficient is intensive and the free energy Eq. 2.27, is well-defined and extensive. The factors w^{-n} in front of the integrals are due to the fact that the molecules have other than spatial degrees of freedom. In this formulation, Eqs. 2.27, the n'th virial coefficient corresponds to the $(n - 1)$'th power of ρ, yielding terms $B_n\rho^{n-1}$. However, the virial series is originally defined for the equation of state (pressure). Taking the derivative (see Eq. 2.11) of the free energy, virial terms $B_n\rho^n$ appear, where the nth virial coefficient corresponds to nth power of the density.

Cutting off the virial expansion beyond the nth virial coefficient, we obtain the nth virial approximation. In this thesis, we will be concerned with only the second virial approximation. A problem with above equations is that implicitly, it has been assumed that there is no ordering of the molecules whatsoever. Therefore, the approach using the virial series is only valid in the homogeneous isotropic fluid phase. This issue will be addressed in Sec.2.3.

2.2.4. Hard Particles. The reason we could perform the virial expansion is because the Mayer function is short-ranged. In this thesis we consider impenetrable or hard particles which have an extremely short-ranged pair-potential,

$$u_{\text{pot}}(\mathbf{q}, \mathbf{q}') = \begin{cases} \infty & \text{if overlap} \\ 0 & \text{if no overlap} \end{cases}, \tag{2.30}$$

and therefore, so does the Mayer function,

$$\phi_M(\mathbf{q}, \mathbf{q}') = \begin{cases} -1 & \text{if overlap} \\ 0 & \text{if no overlap} \end{cases}. \tag{2.31}$$

Then, the virial coefficients get a very intuitive meaning; the second probes if two particles are overlapping, the third if three are overlapping simultaneously etc. Furthermore, if we use that the Mayer function is invariant to translations, $\phi_M(\mathbf{q}, \mathbf{q}') =$

$\phi_M(\mathbf{r} - \mathbf{r}', \Omega, \Omega')$, with Ω the 'other' degrees of freedom, we can define what is called the excluded volume of two molecules

$$\mathcal{E}(\Omega, \Omega') = -\int d\mathbf{r}\phi_M(\mathbf{r}, \Omega, \Omega') \tag{2.32}$$

and the second virial coefficient becomes

$$B_2 = \frac{1}{2w^2}\int d\Omega d\Omega' \mathcal{E}(\Omega, \Omega'). \tag{2.33}$$

The excluded volume plays a central role in fluid phases of hard particles as we will see later.

Another property of hard particle systems, we address here, is that there is no energy scale. Because, temperature does not appear in Eq. 2.30, all virial coefficients are also independent of temperature and therefore, entropic in nature. From Eq. 2.27, we observe that all terms scale linearly with T and this can therefore be scaled out, yielding $\beta_B F$. Note, there is still a temperature dependence in $\mathcal{V}_T$, but this term only shifts the zero of energy and has therefore no effect.

2.3. Density Functional Theory

In this thesis, we are interested in systems of molecules which can undergo phase transitions. However, phase transitions are not included in statistical mechanics as it is formulated in the previous section. The reason is rather subtle and basically due to the fact that the Hamiltonian of our system is invariant to global translations and rotations. Only in the so-called thermodynamic limit ($N, V, U \to \infty$ with their ratios finite) statistical mechanics yields full thermodynamics, and true phase transitions and spontaneous symmetry breaking can occur. One can get around this by, for instance, including infinitesimal fields of some symmetry in the Hamiltonian, thus loosing its translational and orientational invariance, but this is rather tedious [44]. Another more natural approach is called density functional theory (DFT) and is the subject of this section [44, 45]. We roughly follow Ref. [13].

DFT reformulates classical statistical mechanics in terms of the single-molecule distribution function (SDF),

$$\rho^{(1)}(\mathbf{q}) = \frac{\int d\mathbf{q}^N \sum_{i=1}^N \delta(\mathbf{q} - \mathbf{q}_i) \exp[-\beta_B U_{pot}(\mathbf{q}^N)]}{\int d\mathbf{q}^N \exp[-\beta_B U_{pot}(\mathbf{q}^N)]}. \tag{2.34}$$

The sum runs over all particles and the delta functions are used to allow the averaging. Note that the SDF is normalized,

$$\int d\mathbf{q}\rho^{(1)}(\mathbf{q}) = N \tag{2.35}$$

Then, DFT asserts that there exists a functional $\Xi[\rho^{(1)}]$ which has the following properties

(1) For all single-particle distribution functions $\rho^{(1)}(\mathbf{q})$, the following inequality $\Xi[\rho^{(1)}] \geq \Xi[\rho_{eq}^{(1)}]$ holds, with $\rho_{eq}^{(1)}(\mathbf{q})$ the equilibrium distribution.
(2) For the equilibrium distribution, the functional $\Xi[\rho_{eq}^{(1)}] = \Xi_{eq}$, where Ξ_{eq} is the equilibrium value of the grand canonical potential.

Conveniently, this can immediately be recognized as a variational principle for obtaining the equilibrium distributions and the thermodynamic grand canonical potential. Also, it is a rather pleasant surprise that the formulation is in terms of SDF and not the full N-particle distribution function. In fact, it can be shown, that there is a one-to-one correspondence between these two, so the equations, *fully* describing the system, can be written in terms of the SDF. In turn, from the SDF, it can be directly observed in which way the system is ordered and what are the symmetries of the phase. There is one major drawback and that is that DFT proves the existence of such a functional, but does not supply it [3].

Before turning to this, we explore the formal structure of the theory a bit more. Recalling the thermodynamic relation, $\Xi = F - \mu N$, we proceed by defining a functional $\mathcal{F}[\rho^{(1)}]$,

$$\mathcal{F}[\rho^{(1)}] = \Xi[\rho^{(1)}] + \mu \int d\mathbf{q} \rho^{(1)}(\mathbf{q}), \tag{2.36}$$

which we call, in anticipation, the Helmholtz free energy functional. The ideal part of free energy functional is rather straightforwardly proposed,

$$\beta_{\mathrm{B}} \mathcal{F}[\rho^{(1)}] = \int d\mathbf{q} \rho^{(1)}(\mathbf{q}) \left(\log \left(\rho^{(1)}(\mathbf{q}) \mathcal{V}_T \right) - 1 \right) + \beta_{\mathrm{B}} \mathcal{F}_{\mathrm{single}}[\rho^{(1)}] + \beta_{\mathrm{B}} \mathcal{F}_{\mathrm{excess}}[\rho^{(1)}]. \tag{2.37}$$

Two extra unspecified contributions have been included as well. The second term on the right side is the internal energy of a molecule or the single-particle free energy. This can be due to internal degrees of freedom with different potential energies (which we promised to reinsert) or due to an external field acting on the molecules. In both cases, this term has the following structure

$$\beta_{\mathrm{B}} \mathcal{F}_{\mathrm{single}}[\rho^{(1)}] = \beta_{\mathrm{B}} \int d\mathbf{q} \rho^{(1)}(\mathbf{q}) U_{\mathrm{single}}(\mathbf{q}) \tag{2.38}$$

The last term in Eq. 2.37 is the excess free energy and governs the interactions between the molecules. This term is the hard part to obtain knowledge about and, as we did in the formulation of statistical mechanics in the previous section, we will have to resort additional approximations or conjectures to treat the intermolecular interactions. In this thesis, we use the second virial approximation,

$$\beta_{\mathrm{B}} \mathcal{F}_{\mathrm{excess}}[\rho^{(1)}] = -\frac{1}{2} \int d\mathbf{q} d\mathbf{q}' \rho^{(1)}(\mathbf{q}) \rho^{(1)}(\mathbf{q}') \phi_{\mathrm{M}}(\mathbf{q}, \mathbf{q}') \tag{2.39}$$

This term is a direct generalization of the second virial coefficient, Eq. 2.28, in the previous section. In his paper [7] on fluids of hard rods undergoing a transition from isotropic to orientationally ordered (nematic), Onsager already used a free energy functional containing the ideal term of Eq. 2.37 and the latter generalized second virial coefficient. He obtained these by considering the fluid as a mixture of rods with fixed orientations, long before the actual formulation of DFT. Onsager also argued, that the second virial approximation is exact for very long hard rods in the isotropic fluid phase. We will come back to this in Sec. 2.5.

---

[3]It is easily seen that there is never just one functional but a whole family of functionals, as the only requirement is that they need to be the same in their minimum.

Formulating a variational principle the terms of functional derivatives,

$$0 = \left.\frac{\delta\Xi[\rho^{(1)}]}{\delta\rho^{(1)}(\mathbf{q})}\right|_{\rho^{(1)}=\rho^{(1)}_{\mathrm{eq}}} = \left.\frac{\delta\mathcal{F}[\rho^{(1)}]}{\delta\rho^{(1)}(\mathbf{q})}\right|_{\rho^{(1)}=\rho^{(1)}_{\mathrm{eq}}} - \mu, \tag{2.40}$$

where the chemical potential μ acts as Lagrange multiplier. From this, we see immediately that $\mathcal{F}[\rho^{(1)}_{\mathrm{eq}}] = F_{\mathrm{eq}}$, which ensures the generating role of $\mathcal{F}$ in the canonical ensemble. Performing the variation of Eq. 2.37, we obtain

$$\rho^{(1)}(\mathbf{q}) = \frac{1}{\mathcal{V}_T}\mathrm{e}^{\beta_{\mathrm{B}}\mu}\exp\left(-\beta_{\mathrm{B}}U_{\mathrm{single}}(\mathbf{q}) - \beta_{\mathrm{B}}\frac{\delta\mathcal{F}_{\mathrm{excess}}[\rho^{(1)}]}{\delta\rho^{(1)}(\mathbf{q})}\right), \tag{2.41}$$

where now, μ has to be determined using the normalization condition, Eq. 2.35. Also using the second virial approximation Eq. 2.39,

$$\rho^{(1)}(\mathbf{q}) = N\frac{\exp\left(-\beta_{\mathrm{B}}U_{\mathrm{single}}(\mathbf{q}) + \int d\mathbf{q}'\phi_{\mathrm{M}}(\mathbf{q},\mathbf{q}')\rho^{(1)}(\mathbf{q}')\right)}{\int d\mathbf{q}\exp\left(-\beta_{\mathrm{B}}U_{\mathrm{single}}(\mathbf{q}) + \int d\mathbf{q}'\phi_{\mathrm{M}}(\mathbf{q},\mathbf{q}')\rho^{(1)}(\mathbf{q}')\right)}. \tag{2.42}$$

This nonlinear integral equation supplies the distributions for which the functional is stationary. Needless, to say that this equation is still, generally, not solvable. In the simplified case that $U_{\mathrm{single}} = 0$, we can find the trivial isotropic fluid distribution, $\rho^{(1)}_{\mathrm{iso}} = \rho/w$. When, $U_{\mathrm{single}} \neq 0$, the isotropic solution will still exist but it depends on U_{single} and sometimes more approximations are needed to get it in closed form. For polymers, this is one of the topics of Chap. 3. In the next chapter, we present how low symmetry solutions branch off high symmetry solutions in the above formalism.

2.4. Bifurcation Analysis

As stated before, it may be very difficult, if not impossible to solve the stationarity equation Eq. 2.42, and obtain a full solution in a certain phase. However, many phase transitions involve a breaking of symmetry. For instance, in case of a system of spherical particles, clearly the fluid phase has different symmetry than the crystalline phase. In the fluid phase there is full translational symmetry, whereas in the crystal only translations which map the lattice on itself do not change the system. In the above case, the fluid is the high-symmetry solution and the crystal is the low-symmetry solution. Often (not in the above case though), symmetry breaking phase transitions involve a bifurcation point. At the bifurcation point a low-symmetry solution branches off from the high-symmetry one. If the high-symmetry or parent solution is known, one can look for solutions with a lower symmetry in its neighbourhood by means of a perturbation analysis. This study of the bifurcation point and its direct surroundings is bifurcation analysis. The phase transitions considered in this thesis (from an isotropic to a nematic fluid) are very well accessible to a bifurcation analysis, and we consequently use it frequently. In this section, we show the basic principles but do not go into details too much as this is done in the appropriate chapters.

We start with a perturbed SDF of the form,

$$\rho^{(1)}(\mathbf{q}) = \rho^{(1)}_0(\mathbf{q}) + \varepsilon\rho^{(1)}_1(\mathbf{q}). \tag{2.43}$$

The infinitesimal parameter ε is arbitrary, $\rho^{(1)}_0(\mathbf{q})$ is the parent solution and $\rho^{(1)}_1(\mathbf{q})$ has lower symmetry and is the bifurcating solution. In principle, Eq. 2.43 is an expansion in increasing powers of ε, but (for now) we are only interested in the first order. Due to

the normalizations, $\int d\mathbf{q}\rho^{(1)}(\mathbf{q}) = \int d\mathbf{q}\rho_0^{(1)}(\mathbf{q}) = N$, and we have $\int d\mathbf{q}\rho_1^{(1)}(\mathbf{q}) = 0$. Also, we require them to be perpendicular, $\int d\mathbf{q}\rho_1^{(1)}(\mathbf{q})\rho_0^{(1)}(\mathbf{q}) = 0$. Inserting Eq. 2.43 in 2.42, we linearize the exponent,

$$
\begin{aligned}
&\exp\left[-\beta U_{\text{single}}(\mathbf{q}) + \int d\mathbf{q}'\rho^{(1)}(\mathbf{q}')\phi_M(\mathbf{q},\mathbf{q}')\right] = \\
&\exp\left[-\beta U_{\text{single}}(\mathbf{q}) + \int d\mathbf{q}'\rho_0^{(1)}(\mathbf{q}')\phi_M(\mathbf{q},\mathbf{q}')\right]\left(1 + \varepsilon\int d\mathbf{q}'\rho_1^{(1)}(\mathbf{q}')\phi_M(\mathbf{q},\mathbf{q}')\right).
\end{aligned}
\tag{2.44}
$$

Using this in the nominator as well as in the denominator, we obtain in first order of ε (the zeroth order is trivial),

$$
\begin{aligned}
\rho_1^{(1)}(\mathbf{q}) = {}&\rho_0^{(1)}(\mathbf{q})\int d\mathbf{q}'\rho_1^{(1)}(\mathbf{q}')\phi_M(\mathbf{q},\mathbf{q}') \\
&- \frac{1}{N_0}\rho_0^{(1)}(\mathbf{q})\int d\mathbf{q}'d\mathbf{q}''\rho_0^{(1)}(\mathbf{q}')\rho_1^{(1)}(\mathbf{q}'')\phi_M(\mathbf{q}',\mathbf{q}''),
\end{aligned}
\tag{2.45}
$$

where the second term on the right side enforces the normalization. However, in all relevant cases, this last terms vanishes in the thermodynamic limit, yielding

$$
\rho_1^{(1)}(\mathbf{q}) = \rho_0^{(1)}(\mathbf{q})\int d\mathbf{q}'\rho_1^{(1)}(\mathbf{q}')\phi_M(\mathbf{q},\mathbf{q}')
\tag{2.46}
$$

This last equation does not seem to depend on U_{single} anymore, but that is misleading as the parent solution $\rho_0^{(1)}$ will generally depend on U_{single}. And of course, the parent solution still has to satisfy Eq. 2.42 and can be hard to obtain.

In practice, there is a control parameter driving the phase transition. We have been building up the formalism around the virial expansion which is a series in the density. We therefore consider

$$
\rho^{(1)}(\mathbf{q}) = \rho f(\mathbf{q}),
\tag{2.47}
$$

where ρ, as usual, is the number density, and f is a differently normalized version of the SDF, $V^{-1}\int d\mathbf{q}f(\mathbf{q}) = 1$ (do not confuse this f here with the free energy per molecule in Sec. 2.1). Expanding also ρ and f in terms of ε, in the usual way,

$$
\begin{aligned}
f(\mathbf{q}) &= f_0(\mathbf{q}) + \varepsilon f_1(\mathbf{q}) \\
\rho &= \rho_0 + \varepsilon\rho_1
\end{aligned}
\tag{2.48}
$$

we can make the identifications, $\rho_0^{(1)}(\mathbf{q}) = \rho_0 f_0(\mathbf{q})$ and $\rho_1^{(1)}(\mathbf{q}) = \rho_0 f_1(\mathbf{q}) + \rho_1 f_0(\mathbf{q}) = \rho_0 f_1(\mathbf{q})$, because $\rho_0^{(1)}(\mathbf{q})$ is perpendicular to $\rho_1^{(1)}(\mathbf{q})$. Substituting this into Eq. 2.46, we obtain

$$
f_1(\mathbf{q}) = \rho_0 f_0(\mathbf{q})\int d\mathbf{q}'f_1(\mathbf{q}')\phi_M(\mathbf{q},\mathbf{q}').
\tag{2.49}
$$

This last equation is usually called *the* bifurcation equation. It is an generalized linear eigenvalue equation, which it may not appear at first, but which becomes clear after the

transformations

$$g(\mathbf{q}) = f_1(\mathbf{q}) \Big/ \sqrt{f_0(\mathbf{q})}$$

$$K(\mathbf{q}, \mathbf{q}') = \phi_{\mathrm{M}}(\mathbf{q}, \mathbf{q}') \sqrt{f_0(\mathbf{q}) f_0(\mathbf{q}')} \qquad (2.50)$$

yielding

$$g(\mathbf{q}) = \rho_0 \int d\mathbf{q}' g(\mathbf{q}') K(\mathbf{q}, \mathbf{q}'). \qquad (2.51)$$

Given that we know the parent solution $f_0(\mathbf{q})$, Eq. 2.49 can be solved for ρ_0. Usually, there is a whole family of solutions $f_1(\mathbf{q})$, satisfying Eq. 2.49 corresponding to an infinitely increasing number of different ρ_0. The 'physical' bifurcation density is then determined to be the lowest of those ρ_0.

So far, we have only performed the bifurcation analysis to first order in ε. And Eq. 2.49 gives us the bifurcation density ρ_0 and all degenerate eigenfunctions $h_l(\mathbf{q})$ (if there are) corresponding to this density. However, it does not supply us with the exact linear combination of these eigenfunctions, $f_1(\mathbf{q}) = \sum_l c_l h_l(\mathbf{q})$. Nor does it yield the 'direction' of bifurcation, ρ_1. This quantity ρ_1 can be shown to relate to the cubic terms in a Landau expansion of the free energy in terms of the order parameters. As is wellknown, a nonzero cubic term in the Landau exansion usually gives rise to a first-order phase transition. Similarly, $\rho_1 \neq 0$ is characteristic for a first-order transition. If $\rho_1 = 0$, this might indicate a continuous phase transition (although it may still be found to correspond to a first-order phase transition). To find the value of ρ_1 and the coefficients c_l, we need to include the second order ε^2, in the bifurcation analysis. And in case we find that $\rho_1 = 0$, we even need to include the next order ε^3, to find the c_l and ρ_2. Solving the bifurcation equations in this way, one by one, order by order, may allow a construction of the bifurcating solution quite far away from the actual bifurcation point. In fact, in their landmark paper, Kayser and Raveché did so for the case of the isotropic-to-nematic transition of the Onsager model [37]. The treatment we have given above draws freely on Mulder [46, 47] We have not given the second order bifurcation analysis here, but we do so in Chap. 5, for a system of branched heteropolymers.

We make a few more comments of quite general character, illustrated in the case of the Onsager model (see Fig. 2.2 and next section). At the bifurcation point, the parent phase changes stability. This means that in the space of order parameters it changes from being a minimum to being a saddle point. And at the bifurcation point, the second derivative of the free energy with respect to (some of) the order parameters is zero and as such we can call the bifurcation point a spinodal point (see Fig. 2.2). So, coming from the low-density phase, the bifurcation density is the highest possible density to which we might be able to compress the system. There is also a spinodal point corresponding to expansion of the high-density phase; in Fig. 2.2 this is depicted.

In this section, we have discussed the tool of bifurcation analysis to study symmetry-breaking phase transitions. Having knowledge of the so-called parent solution, we only need to solve a relatively simple (linear) equation to get some properties of the bifurcating phase and the transition. These properties include the bifurcation density ρ_0, the 'direction' of bifurcation ρ_1 and the infinitesimal eigenfunction $f_1(\mathbf{q})$ (if one proceeds as far as the second-order bifurcation equation). The requirement that we need to know
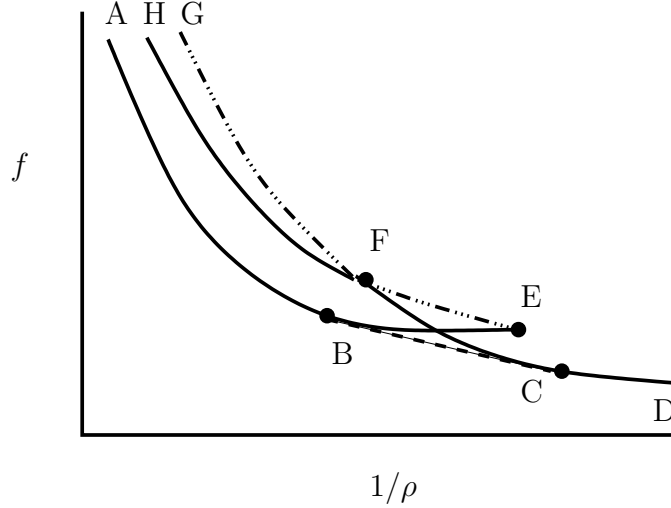
FIGURE 2.2. Generic plot of the isotropic and nematic solutions for the On-sager model. The curve DFG is the isotropic solution and ABEFH is the ne-matic solution. Full parts of the curve are (meta)stable, Dashed-dotted parts are unstable, the dashed part is the common tangent. Point F is the bifurcation point. The isotropic solution is stable for low densities, DF and unstable for high densities, FG. At the bifurcation point F, the nematic solution branches off and has two arms. The physical nematic solution FEBA, is first unstable, then metastable and beyond B, stable. The other nematic solution FH is metastable and unphysical. Points E and F can be considered spinodal points, and B and C are the binodal points.

the parent solution is in practice the most restrictive one, as this solution still has to satisfy Eq. 2.42. Therefore, often, the analysis is applied to phases which branch off the (isotropic) fluid solution, where $f_0(\mathbf{q})$ is trivial, or rather straightforward to obtain (approximately).

2.5. Hard Rods and the Nematic Phase

In this section we briefly review one of the standard models of liquid crystals: the Onsager model. The kind of systems we are concerned with in this thesis are similar to Onsager's original model.

In 1949, Onsager published a monumental paper on the isotropic-to-nematic transi-tion in a system of slender hard rods [7]. A generic plot of the free energy solutions is given in Fig. 2.2. Many of the results have been generated (approximately) by Onsager himself. The model, henceforth referred to as Onsager model, describes the hard rods as having a length l and a width d, where $l \gg d$. The coordinates of the rods are specified by a position $\mathbf{r}$ and an orientation $\hat{\omega}$, so $\mathbf{q} = (\mathbf{r}, \hat{\omega})$. There is no internal energy associated with a single particle, so $U_{\text{single}}(\mathbf{q}) = 0$ and Onsager used the second virial ap-proximation. Consequently, from Eq. 2.42, the SDF in the isotropic fluid phase becomes $\rho^{(1)} = \rho/4\pi$, where $w = \int d\hat{\omega} = 4\pi$. Considering two fluid phases, $\rho^{(1)}(\mathbf{q}) = \rho f(\hat{\omega})$, the
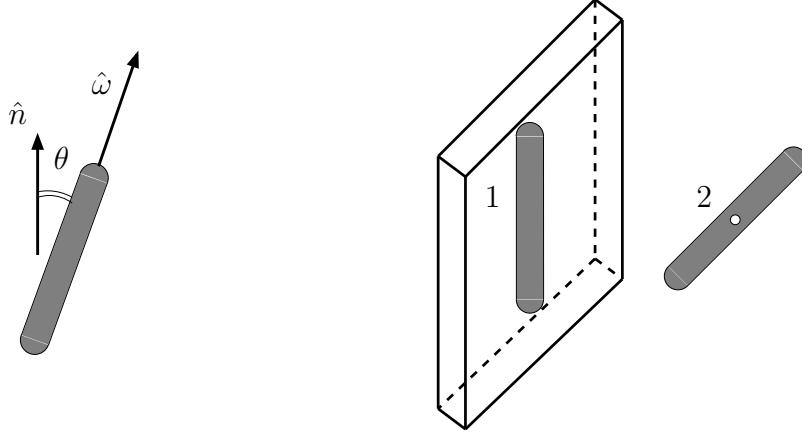
FIGURE 2.3. Onsager rods. Left, one rod is characterized by its orientation $\hat{\omega}$, pointing along the long axis. In the nematic phase, the distribution function is only a function of the angle θ between $\hat{\omega}$ and the nematic director $\hat{n}$. Right, a schematic drawing of the excluded volume between two rods. Picking up rod 2 at the white dot and moving it around space, we see that it (the white dot) can not enter the box due to the presence of rod 1.

excess free energy becomes

$$\beta_{\mathrm{B}}\mathcal{F}_{\mathrm{excess}} = \frac{1}{2}N\rho \int d\hat{\omega}d\hat{\omega}' f(\hat{\omega})f(\hat{\omega}')\mathcal{E}(\hat{\omega},\hat{\omega}'), \tag{2.52}$$

and the relevant quantity is the excluded volume between two rods

$$\mathcal{E}(\hat{\omega},\hat{\omega}') = 2l^2d|\sin\gamma(\hat{\omega},\hat{\omega}')| \tag{2.53}$$

where $\gamma(\hat{\omega},\hat{\omega}')$ is the plane angle between $\hat{\omega}$ and $\hat{\omega}'$ (see Fig. 2.3, right). Increasing the density ρ, the system will go into a nematic phase, where the rods are ordered orientationally with respect to a certain direction $\hat{n}$ (and the integral in Eq. 2.52 is lower than in the isotropic phase). Around $\hat{n}$, there is cylindrical symmetry and the SDF is function of only one polar angle, $f(\hat{\omega}) = f(\theta)$ with $\cos\theta = \hat{n}\cdot\hat{\omega}$ (see Fig. 2.3, left). The phase is also up-down symmetric, and consequently, the SDF $f(\theta)$ can be expanded in even Legendre polynomials, $P_{2n}(\cos\theta)$. The weigthed average over the second Legendre polynomial

$$\langle P_2 \rangle = \frac{1}{2}\int_{-1}^{1} d\cos\theta P_2(\cos\theta)f(\theta) \tag{2.54}$$

is used as order parameter. The phase transition is first-order and the coexistence densities are $\rho_{\mathrm{iso}}(\pi l^2 d/4) = 3.290$ and $\rho_{\mathrm{nem}}(\pi l^2 d/4) = 4.191$ with the order parameter at the phase transition being $\langle P_2\rangle_{\mathrm{nem}} = 0.7922$. The bifurcation analysis has been performed by Kayser and Raveché [37]. The bifurcation density is $\rho_0(\pi l^2 d/4) = 4$ and the eigenfunction is $P_2(\cos\theta)$. The first-order character of the phase transition is confirmed by $\rho_1(\pi l^2 d/4) = -4/7$. Onsager showed that in the limit of $l \to \infty$, $d \to 0$ and $l^2 d$ finite, and in the isotropic phase, the second virial approximation is exact. In
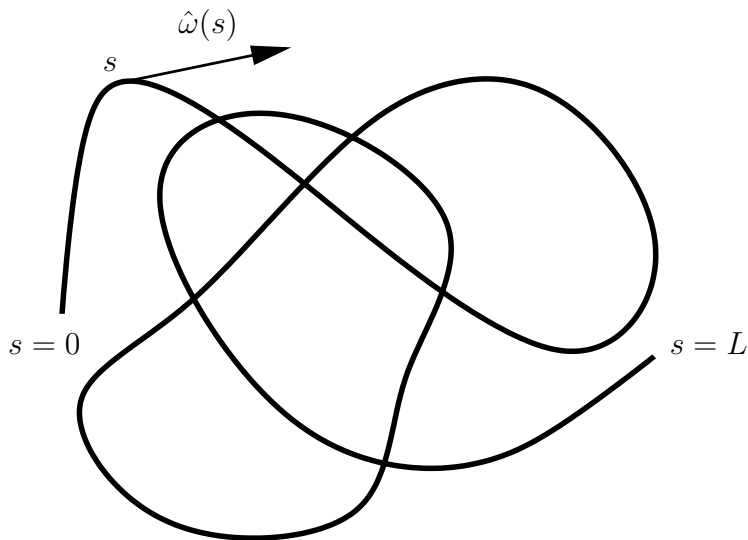
FIGURE 2.4. A wormlike chain.

fact he used geometrical arguments to show that the third virial coefficient scales as

$$\frac{B_3^{\text{iso}}}{(B_2^{\text{iso}})^2} \sim \frac{d}{l} \log \frac{l}{d}. \tag{2.55}$$

Note that in the above limit of infinitely slender rods, there are no free parameters in this model. From hereon, we sometimes refer to the second virial approximation as the Onsager approximation. A good and quite extensive review of the Onsager model is given in Ref. [48].

2.6. The Wormlike Chain Model

There exist many different models for polymers, ranging from random walks on a lattice to 'real' atomic level descriptions used in simulation packages. Evidently, it depends very much on the type of physical phenomenon under study which (specific) polymer properties need to be included. The type of liquid crystalline transitions we are interested in, require anisotropic interactions between the polymers. Consequently, we need to consider polymers, which, apart from the total or contour length, are also characterized by a finite and more or less rigid 'segment' length. A natural and frequently used candidate is the so-called wormlike chain model which is due to Kratky and Porod [49]. The wormlike chain concept plays a central role in this thesis, and in this section, we discuss some of its properties [50, 51].

The wormlike chain can be viewed as a continuous curve in space. Its coordinates $\mathbf{q}$, are specified fully by its position $\mathbf{R}$ and its orientations $\{\hat{\omega}(s)\}$ at every position $s \in [0, L]$ along the chain (see Fig. 2.4). An additional length scale is introduced as the length over which, on average, the chain looses its orientation. This is the persistence length P, and is defined through

$$\langle \hat{\omega}(s) \cdot \hat{\omega}(s') \rangle = \exp[-|s - s'|/P], \tag{2.56}$$

in which the average $\langle \ \rangle$ is over all (weighted) conformations of an isolated wormlike chain (no external field). From the above formula it can be shown that

$$P = \langle \hat{\omega}(s) \cdot \int_s^\infty ds' \hat{\omega}(s') \rangle, \tag{2.57}$$

where one should note that the upper integration limit is ∞ instead of L. Often, this is taken to be the definition of persistence length. Defining the end-to-end distance of a wormlike chain,

$$\mathbf{r}_{0,L} = \int_0^L ds' \hat{\omega}(s'), \tag{2.58}$$

we can identify the persistence length as half of the average projection of $\hat{\omega}(s)$ on the end-to-end distance for infinitely long polymers,

$$P = \frac{1}{2} \lim_{L \to \infty} \langle \hat{\omega}(0) \cdot \mathbf{r}_{-L/2, L/2} \rangle. \tag{2.59}$$

For wormlike chains, the mean-square end-to-end distance is

$$\langle \mathbf{r}_{0,L}^2 \rangle = 2LP \left(1 - \frac{P}{L} \left(1 - \exp[-L/P] \right) \right) \tag{2.60}$$

In case of long chains, $L \gg P$, the above expression goes to $2LP$, which is the Gaussian chain result, and for very short chains, $L \ll P$, the answer is L^2 conform the rigid rod result. Another quantity which is often used concerning polymers is the so-called radius of gyration, which is defined as the average distance of all parts of the polymer to its center of mass. For long chains it is typically 6 times as small as the mean-square end-to-end distance.

In our formulation, $\mathbf{q} = (\mathbf{r}, \{\hat{\omega}(s)\})$ and $\int d\mathbf{q} = \int d\mathbf{r} \int d\{\hat{\omega}(s)\}$ is a path integration. In order for the wormlike chain not to bend on length scales of the order of the persistence length, we need the following internal energy

$$\beta_{\mathrm{B}} U_{\mathrm{single}}(\mathbf{q}) = \frac{1}{2} P \int_0^L ds \left(\frac{\partial \hat{\omega}(s)}{\partial s} \right)^2 \tag{2.61}$$

with the weighted average

$$\langle A(\mathbf{q}) \rangle = \frac{\int d\mathbf{q} A(\mathbf{q}) \exp[-\beta_{\mathrm{B}} U_{\mathrm{single}}(\mathbf{q})]}{\int d\mathbf{q} \exp[-\beta_{\mathrm{B}} U_{\mathrm{single}}(\mathbf{q})]}. \tag{2.62}$$

Together, Eqs. 2.61 and 2.62 yield again Eq. 2.56. Also, as we are interested in liquid crystalline polymer phases, we need to specify how these wormlike chains interact. Assuming them to be impenetrable, we set the width equal to d. Consequently, our wormlike chains are described by three model parameters; L, P and d where we require that $L, P \gg d$.

Although a wormlike chain is naturally characterized in terms of its persistence length, the concept of persistence length does not exclusively apply to wormlike chains. In fact in Chap. 3, we calculate the persistence length for segmented chains. Therefore, we consider a persistent chain to be any chain for which a persistence length can be defined. With wormlike chains, we refer to molecules which can be represented by a *continuous* curve through space. Note, that in this definition also a rigid rod is a wormlike chain (which makes sense as this is the limit, $L \ll P$). Often, people use the

term semiflexible polymers, referring to polymers with $L \gg P \gg d$. We will not use this, as this limit $L \gg P$ is not at all necessary in our analysis.

Other concepts are drawn sometimes from other polymer models. A Kuhn chain is defined as a freely jointed chain of N_K rigid segments, with lengths l_K. The mean-square end-to-end distance of a Kuhn chain is $N_K l_K^2$. Kuhn chains are used by stating that for a very long polymer an equivalent Kuhn chain can be defined in such a way that $\langle \mathbf{r}_{0,L}^2 \rangle = N_K l_K^2$. In this way, for very long polymers one can use the concept of effective Kuhn segment length and its number in the chain. In case of very long wormlike chains, we have $2LP = N_K l_K^2$ and consequently, $P = l_K/2$. In this thesis, we do not use the concept of Kuhn lengths. It may be rather confusing as we are considering segmented chains with bending potentials between the segments. These segments are not related in any way to the Kuhn segments.

The persistence length of a wormlike chain has been defined for an isolated chain. However, the systems we are considering in this thesis consist of many interacting polymers. Still, in the isotropic fluid phase the effective field is constant and not dependent on the coordinates $\mathbf{q}$. Consequently, this has no effect on the chain average, and the wormlike chain is well characterized by its persistence length. On the other hand, in the nematic phase, there is an anisotropic field and the persistence length, defined in the isotropic phase, will not be the correct length scale over which the chain looses its orientational correlation. In this respect, we mention that for high-density nematics, even an extra length scale appears, which is the deflection length due to Odijk [52] [4]. Whereas in the nematic the persistence length is larger than in the isotropic phase, the deflection length is considerably smaller than the persistence length. Both these (additional) length scales are not considered in this thesis. The most important tool, we use, is bifurcation analysis and investigates the stability of the isotropic phase. The 'bare' persistence length should still be the appropriate length scale in this case.

---

[4]The deflection length is the length scale on which the chain is on average deflected by its neighbors.

Part 1

Homopolymeric Chains

3
Uniaxial Polymers

The concept of segmented chains is introduced. We derive the stationarity equations and identify the approximations needed. The wormlike chain limit can be applied at various stages in the description. Bifurcation as well as numerical techniques are used to obtain the phase behaviour. An advantage of segmented chains is the rather direct generalization to branched heteropolymers.

3.1. Introduction

It is by now well established that excluded volume effects in non-spherically shaped particles can drive phase transitions towards liquid crystalline phases [13]. Long flexible molecules with mutual steric interactions are in that sense no exception. It is only the internal degrees of freedom of these molecules which considerably complicate the mechanism of liquid crystalline ordering. In the 1980's Khokhlov and Semenov (henceforth addressed as KS) published a seminal series of papers on the isotropic-to-nematic (I-N) transition in a system of semiflexible molecules [32, 33]. Semiflexible molecules are linear chains in which the persistence length, i.e. the length over which the chain looses its orientational memory, is typically much bigger than the width of the chain but also, much smaller than the total length of the molecule. The chains of KS are wormlike objects with flexibility distributed along them continuously. Their main result is the derivation of the conformational entropy of these chains as a functional of partial partition functions of the chain [33]. From this the thermodynamical behaviour of these systems can be derived, most prominently their phase behaviour. Ever since, this theory is widely used to describe the phase behaviour of long persistent molecules like e.g. DNA.

In spite of its intuitive appeal and its succes in dealing with the phenomenology of the I-N transition in liquid crystalline polymers, the KS approach does have some drawbacks. First, the excluded volume interaction term in the free energy is introduced by heuristic analogy with the Onsager theory, giving little insight into the various approximations that enter the theory and, hence, on its regime of validity. Secondly, focussing as it does on chemically homogeneous chains with continuously distributed flexibility, the theory is less well generalizable to situations in which molecules are composed of chemically different parts, with e.g. varying degrees of stiffness, as is the rule in real world liquid crystalline materials. Therefore, most extensions to the KS approach that dealt with composite molecules have taken the indirect route of "glueing together" rigid segments with persistent spacers, or "tacking on" rigid side chains to persistent backbones. Finally, working with continuous objects does not present an obvious computational advantage.

In fact, the various phase diagrams derived from the theory were invariably in limits where the distribution of local order along the molecules i.e. the finite size effects were negligible. Detailed consideration of these effects, as first performed by Chen [36], require involved numerical work, ultimately relying on discretisation of the continuous equations. Our aim in this work is to develop a flexible formalism for describing orientational ordering in non-rigid, elongated molecules that addresses (at least partially) all three drawbacks discussed above.

We do this by starting from a fully *discrete* description of our molecules. These consist of elongated hard uniaxial segments connected end-to-end to form chains. Flexibility is introduced through (tunable) bending potentials between neighbouring segments meeting at a joint. Through a series of explicit approximations a density functional theory is constructed for systems composed of such chains. The resultant theory is by construction generalizable to heteropolymeric, and even non-linear, branched, molecular morphologies, possibly composed of axially symmetric segments. These generalizations will be undertaken in later chapters. In this chapter we focus on the basic idea as applied to linear, homopolymeric chains of uniaxially symmetric segments, and the relationship with the KS formalism. We first show that the formal solution to the theory can be mapped onto the problem of a single chain in a (self-consistently determined) effective orientational potential, that acts equally on all segments. This essentially one-dimensional statistical system can be cast into a variational framework, involving sets of local (to each segment) "fields", along the lines of the Cluster Variation Method [53], well-known in the area of discrete spin systems. We then show that the passage to chains with continuous flexibility, implemented by applying the so-called Wormlike Chain Limit (WCL) to the reduced free-energy functional obtained in the previous step, directly leads to the KS functional, thus rederiving it "from below". In the results sections we further illustrate the utility of our "discrete" approach. A first investigation of the I-N transition is made through a bifurcation analysis around the spinodal density, which can be carried out fully analytically. Several new results are obtained, which can be mapped onto the continuous chain case *a posteriori* by applying the WCL. Finally, we perform numerical calculations to determine the actual location and characteristics of the thermodynamic transition. Although readily able to tackle a wide range of molecular flexibilities, we can again, compare directly with the continuous case by taking appropriate values of our parameters, showing that a suitably chosen discrete chain model can provide an accurate "physical" discretisation of the continuous model.

3.2. Formalism

3.2.1. Definition of the Model. Consider a fluid of N chains in a volume V. Each chain consists of M cylindrically symmetric rodlike segments labelled with a number m, running from 1 to M. The segments have length l and diameter d with $l \gg d$. The orientation of each segment is specified by a unit vector $\hat{\omega}_m$, which points along the long axis of the segment towards the next segment. The configuration of a single chain is denoted by ξ and is specified by the location $\mathbf{R}$ of the free end of the first segment and the conformation $\mathbf{\Omega} = (\hat{\omega}_1, \hat{\omega}_2, \cdots, \hat{\omega}_M)$. With these definitions the position of the starting point of the m'th segment is given by $\mathbf{r}_m = \mathbf{R} + l \sum_{k=1}^{m-1} \hat{\omega}_k$.
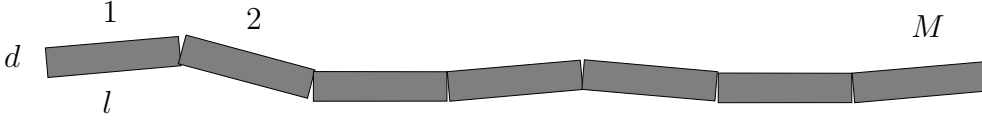
FIGURE 3.1. A segmented chain.

The most convenient formalism for describing anisotropic fluids is density functional theory (DFT). Within DFT, the free energy of a fluid of chains is formulated in terms of the single particle (=chain) configuration distribution function $\rho^{(1)}(\xi)$ [45],

$$
\begin{aligned}
\beta_{\mathrm{B}} \mathcal{F}\left[\rho^{(1)}\right] &= \beta_{\mathrm{B}} \mathcal{F}_{\mathrm{ideal}}[\rho^{(1)}] + \beta_{\mathrm{B}} \mathcal{F}_{\mathrm{single\text{-}chain}}[\rho^{(1)}] + \beta_{\mathrm{B}} \mathcal{F}_{\mathrm{excess}}[\rho^{(1)}] \\
&= \int d\xi \rho^{(1)}(\xi) \left[\log\left(\mathcal{V}_{\mathrm{T}} \rho^{(1)}(\xi)\right) - 1\right] + \beta_{\mathrm{B}} \int d\xi \rho^{(1)}(\xi) U(\xi) + \beta_{\mathrm{B}} \mathcal{F}_{\mathrm{excess}}[\rho^{(1)}].
\end{aligned}
\tag{3.1}
$$

where the three terms denote respectively the ideal contribution, the single particle contribution stemming from *intra*chain interactions or the interaction with an external field and finally the excess free energy due to interactions between the particles. The integrals are over the single-chain configuration space ($d\xi = d\mathbf{R}d\mathbf{\Omega}$) and $\rho^{(1)}(\xi)$ is normalized to the total number of particles $\int \rho^{(1)}(\xi)d\xi = N$. The factor β_{B} denotes the standard dimensionless inverse temperature $(k_B T)^{-1}$ in which k_B is Boltzmann's constant and T the temperature. The 'thermal volume' $\mathcal{V}_{\mathrm{T}}$ is a product of the de Broglie thermal wavelengths of the chains [43].

In the following we will focus on spatially homogeneous phases, so we assume the single-chain configuration distribution function to be independent of $\mathbf{R}$. This means we can write $\rho^{(1)}(\xi) = \rho f(\mathbf{\Omega})$, with $\rho = N/V$ the (homogeneous) number density of the chains. The remaining part $f(\mathbf{\Omega})$ we call the conformational distribution function (CDF) and it is normalized to unity, $\int f(\mathbf{\Omega})d\mathbf{\Omega} = 1$.

To turn the DFT formalism sketched above into an actual model we need to specify the components of the functional in more detail. We start with the single-chain contribution. We assume there is no external field present, so we focus on the contribution due to the internal energy of the chains. We wish to endow the chains with a tunable degree of flexibility. The simplest mechanism for this is to assume a bending potential operative between neighbouring segments of the chain, i.e.

$$
U(\mathbf{\Omega}) = \sum_{m=1}^{M-1} u(\hat{\omega}_m, \hat{\omega}_{m+1}).
\tag{3.2}
$$

Such an intrachain potential of course does not describe more elaborate effects like rotational-isomeric states, but that is in keeping with our interpretation of the segments representing larger stiff subunits of real chains. More importantly it neglects steric self-interactions between segments located on the same chain, an approximation we nevertheless adopt without further justification. For our purposes it is sufficient to consider a simple bending potential of a generic type which favours the fully stretched

conformation,

$$u(\hat{\omega}_m, \hat{\omega}_{m+1}) = -J\hat{\omega}_m \cdot \hat{\omega}_{m+1}, \tag{3.3}$$

in which J is the strength of the interaction.

We assume that the segments of the chains are hard bodies. Chains will thus interact pairwise with a potential $v(\xi, \xi')$ which is infinite when the chains are in an overlapping configuration and zero otherwise. This chain-chain interaction potential is just a sum over pairwise hard interactions between the segments of the chains

$$v(\xi, \xi') = \sum_{m,m'=1}^{M} v_{m,m'}\left(\hat{\omega}_m, \hat{\omega}'_{m'}, \mathbf{r}_{m,m'}\right) \tag{3.4}$$

where $\mathbf{r}_{m,m'} = \mathbf{r}_m - \mathbf{r}_{m'} = \mathbf{R} - \mathbf{R}' + l\sum_{i=1}^{m}\hat{\omega}_i - l\sum_{i'=1}^{m'}\hat{\omega}_{i'}$. In principle we can now expand the excess free energy into a virial series. The chain-chain Mayer function is simply given by,

$$\Phi(\xi, \xi') \equiv \exp(-\beta_{\mathrm{B}} v(\xi, \xi')) - 1 = \left\{ \begin{array}{ll} -1 & \text{if overlap} \\ 0 & \text{if } no \text{ overlap} \end{array} \right. . \tag{3.5}$$

In his landmark paper [7] Onsager already argued that in an isotropic system of hard rods with infinite length-to-width ratio all virial coefficients with order higher than 2 are vanishingly small. Although for chains, whose conformations, especially in the isotropic phase, deviate strongly from being straight, this assumption may not be justified, we assume that we can approximate the excess free energy by just the second virial term

$$\beta_{\mathrm{B}} \mathcal{F}_{\mathrm{excess}}[\rho^{(1)}] = -\frac{1}{2} \int \int d\xi d\xi' \rho^{(1)}(\xi) \rho^{(1)}(\xi') \Phi(\xi, \xi'). \tag{3.6}$$

This is the so-called second virial or Onsager approximation. Due to translational invariance the Mayer function only depends on the relative position of two chains $\mathbf{r} = \mathbf{R} - \mathbf{R}'$. Consequently in the spatially homogeneous phases we are considering here we can perform the spatial integrations to obtain

$$\beta_{\mathrm{B}} \mathcal{F}_{\mathrm{excess}}[f] = \frac{1}{2} N\rho \int \int d\mathbf{\Omega} d\mathbf{\Omega}' f(\mathbf{\Omega}) f(\mathbf{\Omega}') \mathcal{E}(\mathbf{\Omega}, \mathbf{\Omega}') \tag{3.7}$$

where the excluded volume $\mathcal{E}$ as a function of the conformations of the two chains is defined by,

$$\mathcal{E}(\mathbf{\Omega}, \mathbf{\Omega}') = -\int d\mathbf{r} \Phi(\mathbf{\Omega}, \mathbf{\Omega}', \mathbf{r}). \tag{3.8}$$

The chain-chain Mayer function (and the excluded volume as a consequence) is a complicated function of the conformations of both chains. However, using Eq. (3.4) we can expand Φ in terms of the segment-segment Mayer functions $\phi_{m,m'} = e^{-\beta_{\mathrm{B}} v_{m,m'}} - 1$

$$\Phi = \prod_{m,m'} \left(1 + \phi_{m,m'}\right) - 1$$
$$= \sum_{m,m'} \phi_{m,m'} + \sum_{(m_1,m_1') \neq (m_2,m_2')} \sum \phi_{m_1,m_1'} \phi_{m_2,m_2'} + \cdots, \tag{3.9}$$

where for brevity we have dropped all the function arguments. In this series, the first term on the right counts only the independent segment-segment overlaps. The second

term takes into account the fact that two different pairs of segments can overlap simultaneously and so on. If the rods are very slender, as we assume in our model, multiple segment overlaps should be rare for fixed relative conformations. We therefore neglect all terms in Eq. (3.9) except the first. The upshot is that the chain-chain excluded volume is approximated by the sum

$$\mathcal{E}(\boldsymbol{\Omega}, \boldsymbol{\Omega}') = \sum_{m,m'} e(\hat{\omega}_m, \hat{\omega}'_{m'}) \tag{3.10}$$

over the segment-segment excluded volumes

$$e(\hat{\omega}_m, \hat{\omega}'_{m'}) = -\int d\mathbf{r}_{m,m'} \phi_{m,m'}(\hat{\omega}_m, \hat{\omega}'_{m'}, \mathbf{r}_{m,m'}) = 2l^2 d \sin\gamma(\hat{\omega}_m, \hat{\omega}'_{m'}), \tag{3.11}$$

in which $\gamma(\hat{\omega}_m, \hat{\omega}'_{m'})$ is the planar angle between $\hat{\omega}_m$ and $\hat{\omega}'_{m'}$.

Having fixed the details of the interactions between segments within the same chain and in different chains, we resubstitute them in the free energy. Also performing the (remaining) spatial integrations and dividing by N, we obtain the free energy per chain as a functional of the CDF,

$$\frac{\beta_{\mathrm{B}} \mathcal{F}[f]}{N} = \log\left(\rho \mathcal{V}_{\mathrm{T}}\right) + \int d\boldsymbol{\Omega} f(\boldsymbol{\Omega}) \left[\log f(\boldsymbol{\Omega}) - 1\right] + \beta_{\mathrm{B}} \int d\boldsymbol{\Omega} f(\boldsymbol{\Omega}) U(\boldsymbol{\Omega})$$
$$+ \frac{1}{2} \rho \int d\boldsymbol{\Omega} d\boldsymbol{\Omega}' f(\boldsymbol{\Omega}) f(\boldsymbol{\Omega}') \mathcal{E}(\boldsymbol{\Omega}, \boldsymbol{\Omega}'), \tag{3.12}$$

in which U and $\mathcal{E}$ are defined by Eqs. (3.2) and (3.10) respectively.

In thermodynamic equilibrium, the free energy reaches a minimum and the functional is stationary. Therefore, we consider the variation of Eq. 3.12 with respect to the CDF,

$$\frac{\delta}{\delta f(\boldsymbol{\Omega})} \frac{\beta_{\mathrm{B}} \mathcal{F}}{N} - \beta_{\mathrm{B}} \mu = 0 \tag{3.13}$$

with the chemical potential μ playing the role of Lagrange multiplier needed to enforce normalization. Eliminating μ from Eq. 5.2 yields the stationarity equation,

$$f(\boldsymbol{\Omega}) = Q^{-1}[f] \exp\left[-\beta_{\mathrm{B}} U(\boldsymbol{\Omega}) - \rho \int d\boldsymbol{\Omega}' f(\boldsymbol{\Omega}') \mathcal{E}(\boldsymbol{\Omega}, \boldsymbol{\Omega}')\right] \tag{3.14}$$

in which Q is the factor due to normalization,

$$Q[f] = \int d\boldsymbol{\Omega} \exp\left[-\beta_{\mathrm{B}} U(\boldsymbol{\Omega}) - \rho \int d\boldsymbol{\Omega}' f(\boldsymbol{\Omega}') \mathcal{E}(\boldsymbol{\Omega}, \boldsymbol{\Omega}')\right]. \tag{3.15}$$

Next, we define the n-segment distribution function by integrating over the 'other' degrees of freedom,

$$f^{(n)}_{i_1,\cdots,i_n}(\hat{\omega}_{i_1}, \cdots, \hat{\omega}_{i_n}) = \int \prod_{m \neq i_1,\cdots,i_n} d\hat{\omega}_m f(\boldsymbol{\Omega}), \tag{3.16}$$

in which $\{i_1, \cdots, i_n\}$ is a subset of $\{1, \cdots, M\}$. Obviously, $f^{(M)}_{1,\cdots,M}$ is the CDF, and the functions $f^{(1)}_m$ we call the single-segment orientational distribution functions (SDF's). Usually, we drop the upper index and write f_m for the SDF of the mth segment. It is obvious that all n-segment distribution functions are normalized according to $\int \prod_{m=i_1,\cdots,i_n} d\hat{\omega}_m f^{(n)}_{i_1,\cdots,i_n}(\hat{\omega}_{i_1}, \cdots, \hat{\omega}_{i_n}) = 1$. Inserting the details of the interactions

(Eqs. 3.2 and 3.10) and using the projection Eq. 3.16, the stationarity equation Eq. 3.14 splits into a set of equations; one for each segment ($m = 1, \cdots, M$),

$$f_m(\hat{\omega}_m) = Q^{-1} \int \prod_{k \neq m} d\hat{\omega}_k$$

$$\times \prod_{k=1}^{M-1} w(\hat{\omega}_k, \hat{\omega}_{k+1}) \prod_{k=1}^{M} \exp\left[-\frac{\eta}{M} \sum_{k'=1}^{M} \int d\hat{\omega}'_{k'} f_{k'}(\hat{\omega}'_{k'}) \sin\gamma(\hat{\omega}_k, \hat{\omega}'_{k'})\right]. \quad (3.17)$$

In order to ease notation, we have introduced the Boltzmann weight for the successive segment-segment interaction,

$$w(\hat{\omega}_k, \hat{\omega}_{k+1}) = \mathrm{e}^{-\beta_{\mathrm{B}} u(\hat{\omega}_k, \hat{\omega}_{k+1})}, \tag{3.18}$$

and a dimensionless segment density

$$\eta = 2M\rho l^2 d \tag{3.19}$$

(='segment density', $M\rho \times$ 'maximum excluded volume of two segments', $2l^2 d$).

In ending this section, for clarity, we briefly list the approximations needed to arrive at Eqs. 3.17. Three approximations have been made: first, the second virial approximation has been used, not taking into account simultaneous interactions between three or more polymers. Second, the full chain-chain Mayer function has been approximated as the sum of all the segment-segment Mayer functions, discarding simultaneous interactions of two or more pairs of segments on these two chains. Third, the energy within a chain has been taken to be of a simple local bending type, meaning that interactions between remote parts on the same chain are not considered.

3.2.2. A Single Chain in an External Field. Although the stationarity equations Eq. (3.17) form a closed set involving only the SDF's it is not possible to formulate the free energy of the system as a functional of the same. In this section, however, we will show that both the conformational entropy and the interaction terms of the free energy functional can be decomposed in terms of the SDF's in combination with the two-particle distribution functions of nearest neighbour segments $f_{m,m+1}^{(2)}$ (from Eq. 3.16). The result is a well-founded variational theory with the free energy in terms of the variational variables f_m and $f_{m,m+1}^{(2)}$. We can even go one step further and express the free energy fully in terms of sets of *local* functions. The SDF's are mere simple products of these functions. Apart from the intrinsic advantage of employing a variational theory and the fact that the free energy can be expressed in terms of these local functions, there is another important reason for presenting this approach. In the next section, we will show how the Khokhlov and Semenov theory for nematic polymers is obtained from applying the 'wormlike chain limit' to the resulting free energy of this section.

As a first step in this programme, we reformulate the stationarity equations, writing them as

$$f_m(\hat{\omega}_m) = Q^{-1} \int \prod_{k \neq m} d\hat{\omega}_k \prod_{k=1}^{M-1} w(\hat{\omega}_k, \hat{\omega}_{k+1}) \prod_{k=1}^{M} \exp\left[-\beta_{\mathrm{B}} \mathcal{H}(\hat{\omega}_k)\right], \tag{3.20}$$

where we define an effective field

$$\beta_B \mathcal{H}(\hat{\omega}_m) = \frac{\eta}{M} \sum_{m'=1}^{M} \int d\hat{\omega}'_{m'} f_{m'}(\hat{\omega}'_{m'}) \sin \gamma(\hat{\omega}_m, \hat{\omega}'_{m'}), \qquad (3.21)$$

which acts equally on all segments. Conceptually this splits the stationarity equations in two parts: (I) the problem of a single chain of which all the segments are subjected to the same external effective field (Eq. 3.20) and (II) this effective field in turn then needs to be determined selfconsistently on in terms of the SDF's of all the segments (Eq. 3.21). This is exactly the type of scenario one would get using a mean field approximation, with the total mean field given by $\mathcal{H}(\Omega) = \sum_m \mathcal{H}(\hat{\omega}_m)$. In fact, in Ref. [54] an identical free energy is derived from a mean field theory for a system of chains with an effective pair potential between the chains.

We now focus on the problem of a single chain in an external (conformational) field. The free energy in terms of the CDF is

$$\beta_B \mathcal{F}_0[f] = \int d\Omega f(\Omega) \left[\log f(\Omega) - 1\right] + \beta_B \int d\Omega f(\Omega) \left[U(\Omega) + \mathcal{H}(\Omega)\right], \qquad (3.22)$$

in which all symbols stand for the same quantities as in the previous section. Considering Eq. 3.16, it is clear that we can rewrite the contribution of the intramolecular energy and that of the external field in Eq. 3.22 (i.e the second) completely in terms of the SDF's $-f_m^{(1)}-$ and the nearest neighbour segment–segment distribution functions $-f_{m,m+1}^{(2)}-$. At first sight such a decomposition does not appear to be possible for the first term, the orientational entropy. However, using the fact that the chain is linear and that there are only nearest neighbour interactions along it, it is possible to also decompose the first integral of Eq. 3.22 in a similar way. Consider to that end a chain of which the orientation $\hat{\omega}_m$ of the m'th segment is kept fixed. Then, because of the fact that the chain effectively decouples in two independent parts, the conditional probability density of finding a chain with fixed m'th segment factorizes as follows

$$f_{1,\cdots,m-1,m+1,\cdots,M}^{(M-1)}(\hat{\omega}_1, \cdots, \hat{\omega}_{m-1}, \hat{\omega}_{m+1}, \cdots, \hat{\omega}_M | \hat{\omega}_m) =$$
$$f_{1,\cdots,m-1}^{(m-1)}(\hat{\omega}_1, \cdots, \hat{\omega}_{m-1} | \hat{\omega}_m) f_{m+1,\cdots,M}^{(M-m)}(\hat{\omega}_{m+1}, \cdots, \hat{\omega}_M | \hat{\omega}_m).$$

Using the standard formula relating the conditional probability for an event A given B to the probability of the combined event $A \cup B$ (see e.g. Ref. [55]),

$$P(A|B) = P(A \cup B)/P(B), \qquad (3.23)$$

we obtain,

$$f(\Omega) = \frac{f_{1,\cdots,m}^{(m)}(\hat{\omega}_1, \cdots, \hat{\omega}_m) f_{m,\cdots,M}^{(M-m+1)}(\hat{\omega}_m, \cdots, \hat{\omega}_M)}{f_m^{(1)}(\hat{\omega}_m)}. \qquad (3.24)$$

We now have an expression for the CDF in terms of the *unconditional* distribution functions of parts of the chain (one could say that these are the CDF's of the subchains $1, \cdots, m$ and $m, \cdots, M$). Proceeding, and applying the same process recursively on the remaining distribution functions until all interior segments have been exhausted, we

arrive at the result

$$f(\mathbf{\Omega}) = \frac{\prod_{m=1}^{M-1} f_{m,m+1}^{(2)}(\hat{\omega}_m, \hat{\omega}_{m+1})}{\prod_{m=2}^{M-1} f_m^{(1)}(\hat{\omega}_m)}. \tag{3.25}$$

We have thus expressed the CDF completely in terms of the SDF's and the nearest-neighbour 2-segment distribution functions. From hereon, we will drop the upper indices and refer to the $f_{m,m+1}$'s as the pair distribution functions (PDF's). We can now rewrite the orientational entropy and thus the free energy (Eq. 3.22) as a functional of the PDF's and the SDF's,

$$\beta_\mathrm{B} \mathcal{F}_0[f_{m,m+1}, f_m] =$$

$$\sum_{m=1}^{M-1} \int d\hat{\omega}_m \hat{\omega}_{m+1} f_{m,m+1}(\hat{\omega}_m, \hat{\omega}_{m+1}) \left[\log f_{m,m+1}(\hat{\omega}_m, \hat{\omega}_{m+1}) + \beta_\mathrm{B} u(\hat{\omega}_m, \hat{\omega}_{m+1}) \right]$$

$$- \sum_{m=2}^{M-1} \int d\hat{\omega}_m f_m(\hat{\omega}_m) \log f_m(\hat{\omega}_m) + \beta_\mathrm{B} \sum_{m=1}^{M} \int d\hat{\omega}_m f_m(\hat{\omega}_m) \mathcal{H}(\hat{\omega}_m). \tag{3.26}$$

This decomposition of the entropy, specifically for the one-dimensional Ising system, was first discussed by Woodbury [56]. It is at the same time an illustration of the fact that the cluster variation method, most generally formulated by Morita [53], is exact for one-dimensional systems with nearest-neighbour interactions when the bonds are chosen as conserved clusters.

In order to obtain the equilibrium distributions, we must vary the functional Eq. (3.26) with respect to the PDF's and the SDF's to locate the stationary distributions. As usual, we require these distribution functions to be normalized,

$$\begin{array}{l} \int d\hat{\omega}_m f_m(\hat{\omega}_m) = 1, \\ \int d\hat{\omega}_m \hat{\omega}_{m+1} f_{m,m+1}(\hat{\omega}_m, \hat{\omega}_{m+1}) = 1, \end{array} \tag{3.27}$$

but this time, we also have to make sure that they are mutually consistent,

$$\begin{array}{l} \int d\hat{\omega}_m f_{m,m+1}(\hat{\omega}_m, \hat{\omega}_{m+1}) = f_{m+1}(\hat{\omega}_{m+1}), \\ \int d\hat{\omega}_{m+1} f_{m,m+1}(\hat{\omega}_m, \hat{\omega}_{m+1}) = f_m(\hat{\omega}_m). \end{array} \tag{3.28}$$

The implementation of the normalization constraints is straightforward, i.e. we add to the functional Lagrange terms of the type

$$\begin{array}{l} \mathcal{N}_m = \nu_m \int d\hat{\omega}_m f_m(\hat{\omega}_m), \\ \mathcal{N}_{m,m+1} = \nu_{m,m+1} \int d\hat{\omega}_m \hat{\omega}_{m+1} f_{m,m+1}(\hat{\omega}_m, \hat{\omega}_{m+1}). \end{array} \tag{3.29}$$

The Lagrange terms enforcing compatibility are a bit more complicated,

$$\begin{array}{l} \mathcal{C}_{m,m+1}^{(+)} = \int d\hat{\omega}_m \xi_m^{(+)}(\hat{\omega}_m) \left\{ \int d\hat{\omega}_{m+1} f_{m,m+1}(\hat{\omega}_m, \hat{\omega}_{m+1}) - f_m(\hat{\omega}_m) \right\}, \\ \mathcal{C}_{m,m+1}^{(-)} = \int d\hat{\omega}_{m+1} \xi_{m+1}^{(-)}(\hat{\omega}_{m+1}) \left\{ \int d\hat{\omega}_m f_{m,m+1}(\hat{\omega}_m, \hat{\omega}_{m+1}) - f_{m+1}(\hat{\omega}_{m+1}) \right\}. \end{array} \tag{3.30}$$

The quantities $\xi_m^{(\pm)}$ are as yet unknown fields acting as continuous Lagrange multipliers. Defining $q_m^{(\pm)}(\hat{\omega}_m) = \exp(\beta_\mathrm{B} \mathcal{H}(\hat{\omega}_m) - \xi_m^{(\pm)}(\hat{\omega}_m))$ and changing constants, $Z_m = \mathrm{e}^{1-\nu_m}$

and $Z_{m,m+1} = e^{1+\nu_{m,m+1}}$, variation to the SDF's and the PDF's yields the following equilibrium distributions

$$f_m(\hat{\omega}_m) = Z_m^{-1} q_m^{(+)}(\hat{\omega}_m) e^{-\beta_B \mathcal{H}(\hat{\omega}_m)} q_m^{(-)}(\hat{\omega}_m)$$

$$f_{m,m+1}(\hat{\omega}_m, \hat{\omega}_{m+1}) = \tag{3.31}$$

$$Z_{m,m+1}^{-1} q_m^{(+)}(\hat{\omega}_m) e^{-\beta_B \mathcal{H}(\hat{\omega}_m)} w(\hat{\omega}_m, \hat{\omega}_{m+1}) e^{-\beta_B \mathcal{H}(\hat{\omega}_{m+1})} q_{m+1}^{(-)}(\hat{\omega}_{m+1}).$$

Next, application of the normalization constraints (Eqs. 3.27) is straightforward and gives expressions for the normalization constants Z_m and $Z_{m,m+1}$,

$$Z_m = \int d\hat{\omega}_m q_m^{(+)}(\hat{\omega}_m) e^{-\beta_B \mathcal{H}(\hat{\omega}_m)} q_m^{(-)}(\hat{\omega}_m)$$

$$Z_{m,m+1} = \int d\hat{\omega}_m d\hat{\omega}_{m,m+1} \tag{3.32}$$

$$q_m^{(+)}(\hat{\omega}_m) e^{-\beta_B \mathcal{H}(\hat{\omega}_m)} w(\hat{\omega}_m, \hat{\omega}_{m+1}) e^{-\beta_B \mathcal{H}(\hat{\omega}_{m+1})} q_{m+1}^{(-)}(\hat{\omega}_{m+1}).$$

Forcing the stationarity equations to be mutually consistent (Eqs. 3.28) yields relations between the $q_m^{(\pm)}$-functions,

$$q_m^{(\pm)}(\hat{\omega}_m) = \frac{Z_m}{Z_{m,m\mp 1}} \int d\hat{\omega}_{m\mp 1} w(\hat{\omega}_m, \hat{\omega}_{m\mp 1}) e^{-\beta_B \mathcal{H}(\hat{\omega}_{m\mp 1})} q_{m\mp 1}^{(\pm)}(\hat{\omega}_{m\mp 1}). \tag{3.33}$$

The functions on the ends, $q_1^{(+)}$ and $q_M^{(-)}$, turn out to be constant and can be choosen freely, so we set them both equal to one.

In retrospect, the most striking aspect of these stationarity equations is the appearance of the new quantities $q_m^{(+)}$ and $q_m^{(-)}$. These emerge from the process of variation as some unknown fields enforcing compatibility. However, we now recognize (apart from the normalization constants) these fields as being the partition functions of parts of the chain, i.e. $q_m^{(+)}(\hat{\omega}_m)$ is the partition function of a chain of m segments under the condition that the m'th segment has orientation $\hat{\omega}_m$. Hence, the functions $q_m^{(+)}$ and $q_m^{(-)}$ are called the forward and backward partial partition functions respectively. In Eqs. 3.31, these partial partition functions represent the contributions due to orientational coupling with the lower ($< m$) and upper ($> m$) parts of the chain. In this context, it makes sense that $q_1^{(+)}$ and $q_M^{(-)}$ are constant, consistent with the ends of the chain being free. The appearence of the normalization factors in the right side of Eq. 3.33 is a consequence of the variation. However, considering the definitions of the SDF's, which are the physically relevant quantities in this system, it becomes clear that these constants are in fact quite arbitrary and can easily be scaled away.

In concluding this section, we resubstitute the stationarity equations (Eqs. 3.31) in the free energy Eq. 3.26. The result is an expression for the free energy as a functional solely of the *local* $q_m^{(\pm)}$-functions

$$\beta_B \mathcal{F}_0[q_m^{(\pm)}] = \sum_{m=2}^{M-1} \log Z_m[q_m^{(\pm)}] - \sum_{m=1}^{M-1} \log Z_{m,m+1}[q_m^{(+)}, q_{m+1}^{(-)}]$$

$$+ \int d\hat{\omega}_1 f_1(\hat{\omega}_1) \log q_1^{(+)}(\hat{\omega}_1) + \int d\hat{\omega}_M f_M(\hat{\omega}_M) \log q_M^{(-)}(\hat{\omega}_M). \tag{3.34}$$

The normalization factors are given by Eqs. 3.32 and the end-SDF's f_1 and f_M have to be replaced by the appropriate expressions from Eqs. 3.31. Variation of this functional to the $q_m^{(\pm)}$'s yields the recurrence relations Eqs. 3.33. As there are no constraints to the partial partition functions, no Lagrange terms are needed. In the next section, we will use this free energy (Eq. 3.34) to derive the Khokhlov and Semenov free energy for continuously flexible nematic polymers.

3.2.3. The Wormlike Chain Limit. In the 1980's, an impressive series of papers was published by Khokhlov and Semenov (KS) on liquid crystalline ordering in fluids of wormlike chains (Ref. [32, 33, 57] and references therein). A wormlike chain can be regarded as an elastic contour in three-dimensional space with flexibility distributed continuously along it (Ref. [49, 50, 48]). The main result of KS is the derivation of the orientational entropy of these chains as a functional of two fields (continuous analogues of the $q_m^{(\pm)}$-functions we introduced in the previous section). In this section, we rederive the KS free energy for nematic wormlike polymers by transforming our discrete Onsager chains into these wormlike objects. The transformation itself is called the 'wormlike chain limit' (WCL) and consists of taking the following three limits simultaneously – (i) $l \to 0$; the length of the segments goes to zero (ii) $M \to \infty$; the number of segments goes to infinity and (iii) $\beta_{\mathrm{B}} J \to \infty$; the chain locally becomes infinitely stiff – while keeping the total length, Ml, and the bending energy per segment, $\beta_{\mathrm{B}} J/M$, constant.

The natural length scale (apart from the total length) to characterize wormlike chains is the so-called persistence length. This is the distance along the chain over which it loses its orientational correlation. In case of the Onsager chains, the (bare) persistence length P is defined as one half of the average projection of the unit vector $\hat{\omega}_m$ on the end-to-end distance $\mathbf{r}_M - \mathbf{r}_0$, in the limit of an infinitely long isolated polymer (and m infinitely far from both ends) [50]. With the average over the isolated chain defined by,

$$\langle g \rangle_w = \frac{\int \prod_{k=1}^{M} d\hat{\omega}_k \, g\left(\{\hat{\omega}_k\}\right) \prod_{k=1}^{M-1} w(\hat{\omega}_k, \hat{\omega}_{k+1})}{\int \prod_{k=1}^{M} d\hat{\omega}_k \prod_{k=1}^{M-1} w(\hat{\omega}_k, \hat{\omega}_{k+1})} \tag{3.35}$$

the persistence length becomes,

$$P \equiv \tfrac{1}{2} \lim_{m,M \to \infty} \langle \hat{\omega}_m \cdot (\mathbf{r}_M - \mathbf{r}_0) \rangle_w$$

$$= \tfrac{1}{2} l \langle \hat{\omega}_m \cdot \hat{\omega}_m \rangle_w + l \sum_{k=m+1}^{\infty} \langle \hat{\omega}_m \cdot \hat{\omega}_k \rangle_w$$

$$= \tfrac{1}{2} l + l \sum_{k=m+1}^{\infty} \langle (\hat{\omega}_m \cdot \hat{\omega}_{k-1})(\hat{\omega}_k \cdot \hat{\omega}_{k-1}) + (\hat{\omega}_m \times \hat{\omega}_{k-1}) \cdot (\hat{\omega}_k \times \hat{\omega}_{k-1}) \rangle_w \tag{3.36}$$

$$= \tfrac{1}{2} l + l \sum_{k=m+1}^{\infty} \langle (\hat{\omega}_m \cdot \hat{\omega}_{m+1}) \cdots (\hat{\omega}_{k-2} \cdot \hat{\omega}_{k-1})(\hat{\omega}_{k-1} \cdot \hat{\omega}_k) \rangle_w,$$

where we have repeatedly used the identity for unit vectors $\hat{u} \cdot \hat{u}' = (\hat{u} \cdot \hat{v})(\hat{u}' \cdot \hat{v}) + (\hat{u} \times \hat{v}) \cdot (\hat{u}' \times \hat{v})$, with $\hat{v}$ a third (arbitrary) unit vector, and the fact that $\langle (\hat{\omega}_{k'} \times \hat{\omega}_{k-1}) \cdot$

$(\hat{\omega}_k \times \hat{\omega}_{k-1})\rangle_w = 0$ for all $k' < k - 1$. So, the persistence length becomes

$$P = \tfrac{1}{2}l + l \sum_{k=1}^{\infty} \left(\langle \cos\theta \rangle_w\right)^k = \tfrac{1}{2}l \frac{\beta_{\mathrm{B}}J + \beta_{\mathrm{B}}J \coth \beta_{\mathrm{B}}J - 1}{\beta_{\mathrm{B}}J - \beta_{\mathrm{B}}J \coth \beta_{\mathrm{B}}J + 1}, \tag{3.37}$$

On taking the WCL we find that $P \to l\beta_{\mathrm{B}}J = Ml \times \beta_{\mathrm{B}}J/M$ is a well defined constant. The wormlike chain is thus defined by its persistence length P and its total length L, or equivalently its effective number of segments $\bar{M} = L/P$. The label of an individual segment along the chain has now become a continuous parameter $\bar{m} = \frac{m}{M}\bar{M} = \frac{m}{\beta_{\mathrm{B}}J}$ which runs from 0 to $\bar{M}$. In the following we will also employ an appropriately rescaled definition of the segment density $\bar{\eta} = 2\bar{M}\rho P^2 d = \beta_{\mathrm{B}}J\eta$ (cf. Eq. (3.19)). We follow the convention that quantities related to the wormlike chain are denoted by an overbar.

To that end, we first determine how various ingredients of the theory behave in the WCL, and in doing so we define their continuous (wormlike) analogues. The first step is to rewrite the partial partion functions in terms of the continuous field $q_m^{(\pm)}(\hat{\omega}) \to \bar{q}^{(\pm)}(\bar{m}, \hat{\omega})$ (with the arrow denoting the WCL throughout). The effective fields become much smaller (because of the rescaling of the segment length l), and are in leading order of $(\beta_{\mathrm{B}}J)^{-1}$ given by,

$$\beta_{\mathrm{B}}\mathcal{H}_m(\hat{\omega}) \to (\beta_{\mathrm{B}}J)^{-1}\beta_{\mathrm{B}}\bar{\mathcal{H}}(\hat{\omega}) = (\beta_{\mathrm{B}}J)^{-1}\frac{\bar{\eta}}{\bar{M}}\int_0^{\bar{M}} d\bar{m}' \int d\hat{\omega}' \sin\gamma(\hat{\omega}, \hat{\omega}')\bar{f}(\bar{m}', \hat{\omega}'), \tag{3.38}$$

in which $\sum_{m=1}^{M} \to \beta_{\mathrm{B}}J \int_0^{\bar{M}} d\bar{m}$. As the fields $q_m^{(\pm)}$ retain their magnitude in the WCL, it is clear from Eq. (3.31), that the explicit dependence of SDF on the effective field vanishes, as $\exp\left(-\beta_{\mathrm{B}}\mathcal{H}(\hat{\omega})\right) \to 1 + \mathcal{O}((\beta_{\mathrm{B}}J)^{-1})$. However, the effective field will still contribute indirectly through the $\bar{q}^{(\pm)}$'s, as will be shown shown further on. So, the SDF at point $\bar{m}$ along the wormlike chain is given by,

$$\bar{f}(\bar{m}, \hat{\omega}) = \bar{q}^{(+)}(\bar{m}, \hat{\omega})\bar{q}^{(-)}(\bar{m}, \hat{\omega})/\bar{Z}(\bar{m}), \tag{3.39}$$

and normalized in the usual way, $\bar{Z}(\bar{m}) = \int d\hat{\omega}\bar{q}^{(+)}(\bar{m}, \hat{\omega})\bar{q}^{(-)}(\bar{m}, \hat{\omega})$. Next, we also need the difference between two neighbouring $q_m^{(\pm)}$-functions,

$$\left(q_{m+1}^{(\pm)}(\hat{\omega}) - q_m^{(\pm)}(\hat{\omega})\right) \to (\beta_{\mathrm{B}}J)^{-1}\frac{\partial \bar{q}^{(\pm)}}{\partial \bar{m}}(\bar{m}, \hat{\omega}), \tag{3.40}$$

and finally the action of the flexibility weight on an arbitrary function g,

$$\int d\hat{\omega}' w(\hat{\omega}, \hat{\omega}') g(\hat{\omega}') \to w_0 \left(1 + \tfrac{1}{2}(\beta_{\mathrm{B}}J)^{-1}\Delta_{\hat{\omega}}\right) g(\hat{\omega}), \tag{3.41}$$

in which $\Delta_{\hat{\omega}}$ is the Laplace operator on a sphere and $w_0 = 4\pi \frac{\sinh \beta_{\mathrm{B}}J}{\beta_{\mathrm{B}}J}$ is the zeroth Legendre coefficient of w (see Eq. (3.52)), and a divergent function of $\beta_{\mathrm{B}}J$. An explicit proof, in our opinion often alluded to, but never actually presented in the literature, of Eq. (3.41), employing spherical coordinates is given in the Appendix.

Having assembled all the necessary components, we return to the free energy Eq. (3.34), and consider the normalization constants in terms of which it was formulated (Eq. 3.32).

These we need to expand to first order in $(\beta_B J)^{-1}$ because the leading terms will turn out to cancel,

$$Z_m \to \bar{Z}(\bar{m}) \left[1 - (\beta_B J)^{-1} \int d\hat{\omega} \bar{f}(\bar{m}, \hat{\omega}) \beta_B \bar{\mathcal{H}}(\hat{\omega}) \right]. \qquad (3.42)$$

$$Z_{m,m+1} \to w_0 \bar{Z}(\bar{m}) \left[1 + (\beta_B J)^{-1} \bar{Z}^{-1}(\bar{m}) \int d\hat{\omega} \left(\tfrac{1}{2} \bar{q}^{(+)}(\bar{m}, \hat{\omega}) \Delta_{\hat{\omega}} \bar{q}^{(-)}(\bar{m}, \hat{\omega}) \right. \qquad (3.43)$$

$$\left. + \bar{q}^{(+)}(\bar{m}, \hat{\omega}) \frac{\partial \bar{q}^{(-)}}{\partial \bar{m}}(\bar{m}, \hat{\omega}) - 2\bar{q}^{(+)}(\bar{m}, \hat{\omega}) \beta_B \bar{\mathcal{H}}(\hat{\omega}) \bar{q}^{(-)}(\bar{m}, \hat{\omega}) \right) \right].$$

Combining the two summations in Eq. (3.34) into single one,

$$- \sum_{m=1}^{M-1} \log Z_{m,m+1} + \sum_{m=2}^{M-1} \log Z_m =$$

$$- \sum_{m=1}^{M-1} \log \left(Z_{m,m+1} / \sqrt{Z_m Z_{m+1}} \right) - \tfrac{1}{2}(\log Z_1 + \log Z_M) \qquad (3.44)$$

immediately shows that the overall factors $\bar{Z}(\bar{m})$ in front of Eqs. (3.42) and (3.43) drop out, and extra boundary terms appear. Collecting the above and substituting in Eq. (3.34), we obtain an expression for the free energy of a single wormlike chain in an external field,

$$\beta_B \bar{\mathcal{F}}_0 \left[\bar{q}^{(\pm)} \right] = \int_0^{\bar{M}} d\bar{m} \int d\hat{\omega} \bar{f}(\bar{m}, \hat{\omega}) \beta_B \bar{\mathcal{H}}(\hat{\omega})$$

$$- \tfrac{1}{2} \int_0^{\bar{M}} d\bar{m} \int d\hat{\omega} \bar{Z}^{-1}(\bar{m}) \left(\bar{q}^{(+)}(\bar{m}, \hat{\omega}) \Delta_{\hat{\omega}} \bar{q}^{(-)}(\bar{m}, \hat{\omega}) + 2\bar{q}^{(+)}(\bar{m}, \hat{\omega}) \frac{\partial \bar{q}^{(-)}}{\partial \bar{m}}(\bar{m}, \hat{\omega}) \right)$$

$$+ \int d\hat{\omega} \left(\bar{f}(0, \hat{\omega}) \log \frac{\bar{q}^{(+)}(0, \hat{\omega})}{\sqrt{\bar{Z}(0)}} + \bar{f}(\bar{M}, \hat{\omega}) \log \frac{\bar{q}^{(-)}(\bar{M}, \hat{\omega})}{\sqrt{\bar{Z}(\bar{M})}} \right), \qquad (3.45)$$

in which we have left out the (diverging) constant term $-\beta_B J \bar{M} \log w_0$. Finally, to clean up, we can symmetrize the Laplace term by partial integration, and the derivative to $\bar{m}$ by considering the symmetry in the fields: $\bar{q}^{(+)}(\bar{m}, \hat{\omega}) = \bar{q}^{(-)}(\bar{M} - \bar{m}, \hat{\omega})$, which is due to the chain being symmetric in $+$ and $-$ direction, and change to variables, $\psi^{(\pm)}(\bar{m}, \hat{\omega}) = \bar{q}^{(\pm)}(\bar{m}, \hat{\omega}) / \sqrt{\bar{Z}(\bar{m})}$. This leads to

$$\beta_B \bar{\mathcal{F}}_0 \left[\psi^{(\pm)} \right] =$$

$$\tfrac{1}{2} \int_0^{\bar{M}} d\bar{m} \int d\hat{\omega} \left(\nabla_{\hat{\omega}} \psi^{(+)}(\bar{m}, \hat{\omega}) \cdot \nabla_{\hat{\omega}} \psi^{(-)}(\bar{m}, \hat{\omega}) + \psi^{(-)}(\bar{m}, \hat{\omega}) \frac{\partial \psi^{(+)}}{\partial \bar{m}}(\bar{m}, \hat{\omega}) \right.$$

$$\left. - \psi^{(+)}(\bar{m}, \hat{\omega}) \frac{\partial \psi^{(-)}}{\partial \bar{m}}(\bar{m}, \hat{\omega}) \right) + \int_0^{\bar{M}} d\bar{m} \int d\hat{\omega} \bar{f}(\bar{m}, \hat{\omega}) \beta_B \bar{\mathcal{H}}(\hat{\omega})$$

$$+ \int d\hat{\omega} \left(\bar{f}(0, \hat{\omega}) \log \psi^{(+)}(0, \hat{\omega}) + \bar{f}(\bar{M}, \hat{\omega}) \log \psi^{(-)}(\bar{M}, \hat{\omega}) \right), \qquad (3.46)$$

in which the orientational distribution function now equals $\bar{f} = \psi^{(+)}\psi^{(-)}$. Apart from the external field, this is exactly the KS result for the free energy [33]. The only difference is the factor $\frac{1}{2}$ in front of the term with the derivatives, which is due to the fact that we use the persistence length P as our unit of length rather than the Kuhn length $2P$ employed by KS.

As in the previous section, we can directly apply a variation principle to the free energy Eq. (3.46) in terms of the fields $\psi^{(\mp)}$. To ensure that $\bar{f}$ is normalized at every point along the chain we add a Lagrange term,

$$\int_0^{\bar{M}} d\bar{m}\lambda(\bar{m}) \int d\hat{\omega}\psi^{(+)}(\bar{m},\hat{\omega})\psi^{(-)}(\bar{m},\hat{\omega}), \tag{3.47}$$

in which $\lambda(\bar{m})$ is the continuous Lagrange multiplier. This variation yields the diffusion equation,

$$\pm\frac{\partial\bar{\psi}^{(\pm)}}{\partial\bar{m}}(\bar{m},\hat{\omega}) = \tfrac{1}{2}\Delta_{\hat{\omega}}\bar{\psi}^{(\pm)}(\bar{m},\hat{\omega}) - \beta_{\mathrm{B}}\bar{\mathcal{H}}'(\bar{m},\hat{\omega})\bar{\psi}^{(\pm)}(\bar{m},\hat{\omega}), \tag{3.48}$$

with the parameter $\bar{m}$ playing the role of time, and $\Delta_{\hat{\omega}}$ the Laplace operator on a sphere. The primed effective fields have to be determined selfconsistently,

$$\beta_{\mathrm{B}}\bar{\mathcal{H}}'(\bar{m},\hat{\omega}) = \lambda(\bar{m}) + \frac{\bar{\eta}}{\bar{M}}\int_0^{\bar{M}} d\bar{m}' \int d\hat{\omega}' \sin\gamma(\hat{\omega},\hat{\omega}')\bar{f}(\bar{m}',\hat{\omega}'), \tag{3.49}$$

and $\lambda(\bar{m})$ is tuned to achieve the normalization. Variation with respect to the terminal fields $\psi^{(+)}(0,\hat{\omega})$ and $\psi^{(-)}(\bar{M},\hat{\omega})$ yields that both are constant. Of course, Eq. (3.48) can also be obtained by direct application of the WCL on the recurrence relation Eq. (3.33).

3.3. Results

3.3.1. Bifurcation Analysis. We are now in a position to apply the formal results of the previous sections to adress the description of the isotropic to nematic (I-N) transition in our sytem. In the next section, we numerically compute solutions which minimize the free energy and so determine the coexistence densities and the degree of ordering at the transition. In the present section, we will use a linear stability analysis to analytically determine the location of the I-N bifurcation (spinodal) density. At the bifurcation point a nematic solution to the stationarity equation branches off from the isotropic solution, which changes stability there; for densities lower than the bifurcation density it is (meta)stable, for higher densities unstable. Consequently, close to the bifurcation point, the solutions to the stationarity equation can be written as the isotropic solution with small nematic perturbations [37]. Then, the (lowest) density for which such perturbed distributions are solutions to the stationarity equations is the bifurcation density.

Before we start however, we have to choose a convenient order parameter to distinguish between the isotropic and the nematic phases. Both the segments and the phases we consider have azimuthal symmetry. This means that the SDF's can be written as a function of only one polar angle θ (or $\cos\theta$), measured with respect to some nematic director $\hat{n}$. Consequently, we expand the SDF's in series of Legendre polynomials,

$$f_m(\hat{\omega}_m \cdot \hat{n}) = \sum_{n=0}^{\infty} \frac{2n+1}{4\pi} a_n^{(m)} P_n(\hat{\omega}_m \cdot \hat{n}), \tag{3.50}$$

in which the coefficients are given by

$$a_n^{(m)} = \int d\hat{\omega} f_m(\hat{\omega} \cdot \hat{n}) P_n(\hat{\omega} \cdot \hat{n}), \tag{3.51}$$

Clearly, $a_0^{(m)} = 1$, because of the normalization of f_m, and due to the up-down symmetry of the segments and the phase (f_m is invariant under $\theta \leftrightarrow \pi - \theta$), all $a_n^{(m)} = 0$ for odd n. Consequently, the lowest nonzero coefficient different in the isotropic and nematic phase is $a_2^{(m)}$. We choose this set of coefficients $a_2^{(m)}$ to be our order parameters. These coefficients, which are of course the well-known Maier-Saupe order parameters for the segments, are 0 in the isotropic phase, and between 0 and 1 when there is orientational ordering in the direction of the nematic axis. Frequently, we will also use the average order parameter of the chain $a_2 = (1/M) \sum_{m=1}^{M} a_2^{(m)}$.

The results are presented more easily by defining the following invariant expansions as well,

$$\begin{bmatrix} w(\hat{\omega} \cdot \hat{n}) \\ \sin \theta(\hat{\omega}, \hat{n}) \end{bmatrix} = \sum_{n=0}^{\infty} \frac{2n+1}{4\pi} \begin{bmatrix} w_n \\ s_n \end{bmatrix} P_n(\hat{\omega} \cdot \hat{n}), \tag{3.52}$$

in which the coefficients are given by similar relations as for the SDF's (Eq. 3.51). Both s_n and w_n can be expressed completely in analytical terms [58]. For the bifurcation analysis we will only need

$$
\begin{aligned}
w_0 &= 4\pi \sinh \beta_{\mathrm{B}} J / \beta_{\mathrm{B}} J & s_0 &= \pi^2 \\
w_2 &= 4\pi \left((1 + 3/(\beta_{\mathrm{B}} J)^2) \sinh \beta_{\mathrm{B}} J / \beta_{\mathrm{B}} J - 3 \cosh \beta_{\mathrm{B}} J / (\beta_{\mathrm{B}} J)^2 \right) & s_2 &= -\pi^2/8.
\end{aligned}
\tag{3.53}
$$

Also, the coefficients $s_n = 0$ for odd values of n.

In the isotropic phase, the SDF's are simply constant, so due to normalization, $f_m(\theta_m) = 1/4\pi$. It is easily checked that the isotropic distribution is a solution to the stationarity equations Eqs. (3.17) for every density η. At higher densities, however, the isotropic phase is unstable and the system will favour an orientationally ordered phase. The density at which the isotropic solution becomes absolutely unstable (and the nematic solution branches off) can be found by investigating the stability of small nematic perturbations added to the isotropic distributions. That is, we assume the SDF's to have the form,

$$f_m(\hat{\omega}_m \cdot \hat{n}) = \frac{1}{4\pi} + \varepsilon_m P_2(\hat{\omega}_m \cdot \hat{n}), \tag{3.54}$$

in which ε_m are a set of infinitesimally small parameters. Substituting these SDF's in Eqs. (3.17), yields

$$
\begin{aligned}
\frac{1}{4\pi} + \varepsilon_m P_2(\hat{\omega}_m \cdot \hat{n}) = {} & \frac{1}{4\pi} \int \prod_{j \neq m} d\hat{\omega}_j \\
& \times \prod_{j=1}^{M-1} \frac{w(\hat{\omega}_j \cdot \hat{\omega}_{j+1})}{w_0} \prod_{k=1}^{M} \exp \left[-\frac{\eta}{M} \sum_{k'=1}^{M} \varepsilon_{k'} \int d\hat{\omega}_{k'}' P_2(\hat{\omega}_{k'}' \cdot \hat{n}) \sin \gamma(\hat{\omega}_k, \hat{\omega}_{k'}') \right],
\end{aligned}
\tag{3.55}
$$

in which γ is the planar angle between $\hat{\omega}_k$ and $\hat{\omega}'_{k'}$, $\sin\gamma(\hat{\omega}_k, \hat{\omega}'_{k'}) = |\hat{\omega}_k \times \hat{\omega}'_{k'}| = \sqrt{1 - (\hat{\omega}_k \cdot \hat{\omega}'_{k'})^2}$. We now apply the addition theorem to the Legendre function $P_2(\hat{\omega}'_{k'} \cdot \hat{n})$ to express it in terms of spherical harmonics with polar vector $\hat{\omega}_k$

$$P_2(\hat{\omega}'_{k'} \cdot \hat{n}) = \frac{4\pi}{5} \sum_{m=-2}^{2} Y_{2,m}^*(\hat{\omega}'_{k'}|\hat{\omega}_k) Y_{2,m}(\hat{n}|\hat{\omega}_k). \tag{3.56}$$

As $\sin\gamma(\hat{\omega}_k, \hat{\omega}'_{k'})$ only depends on $(\hat{\omega}_k \cdot \hat{\omega}'_{k'})$ it is orthogonal to any spherical harmonic $Y_{2,m}(\hat{\omega}'_{k'}|\hat{\omega}_k)$ with $m \neq 0$. Consequently,

$$-\frac{\eta}{M} \sum_{k'=1}^{M} \varepsilon_{k'} \int d\hat{\omega}'_{k'} P_2(\hat{\omega}'_{k'} \cdot \hat{n}) \sin\gamma(\hat{\omega}_k, \hat{\omega}'_{k'}) = -\frac{\eta s_2}{M} \left(\sum_{k'=1}^{M} \varepsilon_{k'} \right) P_2(\hat{\omega}_k \cdot \hat{n}) \tag{3.57}$$

Linearizing the exponential with respect to the (small) ε_m and subtracting the isotropic contribution $1/4\pi$, Eq. (3.55) becomes to first order in ε_m

$$\varepsilon_m P_2(\hat{\omega}_m \cdot \hat{n}) = -\frac{\eta s_2}{4\pi M} \left(\sum_{k'=1}^{M} \varepsilon_{k'} \right) \int \prod_{j \neq m}^{M-1} d\hat{\omega}_j \prod_{j=1}^{M-1} \frac{w(\hat{\omega}_j \cdot \hat{\omega}_{j+1})}{w_0} \sum_{k=1}^{M} P_2(\hat{\omega}_k \cdot \hat{n}). \tag{3.58}$$

The right hand side of this equation can be interpreted as the sum over the contributions due to orientational perturbations of the form $\left(\sum_{k'=1}^{M} \varepsilon_{k'} \right) P_2(\hat{\omega}_k \cdot \hat{n})$ operating on each single segment in turn. Focus for a moment on a term with $k < m$. The integration over the flexibility Boltzmann weights for $j < k$, as well as those for $j \geq m+1$ are trivially performed, and yield a factor $w_0/w_0 = 1$ each. The effect of the remaining integrations is to "pass on" the orientational perturbation at the k'th segment to the $(k+1)$'th segment and so on until the target segment m is reached. The first integration is given by

$$\int d\hat{\omega}_k \frac{w(\hat{\omega}_k \cdot \hat{\omega}_{k+1})}{w_0} P_2(\hat{\omega}_k \cdot \hat{n}) = \frac{w_2}{w_0} P_2(\hat{\omega}_{k+1} \cdot \hat{n}), \tag{3.59}$$

where we again employed the addition theorem for $P_2(\hat{\omega}_k \cdot \hat{n})$. Clearly the following steps are similar, each step picking up an additional factor w_2/w_0. The total factor picked up on reaching segment m is $(w_2/w_0)^{m-k}$. By the same token for $k > m$, we pick up a factor $(w_2/w_0)^{k-m} = (w_2/w_0)^{|m-k|}$. Substituting these results in Eq. (3.58), we obtain

$$\varepsilon_m P_2(\hat{\omega}_m \cdot \hat{n}) = -\frac{\eta s_2}{4\pi M} \left(\sum_{k'=1}^{M} \varepsilon_{k'} \right) \sum_{k=1}^{M} \left(\frac{w_2}{w_0} \right)^{|m-k|} P_2(\hat{\omega}_m \cdot \hat{n}). \tag{3.60}$$

Next, we cancel the P_2's, substitute $s_2 = -\pi^2/8$, define $\sigma = w_2/w_0$ and perform the summation over k. This yields

$$\varepsilon_m = \frac{\eta\pi}{32M} \frac{1 + \sigma - \sigma^m - \sigma^{M-m+1}}{1 - \sigma} \sum_{k'=1}^{M} \varepsilon_{k'}. \tag{3.61}$$

The new parameter σ serves as a convenient measure of the chain stiffness since it ranges from 0 in absence of intrachain interactions to 1 in case of $\beta_B J \to \infty$ (see Eqs. 3.53).

Summing both sides over m, we can drop the sum over ε_m, and obtain an expression for the bifurcation density,

$$\eta^* = \frac{32}{\pi} \left(\frac{1}{M} \sum_{m=1}^{M} \frac{1 + \sigma - \sigma^m - \sigma^{M-m+1}}{1 - \sigma} \right)^{-1} = \frac{32}{\pi} \left(\frac{1 + \sigma}{1 - \sigma} - \frac{2\sigma}{M} \frac{1 - \sigma^M}{(1 - \sigma)^2} \right)^{-1}.$$

(3.62)

Let us check a few limiting cases, and compare with the known results on the bifurcation density for hard rods in the Onsager approximation following Ref. [37] (who use the density $c = \eta\pi/8$). For $M = 1$, we have a single hard rod and find $\eta^*\pi/8 = 4$. When $\sigma = 1$, we effectively have rigid rods of length $L = Ml$ yielding a bifurcation density, $M\eta^*\pi/8 = \pi(Ml)^2 d\rho_*/4 = 4$, where ρ is the *chain* density. Finally, for very floppy chains with $\sigma = 0$ the bifurcation density is the same as for unconnected rods, $\eta^*\pi/8 = 4$.

In the previous section, we showed that one of the strengths of our model is the fact that the KS-theory can be recovered by applying the WCL. We illustrate this here on the level of the bifurcation results. In the WCL, the σ-parameter behaves as $\sigma \to 1 - 3(\beta_B J)^{-1}$, so the bifurcation density becomes

$$\bar{\eta}^* = \frac{48}{\pi} \left(1 - \frac{1 - e^{-3\bar{M}}}{3\bar{M}} \right)^{-1},$$

(3.63)

which is the result given by KS in Ref. [33]. In the limit of very long wormlike chains, $\bar{\eta}^* = 48/\pi$. Another interesting case is the rigid rod limit, $\bar{M} \to 0$, where we need to rescale the density, $\bar{\eta}^* \bar{M} = 2\rho^* L^2 d \to (32/\pi)(1 + \bar{M} + \mathcal{O}(\bar{M}^2))$.

From Eqs. (3.50) and (3.54), we see that the nematic perturbations ε_m are proportional to the order parameters $a_2^{(m)}$. And although these perturbations are very small, Eq. (3.61) readily yields the distribution of *relative* order along the chain. Applying the WCL to Eq. (3.61), we obtain a normalized expression for the order distribution along a wormlike chain,

$$\frac{\bar{\varepsilon}(\bar{m})}{\langle \bar{\varepsilon}(\bar{m}) \rangle} = \frac{3}{2} \frac{\left((1 - e^{-3\bar{m}}) + (1 - e^{-3(\bar{M}-\bar{m})}) \right)}{1 - \left(1 - e^{-3\bar{M}} \right)/3\bar{M}},$$

(3.64)

with $\varepsilon_m \to \bar{\varepsilon}(\bar{m})$ and $\langle \bar{\varepsilon}(\bar{m}) \rangle = \frac{1}{\bar{M}} \int_0^{\bar{M}} d\bar{m} \bar{\varepsilon}(\bar{m})$. So, for instance, the ratio of the order in the middle of the chain to that at the chain ends is given by

$$\frac{\bar{\varepsilon}(\frac{1}{2}\bar{M})}{\bar{\varepsilon}(0)} = \frac{2}{1 + e^{-\frac{3}{2}\bar{M}}}.$$

(3.65)

This means that, already at the bifurcation point, the middle of the chain is more strongly ordered than the ends. For very long chains ($\bar{M} \to \infty$) this factor is exactly equal to 2. The heuristic explanation is that for very long chains the middle feels an equal orientational "pull" from both sides of the chain, whereas the ends feels the same effect but only from one side. This was first discussed by KS in Ref. [33] using a more general argument.
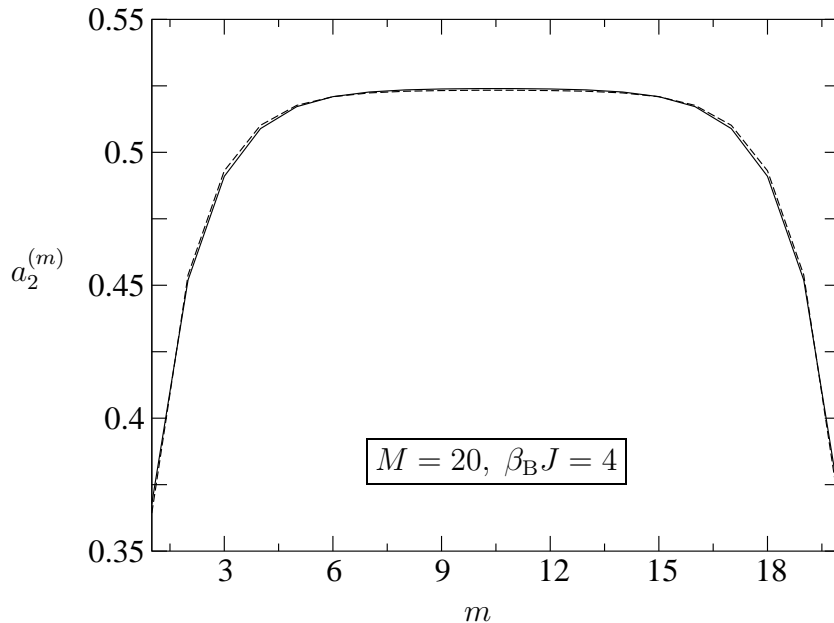
FIGURE 3.2. Order along a segmented chain of $M = 20$ segments and coupling constant $\beta_{\mathrm{B}} J = 4$ (so $P \approx M/\beta_{\mathrm{B}} J = 5$). The full curve is the real order $a_{2,\mathrm{nem}}^{(m)}$ at the phase transition, $\eta_{\mathrm{nem}} = 3.205$. The dashed curve is the rescaled order at the bifurcation point $\eta_* = 4.218$. The bifurcating order $\varepsilon_m / \sum_k \varepsilon_k$ (from Eq. 3.61) normally has average 1, but has been rescaled here to the same average order as at the phase transition $a_{2,\mathrm{nem}} = 0.495$. The fact that the two profiles nearly overlap suggests that the relative order profile at the bifurcation point gives a good estimate for the real order profile at the transition. Absolute values of the average order at the transition can not be obtained from bifurcation analysis. The numerical order profile at the phase transition is calculated in the next section and also given in Fig. 3.4(right).

3.3.2. Numerical Analysis. In the previous section, we determined the location of the I-N bifurcation (spinodal) density. However, for a system like this, with a first-order I-N phase transition, the densities characterizing the coexistence between two stable thermodynamic phases are the coexistence (binodal) densities η_{iso} and η_{nem}. In the coexistence region, the system phase seperates into an isotropic and a nematic part of respective (coexistence) densities. The order parameters in the nematic part of the coexisting phases are denoted by $a_{2,\mathrm{nem}}$ and $a_{2,\mathrm{nem}}^{(m)}$. In this section, we numerically calculate the coexistence densities and the order parameters at the phase transition for a range of chain stiffnesses and various values of the chain lengths.

For a given density, we numerically calculate the equilibrium distributions analogue to Ref. [59], i.e. we solve the stationarity equations (Eqs. 3.17) iteratively by means of repeated numerical integrations. To that end, we perform all integrations over ϕ in advance and the remaining (θ-)integrations numerically on a grid. The external field is

given by

$$\beta_{\mathrm{B}}\mathcal{H}(\theta) = \eta \int_0^\pi d\theta' \sin\theta' K(\theta, \theta') f_{\mathrm{av}}(\theta') \tag{3.66}$$

in which

$$K(\theta, \theta') = \int_0^{2\pi} d\phi \sin\gamma(\hat{\omega}, \hat{\omega}') = \int_0^{2\pi} d\phi\sqrt{1 - (\cos\theta\cos\theta' + \sin\theta\sin\theta'\cos\phi)^2} \tag{3.67}$$

and with $f_{\mathrm{av}}(\theta) = (1/M)\sum_{m'=1}^M f_{m'}(\theta)$ the average SDF in the chain. The kernel $K(\theta, \theta')$ has to be computed numerically only once (on a square θ-grid) and can be used every iteration cycle again. The $(M-1)$ flexibility integrations become,

$$q_{m+1}(\theta) = \int_0^\pi d\theta' \sin\theta' W(\theta, \theta') \mathrm{e}^{-\beta_{\mathrm{B}}\mathcal{H}(\theta')} q_m(\theta') \tag{3.68}$$

with of course $q_1 = 1$. Here, the kernel $W(\theta, \theta')$ is given by

$$W(\theta, \theta') = \int_0^{2\pi} d\phi w(\hat{\omega}, \hat{\omega}') = \int_0^{2\pi} d\phi \exp\left[\beta_{\mathrm{B}} J \left(\cos\theta\cos\theta' + \sin\theta\sin\theta'\cos\phi\right)\right]$$
$$= 2\pi \exp\left[\beta_{\mathrm{B}} J \cos\theta\cos\theta'\right] I_0\left(\beta_{\mathrm{B}} J \sin\theta\sin\theta'\right), \tag{3.69}$$

with I_0 the modified Bessel function of zeroth order. In Eq. 3.68, we have dropped the superscript $\pm$ because due to symmetry $(q_m^{(+)}(\theta) = q_{M-m+1}^{(-)}(\theta))$ we only need to compute one of the two. The SDF's are then given by

$$f_m(\theta) = Q^{-1} q_m(\theta) \mathrm{e}^{-\beta_{\mathrm{B}}\mathcal{H}(\theta)} q_{M-m+1}(\theta), \tag{3.70}$$

with,

$$Q = 2\pi \int_0^\pi d\theta q_m(\theta) \mathrm{e}^{-\beta_{\mathrm{B}}\mathcal{H}(\theta)} q_{M-m+1}(\theta). \tag{3.71}$$

The normalization constant Q is of course the same for all m. Then, going through Eqs. 3.66 to 3.71 and using the SDF's from Eq. 3.70 as input for Eq. 3.66, we have a closed (iterative) loop. Using extreme nematic distributions (normalized delta peaks around $\theta = 0$) as a seed, this iteration will converge to the nematic solutions of the stationarity equations, if they exist for the density selected. In the isotropic phase, $f_m = 1/4\pi$ and consequently $\beta_{\mathrm{B}}\mathcal{H}_{\mathrm{iso}}(\eta) = \pi\eta/4$ and $Q_{\mathrm{iso}}(\eta) = 4\pi w_0^{M-1}\exp[-\pi\eta M/4]$.

Then, having computed equilibrium distributions for a given density, we also want to calculate the free energy of the two phases. In section 3.2.1 we found that we could not *a priori* derive an expression for the free energy solely in terms of the SDF's. However, we can use the *equilibrium* distributions themselves (having already computed them), and resubstitute them in the the free energy (Eq. 3.14 in 3.12). This yields

$$\frac{\beta_{\mathrm{B}}\mathcal{F}^{(\mathrm{eq})}(\rho)}{N} = -\log\int d\mathbf{\Omega}\exp\left[-\beta_{\mathrm{B}} U(\mathbf{\Omega}) - \rho\int d\mathbf{\Omega}' f^{(\mathrm{eq})}(\mathbf{\Omega}')\mathcal{E}(\mathbf{\Omega}, \mathbf{\Omega}')\right]$$
$$+ \log(\rho\mathcal{V}_{\mathrm{T}}) - 1 - \tfrac{1}{2}\rho\int d\mathbf{\Omega} d\mathbf{\Omega}' f^{(\mathrm{eq})}(\mathbf{\Omega}) f^{(\mathrm{eq})}(\mathbf{\Omega}')\mathcal{E}(\mathbf{\Omega}, \mathbf{\Omega}'), \tag{3.72}$$

where we have added superscripts to denote the equilibrium character. We can then numerically compute the free energy by using the (equilibrium) results from the above iterative procedure for a particular density

$$\frac{\beta_{\mathrm{B}}\mathcal{F}^{(\mathrm{eq})}(\eta)}{N} =$$

$$\log \eta - \log Q^{(\mathrm{eq})}(\eta) - \frac{\eta}{2M} \sum_{m,m'=1}^{M} \int \int d\hat{\omega} d\hat{\omega}' f_m^{(\mathrm{eq})}(\hat{\omega}) f_{m'}^{(\mathrm{eq})}(\hat{\omega}') \sin \gamma(\hat{\omega}, \hat{\omega}')$$

$$= \log \eta - \log Q^{(\mathrm{eq})}(\eta) - \pi \eta M \int_0^\pi d\theta \sin \theta \int_0^\pi d\theta' \sin \theta' f_{\mathrm{av}}^{(\mathrm{eq})}(\theta) f_{\mathrm{av}}^{(\mathrm{eq})}(\theta') K(\theta, \theta'),$$

$$(3.73)$$

where we have also dropped the (irrelevant) constant term $\log (\mathcal{V}_{\mathrm{T}}/2l^2 dM) - 1$. In the isotropic phase, this free energy reduces to

$$\beta_{\mathrm{B}}\mathcal{F}_{\mathrm{iso}}^{(\mathrm{eq})}(\eta)/N = \log(\eta/4\pi) - (M-1)\log w_0 + \pi \eta M/8. \tag{3.74}$$

Two phases in coexistence need to be in mechanical and chemical equilibrium. Consequently, we derive expressions for pressure P and chemical potential μ, using Eq. 3.72,

$$\beta_{\mathrm{B}}P(\rho) = -\left(\frac{\partial \beta_{\mathrm{B}}\mathcal{F}^{(\mathrm{eq})}}{\partial V}\right)_N = \rho^2 \frac{\partial(\beta_{\mathrm{B}}\mathcal{F}^{(\mathrm{eq})}/N)}{\partial \rho} \tag{3.75}$$

$$= \rho + \tfrac{1}{2}\rho^2 \int d\mathbf{\Omega} d\mathbf{\Omega}' f^{(\mathrm{eq})}(\mathbf{\Omega}) f^{(\mathrm{eq})}(\mathbf{\Omega}') \mathcal{E}(\mathbf{\Omega}, \mathbf{\Omega}'),$$

$$\beta_{\mathrm{B}}\mu(\rho) = \left(\frac{\partial \beta_{\mathrm{B}}\mathcal{F}^{(\mathrm{eq})}}{\partial N}\right)_V = \frac{\beta_{\mathrm{B}}\mathcal{F}^{(\mathrm{eq})}}{N} + \rho \frac{\partial(\beta_{\mathrm{B}}\mathcal{F}^{(\mathrm{eq})}/N)}{\partial \rho} \tag{3.76}$$

$$= \log (\rho \mathcal{V}_{\mathrm{T}}) - \log \int d\mathbf{\Omega} \exp\left[-\beta_{\mathrm{B}}U(\mathbf{\Omega}) - \rho \int d\mathbf{\Omega}' f^{(\mathrm{eq})}(\mathbf{\Omega}') \mathcal{E}(\mathbf{\Omega}, \mathbf{\Omega}')\right].$$

In simplified terms, these are

$$(2l^2 dM)\beta_{\mathrm{B}}P(\eta) =$$

$$\eta + \pi \eta^2 M \int_0^\pi d\theta \sin \theta \int_0^\pi d\theta' \sin \theta' f_{\mathrm{av}}^{(\mathrm{eq})}(\theta) f_{\mathrm{av}}^{(\mathrm{eq})}(\theta') K(\theta, \theta'), \tag{3.77}$$

$$\beta_{\mathrm{B}}\mu(\eta) = \log \eta - \log Q^{(\mathrm{eq})}(\eta). \tag{3.78}$$

in which we have multiplied the pressure with $2l^2 dM$ in order to make it dimensionless. Further, we have dropped a term $\log (\mathcal{V}_{\mathrm{T}}/2l^2 dM)$ in the chemical potential. In the isotropic phase these expressions reduce to

$$(2l^2 dM)\beta_{\mathrm{B}}P_{\mathrm{iso}}(\eta) = \eta + \pi \eta^2 M/8, \tag{3.79}$$

$$\beta_{\mathrm{B}}\mu_{\mathrm{iso}}(\eta) = \log(\eta/4\pi) - (M-1)\log w_0 + \pi \eta M/4. \tag{3.80}$$

Then, the conditions for coexistence are

$$P(\eta_{\mathrm{nem}}) = P_{\mathrm{iso}}(\eta_{\mathrm{iso}}) \quad \text{and} \quad \mu(\eta_{\mathrm{nem}}) = \mu_{\mathrm{iso}}(\eta_{\mathrm{iso}}), \tag{3.81}$$

which are two equations with two unknown variables. Numerical rootfinding methods can then be used to find the solution with $\eta_{\mathrm{nem}} \neq \eta_{\mathrm{iso}}$. Geometrically, this corresponds
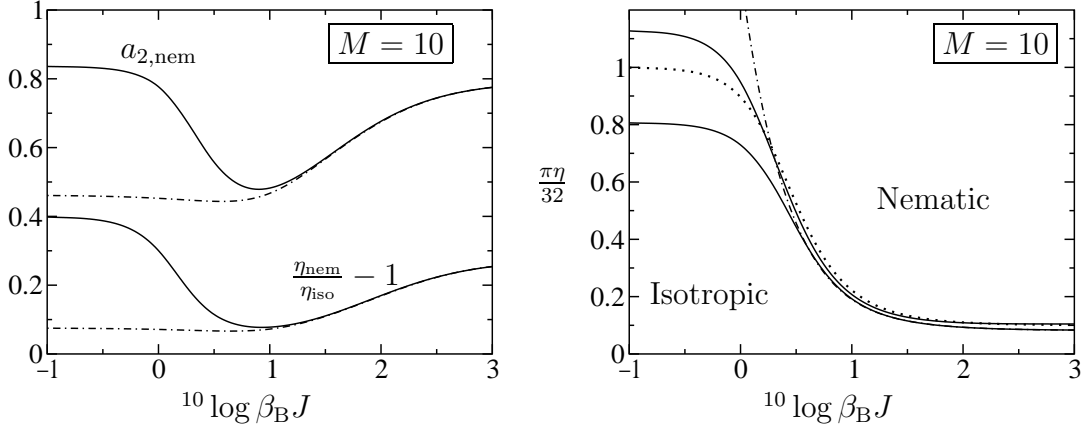
FIGURE 3.3. Results for the I-N transition of chains with $M = 10$ segments, and a comparison with the results of Chen [36]. Chen uses a 'flexibility parameter' α which we have set equal to $M/2\beta_B J$ (in fact, α is defined as the total length over the Kuhn length). In the left graph, we have plotted the order parameter at the phase transition $a_{2,\mathrm{nem}}$ and the relative width of the coexistence region $\eta_{\mathrm{nem}}/\eta_{\mathrm{iso}} - 1$, both as a function of the stiffness parameter, $\beta_B J$. The full curves are the present work, and the dashed-dotted are due to Chen. In the right graph, we have given the transition densities as a function of $\beta_B J$. The full curves are the coexistence densities, η_{nem} and η_{iso}, the dotted curve is the bifurcation density, η_* and the dashed-dotted is the result for η_{iso} due to Chen. To compare, the rigid rod results can be found in the text.

to finding the so-called common tangents (which cancel the non-convexity of the free energy surface).

We determined the coexistence densities η_{iso} and η_{nem} and the order parameter at the phase transition for a range of coupling strengths J and chain lengths M. Some results are plotted in Fig. 3.3. For wormlike chains similar figures are calculated by Chen [36]. Here, we only compare these quantities for a chain of $M = 10$ segments with Chen's results (Fig. 3.3), because the effect is qualitatively the same for other chain lengths. We have also plotted the bifurcation density as a function of the coupling (Eq. 3.62), to show the relation with the coexistence densities. Clearly, there are two regimes, one (for high $\beta_B J$) where the segmented chains give quite accurately the same results as wormlike chains and a regime (for low $\beta_B J$) where the results are quite different. We will discuss this illustrated by the $\beta_B J$-dependence of $a_{2,\mathrm{nem}}$ (Fig. 3.3, left). We start from infinite stiffness (so on the left side of the plot, where we have effectively a system of rigid rods of length $Ml \Rightarrow a_{2,\mathrm{nem}} = 0.7922, \pi\eta_{\mathrm{iso}}/32 = 0.8225/M = 0.08225$ and $\pi\eta_{\mathrm{nem}}/32 = 1.048/M = 0.1048$ [48, 60]) Decreasing J, the chains become more flexible and this allows them to postpone the I-N phase transition to higher densities (Fig. 3.3, right) and simultaneously they can assume a more disordered state at the phase transition. This results in a decrease of the order parameter in exactly the same way as for the wormlike chains. Decreasing the coupling even further, however, the dependence reaches a minimum and then goes up again, whereas for the wormlike chains it stays down (actually, it goes slightly up). Apparently, segmented chains, with segments of length
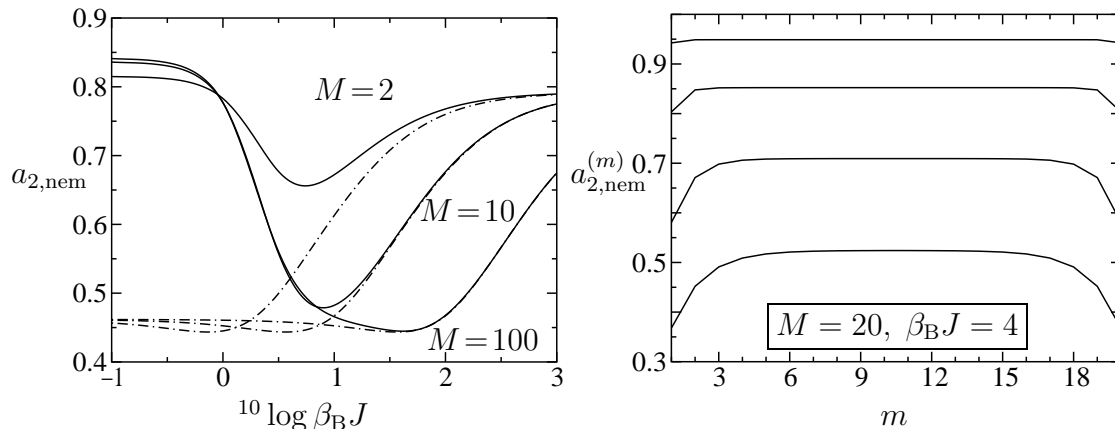
FIGURE 3.4. Order parameter at the phase transition $a_{2,\text{nem}}$, vs. stiffness $\beta_{\text{B}}J$, for various values of M (left) and order parameter a_2, as a function of chain label m for various values of the density η (right). In the left graph, the full curves are the present work, for $M = 2$, $M = 10$ and $M = 100$, and the dashed-dotted are due to Chen where Chen's flexibility parameter α is set equal to $M/2\beta_{\text{B}}J$ (for $M = 2$, $M = 10$ and $M = 100$, Chen's curves are all the same but shifted with respect to each other due to the logarithm of the x-axis). In the right graph, the order along the chain is plotted for a chain with $M = 20$ and $\beta_{\text{B}}J = 4$ (so $P \approx M/\beta_{\text{B}}J = 5$). The segments are discrete and located at the integer values, 1,2, etc. the full lines are connecting them. The lower curve is for density $\eta = \eta_{\text{nem}} = 3.205$, the one above that for $\eta = 4.224$, the next for $\eta = 7.280$ and the upper for $\eta = 15.43$. The lower curve is also given in Fig. 3.2 and compared with the bifurcation result.

l, without coupling ($\beta_{\text{B}}J = 0$) behave more or less the same as a fluid of independent rods of length l. (Actually, there is a small difference due to the fact that the ideal gas term in the free energy is different.) Wormlike chains, however, do not have a segmented character and can in principle be made infinitely flexible ($\bar{M} \to \infty$). Summarizing, for high values of $\beta_{\text{B}}J$, segmented chains behave much like wormlike chains. In this regime, the segmented character does not show, as many segments act as one persistence length. Furthermore, the persistence length scales linearly with $\beta_{\text{B}}J$ so a direct identification with wormlike chains is possible. Below some treshold value of $\beta_{\text{B}}J$ (we come back to this later), the segmented character of the chains shows and the results differ from the wormlike chains. Also, for low $\beta_{\text{B}}J$, the persistence length of segmented chains does not scale simply linear with $\beta_{\text{B}}J$ (see Eq. 3.37).

In order to study the question when a segmented chain does behave like a wormlike chain, we have plotted some more dependences in Fig. 3.4 (left), for various values of M. We find that for chains of many segments, like $M = 100$, the dividing line between the two regimes lies at about $\beta_{\text{B}}J = 10$ as it does for chains of $M = 10$ segments. However, shorter chains, with $M < 10$, show a divergence from the wormlike behaviour already at higher $\beta_{\text{B}}J > 10$ (for $M = 2$, this dividing line lies at about $\beta_{\text{B}}J = 100$). Therefore,

we propose the following 'rule of thumb',

$$\begin{array}{ll} \beta_{\mathrm{B}}J = 10 & \text{if} \quad M \geq 10 \\ \beta_{\mathrm{B}}J = -20M + 210 & \text{if} \quad M < 10 \end{array} . \qquad (3.82)$$

We will use this rule in Chap. 7, where we numerically study I-N behaviour of side chain LCP's. It is of course always possible to use a more accurate estimate, which we do in Chap. 7 as well, but there we explicitly mention it.

Finally, in Fig. 3.4 (right), we give order profiles of a chain in the nematic phase. Starting at the phase transition, the average order is still quite low and the chain end effects are visible to a length scale of about the persistence length. Increasing the density, the nematic field gets stronger, and the average order goes up. At the same time, influences due to chain stiffness become less pronounced, and the order profile becomes more flat. This is because the nematic field scales linearly with the density whereas the stiffness of the chain is independent of it.

3.4. Conclusion

We have presented a DFT approach to nematic ordering in liquid crystalline polymers which are modelled by uniaxial segmented chains. The approximations, we make, are formulated explicitly and are basically: the use of the second virial approximation (1), we allow only nearest-neighbor interactions within the chains (2) and we assume that two chains interact with only one 'interaction site' at a time (3). The problem is formally equivalent to that of a single chain in an effective field, allowing us to use techniques developed in the field of discrete spin systems. Wormlike chains are a limiting case of our segmented chains and the Khokhlov and Semenov free energy for nematic polymers can be obtained from our formulation by applying the 'wormlike chain limit'. The I-N transition for the segmented chains is located by means of a bifurcation analysis of the spinodal point, and by numerically locating the coexistence points.

The main advantage in working with segmented chains is the rather direct generalization to heterochains (consisting of different types of segments) and chains with various branches. We use the segmented chain approach to main chain polymers and side chain polymers, in Part 2 of this thesis. Secondly, the wormlike chain limit can be applied at virtually any stage of the analysis, i.e. directly to the free energy functional but also to the results of the bifurcation analysis. Even the numerical results show a rather clear regime where segmented chains behave as wormlike chains. This allows us to use the concept of segmented chains 'all the way' and interpret the results at the end in terms of wormlike chains. This property will also be used in Part 2.

Appendix

When coupling constant J, in case of nearest neighbour bending potential (Eq. 3.3) becomes very large (i.e. in the wormlike chain limit in section 3.2.3) the typical angles between successive segments in the chains become very small. In this appendix, we show the limiting behaviour of the flexibility integration in case of $\beta_{\mathrm{B}}J \to \infty$ (Eq. 3.41) to be

$$w_0^{-1} \int d\hat{\omega}' w(\hat{\omega}, \hat{\omega}') g(\hat{\omega}') \to \left(1 + \tfrac{1}{2} \left(\beta_{\mathrm{B}}J\right)^{-1} \Delta_{\hat{\omega}}\right) g(\hat{\omega}), \qquad (3.83)$$

with $\Delta_{\hat{\omega}}$ the Laplace operator on a sphere, w_0 the first Legendre coefficient of $w(\hat{\omega}, \hat{\omega}') = \exp(\beta_{\mathrm{B}} J \hat{\omega} \cdot \hat{\omega}')$ (see Eq. 3.52) and $g(\hat{\omega})$ a sufficiently smooth function (in our case: $\exp(-\beta_{\mathrm{B}} H(\hat{\omega})) q_m^{(\pm)}(\hat{\omega})$).

Rather than focus on the specific bending potential of our model, we prove that the property in question holds for any weight function that is symmetric and sufficiently peaked around a preferred direction. Consider thereto a function $\psi_{\varepsilon, \hat{z}}(\hat{\omega})$ on the unit sphere, whose definition involves a parameter ε and a preferred axis denoted by the unit vector $\hat{z}$, that satisfies the following conditions:

(1) It is normalized: $\displaystyle\int d\hat{\omega} \psi_{\varepsilon, \hat{z}}(\hat{\omega}) = 1$

(2) It is invariant under rotations $\mathbf{R}_{\hat{z}}(\gamma)$ over an arbitrary angle γ around the preferred axis $\hat{z}$: $\psi_{\varepsilon, \hat{z}}(\mathbf{R}_{\hat{z}}(\gamma)\hat{\omega}) = \psi_{\varepsilon, \hat{z}}(\hat{\omega})$

(3) For small values, the parameter ε measures the second moment of $\psi_{\varepsilon, \hat{z}}(\hat{\omega})$ with respect to deviations in polar angle from the preferred axis: $\lim_{\varepsilon \downarrow 0} \varepsilon^{-1} \int d\hat{\omega} \psi_{\varepsilon, \hat{z}}(\hat{\omega}) \times \theta^2 = 1$ with θ and the angle between $\hat{z}$ and $\hat{\omega}$.

We now prove that:

$$\lim_{\varepsilon \downarrow 0} \varepsilon^{-1} \left\{ \int d\hat{\omega} \psi_{\varepsilon, \hat{z}}(\hat{\omega}) g(\hat{\omega}) - g(\hat{z}) \right\} = \tfrac{1}{4} \Delta_{\hat{z}} g(\hat{z}) \tag{3.84}$$

for g sufficiently smooth.

First, we expand the function g in spherical harmonics with $\hat{z}$ as the polar axis,

$$g(\hat{\omega}) = \sum_{n=0}^{\infty} \sum_{m=-n}^{n} g_{n,m} Y_{n,m}(\hat{\omega}|\hat{z}), \tag{3.85}$$

The spherical harmonics are explicitly given by

$$Y_{n,m}(\hat{\omega}|\hat{z}) = (-1)^m \left[\frac{2n+1}{4\pi} \frac{(n-m)!}{(n+m)!} \right]^{1/2} \mathrm{e}^{im\phi} P_n^m(\cos\theta) \quad m \geq 0,$$

$$Y_{n,-m} = (-1)^m Y_{n,m}^*$$

where the polar angle is defined through $\cos\theta = \hat{\omega} \cdot \hat{z}$ and the azimuthal angle ϕ is defined with respect to an arbitrary axis $\hat{x} \perp \hat{z}$. Using this expansion we can write

$$\int d\hat{\omega} \psi_{\varepsilon, \hat{z}}(\hat{\omega}) g(\hat{\omega}) = \sum_{n=0}^{\infty} \sum_{m=-n}^{n} g_{n,m} \int d\hat{\omega} \psi_{\varepsilon, \hat{z}}(\hat{\omega}) Y_{n,m}(\hat{\omega}|\hat{z}). \tag{3.86}$$

By condition 2. above on $\psi_{\varepsilon, \hat{z}}$ we have for arbitrary γ

$$\int d\hat{\omega} \psi_{\varepsilon, \hat{z}}(\hat{\omega}) Y_{n,m}(\hat{\omega}|\hat{z}) = \int d\hat{\omega} \psi_{\varepsilon, \hat{z}}(\mathbf{R}_{\hat{z}}(\gamma)\hat{\omega}) Y_{n,m}(\hat{\omega}|\hat{z}) =$$

$$\int d\hat{\omega}' \psi_{\varepsilon, \hat{z}}(\hat{\omega}') Y_{n,m}(\mathbf{R}_{\hat{z}}^{-1}(\gamma)\hat{\omega}'|\hat{z}) = \mathrm{e}^{-im\gamma} \int d\hat{\omega}' \psi_{\varepsilon, \hat{z}}(\hat{\omega}') Y_{n,m}(\hat{\omega}'|\hat{z}), \tag{3.87}$$

so that

$$\int d\hat{\omega} \psi_{\varepsilon, \hat{z}}(\hat{\omega}) Y_{n,m}(\hat{\omega}|\hat{z}) = \delta_{m,0} \sqrt{\frac{2n+1}{4\pi}} \int d\hat{\omega} \psi_{\varepsilon, \hat{z}}(\hat{\omega}) P_n(\hat{\omega} \cdot \hat{z}). \tag{3.88}$$

Next, we exploit the fact that for small ε the angle θ between $\hat{\omega}$ and $\hat{z}$ is very small. In that limit the Legendre polynomials have the form $P_n(\cos\theta) = 1 + \alpha_n\theta^2 + \mathcal{O}(\theta^4)$. From the recursive equality for Legendre polynomials ([58], 8.914),

$$(n+1)P_{n+1}(\cos\theta) - (2n+1)\cos\theta P_n(\cos\theta) + nP_{n-1}(\cos\theta) = 0 \tag{3.89}$$

it is straightforward to prove that $\alpha_n = -\frac{1}{4}n(n+1)$. We also recall the identity

$$\delta_{m,0} = \sqrt{\frac{4\pi}{2n+1}}Y_{n,m}(\hat{z}|\hat{z}), \tag{3.90}$$

which leads to the result

$$\int d\hat{\omega}\,\psi_{\varepsilon,\hat{z}}(\hat{\omega})Y_{n,m}(\hat{\omega}|\hat{z}) = \left\{1 - \frac{1}{4}n(n+1)\varepsilon + \mathcal{O}\left(\varepsilon^2\right)\right\}Y_{n,m}(\hat{z}|\hat{z})$$

$$= Y_{n,m}(\hat{z}|\hat{z}) + \frac{1}{4}\varepsilon\Delta_{\hat{z}}Y_{n,m}(\hat{z}|\hat{z}) + \mathcal{O}\left(\varepsilon^2\right) \tag{3.91}$$

where we used the fact that the spherical harmonics are eigenfunctions of the spherical Laplacian. Insertion into Eq. (3.86) and resumming the expansion then directly leads to the desired result

$$\int d\hat{\omega}\,\psi_{\varepsilon,\hat{z}}(\hat{\omega})g(\hat{\omega}) = g(\hat{z}) + \frac{1}{4}\varepsilon\Delta_{\hat{z}}g(\hat{z}) + \mathcal{O}(\varepsilon^2) \tag{3.92}$$

We now make the identification of $w_0^{-1}w(\hat{\omega}, \hat{z})$ with $\psi_{\varepsilon,\hat{z}}(\hat{\omega})$ and of the small parameter ε with $2(\beta_B J)^{-1}$ (as $\langle\theta^2\rangle_w \approx 2(\beta_B J)^{-1}$). Ignoring the higher order terms then immediately yields Eq. (3.83).

4

BIAXIAL POLYMERS

We construct a theory for nematic ordering in a fluid of biaxial polymers. This is a combination of the theory for wormlike polymers (by Khokhlov and Semenov) and the theory for biaxial particles (by Mulder). We use the approach of segmented chains developed in Chapter 3. The I-N bifurcation density is computed as a function of 4 model parameters.

4.1. Introduction

Model fluids of hard particles of great anisotropy (length $\gg$ width) are seen to have an isotropic-to-nematic (I-N) phase transition on increasing density [7]. In most cases, it suffices to use hard rods with cylindrical symmetry around their long axis and as a consequence, the resulting nematic phase is uniaxial (UN), which means it is symmetric around the nematic director. To investigate more realistic situations, one could choose to drop the cylindrical symmetry of the molecules, and study the effect of 'molecular biaxiality' on the phase behaviour. Biaxial particles are in principle capable of forming a biaxial nematic phase (BN, with two nematic directors), where the long axis of a molecule orders with respect to one and a short axis with respect to another director. For rods with small biaxiality, the system still prefers the UN phase and the BN phase is postponed to high densities (where it is usually preceded by a spatially ordered phase like a smectic). Opposed to rods, which have one long axis and two short axes, disks have two long axes and one short axis. A fluid of disks also prefers the UN phase, with the essential difference that the *short* axis of a disk orders with respect to the nematic director. If we start with a rod and continuously deform it into a disk (by increasing one of the two shorter axes until it is as large as the long axis), we find that the preferred nematic phase changes from UN (with ordering of the long axis) to UN (with ordering of the short axis). Somewhere in between (halfway this process), where the ordering of long and short axes is equally strong, we expect to find a direct transition to the biaxial nematic.

The BN phase was first predicted by Freiser [61], in 1970, who considered the Maier-Saupe model for biaxial molecules using an extra (biaxial) order parameter. Later, Alben [62] used a Landau approach and calculated (what now seems to be) the general phase behaviour as a function of molecule asymmetry. He established that there is an intermediate particle-shape (between rodlike and disklike) where the system undergoes a second-order transition from I to BN. Straley [63] was the first to use the full set of four order parameters to describe BN behaviour. In the eighties, Mulder used bifurcation

analysis [64, 65] to solve Onsager's model for a specific kind of long biaxial particles, called spheroplatelets. Monte Carlo simulations on systems of biaxial molecules were done by Allen [66] confirming the general phase diagram predicted by Refs. [62, 63]. Sarman [67] found a BN by computing diffusion coefficients and autocorrelation functions in fluids of biaxial particles, using molecular dynamics simulations.

The first experimental observation of a biaxial phase was reported in 1980, by Yu and Saupe [68], in a system of micelle-forming amphiphiles. More work and claims followed, on similar amphiphilic systems as well as on thermotropic liquid crystals. A question which complicates the analysis of micellar systems is the ability of the micelles to deform, which may have a pronounced effect on the phase diagram [69]. In case of thermotropic liquid crystals at least some of the initial claims for low-molecular weight systems have been called into doubt later [70, 71] and the search continues [72]. For liquid crystalline polymers, BN phases have been reported [73, 74], but also here, the evidence is weak [27].

Parallel to the above, a lot of effort has gone into finding the BN phase in mixtures of rods and disks. Putting few rods in a UN of disks will cause the rods to order perpendicular to the director, and vice versa, in a UN of rods, few disks also order perpendicular to the director. For intermediate concentrations, a BN phase can form, although demixing into two coexisting nematic phases (one rod-rich and one disk-rich) can interfere. Experimentally, no BN phase in these systems has been reported yet. Some references are [75, 76, 77, 78].

Summarizing, the biaxial nematic phase is far from a common phenomenon. Although both theory and simulations predict its existence in fluids of biaxial molecules as well as mixtures of rods and disks, experimental confirmation of these results has proven extremely hard. Some systems of sidechain LC polymers seem to exhibit some degree of (local) biaxial ordering [73, 74]. Side chain polymers consist of a backbone and side chains hinged more or less perpendicular to it. These side chains can have an orientational coupling with neighbouring sidechains causing the polymers to be effectively lath-like (biaxial). For long backboned polymers, flexibility of the laths (bending, twisting) can have a pronounced effect on the phase behaviour. The interplay between molecular flexibility and biaxiality is the topic of this chapter.

We construct an Onsager-like theory for orientational ordering in a fluid of impenetrable biaxial (lath-like) but (somewhat) flexible polymers. The resulting theory is a combination of Khokhlov and Semenov's theory for nematic order in wormlike chains [32, 33] and Mulder's analysis of fluids of long platelets [64]. The approach we use is similar to that of chapter 3; i.e. we start with segmented chains which have flexibility located at the joints (Sec. 4.2) and later take the limit where the segments become very small, their number and the joint stiffnesses very large, thus obtaining continuously flexible chains (Sec. 4.3). Using bifurcation analysis, we calculate the I-N bifurcation density. We focus on biaxialities comparable to the thickness of the polymer, for which the resulting phase is always uniaxial. The resulting theory for continuously flexible polymers (which we call ribbonlike polymers) has 4 (dimensionless) model parameters: the effective biaxiality of the polymer Δ/d and three persistence lengths, corresponding to one twisting $P_{1,2}/L$ and two bending modes $P_{1,3}/L, P_{2,3}/L$.
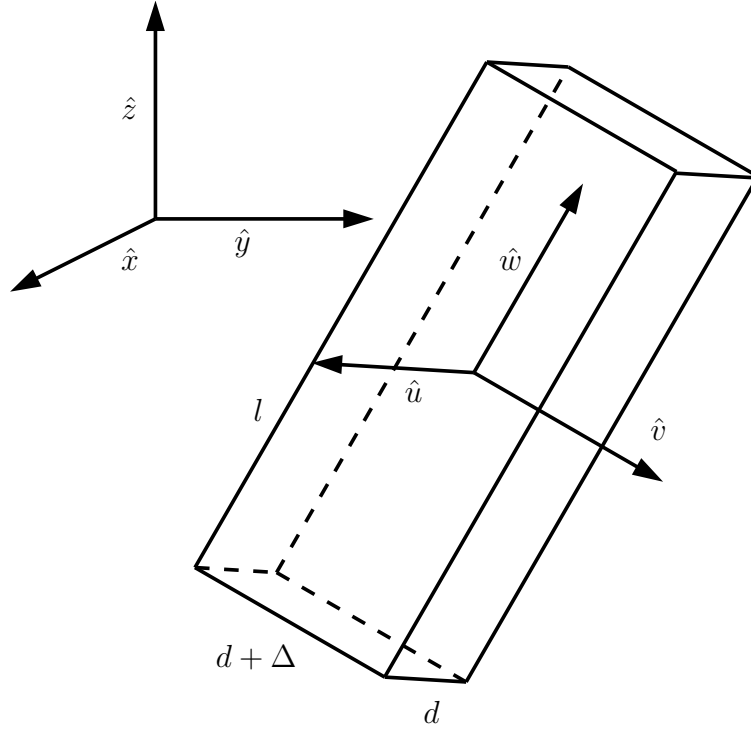
FIGURE 4.1. A biaxial segment.

4.2. Segmented Biaxial Chains

4.2.1. The Model. We consider a fluid of N interacting chains in a volume V. The chains are discrete and consist of M segments and every segment has a label $m \in \{1 \cdots M\}$. The segments are modeled as platelets which have dimensions $d, d+\Delta$ and l with $d, \Delta \ll l$ (see Fig. 4.1) and are connected to their neighbours with the sides of their smallest surfaces (i.e. with dimensions $d, d + \Delta$, see Fig. 4.2). The total length of the chain is $L = Ml$. Every segment has a $(\hat{u}, \hat{v}, \hat{w})$-frame attached to it, with $\hat{u}$ pointing along the d-side, $\hat{v}$ along the $(d + \Delta)$-side and $\hat{w}$ along the l-side. The orientation of segment m is Ω_m and is uniquely described in terms of the Euler angles $(\alpha_m, \beta_m, \gamma_m)$ with respect to the lab-fixed frame $(\hat{x}, \hat{y}, \hat{z})$. The Euler angles can be visualized as three successive rotations around axes of the segment-fixed frame, with two successive axes not around the same axis, and starting from the situation where $(\hat{u}_m, \hat{v}_m, \hat{w}_m) = (\hat{x}, \hat{y}, \hat{z})$. In our case, we take the first and the third rotation, α_m and γ_m, around the $\hat{w}_m$-axis and the second, β_m, around the $\hat{v}_m$-axis, and positive when the rotation is counterclockwise (which is the same as in Refs. [79, 80]). Finally, $\alpha_m, \gamma_m \in [0, 2\pi]$ and $\beta_m \in [0, \pi]$. The conformation of each chain is $\boldsymbol{\Omega}$ and is specified by all orientations of the individual segments, $\boldsymbol{\Omega} = \{\Omega_1, \cdots, \Omega_M\}$.

Within each chain, we assume there is a conformation-dependent energy $U(\boldsymbol{\Omega})$ which is high when the conformation is rather bended or twisted (or both) and low when it is not. To this end, we assume a potential between successive segments, u,

$$U(\boldsymbol{\Omega}) = \sum_{m=1}^{M-1} u(\Omega_m, \Omega_{m+1}), \tag{4.1}$$
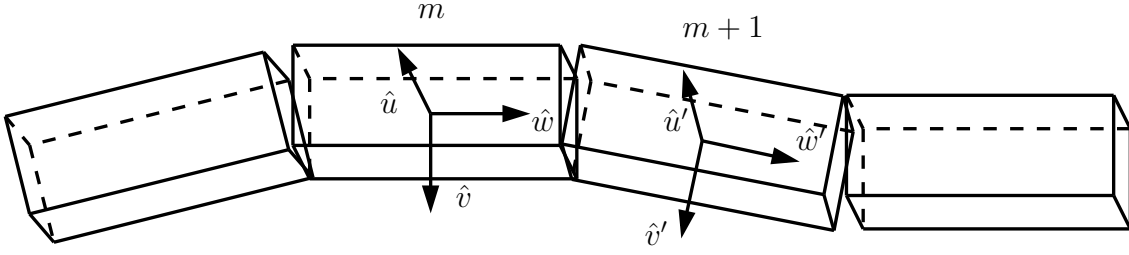
FIGURE 4.2. A chain of biaxial segments.

which opposes bending and twisting in a generic fashion,

$$
\begin{aligned}
u(\Omega, \Omega') = & - J_1 \hat{u} \cdot \hat{u}' - J_2 \hat{v} \cdot \hat{v}' - J_3 \hat{w} \cdot \hat{w}' \\
= & - J_1 (\cos\alpha \cos\beta \cos\gamma - \sin\alpha \sin\gamma) \\
& - J_2 (\cos\alpha \cos\gamma - \cos\beta \sin\alpha \sin\gamma) - J_3 \cos\beta.
\end{aligned}
\tag{4.2}
$$

in which $(\Omega)^{-1}\Omega' = \tilde{\Omega} = (\alpha, \beta, \gamma)$ is the Cartesian rotation to go from the unprimed to the primed frame and is represented by a matrix. The parameters J_1, J_2 and J_3 are the coupling parameters between the corresponding unit vectors of the two segments. An important feature of the potential is that for small angles the interaction is locally harmonic (we will use this later).

In interaction with other chains, we model the molecules as being hard objects, so the potential is infinity when the chains overlap, and zero when they do not. Using the second virial approximation and considering only spatially homogeneous phases, the quantity which is most suitable of describing the interaction is the volume which a chain cannot enter due to the presence of another. This is the excluded volume, $\mathcal{E}(\boldsymbol{\Omega}, \boldsymbol{\Omega}')$, and is a function of the conformations of both chains. This excluded volume between two chains, we approximate as being the sum of excluded volumes of the segments of which they are composed,

$$
\mathcal{E}(\boldsymbol{\Omega}, \boldsymbol{\Omega}') = \sum_{m,m'=1}^{M} e(\Omega_m, \Omega'_{m'}).
\tag{4.3}
$$

The last approximation is discussed to some extend in Chap. 3. The excluded volume between two platelets (which the segments are) is calculated by Mulder (see Ref. [64]) and is (in leading order of l^2)

$$
\begin{aligned}
e(\Omega, \Omega') & = 2l^2 d \left[\sqrt{1 - (\hat{w} \cdot \hat{w}')^2} + \frac{\Delta}{2d} \left(|\hat{w} \cdot \hat{u}'| + |\hat{u} \cdot \hat{w}'| \right) \right] \\
& = 2l^2 d \sin\beta \left[1 + \frac{\Delta}{2d} \left(|\cos\alpha| + |\cos\gamma| \right) \right].
\end{aligned}
\tag{4.4}
$$

Here, again, $(\Omega)^{-1}\Omega' = \tilde{\Omega} = (\alpha, \beta, \gamma)$. From the excluded volume, we see that if the segments have no biaxiality and $\Delta = 0$, we just have ordinary Onsager rods (although the successive-segment potential, Eq. 4.2, still includes bending as well as twisting). The

other limit, where $d = 0$ and Δ remains finite, is new and the segments correspond to infinitely thin platelets.

4.2.2. The Stationarity Equation. The free energy functional for a fluid of hard molecules in the second virial approximation with no spatial order is given by (see Chap. 3),

$$\frac{\beta_{\mathrm{B}}\mathcal{F}[f]}{N} = \log\left(\rho\mathcal{V}_{\mathrm{T}}\right) + \int d\mathbf{\Omega} f(\mathbf{\Omega})\left[\log f(\mathbf{\Omega}) - 1\right] + \beta_{\mathrm{B}}\int d\mathbf{\Omega} f(\mathbf{\Omega})U(\mathbf{\Omega})$$

$$+ \tfrac{1}{2}\rho\int d\mathbf{\Omega}d\mathbf{\Omega}' f(\mathbf{\Omega})f(\mathbf{\Omega}')\mathcal{E}(\mathbf{\Omega},\mathbf{\Omega}'). \tag{4.5}$$

$\beta_{\mathrm{B}} = 1/k_{\mathrm{B}}T$ is the Boltzmann factor, with T the temperature and k_{B} Boltzmann's constant. $\rho = N/V$ is the number density of chains and $\mathcal{V}_{\mathrm{T}}$ the "thermal volume". The function $f(\mathbf{\Omega})$ is the conformational distribution function (CDF) and is the normalized probability ($\int d\mathbf{\Omega} f(\mathbf{\Omega}) = 1$) of finding a chain with conformation $\mathbf{\Omega}$. Further, $\int d\mathbf{\Omega} = \int d\Omega_1 \cdots d\Omega_M$ and $\int d\Omega = \int_0^{2\pi} d\alpha \int_0^{\pi} d\beta \sin\beta \int_0^{2\pi} d\gamma$. In the isotropic phase, the second virial approximation (or Onsager approximation) is exact when $l \gg d, \Delta$ with $l^2 d$ and $l^2\Delta$ finite.

In thermodynamic equilibrium, the free energy reaches a minimum and the functional is stationary. Therefore, we consider the variation of Eq. 4.5 with respect to the CDF,

$$\frac{\delta}{\delta f(\mathbf{\Omega})}\frac{\beta_{\mathrm{B}}\mathcal{F}}{N} - \beta_{\mathrm{B}}\mu = 0 \tag{4.6}$$

with the chemical potential μ playing the role of Lagrange multiplier needed to enforce normalization. Eliminating μ from Eq. 5.2 yields the stationarity equation,

$$f(\mathbf{\Omega}) = Z^{-1}[f]\exp\left[-\beta_{\mathrm{B}}U(\mathbf{\Omega}) - \rho\int d\mathbf{\Omega}' f(\mathbf{\Omega}')\mathcal{E}(\mathbf{\Omega},\mathbf{\Omega}')\right] \tag{4.7}$$

in which Z is the factor due to normalization,

$$Z[f] = \int d\mathbf{\Omega}\exp\left[-\beta_{\mathrm{B}}U(\mathbf{\Omega}) - \rho\int d\mathbf{\Omega}' f(\mathbf{\Omega}')\mathcal{E}(\mathbf{\Omega},\mathbf{\Omega}')\right]. \tag{4.8}$$

The single-segment orientational distribution function (ODF) of the mth segment can be defined by integrating the conformational distribution function over all degrees of freedom but the mth,

$$f_m(\Omega_m) = \int \prod_{k\neq m} d\Omega_k f(\mathbf{\Omega}). \tag{4.9}$$

The ODF is normalized in the same way, $\int d\Omega_m f_m(\Omega_m) = 1$. Inserting the expressions for U and $\mathcal{E}$ (Eqs. 4.1 to 4.4) in Eq. 4.7 and using Eq. 4.9, yields a set of stationarity equations,

$$f_m(\Omega_m) = Z^{-1}\int \prod_{k\neq m} d\Omega_k$$

$$\times \prod_{k=1}^{M-1} w(\Omega_k,\Omega_{k+1})\prod_{k=1}^{M}\exp\left[-\rho\sum_{k'=1}^{M}\int d\Omega'_{k'}e(\Omega_k,\Omega'_{k'})f_{k'}(\Omega'_{k'})\right], \tag{4.10}$$

in which

$$w(\Omega_k, \Omega_{k+1}) = \exp\left[-\beta_B u(\Omega_k, \Omega_{k+1})\right]. \tag{4.11}$$

In the analysis we present in here, we will only need the average ODF (with respect to the whole chain), $f^{(\text{av})}(\Omega) = \frac{1}{M}\sum_{m=1}^{M} f_m(\Omega)$. Then, the stationarity equations become

$$f^{(\text{av})}(\Omega) = \frac{1}{MZ}\sum_{m=1}^{M}\int\prod_{k=1}^{M} d\Omega_k \delta(\Omega - \Omega_m)$$

$$\times \prod_{k=1}^{M-1} w(\Omega_k, \Omega_{k+1})\prod_{k=1}^{M}\exp\left[-\rho M\int d\Omega' e(\Omega_k, \Omega')f^{(\text{av})}(\Omega')\right], \quad (4.12)$$

in which $\delta(\Omega - \Omega_m)$ is the Dirac delta function.

It is straightforward to show that the isotropic distribution, $f_{\text{iso}}^{(\text{av})} = 1/8\pi^2$, is always a solution to Eq. 4.12,

$$\rho M\int d\Omega' e(\Omega_k, \Omega')f_{\text{iso}}^{(\text{av})} = \frac{\rho M e_0^{0,0}}{8\pi^2} \tag{4.13}$$

and

$$Z_{\text{iso}} = 8\pi^2 \left(w_0^{0,0}\right)^{M-1}\exp[-\rho M^2 e_0^{0,0}/8\pi^2]. \tag{4.14}$$

Here, $e_0^{0,0}$ and $w_0^{0,0}$ are $\int d\Omega e(\Omega)$ and $\int d\Omega w(\Omega)$, respectively (as we will see again next subsection).

4.2.3. Symmetries, Expansions and Order Parameters. In general, any function of the Euler angles $\Omega = (\alpha, \beta, \gamma)$ can be expanded in the rotation matrix elements $\mathcal{D}_{i,j}^n(\Omega)$ (we use labels n, i, j because l and m are used elsewhere). In case of the mean ODF, this becomes

$$f^{(\text{av})}(\Omega) = \sum_{n=0}^{\infty}\sum_{i,j=-n}^{n}\frac{2n+1}{8\pi^2}a_n^{i,j}\mathcal{D}_{i,j}^n(\Omega), \tag{4.15}$$

and the coefficients are given by

$$a_n^{i,j} = \int d\Omega f^{(\text{av})}(\Omega)\left(\mathcal{D}_{i,j}^n(\Omega)\right)^*. \tag{4.16}$$

The asterisk refers to the complex conjugate and for a list of the properties of these matrix elements and the relations between them, we refer to Ref. [80]. Next, we investigate the symmetries present in this system, as these will simplify the analysis following. The phase we are interested in, the nematic phase, has inversion symmetry (symmetry operation I) as well as symmetry with respect to the elements of the rotation group $D_2 = \{1, R_{\hat{x}}(\pi), R_{\hat{y}}(\pi), R_{\hat{z}}(\pi)\}$ in which the operations $R_\sigma(\pi)$ are rotations of π around the σ-axis. This means that if $g \in I \otimes D_2 = D_{2h}$, the ODF's are invariant under the operation of g in the following way: $f(\Omega) = f(g\Omega)$. The same symmetry holds for the segments of the chain, i.e. the platelets are also invariant under the operation $g \in D_{2h}$; $f(\Omega) = f(\Omega g)$. Using these symmetries, it is not difficult to show that only the elements $\mathcal{D}_{i,j}^n$ for which n, i, j are even contribute and that furthermore

$a_n^{i,j} = a_n^{-i,j} = a_n^{i,-j} = a_n^{-i,-j}$. Having observed these symmetries, we proceed by combining the $\mathcal{D}_{i,j}^n$-functions and define

$$Q_{i,j}^n = \left(\tfrac{1}{2}\sqrt{2}\right)^{2+\delta_{i,0}+\delta_{j,0}} \left(\mathcal{D}_{i,j}^n + \mathcal{D}_{-i,j}^n + \mathcal{D}_{i,-j}^n + \mathcal{D}_{-i,-j}^n\right). \tag{4.17}$$

The factor $\tfrac{1}{2}\sqrt{2}$ is to obtain correct normalization and the $\delta_{i,j}$ are Kronecker delta functions. Eq. 4.15 can then be written as

$$f^{(\mathrm{av})}(\Omega) = \sum_{n=0}^{\infty} \sum_{i,j=0}^{n} \frac{2n+1}{8\pi^2} q_n^{i,j} Q_{i,j}^n(\Omega), \tag{4.18}$$

with all n, i, j only assuming even (positive) values. Similar to Eq. 4.16, the coefficients become

$$q_n^{i,j} = \int d\Omega f^{(\mathrm{av})}(\Omega) Q_{i,j}^n(\Omega). \tag{4.19}$$

The $Q_{i,j}^n$-functions satisfy the orthogonality conditions,

$$\int d\Omega Q_{i,j}^n(\Omega) Q_{i',j'}^{n'}(\Omega) = \frac{8\pi^2}{2n+1} \delta_{n,n'} \delta_{i,i'} \delta_{j,j'}. \tag{4.20}$$

as well as being a closed set under composite rotations $\Omega'^{-1}\Omega$ (first Ω'^{-1} and then Ω) in the sense that

$$\int d\Omega' Q_{i,j}^n(\Omega') Q_{i',j'}^{n'}(\Omega'^{-1}\Omega) = \frac{8\pi^2}{2n+1} \delta_{n,n'} \delta_{j,i'} Q_{i,j'}^n(\Omega). \tag{4.21}$$

The excluded volume of two platelets has the same symmetry as the ODF (for with $g, g' \in D_{2h}$, it holds that $e(\Omega'^{-1}\Omega) = e(g'^{-1}\Omega'^{-1}\Omega g)$). This yields the following expansion

$$e(\Omega) = \sum_{n=0}^{\infty} \sum_{i,j=0}^{n} \frac{2n+1}{8\pi^2} e_n^{i,j} Q_{i,j}^n(\Omega), \tag{4.22}$$

with again only even (and positive) n, i, j contributing and a similar relation as Eq. 4.19 for the coefficients. Moreover, the excluded volume has an extra symmetry (with respect to the ODF) due to the invariance under the interchange of two particles: $e_n^{i,j} = e_n^{j,i}$. In the bifurcation analysis, which is the topic of the next subsection, we will need the following integral,

$$\int d\Omega' e(\Omega'^{-1}\Omega) Q_{i,j}^n(\Omega') = \sum_{j'=0}^{n} e_n^{j,j'} Q_{i,j'}^n(\Omega), \tag{4.23}$$

which can be derived by combining Eqs. 4.21 and 4.22.

The Boltzmann factor w of two successive segments in the chain has lower symmetry than the excluded volume. It is polar, and as a consequence, there is no inversion symmetry and it is not invariant under the D_2-rotations. The symmetries, which are present, are invariance under $(\alpha, \beta, \gamma) \to (-\alpha, \beta, -\gamma)$, $(\alpha, \beta, \gamma) \to (\gamma, \beta, \alpha)$ and exchange of the two particles, $(\alpha, \beta, \gamma) \to (-\gamma, -\beta, -\alpha)$. Consequently, in the expansion of w,

$w_n^{-i,-j} = w_n^{i,j}$, $w_n^{i,j} = w_n^{j,i}$ and only terms with even $i + j$ contribute,

$$w(\Omega) = \sum_{n=0}^{\infty} \frac{2n+1}{8\pi^2} \sum_{i=-n}^{n} \sum_{j=0}^{n} (\tfrac{1}{2})^{\delta_{j,0}} w_n^{i,j} \left(\mathcal{D}_{i,j}^n(\Omega) + \mathcal{D}_{-i,-j}^n(\Omega) \right). \tag{4.24}$$

The coefficients $w_n^{i,j}$ are given by a relation similar to Eq. 4.16. In the bifurcation analysis, which is the subject of the next subsection, we need the following integral, [1]

$$\int d\Omega w(\Omega'^{-1}\Omega) Q_{i,j}^n(\Omega') = \sum_{j'=0}^{n} W_n^{j,j'} Q_{i,j'}^n(\Omega), \tag{4.25}$$

in which the coefficients $W_n^{j,j'}$ are given by

$$W_n^{j,j'} = \int d\Omega w(\Omega) Q_{j,j'}^n(\Omega). \tag{4.26}$$

These coefficients are also zero for odd $j + j'$. The relation between the two coefficients $w_n^{i,j}$ and $W_n^{i,j}$ is

$$W_n^{i,j} = \left(\tfrac{1}{2}\sqrt{2} \right)^{\delta_{i,0}+\delta_{j,0}} \left(w_n^{i,j} + w_n^{-i,j} \right). \tag{4.27}$$

In concluding this subsection, we introduce the order parameters necessary to distinguish between the isotropic and the nematic phases. Straley [63] and Mulder [64] have shown that for biaxial particles it is necessary and sufficient to use four order parameters. Then, it makes sense to use the lowest order coefficients in the ODF expansion different in the isotropic and the nematic phase (of which there are four). These are

$$q_2^{i,j} = \int d\Omega f^{(\mathrm{av})}(\Omega) Q_{i,j}^2(\Omega), \tag{4.28}$$

in which both i and j can be 0 or 2. These are also the order parameters Straley and Mulder use. In order to be complete, we list the Q^2-functions here

$$\begin{aligned}
Q_{0,0}^2(\Omega) &= \tfrac{1}{2}(3(\hat{z} \cdot \hat{w})^2 - 1) = \tfrac{1}{2}(3\cos^2\beta - 1), \\
Q_{2,0}^2(\Omega) &= \tfrac{1}{2}\sqrt{3}\left((\hat{y} \cdot \hat{w})^2 - (\hat{x} \cdot \hat{w})^2\right) = \tfrac{1}{2}\sqrt{3}\sin^2\beta\cos 2\alpha, \\
Q_{0,2}^2(\Omega) &= \tfrac{1}{2}\sqrt{3}\left((\hat{z} \cdot \hat{v})^2 - (\hat{z} \cdot \hat{u})^2\right) = \tfrac{1}{2}\sqrt{3}\sin^2\beta\cos 2\gamma, \\
Q_{2,2}^2(\Omega) &= \tfrac{1}{2}\left((\hat{x} \cdot \hat{u})^2 - (\hat{y} \cdot \hat{u})^2 + (\hat{y} \cdot \hat{v})^2 - (\hat{x} \cdot \hat{v})^2\right) \\
&= \tfrac{1}{2}(1 + \cos^2\beta)\cos 2\alpha\cos 2\gamma - \cos\beta\sin 2\alpha\sin 2\gamma. \tag{4.29}
\end{aligned}$$

In the isotropic phase all order parameters are identically zero. In the uniaxial nematic phase, the order parameters $q_2^{0,0}$ and $q_2^{0,2}$ are non-zero whereas the other two, $q_2^{2,0}$ and $q_2^{2,2}$, are zero (due to the fact that the $\hat{x}$- and $\hat{y}$-axes are equivalent). In the biaxial nematic phase all four order parameters are non-zero.

---

[1]Eq. 4.25 has been derived using $\int d\Omega' \mathcal{D}_{i,j}^n(\Omega') \mathcal{D}_{i',j'}^{n'}(\Omega'^{-1}\Omega) = \frac{8\pi^2}{2n+1}\delta_{n,n'}\delta_{j,i'}\mathcal{D}_{i,j'}^n(\Omega)$ We would like the reader to note that although w itself cannot be expanded in $Q_{i,j}^n$'s, it does map $Q_{i,j}^n$ onto $\{Q_{i,0}^n, Q_{i,2}^n, \cdots, Q_{i,n}^n\}$ (when it is used as an integration kernel, Eq. 4.25).

4.2.4. Bifurcation Analysis. In this subsection, we will use a linear stability analysis to analytically determine the I-N bifurcation density. At the bifurcation point, the nematic solution branches off the isotropic one which becomes thereafter (for higher densities) unstable (Refs.[37, 65]). Consequently, the bifurcation (or spinodal) density can be found by substituting in the stationarity equation the isotropic solution with small nematic perturbations. Then, one can linearize the equation around the isotropic distribution (assuming these nematic perturbations to be small) and so obtain a linear eigenvalue equation. The (lowest) density for which this eigenvalue equation can be solved is the bifurcation density.

The isotropic distribution with nematic perturbations is simply

$$f^{(\mathrm{av})}(\Omega) = \frac{1}{8\pi^2} + \varepsilon\chi(\Omega), \tag{4.30}$$

in which ε is an infinitesimally small parameter and the function χ is normalized (necessarily) as follows: $\int d\Omega\chi(\Omega) = 0$. Inserting Eq. 4.30 in the stationarity equation Eq. 4.12, and linearizing with respect to ε, to zeroth order we re-obtain the isotropic results (below Eq. 4.12). To first order in ε, we get

$$\chi(\Omega) = -\frac{\rho}{8\pi^2} \sum_{m,m'=1}^{M} \int \prod_{k=1}^{M} d\Omega_k \delta(\Omega - \Omega_m)$$

$$\times \prod_{k=1}^{M-1} \frac{w(\Omega_k, \Omega_{k+1})}{w_0^{0,0}} \int d\Omega' e(\Omega_{m'}, \Omega')\chi(\Omega'). \tag{4.31}$$

This (rather messy looking) linear integral equation is the bifurcation equation. On the basis of previous results, concerning Onsager rods, we expect the system to become unstable for the first time with respect to the $n = 2$-mode,

$$\chi(\Omega) = \sum_{i,j\in\{0,2\}} \frac{5}{8\pi^2} q_2^{i,j} Q_{i,j}^2(\Omega). \tag{4.32}$$

Substitution of this in Eq. 4.31 leaves us with a chain of integrals to be evaluated. The first one is performed using Eq. 4.23,

$$\int d\Omega' e(\Omega'^{-1}\Omega_{m'})\chi(\Omega') = \sum_{i,j,s} \frac{5}{8\pi^2} q_2^{i,j} e_2^{j,s} Q_{i,s}^2(\Omega_{m'}), \tag{4.33}$$

and the summation is over all $i, j, s \in \{0, 2\}$. The integrals with w as a kernel act as a chain in that they "pass on" the perturbation χ at segment m' to segment m. Suppose for now that $m > m'$. Then, we are left with $m - m'$ w-integrals and they are all of the type of Eq. 4.25. The first one yields

$$\int d\Omega_{m'} \frac{w(\Omega_{m'}^{-1}\Omega_{m'+1})}{w_0^{0,0}} \int d\Omega' e(\Omega'^{-1}\Omega_{m'})\chi(\Omega') = \sum_{i,j,s,t} \frac{5}{8\pi^2} q_2^{i,j} e_2^{j,s} \frac{W_2^{s,t}}{w_0^{0,0}} Q_{i,t}^2(\Omega_{m'+1})$$

$$\tag{4.34}$$

From the symmetry analysis in the preceding subsection, we know that the elements $W_2^{s,t}$ are non-zero when $s + t$ is even. Recalling from Eq. 4.33 that s only assumes even

values, this must also be the case for t. So, again the summation is over $i, j, s, t \in \{0, 2\}$. In order to obtain a more convenient notation, we define

$$\sigma_2^{s,t} = W_2^{s,t}/w_0^{0,0}, \tag{4.35}$$

and

$$\mathbf{q}_2^i = \begin{bmatrix} q_2^{i,0} \\ q_2^{i,2} \end{bmatrix} \quad \text{and} \quad \mathbf{Q}_i^2(\Omega) = \begin{bmatrix} Q_{i,0}^2(\Omega) \\ Q_{i,2}^2(\Omega) \end{bmatrix} . \tag{4.36}$$

Then, we can rewrite Eq. 4.34,

$$\int d\Omega_{m'} \frac{w(\Omega_{m'}^{-1}\Omega_{m'+1})}{w_0^{0,0}} \int d\Omega' e(\Omega'^{-1}\Omega_{m'})\chi(\Omega') =$$

$$\sum_{i \in \{0,2\}} \frac{5}{8\pi^2} \left(\mathbf{q}_2^i\right)^{\mathrm{T}} \mathbf{e}_2 \boldsymbol{\sigma}_2 \mathbf{Q}_i^2(\Omega_{m'+1}), \quad (4.37)$$

where $\mathbf{e}_2$ and $\boldsymbol{\sigma}_2$ are 2×2-matrices with corresponding elements, and the superscript T refers to the transposed vector. Applying the w-integration recursively until we reach the mth segment, we obtain

$$\int \prod_{k=m'}^{m-1} d\Omega_k \prod_{k=m'}^{m-1} \frac{w(\Omega_k^{-1}\Omega_{k+1})}{w_0^{0,0}} \int d\Omega' e(\Omega'^{-1}\Omega_{m'})\chi(\Omega') =$$

$$\sum_{i \in \{0,2\}} \frac{5}{8\pi^2} \left(\mathbf{q}_2^i\right)^{\mathrm{T}} \mathbf{e}_2 \boldsymbol{\sigma}_2^{m-m'} \mathbf{Q}_i^2(\Omega_m). \quad (4.38)$$

The case for $m < m'$ obviously works the same, so $m - m'$ has to be replaced by $|m - m'|$. Further, the other $(M - |m - m'| - 1)$ w-integrations all simply yield $W_0^{0,0}/w_0^{0,0} = 1$ (because $W_0^{0,0} = w_0^{0,0}$). So, substituting these results in Eq. 4.31 yields

$$\chi(\Omega) = -\frac{\rho}{8\pi^2} \sum_{i \in \{0,2\}} \frac{5}{8\pi^2} \left(\mathbf{q}_2^i\right)^{\mathrm{T}} \mathbf{e}_2 \left(\sum_{m,m'=1}^{M} \boldsymbol{\sigma}_2^{|m-m'|} \right) \mathbf{Q}_i^2(\Omega). \tag{4.39}$$

Using the relation for the coefficients, $\mathbf{q}_2^{i'} = \int d\Omega \chi(\Omega) \mathbf{Q}_{i'}^2(\Omega)$, Eq. 4.39 reduces to the following eigenvalue equation,

$$\left(\mathbf{q}_2^{i'}\right)^{\mathrm{T}} \left[\frac{8\pi^2}{\rho} + \mathbf{e}_2 \left(\sum_{m,m'=1}^{M} \boldsymbol{\sigma}_2^{|m-m'|} \right) \right] = 0, \tag{4.40}$$

in which the dependence on the index i' is only apparent, as the two problems (for both i') are identical. Taking the transposed of the eigenvalue equation, we obtain a more customary form (drop the index i'),

$$\left[\frac{8\pi^2}{\rho} + \left(\sum_{m,m'=1}^{M} \boldsymbol{\sigma}_2^{|m-m'|} \right) \mathbf{e}_2 \right] \mathbf{q}_2 = 0. \tag{4.41}$$

Defining the 2×2-matrix $\boldsymbol{\alpha}_2$ as follows,

$$\boldsymbol{\alpha}_2 = \left(\frac{1}{M} \sum_{m,m'=1}^{M} \boldsymbol{\sigma}_2^{|m-m'|} \right) \mathbf{e}_2 = \left[\frac{1 + \boldsymbol{\sigma}_2}{1 - \boldsymbol{\sigma}_2} - \frac{2\boldsymbol{\sigma}_2}{M} \frac{1 - \boldsymbol{\sigma}_2^M}{(1 - \boldsymbol{\sigma}_2)^2} \right] \mathbf{e}_2, \tag{4.42}$$

we can immediately write down the solution to Eq. 4.41,

$$\frac{\rho_{\pm}M}{8\pi^2} = -\left(2\det(\boldsymbol{\alpha}_2)\right)^{-1}\left(\text{tr}(\boldsymbol{\alpha}_2) \pm \sqrt{\text{tr}^2(\boldsymbol{\alpha}_2) - 4\det(\boldsymbol{\alpha}_2)}\right), \tag{4.43}$$

and the eigenvector corresponding to $\rho_{\pm}$ is $\mathbf{q}_2 = \begin{pmatrix} 1 \\ v_{\pm} \end{pmatrix}$, with

$$v_{\pm} = (2\alpha_2^{(1,2)})^{-1}\left(\alpha_2^{(2,2)} - \alpha_2^{(1,1)} \mp \sqrt{\text{tr}^2(\boldsymbol{\alpha}_2) - 4\det(\boldsymbol{\alpha}_2)}\right), \tag{4.44}$$

in which $\text{tr}(\boldsymbol{\alpha}_2)$ and $\det(\boldsymbol{\alpha}_2)$ are the trace and determinant of $\boldsymbol{\alpha}_2$ respectively and $\alpha_2^{(i,j)}$ is the (i,j)'th element of $\boldsymbol{\alpha}_2$. The unsual way of writing the matrix multiplication (as a division) in Eq. 4.42 is done to make the connection with Eq. 3.62 in Chap. 3. As $(\mathbf{1} - \boldsymbol{\sigma}_2)^{-1}$ commutes with $\boldsymbol{\sigma}_2$, this does not introduce a duality. Before we can determine which of the two densities is the lower, we need to evaluate the elements of $\mathbf{e}_2$. We use the same hard platelets as Mulder uses in [64], so we give the matrix $\mathbf{e}_2$ here without further comment and only refer to this paper,

$$\mathbf{e}_2 = 2l^2 d s_2 \begin{bmatrix} 1 - \frac{2\Delta}{\pi d} & \sqrt{3}\frac{2\Delta}{\pi d} \\ \sqrt{3}\frac{2\Delta}{\pi d} & 0 \end{bmatrix}, \tag{4.45}$$

with $s_2 = (2\pi)^2 \int_0^{\pi} d\beta \sin^2 \beta P_2(\cos\beta) = -\pi^3/4$. For $M = 1$, $\boldsymbol{\alpha}_2 = \mathbf{e}_2$ and then it is clear that both the determinant and the trace are negative and ρ_+ is the only positive of the two solutions. Consequently, the bifurcation density becomes

$$\frac{\rho_*M}{8\pi^2} = -\left(2\det(\boldsymbol{\alpha}_2)\right)^{-1}\left(\text{tr}(\boldsymbol{\alpha}_2) + \sqrt{\text{tr}^2(\boldsymbol{\alpha}_2) - 4\det(\boldsymbol{\alpha}_2)}\right), \tag{4.46}$$

and the eigenvector, $\mathbf{q}_{2,*} = \begin{pmatrix} 1 \\ v_* \end{pmatrix}$, with

$$v_* = (2\alpha_2^{(1,2)})^{-1}\left(\alpha_2^{(2,2)} - \alpha_2^{(1,1)} - \sqrt{\text{tr}^2(\boldsymbol{\alpha}_2) - 4\det(\boldsymbol{\alpha}_2)}\right). \tag{4.47}$$

The elements of $\boldsymbol{\sigma}_2$ cannot be calculated analytically, and therefore, we calculate asymptotic expressions for the $\sigma_2^{i,j}$ in the appendix. For two out of three k_{μ}'s large (in which $k_{\mu} = \beta_B J_{\mu}$ and $\mu \in \{1, 2, 3\}$), to the first orders in $1/k_{\mu}$, this yields

$$\begin{aligned}
\sigma_2^{0,0} &= 1 + \frac{3}{2}\left(-\frac{1}{k_1 + k_3} - \frac{1}{k_2 + k_3}\right), \\
\sigma_2^{0,2} &= \sigma_2^{2,0} = \frac{1}{2}\sqrt{3}\left(\frac{1}{k_1 + k_3} - \frac{1}{k_2 + k_3}\right) \\
\sigma_2^{2,2} &= 1 - \frac{2}{k_1 + k_2} - \frac{1}{2(k_1 + k_3)} - \frac{1}{2(k_2 + k_3)}
\end{aligned} \tag{4.48}$$

These expressions will be used in the next section, where we consider 'ribbonlike' chains.

The limiting case that $k_1 = k_2 = 0$ and $\Delta = 0$, the bifurcation density reduces to

$$\rho^* M 2l^2 d = \frac{32}{\pi}\left(\frac{1+\sigma}{1-\sigma} - \frac{2\sigma}{M}\frac{1-\sigma^M}{(1-\sigma)^2}\right)^{-1}, \tag{4.49}$$
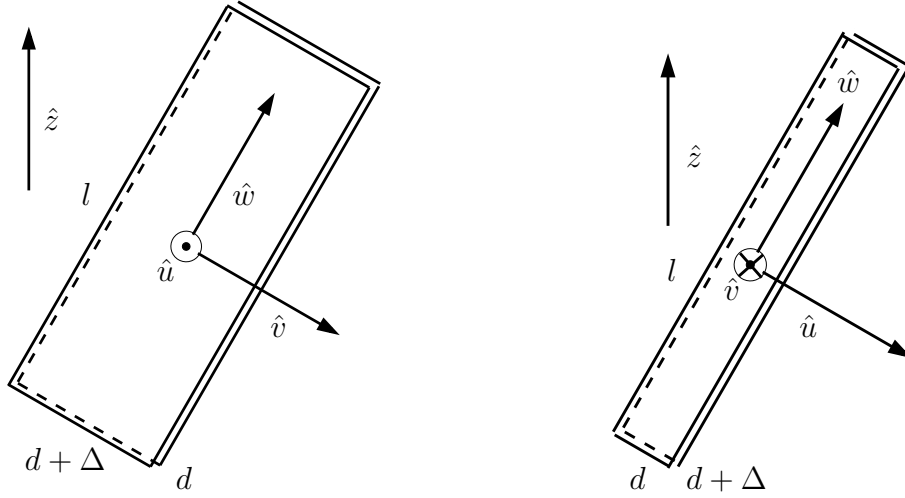
FIGURE 4.3. In a uniaxial nematic phase, the long ($\hat{w}$-) axes of the segments orders with respect to the nematic director, $\hat{z}$. The degree of ordering is measured by the nematic order parameter, $q_2^{0,0}$. With the segments being biaxial however, there will in general also be a difference in the ordering of $\hat{u}$ and $\hat{v}$ with respect to $\hat{z}$. The degree of nonequivalence of these two axis is measured by a second (uniaxial) order parameter, $q_2^{0,2}$. From the excluded volume (Eq. 4.4), we can see that the situation for $\gamma \approx \pi/2, 3\pi/2$ (left) is preferred over $\gamma \approx 0, \pi$ (right) $\Rightarrow q_2^{0,2} < 0$.

with $\sigma = \sigma_2^{0,0} = 1 + 3/k_3^2 - 3\coth(k_3)/k_3$. This is the bifurcation density for a gas of chains of hard rods with only bending (and no twisting) interactions within the chain, as was calculated in Chap. 3 (Eq. 3.62).

At Eq. 4.40, we saw that bifurcation equation split in two identical problems, whose eigenvectors must be the same, up to a constant factor. Therefore, the bifurcating function χ has the following form

$$\chi(\Omega) = Q_{0,0}^2(\Omega) + v_* Q_{0,2}^2(\Omega) + \kappa \left(Q_{2,0}^2(\Omega) + v_* Q_{2,2}^2(\Omega) \right), \tag{4.50}$$

with κ the constant factor. In principle, this κ has to be determined (and more) from the "second order" bifurcation equation (see Ref. [65]). However, we are only considering moderate biaxialities (Δ of the order of d) so the nematic phase is always uniaxial, $f^{(\mathrm{av})}(\beta, \gamma)$, and $\kappa = 0$. $q_{0,0}^2$ is the usual uniaxial nematic (Maier Saupe) order parameter concerning ordering of the long axes ($\hat{w}$) of the molecules with respect to the nematic director $\hat{z}$. In case of biaxial objects, however, the nonequivalence of the short axes ($\hat{u}$ and $\hat{v}$) will result in a different ordering with respect to $\hat{z}$ as well, hence $q_{0,2}^2$. For our system we always find $q_{0,2}^2 < 0$, which means that there is a maximum in the ODF around $\gamma = \pi/2$ and $3\pi/2$ (corresponding to $\hat{v}$ being in the plane spanned by $\hat{z}$ and $\hat{w}$, see Fig. 4.3).

4.3. Ribbonlike Chains

4.3.1. The Ribbonlike Chain Limit. A concept playing an important role in polymer physics is that of the wormlike chain, first introduced by Kratky and Porod [49]. The connection to LC polymers was made by Khokhlov and Semenov [32, 33]. KS's main result is the derivation of the conformational entropy of the wormlike chain. In Chap. 3, we rederived these results by using the concept of a segmented chain model, and applying the so-called 'wormlike chain limit' (WCL). In this section, we generalize the results for wormlike chains (which are (locally) cylindrically symmetric) to continuously flexible biaxial polymers, or ribbonlike chains. This is done by using the results of the previous section (for segmented biaxial chains) in a limit. This limit, we will call the ribbonlike chain limit (RCL) in analogy with the WCL. In our system, the RCL is (remember $k_\mu = \beta_B J_\mu$)

$$l \to 0, \quad M \to \infty, \quad k_\mu \to \infty, \tag{4.51}$$

while the following ratios stay finite,

$$P_\mu = k_\mu l, \quad \bar{M}_\mu = M/k_\mu. \tag{4.52}$$

Note that these three different coupling constants $\beta_B J_\mu$ give rise to *three* different length scales; the persistence lengths P_μ. The $\bar{M}_\mu = L/P_\mu$ are the number of persistence lengths in the chain. Each of these lengths corresponds to the orientational persistence of one of the axes $\hat{u}, \hat{v}$ and $\hat{w}$, i.e. $\mu \in \{1, 2, 3\}$ (where it has to be remembered from Eq. 4.2 that 1 corresponds to $\hat{u}$, 2 to $\hat{v}$ and 3 to $\hat{w}$). However, bending or torquing a chain always affects two axes (e.g. rotating the chain locally around the $\hat{w}$-axis changes both the $\hat{u}$- and the $\hat{v}$-axis). Therefore it makes sense to define

$$P_{\mu,\nu} = P_\mu + P_\nu, \quad \bar{M}_{\mu,\nu} = \frac{\bar{M}_\mu \bar{M}_\nu}{\bar{M}_\mu + \bar{M}_\nu} \quad \text{and} \quad \mu < \nu \tag{4.53}$$

where it still holds that $L = \bar{M}_{\mu,\nu} P_{\mu,\nu}$. Note that there are only *three* length scales $P_{\mu,\nu}$. Then, physically, each of the three length scales $P_{\mu,\nu}$ corresponds to persistence of a certain bending/twisting mode, i.e. (2,3) and (1,3) correspond to bending (respectively, around $\hat{u}$- and $\hat{v}$-axis) and (1,2) to twisting (around $\hat{w}$-axis). Moreover, we also define

$$P = P_1 + P_2 + P_3 \quad \text{and} \quad \bar{M} = \frac{\bar{M}_1 \bar{M}_2 \bar{M}_3}{\bar{M}_1 \bar{M}_2 + \bar{M}_1 \bar{M}_3 + \bar{M}_2 \bar{M}_3}, \tag{4.54}$$

so instead of a discrete m we now have a continuous $\bar{m}$ running along the ribbonlike chain, from 0 to $\bar{M}$; $\bar{m} = \frac{m}{M} \bar{M}$. Note that here too, $L = \bar{M} P$

A ribbonlike chain, as defined above, is characterized by 6 model parameters: i.e. total length L, thickness d, width $d + \Delta$ and the three P_μ. However, using dimensionless quantities, we can reduce them to 4: Δ/d and the three $L/P_\mu = \bar{M}_\mu$. Doing this, also the density needs to be rescaled with a volume factor (with for instance $P^2 d$). Naively, if one considers a ribbonlike object consisting homogeneously of a certain material, one would expect to even loose another model parameter. Instead of having 3 parameters $\bar{M}_\mu$, one might argue that one of them is redundant as it is fixed by the other two and the geometry of the cross-section of the polymer. [2] On the other hand, chemical units

---

[2]In Ref. [81], this is explained in terms of two moduli: the modulus of pure shear K_{ps} and the modulus of hydrodynamic compression K_{hc}.

do not have a straightforward relation between dimensions and rigidity. We have not investigated this further.

Finally, in concluding this subsection, we mention another type of continuously flexible biaxial chain, which is closer related to the wormlike chain than the ribbonlike chain is. In order to obtain ribbonlike chains we had to take the limit where all k_μ become large in a way that k_μ/M stays finite. If now instead, we take the limit where $k_3 \to \infty$ and $k_1, k_2 \to 0$ such that $M/k_3, Mk_1, Mk_2$ stay finite. Then, this case corresponds to a wormlike chain (the k_3-direction is very stiff) with nonzero torsion energy (Mk_1 and Mk_2 are nonzero), i.e. a *weakly biaxial* wormlike chain. In order to get the wormlike chain results from this weakly biaxial wormlike chain, we then have to take the limit $Mk_1, Mk_2 \to 0$. This means that the wormlike chain limit for the biaxial chains studied in this chapter is not well-defined. We do not go into this case any further, but we encounter this furtheron and therefore we mention it.

4.3.2. The Stationarity Equation. In this subsection, we will rewrite the stationarity equations 4.10 in the RCL. To that end, we first introduce another notation in which to express Eqs. 4.10. We define

$$\psi_{m+1}(\Omega) = \int d\Omega' \frac{w(\Omega, \Omega')}{w_0^{0,0}} \exp\left[-\beta_{\mathrm{B}} \mathcal{H}(\Omega')\right] \psi_m(\Omega') \tag{4.55}$$

with for notational purposes, rewritten as a field on a segment,

$$\beta_{\mathrm{B}} \mathcal{H}(\Omega) = \rho \sum_{k'=1}^{M} \int d\Omega' e(\Omega, \Omega') f_{k'}(\Omega'), \tag{4.56}$$

and finally, $Z' = Z/\left(w_0^{0,0}\right)^{M-1}$ and $\psi_1 = 1/\sqrt{Z'}$. Then, in this notation (Eq. 4.10), the ODF becomes

$$f_m(\Omega) = \psi_m(\Omega) \exp\left[-\beta_{\mathrm{B}} \mathcal{H}(\Omega)\right] \psi_{M-m+1}(\Omega). \tag{4.57}$$

Eqs. 4.55 to 4.57 together form the (selfconsistent) stationarity equations. We have introduced the ψ-functions for notational purposes, but from Eq. 4.55 (recurrently formulated), one can see that they also serve as the (renormalized) partition functions of parts of the chain; i.e. $\sqrt{Z'}\psi_m(\Omega) \exp\left[-\beta_{\mathrm{B}} \mathcal{H}(\Omega)\right]$ is the partition function of a chain of m segments with the orientation of the mth segment fixed to Ω.

In the RCL, some quantities have to be rescaled. We choose the factor $\bar{M}/M$ in which to expand and then only keep the lowest-order (relevant) terms. The arrow, $\to$, we use to denote the RCL. The ODF and the ψ-functions do not have to be rescaled,

$$f_m(\Omega) \to \bar{f}(\bar{m}, \Omega) \quad \psi_m(\Omega) \to \bar{\psi}(\bar{m}, \Omega), \tag{4.58}$$

where generally, we use a bar over a symbol to indicate the RCL. It still holds that $\int d\Omega \bar{f}(\bar{m}, \Omega) = 1$. The excluded volume between two segments rescales as follows,

$$e(\Omega) \to \left(\frac{\bar{M}}{M}\right)^2 \bar{e}(\Omega) = \left(\frac{\bar{M}}{M}\right)^2 2P^2 d \sin \beta \left[1 + \frac{\Delta}{2d} \left(|\cos \alpha| + |\cos \gamma|\right)\right], \tag{4.59}$$

and therefore, the field becomes (with $\sum_{m'} \to (M/\bar{M}) \int d\bar{m}'$)

$$\beta_{\mathrm{B}} \mathcal{H}(\Omega) \to \left(\frac{\bar{M}}{M}\right) \beta_{\mathrm{B}} \bar{\mathcal{H}}(\Omega) = \left(\frac{\bar{M}}{M}\right) \rho \int_0^{\bar{M}} d\bar{k}' \int d\Omega' \bar{e}(\Omega, \Omega') \bar{f}(\bar{k}', \Omega'). \tag{4.60}$$

From Eq. 4.60, we can see that the field on a segment goes to zero in the RCL (because the segment length l goes to zero), and therefore

$$\exp\left[-\beta_{\mathrm{B}}\mathcal{H}(\Omega)\right] \to 1 - \left(\frac{\bar{M}}{M}\right)\beta_{\mathrm{B}}\bar{\mathcal{H}}(\Omega), \tag{4.61}$$

so, in the RCL,

$$\bar{f}(\bar{m}, \Omega) = \bar{\psi}(\bar{m}, \Omega)\bar{\psi}(\bar{M} - \bar{m}, \Omega). \tag{4.62}$$

Next,

$$\psi_{m+1}(\Omega) - \psi_m(\Omega) \to \left(\frac{\bar{M}}{M}\right)\frac{\partial\bar{\psi}}{\partial\bar{m}}(\bar{m}, \Omega), \tag{4.63}$$

and we prove in the appendix that

$$\left(\int d\Omega'\frac{w(\Omega'^{-1}\Omega)}{w_0^{0,0}}\psi_m(\Omega')\right) - \psi_m(\Omega) \to$$
$$-\tfrac{1}{2}\left(\frac{\bar{M}}{M}\right)\left(\frac{\bar{M}_{2,3}}{\bar{M}}L_{\hat{u}}^2 + \frac{\bar{M}_{1,3}}{\bar{M}}L_{\hat{v}}^2 + \frac{\bar{M}_{1,2}}{\bar{M}}L_{\hat{w}}^2\right)\bar{\psi}(\bar{m}, \Omega), \quad (4.64)$$

with $\mathbf{L}$ the angular momentum operator of the classical rigid rotator,

$$\mathbf{L} = \begin{pmatrix} L_{\hat{u}} \\ L_{\hat{v}} \\ L_{\hat{w}} \end{pmatrix} = \sqrt{-1}\begin{pmatrix} \cos\alpha\cot\beta\frac{\partial}{\partial\alpha} + \sin\alpha\frac{\partial}{\partial\beta} - \frac{\cos\alpha}{\sin\beta}\frac{\partial}{\partial\gamma} \\ \sin\alpha\cot\beta\frac{\partial}{\partial\alpha} - \cos\alpha\frac{\partial}{\partial\beta} - \frac{\sin\alpha}{\sin\beta}\frac{\partial}{\partial\gamma} \\ -\frac{\partial}{\partial\alpha} \end{pmatrix}, \tag{4.65}$$

where we have used $\sqrt{-1}$ for the imaginary unit, because i is used elsewhere. Combining Eqs. 4.61, 4.63 and 4.64 with Eq. 4.55, we get

$$\frac{\partial\bar{\psi}}{\partial\bar{m}}(\bar{m}, \Omega) = -\tfrac{1}{2}\left(\frac{\bar{M}_{2,3}}{\bar{M}}L_{\hat{u}}^2 + \frac{\bar{M}_{1,3}}{\bar{M}}L_{\hat{v}}^2 + \frac{\bar{M}_{1,2}}{\bar{M}}L_{\hat{w}}^2\right)\bar{\psi}(\bar{m}, \Omega) - \beta_{\mathrm{B}}\bar{\mathcal{H}}(\Omega)\bar{\psi}(\bar{m}, \Omega). \tag{4.66}$$

Eq. 4.66 is a generalized diffusion equation with $\bar{m}$ playing the role of time. With $Z \to \bar{Z}$, the "initial" condition is $\bar{\psi}(\bar{m} = 0) = 1/\sqrt{\bar{Z}}$. Eq. 4.66 together with Eqs. 4.60 and 4.62 form the (selfconsistent) stationarity equations in the RCL. The analogy with wormlike chains is evident; i.e. for wormlike chains (see Ref. [33] and Chap. 3), the unit vector along tangent to the polymer (in our case $\hat{w}$) diffuses on a unit sphere with diffusion constant 1/(persistence length). For the ribbonlike chains, the axis system $(\hat{u}, \hat{v}, \hat{w})$ diffuses on a four-dimensional counterpart of a sphere, with three different diffusion constants.

Defining $\tilde{\mathbf{L}} = \mathrm{diag}\left(\sqrt{\bar{M}_{2,3}/\bar{M}}, \sqrt{\bar{M}_{1,3}/\bar{M}}, \sqrt{\bar{M}_{1,2}/\bar{M}}\right)\mathbf{L}$, Eq. 4.66 becomes

$$\frac{\partial\bar{\psi}}{\partial\bar{m}}(\bar{m}, \Omega) = -\tfrac{1}{2}\tilde{\mathbf{L}}^2\bar{\psi}(\bar{m}, \Omega) - \beta_{\mathrm{B}}\bar{\mathcal{H}}(\Omega)\bar{\psi}(\bar{m}, \Omega). \tag{4.67}$$

Although the analogy with wormlike polymers is clear, it seems nontrivial to make the connection between the equations describing these two systems. Making the system of ribbonlike polymers more 'wormlike' by taking the limit $\Delta = 0$ and $M_1 = M_2 \gg M_3$ one sees from Eq. 4.66 that the term with $L_{\hat{w}}$ dominates on small length scales of P_1 or P_2 (corresponding to diffusion of $\hat{u}$ and $\hat{v}$). The diffusion of the vector $\hat{w}$ itself takes place

on a much larger length scale, i.e. P_3. This is again an appearence of the fact that the wormlike chain limit is ill-defined for biaxial chains.

4.3.3. The Free Energy. Without further comment, we now give the free energy of a fluid of ribbonlike polymers in a nematic field, in a symmetric form,

$$
\beta \bar{\mathcal{F}}[\psi^{(\pm)}] =
$$
$$
- \tfrac{1}{2} \int_0^{\bar{M}} d\bar{m} \int d\Omega \left(\tilde{\mathbf{L}} \psi^{(+)}(\bar{m}, \Omega) \cdot \tilde{\mathbf{L}} \psi^{(-)}(\bar{m}, \Omega) + \psi^{(+)}(\bar{m}, \Omega) \frac{\partial \psi^{(-)}}{\partial \bar{m}}(\bar{m}, \Omega) \right.
$$
$$
\left. - \psi^{(-)}(\bar{m}, \Omega) \frac{\partial \psi^{(+)}}{\partial \bar{m}}(\bar{m}, \Omega) \right) + \int_0^{\bar{M}} d\bar{m} \int d\Omega \bar{f}(\bar{m}, \Omega) \beta_{\mathrm{B}} \bar{\mathcal{H}}(\Omega)
$$
$$
+ \int d\Omega \left(\bar{f}(0, \Omega) \log \psi^{(+)}(0, \Omega) + \bar{f}(\bar{M}, \Omega) \log \psi^{(-)}(\bar{M}, \Omega) \right). \quad (4.68)
$$

Here, $\psi^{(+)}(\bar{m}, \Omega) = \psi(\bar{m}, \Omega)$, $\psi^{(-)}(\bar{m}, \Omega) = \psi(\bar{M} - \bar{m}, \Omega)$ and $\bar{f}(\bar{m}, \Omega) = \psi^{(+)}(\bar{m}, \Omega) \times \psi^{(-)}(\bar{m}, \Omega)$. The derivation of Eq. 4.68 is similar to that of the free energy of a fluid of wormlike polymers in Chap. 3, with the only difference that ∇^2 is replaced by $-\tilde{\mathbf{L}}^2$. Its form compares directly with the free energy KS derived in Ref. [33]. This free energy 4.68 also serves as a functional; i.e. variation to $\psi^{(\pm)}$ again yields Eq. 4.67.

4.3.4. Bifurcation Results. The I-N bifurcation density of these ribbonlike polymers, we calculate not by performing a bifurcation analysis of Eq. 4.66, but by applying the RCL directly to the results for discrete biaxial chains (Eqs. 4.42 to 4.48). First, we rewrite $\boldsymbol{\sigma}_2$ as follows

$$
\boldsymbol{\sigma}_2 = \mathbf{1} - \frac{3}{M} \mathbf{M}, \quad (4.69)
$$

which defines the 2×2-matrix $\mathbf{M}$, and $\mathbf{1}$ is the (two-dimensional) unit matrix. In the RCL, only terms to first order in $1/k_\mu$ contribute, so $\mathbf{M}$ becomes (from Eq. 4.48),

$$
\mathbf{M} \to \bar{\mathbf{M}} = \left[\begin{array}{cc} \frac{1}{2}(\bar{M}_{1,3} + \bar{M}_{2,3}) & \frac{1}{6}\sqrt{3}(\bar{M}_{2,3} - \bar{M}_{1,3}) \\ \frac{1}{6}\sqrt{3}(\bar{M}_{2,3} - \bar{M}_{1,3}) & \frac{2}{3}\bar{M}_{1,2} + \frac{1}{6}(\bar{M}_{1,3} + \bar{M}_{2,3}) \end{array} \right]. \quad (4.70)
$$

The matrix $\mathbf{e}_2$ becomes in the RCL,

$$
M^2 \mathbf{e}_2 \to \bar{\mathbf{e}}_2 = 2L^2 ds_2 \left[\begin{array}{cc} 1 - \frac{2\Delta}{\pi d} & \sqrt{3}\frac{2\Delta}{\pi d} \\ \sqrt{3}\frac{2\Delta}{\pi d} & 0 \end{array} \right]. \quad (4.71)
$$

Then, using the the mathematical identity $\lim_{n \to \infty}(1 + x/n)^n = \exp(x)$, the matrix $\boldsymbol{\alpha}_2$ becomes in the RCL

$$
M \boldsymbol{\alpha}_2 \to \bar{\boldsymbol{\alpha}}_2 = \frac{2}{3\bar{\mathbf{M}}} \left(\mathbf{1} - \frac{1 - \exp(-3\bar{\mathbf{M}})}{3\bar{\mathbf{M}}} \right) \bar{\mathbf{e}}_2, \quad (4.72)
$$

in which the matrix $\exp(\mathbf{A})$ is defined as $\mathbf{1} + \mathbf{A} + \frac{1}{2}\mathbf{A}^2 + \ldots$, and $1/\bar{\mathbf{M}}$ is the regular inverse of $\bar{\mathbf{M}}$. For numerical purposes this is a very unpractical expression, as we have to compute an infinite matrix summation and multiplication. Consequently, we want to write $\bar{\mathbf{M}}$ in the following form,

$$
\bar{\mathbf{M}} = \lambda_+ \mathbf{E}_+ + \lambda_- \mathbf{E}_-, \quad (4.73)
$$

with $\mathbf{E}_\pm = \mathbf{v}_\pm \otimes \mathbf{v}_\pm$ the matrices generated by the external products of the eigenvectors $\mathbf{v}_\pm$ corresponding to eigenvalues $\lambda_\pm$. Then, we get for the expression,

$$\frac{2}{3\bar{\mathbf{M}}}\left(\mathbf{1} - \frac{1 - \exp(-3\bar{\mathbf{M}})}{3\bar{\mathbf{M}}}\right) = \sum_{\tau=\pm} \frac{2}{3\lambda_\tau}\left(1 - \frac{1 - \exp(-3\lambda_\tau)}{3\lambda_\tau}\right)\mathbf{E}_\tau \qquad (4.74)$$

The eigenvalues of $\bar{\mathbf{M}}$ are

$$\lambda_\pm = \frac{1}{3}\left(\bar{M}_{1,2} + \bar{M}_{1,3} + \bar{M}_{2,3}\right) \pm \frac{1}{6}\sqrt{2}\Lambda, \qquad (4.75)$$

with

$$\Lambda = \sqrt{(\bar{M}_{1,2} - \bar{M}_{1,3})^2 + (\bar{M}_{1,2} - \bar{M}_{2,3})^2 + (\bar{M}_{1,3} - \bar{M}_{2,3})^2} \qquad (4.76)$$

and the corresponding eigenvectors,

$$\mathbf{v}_\pm = \frac{1}{C_\pm}\left(\begin{array}{c} 2\bar{M}_{1,2} - \bar{M}_{1,3} - \bar{M}_{2,3} \mp \sqrt{2}\Lambda \\ \sqrt{3}(\bar{M}_{1,3} - \bar{M}_{2,3}) \end{array}\right), \qquad (4.77)$$

with normalization factors,

$$C_\pm = 2\sqrt{\Lambda(\Lambda \pm \tfrac{1}{2}\sqrt{2}(\bar{M}_{1,3} + \bar{M}_{2,3} - 2\bar{M}_{1,2}))}. \qquad (4.78)$$

Then, finally, the RCL bifurcation density is

$$\frac{\rho^*\bar{M}}{8\pi^2} = -\left(2\det(\bar{\boldsymbol{\alpha}}_2)\right)^{-1}\left(\mathrm{tr}(\bar{\boldsymbol{\alpha}}_2) + \sqrt{\mathrm{tr}^2(\bar{\boldsymbol{\alpha}}_2) - 4\det(\bar{\boldsymbol{\alpha}}_2)}\right), \qquad (4.79)$$

and the eigenvector, $\mathbf{q}_2^* = \left(\begin{array}{c} 1 \\ v^* \end{array}\right)$, with

$$v^* = (2\bar{\alpha}_2^{(1,2)})^{-1}\left(\bar{\alpha}_2^{(2,2)} - \bar{\alpha}_2^{(1,1)} - \sqrt{\mathrm{tr}^2(\bar{\boldsymbol{\alpha}}_2) - 4\det(\bar{\boldsymbol{\alpha}}_2)}\right). \qquad (4.80)$$

Eqs. 4.71 to 4.79 together, yield the I-N bifurcation density $\rho^*\bar{M}$ of a fluid of ribbonlike polymers and can be calculated analytically. The bifurcation density in the RCL is dependent on four quantities; i.e. the biaxiality of the polymer (Δ/d), and the number of persistence lengths of the three vectors $P_\mu/L = 1/\bar{M}_\mu$. All other dependences can be scaled out.

In many ways, the matrix $\bar{\mathbf{M}}$ is symmetric with respect to the $\bar{M}_\mu$, i.e. one can see that clearly from the determinant, the trace and as a consequence, from the eigenvalues. Indeed, in deriving $\bar{\mathbf{M}}$ it is nowhere used that one direction $(\hat{u},\hat{v}$ or $\hat{w})$ is special with respect to the others. The reason that $\bar{\mathbf{M}}$ is not fully symmetric is due to the fact that the Q-functions are formulated with respect to a specific coordinate system and this causes the 'symmetry' breaking. The fact that the bifurcation density is dependent in a different way to $\bar{M}_3$ on one hand and $\bar{M}_1$ and $\bar{M}_2$ on the other, is due to the excluded volume matrix $\bar{\mathbf{e}}_2$.

It has already been mentioned before, that effectively the bifurcation density depends only on 4 quantities $(\Delta/d, \bar{M}_\mu)$. That is because a volume factor can be scaled out of the excluded volume matrix and used in the bifurcation density so it becomes dimensionless. In analogy to rods in the Onsager approximation, it makes sense to express this volume
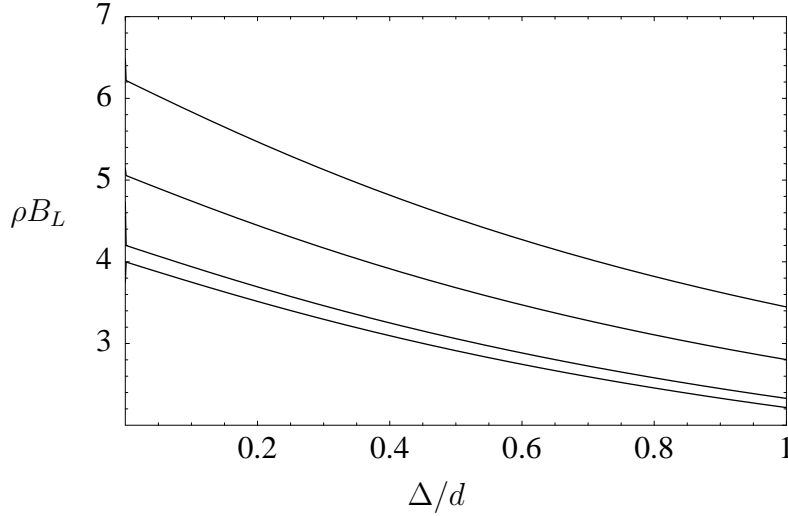
FIGURE 4.4. The bifurcation density vs. biaxiality of the molecule. Four curves, starting from a rigid biaxial particle (bottom curve, $\bar{M}_1 = \bar{M}_2 = \bar{M}_3 = 0$), the flexibility of all bending directions $(\hat{u}, \hat{v}, \hat{w})$ is increased simultaneously. From the bottom curve upward, $\bar{M}_1 = \bar{M}_2 = \bar{M}_3 = 0, 0.1, 0.5$ and $1.$, respectively. The density is scaled with $B_L = \frac{\pi}{4} L^2 d$ which is the same as Mulder used, and the bottom curve is the same as Fig. 6 (Ref. [64]).

factor as (effective segment length)$^2 d$, where the effective segment length is the persistence length of $\hat{w}$. In general, this segment length will be of the order $P = P_1 + P_2 + P_3$ yielding a dimensionless density, $\rho P^2 d$. However if for instance $P_1 \gg P_2, P_3$, then the persistence length (in the direction of $\hat{w}$) is much smaller than P and it is more appropriate to use $P_{2,3} = P_2 + P_3$, so $\rho P_{2,3}^2 d$. Finally, if the resulting effective segment length is larger than the total length of the chain, one should use L to scale, and the dimensionless density becomes $\rho L^2 d$.

On the level of the bifurcation analysis, one limiting case of the ribbonlike polymer is readily taken. Biaxial particles as studied by Mulder in Ref. [64] can be viewed as very stiff biaxial polymers. Taking the limit of all $\bar{M}_\mu \to 0$, then $\boldsymbol{\alpha} \to \mathbf{e}_2$ and the problem reduces to that of Mulder of biaxial particles of dimensions $L, d + \Delta, d$.

It has already been mentioned that wormlike chains are in a sense an ill-defined limiting case of ribbonlike chains. However, on the level of bifurcation analysis, we can get around the problem by taking the limits in a convenient order. If we first put $\Delta = 0$ and $\bar{M}_1 = \bar{M}_2$, the matrices $\mathbf{e}_2$ and $\bar{\mathbf{M}}$ reduce to

$$\bar{\mathbf{e}}_2 = 2L^2 ds_2 \begin{bmatrix} 1 & 0 \\ 0 & 0 \end{bmatrix} \quad \text{and} \quad \bar{\mathbf{M}} = \begin{bmatrix} \bar{M}_{1,3} & 0 \\ 0 & \frac{1}{3}\bar{M}_1 + \frac{1}{3}\bar{M}_{1,3} \end{bmatrix}. \tag{4.81}$$

If we then let $\bar{M}_1 \to \infty$, so $\bar{M}_{1,3} = \bar{M}_3/(1 + \bar{M}_3/\bar{M}_1) \to \bar{M}_3$ and the diverging 2,2-element of $\bar{\mathbf{M}}$ has no effect as both matrices are diagonal. The resulting bifurcation density corresponds to KS's result [33], and our result in Chap. 3.

We have plotted some dependences of the bifurcation density to the model parameters in Figs. 4.4 to 4.5. We don't compare with experiments, but merely want to show what the model (in combination with bifurcation theory) is capable of, as well as exploring its features a bit. Figs. 4.4 and 4.5 are interesting because of the contact we can make
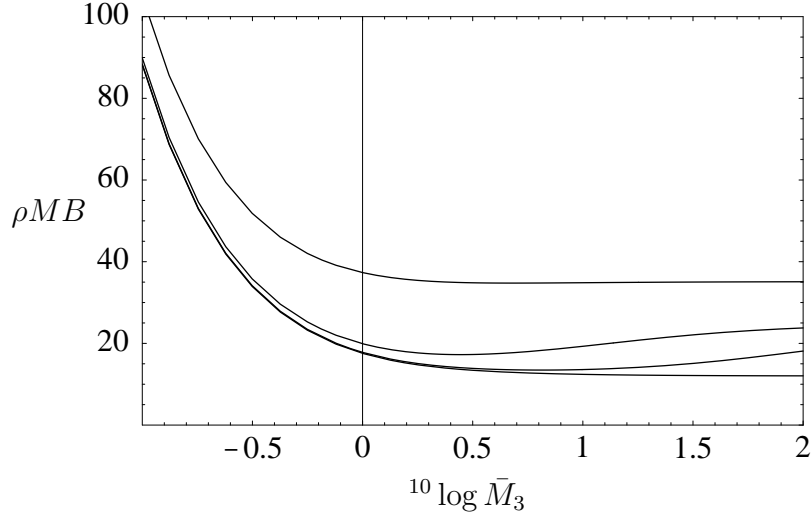
FIGURE 4.5. The bifurcation density vs. flexibility of $\hat{w}$-direction (which is M_3). Four graphs with no biaxiality, $\Delta/d = 0$, starting (effectively) from the wormlike chain (bottom curve, $\bar{M}_1 = \bar{M}_2 \gg \bar{M}_3$) and decreasing $\bar{M}_1 = \bar{M}_2$ simultaneously (i.e. increasing the importance of torsion). From the bottom curve upward, $\bar{M}_1 = \bar{M}_2 = 100000, 100, 10$ and 1, respectively. The lower curve is the same as in Fig. 1 in Ref. [33]. The density is scaled with $MB = \frac{\pi}{2}MP^2d$ which is the same scaling used by KS in Ref. [33]. This scaling is not very appropriate for $\log \bar{M}_3 < 0$ for then $L < P$.

with previous work. In Fig. 4.4, the bottom curve is the biaxiality-dependence of the bifurcation density of a single (rigid) segment, previously calculated by Mulder [64]. The other curves are obtained by introducing some flexibility in this segment. Fig. 4.5 reproduces KS's result (bottom curve) for the dependence of the bifurcation density on the number of persistence lengths in the wormlike polymer [33]. The other curves are obtained with nonzero torque.

In Fig. 4.6, we have calculated a few curves to study the effect of asymmetry in the bending directions. We have set $\bar{M}_2 = 0$, so the $\hat{v}$-direction is completely stiff. Consequently, the chain is only allowed to bend in the plane perpendicular to $\hat{v}$. When $\bar{M}_1$ and $\bar{M}_3$ are small (top curve) there is not much difference with Fig. 4.4, but when $\bar{M}_1$ and $\bar{M}_3$ increase, the shape of the curve changes and in case of the lower curve, a maximum appears. At present, it is not totally clear to us what causes the maximum although it is real. It may have to do with the fact that by increasing Δ, the nematic order parameter $q_{0,2}^2$ (measuring the nonequivalence between the $\hat{u}$- and $\hat{v}$-axes) goes very quickly from 0 to substantial negative values. In this way, in the nematic the entropy of the chain is quite reduced compared to when $\Delta \ll 1$. As a result, the system postpones the I-N transition to higher densities. At some point, increasing Δ simply means adding material to the molecules and that does not affect $q_{0,2}^2$ anymore, so the curve reaches a maximum and goes down. In any case, the system is rather unphysical as one would not easily expect a chain with such unequivalent bending directions.
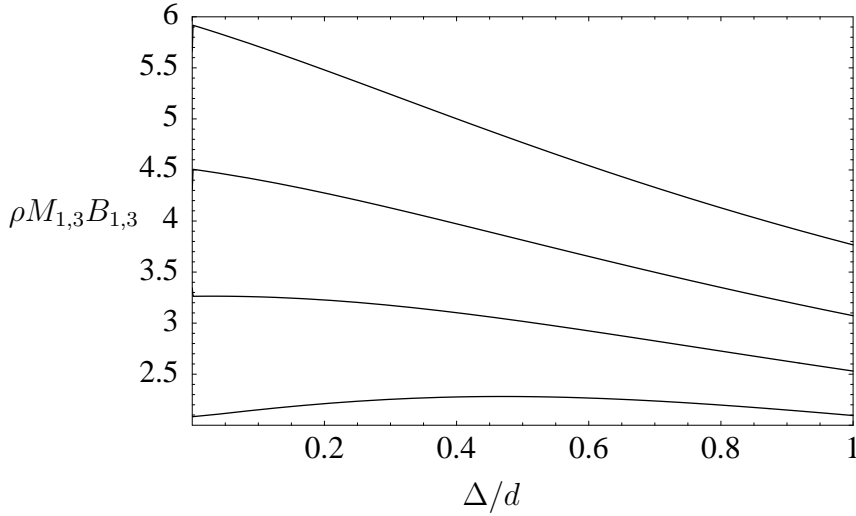
FIGURE 4.6. The bifurcation density vs. biaxiality of the molecule, in which the $\hat{v}$-direction is set completely stiff, $\bar{M}_2 = 0$. Four curves with increasing asymmetry in flexibility of bending directions. From the top curve down, $\bar{M}_1 = \bar{M}_3 = 2, 3, 5$ and 10, respectively. The density is scaled with $M_{1,3} B_{1,3} = \frac{\pi}{2} M_{1,3} P_{1,3}^2 d$. For large asymmetry, a maximum appears (bottom curve).

4.4. Conclusion and Discussion

In this chapter, we developed a theory for nematic ordering in a fluid of biaxial polymers. The biaxial polymers are modeled as chains of platelet-like segments with a bending/twisting potential between them. Nematic ordering in a fluid of platelets has been considered earlier by Mulder [64]. We have taken the segmented-chain approach used earlier in Chap. 3 and calculated the I-N bifurcation density. The ribbonlike chain limit has been applied to these segmented chains, thus obtaining continuously flexible chains, characterized by 4 model parameters. The resulting theory can be viewed as a combination of Refs. [33, 64] for wormlike chains and platelets respectively.

We have chosen, in the present chapter, to consider small biaxialities Δ, where the phase transition is always I-UN. In principle, the analysis holds as well for $P \gg \Delta \gg d$ (or equivalently, $d = 0$ and Δ finite), as long as $P^2 \Delta$ remains finite (so the Onsager approximation still holds). In that case, we are in a regime where one would expect a second-order transition I-BN (the condition for this is $\Delta \sim \sqrt{Pd}$, see Ref. [65]). It would be interesting to perform a second-order bifurcation analysis, to find the combinations of parameter values for which the system has this transition. In general, flexibility might have a pronounced influence on the stability of the biaxial nematic, and especially with respect to the uniaxial nematic, one would expect flexibility to destabilize the biaxial phase.

For the chain of biaxial segments, we have considered in this chapter, we used a nearest-neighbour bending/twisting potential which was symmetric with respect to the interchange of the two segments (Eq. 4.2). It is fairly straightforward to introduce chirality in this system. By simply adding a term $\varepsilon(\hat{u} \cdot \hat{v}' - \hat{u}' \cdot \hat{v})$ to Eq. 4.2 (where ε is small, and the unprimed vectors refer to segment m and the primed to $m + 1$),

one obtains a biaxial chain whose equilibrium conformation is twisted. A fluid of these twisted biaxial chains is expected to have a transition from isotropic to chiral nematic (CN, or cholesteric) instead of UN. However, as a CN phase is spatially modulated, this would complicate a lot the present analysis, where homogeneity of the phases is an essential condition. In the RCL, additionally, $\varepsilon \to 0$ and $M\varepsilon$ should stay finite in order not to loose the twist. We are not aware of much work relating the geometric origin of molecular chirality to cholesteric phase behaviour [45]. In general, many biopolymers, like e.g. DNA and virus particles, are twisted and (somewhat) flexible and these twisted ribbonlike chains could be a useful model.

Appendices

Appendix A: From symmetries to expansion coefficients. In this part of the appendix, we will show for the flexibility interaction how to obtain relations between the expansion coefficients after having identified the symmetries of the interaction. In case of the ODF and the excluded volume expansion, the procedure is analogue and already discussed in Ref. [64] (also for particles and phases with the same symmetries as here). As was already mentioned the symmetries of the flexibility interaction (Eqs. 4.2 and 4.11) are

- invariance under $(\alpha, \beta, \gamma) \to (-\alpha, \beta, -\gamma)$; operator A_1
- invariance under $(\alpha, \beta, \gamma) \to (\gamma, \beta, \alpha)$; operator A_2
- particle exchange symmetry, $\Omega = (\alpha, \beta, \gamma) \to \Omega^{-1} = (-\gamma, -\beta, -\alpha)$; exchange operator E

And the effect of these operations on the matrix elements (see Ref. [80]) $\mathcal{D}_{m,n}^l(\Omega)$,

$$\mathcal{D}_{m,n}^l(A_1\Omega) = (-1)^{m-n}\mathcal{D}_{-m,-n}^l(\Omega), \tag{4.82}$$

$$\mathcal{D}_{m,n}^l(A_2\Omega) = (-1)^{m-n}\mathcal{D}_{n,m}^l(\Omega), \tag{4.83}$$

$$\mathcal{D}_{m,n}^l(E\Omega) = (-1)^{n-m}\mathcal{D}_{-n,-m}^l(\Omega). \tag{4.84}$$

The resulting relations between the flexibility coefficients are then

$$w_l^{-m,-n} = \int d\Omega w(\Omega)\mathcal{D}_{-m,-n}^l(\Omega) = \int d(A_1\Omega)w(A_1\Omega)\mathcal{D}_{-m,-n}^l(A_1\Omega) =$$

$$= (-1)^{n-m}\int d\Omega w(\Omega)\mathcal{D}_{m,n}^l(\Omega) = (-1)^{n-m}w_l^{m,n} \tag{4.85}$$

$$w_l^{n,m} = \int d\Omega w(\Omega)\mathcal{D}_{n,m}^l(\Omega) = (-1)^{n-m}w_l^{m,n} \tag{4.86}$$

$$w_l^{-n,-m} = \int d\Omega w(\Omega)\mathcal{D}_{-n,-m}^l(\Omega) = (-1)^{m-n}w_l^{m,n}. \tag{4.87}$$

Combining these relations, we reach the conclusion that $m+n$ are even and also $w_l^{m,n} = w_l^{-m,-n}$ and $w_l^{m,n} = w_l^{n,m}$. Finally, we want the reader to note that all symmetries found here, hold directly for the interaction itself. In case of e.g. the excluded volume interaction, the symmetries which were found, hold for the particles. Consequently, in that case, e.g. both $e((R_x(\pi))^{-1}\Omega'^{-1}\Omega) = e(R_x(\pi)\Omega'^{-1}\Omega)$ and $e(\Omega'^{-1}\Omega R_x(\pi))$ must be considered separately, and will yield different symmetry relations.

Appendix B: The coefficients $W_2^{p,q}$. In this appendix, we calculate asymptotic expressions for the flexibility coefficients $W_0^{0,0}$ and $W_2^{p,q}$ in the limit of stiff interactions (two out of three k_i's large, with $k_i = \beta_B J_\mu$, for $\mu \in \{1,2,3\}$). First, we will derive expressions of the coefficients $W_2^{p,q}$ in terms of $W_0^{0,0}$ and derivatives of $W_0^{0,0}$ with respect to the k_μ's. Next, we will calculate $W_0^{0,0}$ for high values of the coupling parameters k_μ. To that end, we first rewrite the Boltzmann factor for the flexibility interaction $w(\alpha, \beta, \gamma)$ in terms of the coordinates $(x, y, \beta) = (\alpha + \gamma, \alpha - \gamma, \beta)$,

$$w(x, y, \beta) = \exp\left[k_3 \cos\beta + \tilde{k}(1 + \cos\beta)\cos x + \tilde{k}'(1 - \cos\beta)\cos y\right], \quad (4.88)$$

with $\tilde{k} = \frac{1}{2}(k_1 + k_2)$ and $\tilde{k}' = \frac{1}{2}(k_2 - k_1)$. In terms of these new coordinates, the Q^2-functions become (Eqs. 4.29),

$$Q_{0,0}^2(x, y, \beta) = \frac{1}{2}(3\cos^2\beta - 1),$$

$$Q_{0,2}^2(x, y, \beta) + Q_{2,0}^2(x, y, \beta) = \sqrt{3}\sin^2\beta \cos x \cos y$$

$$Q_{2,2}^2(x, y, \beta) = \frac{1}{2}(1 + \cos^2\beta)(\cos^2 y - \sin^2 x) - \cos\beta(\cos^2 y - \cos^2 x). \quad (4.89)$$

in which $Q_{0,2}^2$ and $Q_{2,0}^2$ have been added because of the symmetry of w with respect to interchange of α and γ. Further, in principle, $\int_{-\pi}^{\pi} d\alpha \int_{-\pi}^{\pi} d\gamma = \frac{1}{2} \int_{-2\pi}^{2\pi} dx \int_{|x|-2\pi}^{2\pi-|x|} dy$, but due to invariance of all integrands, i.e. w and the Q^2-functions, with respect to $x \leftrightarrow 2\pi - x$ and $y \leftrightarrow 2\pi - y$, we just get $\int_{-\pi}^{\pi} d\alpha \int_{-\pi}^{\pi} d\gamma = \int_{-\pi}^{\pi} dx \int_{-\pi}^{\pi} dy$, in which an extra factor 2 cancels with the $\frac{1}{2}$. Next, it is straightforward though time-consuming to show that

$$\frac{\partial^2 w}{\partial k_1^2} = \left(\frac{1}{2}Q_{2,2}^2 - \frac{1}{6}\sqrt{3}(Q_{0,2}^2 + Q_{2,0}^2) + \frac{1}{6}Q_{0,0}^2 + \frac{1}{3}\right)w,$$

$$\frac{\partial^2 w}{\partial k_2^2} = \left(\frac{1}{2}Q_{2,2}^2 + \frac{1}{6}\sqrt{3}(Q_{0,2}^2 + Q_{2,0}^2) + \frac{1}{6}Q_{0,0}^2 + \frac{1}{3}\right)w, \quad (4.90)$$

$$\frac{\partial^2 w}{\partial k_3^2} = \left(\frac{2}{3}Q_{0,0}^2 + \frac{1}{3}\right)w.$$

And consequently, integrating both sides of Eqs. 4.90 ($\int d\Omega$) and rearranging a bit, this yields

$$W_2^{0,0} = \left(\frac{3}{2}\frac{\partial^2}{\partial k_3^2} - \frac{1}{2}\right)W_0^{0,0},$$

$$W_2^{0,2} = W_2^{2,0} = \frac{1}{2}\sqrt{3}\left(\frac{\partial^2}{\partial k_2^2} - \frac{\partial^2}{\partial k_1^2}\right)W_0^{0,0}, \quad (4.91)$$

$$W_2^{2,2} = \left(\frac{\partial^2}{\partial k_1^2} + \frac{\partial^2}{\partial k_2^2} - \frac{1}{2}\frac{\partial^2}{\partial k_3^2} - \frac{1}{2}\right)W_0^{0,0}.$$

Therefore, we only have to compute an expression for $W_0^{0,0}$ and this then gives us automatically expressions for the $W_0^{p,q}$.

Let's first look at some symmetries of $W_0^{0,0}$. Looking at Eq. 4.2, we see that in the flexiblity interaction all dimensions are equivalent (i.e. there is no information on the geometry of the particles etc.). Consequently, integrating over all orientations Ω, it does not matter anymore wether it was k_3 connected to the $\hat{w}$-direction or k_1. This means that

$W_0^{0,0}$ is invariant under interchange of k_μ's mutually. So we can just state that from now on in this appendix, we assume $k_1 \le k_2 \le k_3$, which is without loss of generality. Then, there are four asymptotic regions in which we can try to evaluate $W_0^{0,0}$: $k_1, k_2, k_3 \gg 1$; $k_2, k_3 \gg 1 \gg k_1$; $k_3 \gg 1 \gg k_1, k_2$ and $1 \gg k_1, k_2, k_3$. In practice, however, there are only two, and it is enough to assume that two k_μ's are very large (i.e. k_2 and k_3) or very small (i.e. k_1 and k_2). In this appendix, we will only consider the case of $k_2, k_3 \gg 1$, which is of most interest to us. If $k_2, k_3 \gg 1$, it means that all three particle-fixed axes are strongly correlated with that of its nearest neighbours (it suffices to fix two axis to also fix the third). And therefore, this means that (in terms of (x, y, β)) that $x, \beta \ll 1$, but that y can still be large. The difference between the two Euler angles α and γ can be large as long as *final* orientation is very close to the initial (when $\alpha \approx -\gamma \Rightarrow x \ll 1$ but $y \not\ll 1$). Consequently, we can write

$$w(x, y, \beta) = \mathrm{e}^{k_3 + 2\tilde{k}} \exp\left[-\tfrac{1}{2}(k_3 + \tilde{k})\beta^2 - \tilde{k}x^2 + \tfrac{1}{2}\tilde{k}'\beta^2 \cos y\right]$$
$$\times \left(1 + \tfrac{1}{24}(k_3 + \tilde{k})\beta^4 + \tfrac{1}{4}\tilde{k}\beta^2 x^2 + \tfrac{1}{12}\tilde{k}x^4 - \tfrac{1}{24}\tilde{k}'\beta^4 \cos y + \mathcal{O}(6)\right), \quad (4.92)$$

in which $\mathcal{O}(6)$ are terms of order 6 and higher. Naively, one would say that for very stiff interactions, you need only two (very small) angles, i.e. a polar, β, and an azimuthal, x. The fact that y still appears in Eq. 4.92 is due to that for the interaction it matters at which azimuthal angle the polar angle is applied. We will now integrate Eq. 4.92 over x, y and β (dropping the order-symbol). First the y-integration,

$$\int_{-\pi}^{\pi} dy\, w(x, y, \beta) = 2\pi \mathrm{e}^{k_3 + 2\tilde{k}} \exp\left[-\tfrac{1}{2}(k_3 + \tilde{k})\beta^2 - \tilde{k}x^2\right]$$
$$\times \left(\left(1 + \tfrac{1}{24}(k_3 + \tilde{k})\beta^4 + \tfrac{1}{4}\tilde{k}\beta^2 x^2 + \tfrac{1}{12}\tilde{k}x^4\right) I_0(\tfrac{1}{2}\tilde{k}\beta^2) - \tfrac{1}{24}\tilde{k}'\beta^4 I_1(\tfrac{1}{2}\tilde{k}\beta^2)\right). \quad (4.93)$$

The functions I_0 and I_1 are the modified Bessel functions of zeroth and first order respectively. For the integration over x, we replace the integration boundaries $[-\pi, \pi]$ with $[-\infty, \infty]$. Then,

$$\int_{-\infty}^{\infty} dx \int_{-\pi}^{\pi} dy\, w(x, y, \beta) = 2\pi\sqrt{\frac{\pi}{\tilde{k}}} \mathrm{e}^{k_3 + 2\tilde{k}} \exp\left[-\tfrac{1}{2}(k_3 + \tilde{k})\beta^2\right]$$
$$\times \left(\left(1 + \tfrac{1}{24}(k_3 + \tilde{k})\beta^4 + \tfrac{1}{8}\beta^2 + \tfrac{1}{16}(\tilde{k})^{-1}\right) I_0(\tfrac{1}{2}\tilde{k}\beta^2) - \tfrac{1}{24}\tilde{k}'\beta^4 I_1(\tfrac{1}{2}\tilde{k}\beta^2)\right). \quad (4.94)$$

The error introduced in $\int_{-\infty}^{\infty} dx\, x^n \mathrm{e}^{-\tilde{k}x^2}$ by this approximation is largest for $n = 0$, and is of leading order

$$\int_{-\infty}^{\infty} dx\, \mathrm{e}^{-\tilde{k}x^2} - \int_{-\pi}^{\pi} dx\, \mathrm{e}^{-\tilde{k}x^2} = \sqrt{\frac{\pi}{\tilde{k}}} \mathrm{erfc}(\pi\sqrt{\tilde{k}}) \to \frac{\mathrm{e}^{-\pi^2 \tilde{k}}}{\pi\tilde{k}}, \quad (4.95)$$

which goes to zero much faster than any power of $1/\tilde{k}$. The function erfc is the complementary error function [82]. For the last integration, we again replace the integration boundaries (which is allowed through a similar argument as Eq. 4.95), $[0, \pi] \to [0, \infty]$.

Then, the β-integration yields

$$\int_0^\infty d\beta \left(\beta - \tfrac{1}{6}\beta^3\right) \int_{-\infty}^\infty dx \int_{-\pi}^\pi dy\, w(x,y,\beta) =$$

$$\frac{2\pi\sqrt{\pi}e^{k_3+2\tilde{k}}}{\sqrt{\tilde{k}((k_3+\tilde{k})^2-\tilde{k}'^2)}} \left(1 + \frac{1}{16}\left(\frac{1}{\tilde{k}} + \frac{2}{k_3+\tilde{k}+\tilde{k}'} + \frac{2}{k_3+\tilde{k}-\tilde{k}'}\right)\right), \quad (4.96)$$

in which we have dropped higher order terms (of order $1/k_\mu^2$). Resubstituting, $\tilde{k} = \frac{1}{2}(k_1+k_2)$ and $\tilde{k}' = \frac{1}{2}(k_2-k_1)$, we get an asymptotic expression for $W_0^{0,0}$ until first order in $1/k_\mu$,

$$W_0^{0,0} = \frac{(2\pi)^{3/2}e^{k_1+k_2+k_3}}{\sqrt{(k_1+k_2)(k_1+k_3)(k_2+k_3)}}$$

$$\times \left(1 + \frac{1}{8}\left(\frac{1}{k_1+k_2} + \frac{1}{k_1+k_3} + \frac{1}{k_2+k_3}\right)\right). \quad (4.97)$$

Of course, the same can be done with more terms in Eq. 4.92. Clearly, $W_0^{0,0}$ is symmetric in all three k_μ's. The second derivative of $W_0^{0,0}$ to any k_μ (let's say k_1) is then given by

$$\frac{\partial^2 W_0^{0,0}}{\partial k_1^2} = \frac{(2\pi)^{3/2}e^{k_1+k_2+k_3}}{\sqrt{(k_1+k_2)(k_1+k_3)(k_2+k_3)}}$$

$$\times \left(1 + \frac{1}{8}\left(\frac{1}{k_2+k_3} - \frac{7}{k_1+k_2} - \frac{7}{k_1+k_3}\right)\right). \quad (4.98)$$

and to first order in $1/k_\mu$ the quotient of Eqs. 4.97 and 4.98,

$$\frac{1}{W_0^{0,0}}\frac{\partial^2 W_0^{0,0}}{\partial k_1^2} = 1 - \frac{1}{k_1+k_2} - \frac{1}{k_1+k_3} \quad (4.99)$$

Very straightforward, this yields for the coefficients $\sigma_2^{p,q}$

$$\sigma_2^{0,0} = 1 - \frac{3}{2}\left(\frac{1}{k_1+k_3} + \frac{1}{k_2+k_3}\right),$$

$$\sigma_2^{0,2} = \sigma_2^{2,0} = \frac{1}{2}\sqrt{3}\left(\frac{1}{k_1+k_3} - \frac{1}{k_2+k_3}\right), \quad (4.100)$$

$$\sigma_2^{2,2} = 1 - \frac{2}{k_1+k_2} - \frac{1}{2(k_1+k_3)} - \frac{1}{2(k_2+k_3)}.$$

Appendix C: $w(\Omega)$ in the RCL. In this appendix, we prove that for any function $g(\Omega)$ the integration with kernel $w(\Omega)$ (given by Eq. 4.2 and 4.11) has the following limiting behaviour in the RCL

$$\left(\int d\Omega' \frac{w(\Omega'^{-1}\Omega)}{w_0^{0,0}}g(\Omega')\right) - g(\Omega) \rightarrow$$

$$-\frac{1}{2}\left(\frac{\bar{M}}{M}\right)\left(\frac{\bar{M}_{2,3}}{\bar{M}}L_{\hat{u}}^2 + \frac{\bar{M}_{1,3}}{\bar{M}}L_{\hat{v}}^2 + \frac{\bar{M}_{1,2}}{\bar{M}}L_{\hat{w}}^2\right)g(\Omega), \quad (4.101)$$

with $\mathbf{L}$ the angular momentum operator of the classical rigid rotator given by Eq. 4.65.

First, we assume that $g(\Omega)$ is 'smooth' enough so that it can be expanded in $\mathcal{D}_{i,j}^n$,

$$g(\Omega) = \sum_{n=0}^{\infty} \sum_{i,j=-n}^{n} \frac{2n+1}{8\pi^2} g_n^{i,j} \mathcal{D}_{i,j}^n(\Omega) \qquad (4.102)$$

Defining $\mathcal{O} = (0,0,0)$, so that $w(\Omega'^{-1}\mathcal{O}) = w(\Omega'^{-1}) = w(\Omega')$, then

$$\int d\Omega' \frac{w(\Omega')}{w_0^{0,0}} g(\Omega') = \sum_{n=0}^{\infty} \sum_{i,j=-n}^{n} \frac{2n+1}{8\pi^2} g_n^{i,j} \int d\Omega' \frac{w(\Omega')}{w_0^{0,0}} \mathcal{D}_{i,j}^n(\Omega'). \qquad (4.103)$$

In the RCL, $w(\Omega)$ is very peaked around $(\beta, \alpha + \gamma) = (0,0)$ and therefore, we expect only contributions to the integral of $\mathcal{D}_{i,j}^n$ with β and $x (= \alpha + \gamma)$ small. Furthermore, $w(\Omega)$ is even in (β, x), so odd powers in either of them drop out. Expanding the matrix elements in terms of small (β, x) the only $\mathcal{D}_{i,j}^n$ with even orders of 2 and lower are

$$\mathcal{D}_{i,i}^n(\Omega) = 1 - \tfrac{1}{4}n(n+1)\beta^2 + \tfrac{1}{4}i^2\beta^2 - \tfrac{1}{2}i^2 x^2, \qquad (4.104)$$
$$\mathcal{D}_{i+2,i}^n(\Omega) = \tfrac{1}{8}\sqrt{A_{n,i}}\beta^2 \cos y,$$
$$\mathcal{D}_{i-2,i}^n(\Omega) = \tfrac{1}{8}\sqrt{A'_{n,i}}\beta^2 \cos y,$$

with $y = \alpha - \gamma$ (we will see later that we do not need orders higher than 2). The dummies $A_{n,i}$ and $A'_{n,i}$ are

$$A_{n,i} = (n+i+2)(n+i+1)(n-i)(n-i-1)$$
$$A'_{n,i} = (n+i)(n+i-1)(n-i+2)(n-i+1). \qquad (4.105)$$

So, using this knowledge in Eq. 4.103 we obtain

$$\int d\Omega' \frac{w(\Omega')}{w_0^{0,0}} g(\Omega') = \sum_{n=0}^{\infty} \frac{2n+1}{8\pi^2} \left\{ \sum_{i=-n}^{n} g_n^{i,i} \int d\Omega' \frac{w(\Omega')}{w_0^{0,0}} \mathcal{D}_{i,i}^n(\Omega') \right.$$

$$\left. \sum_{i=-n}^{n-2} g_n^{i+2,i} \int d\Omega' \frac{w(\Omega')}{w_0^{0,0}} \mathcal{D}_{i+2,i}^n(\Omega') + \sum_{i=-n+2}^{n} g_n^{i-2,i} \int d\Omega' \frac{w(\Omega')}{w_0^{0,0}} \mathcal{D}_{i-2,i}^n(\Omega') \right\}. $$
$$(4.106)$$

For two out of three k_μ large (see Eq. 4.48) these integrals equal

$$\int d\Omega \frac{w(\Omega)}{w_0^{0,0}} \mathcal{D}_{i,i}^n(\Omega) =$$

$$1 + (\tfrac{1}{4}i^2 - \tfrac{1}{4}n(n+1)) \left(\frac{1}{k_1+k_3} + \frac{1}{k_2+k_3} \right) - \tfrac{1}{2}i^2 \frac{1}{k_1+k_2},$$

$$\int d\Omega \frac{w(\Omega)}{w_0^{0,0}} \mathcal{D}_{i+2,i}^n(\Omega) = \tfrac{1}{8}\sqrt{A_{n,i}} \left(\frac{1}{k_1+k_3} - \frac{1}{k_2+k_3} \right), \qquad (4.107)$$

$$\int d\Omega \frac{w(\Omega)}{w_0^{0,0}} \mathcal{D}_{i-2,i}^n(\Omega) = \tfrac{1}{8}\sqrt{A'_{n,i}} \left(\frac{1}{k_1+k_3} - \frac{1}{k_2+k_3} \right),$$

Stating that $g_n^{i,j} = 0$ for $|i|, |j| > n$ and realizing that $\mathcal{D}_{i,j}^n(\mathcal{O}) = \delta_{i,j}$, we can rewrite Eq. 4.106 as follows

$$
\int d\Omega' \frac{w(\Omega')}{w_0^{0,0}} g(\Omega') = \sum_{n=0}^{\infty} \frac{2n+1}{8\pi^2}
$$

$$
\times \left\{ \sum_{i,j=-n}^{n} g_n^{i,j} \left(1 + (\tfrac{1}{4}i^2 - \tfrac{1}{4}n(n+1)) \left(\frac{1}{k_1+k_3} + \frac{1}{k_2+k_3} \right) - \tfrac{1}{2}i^2 \frac{1}{k_1+k_2} \right) \right.
$$

$$
\left. + \sum_{i,j=-n-2}^{n+2} \tfrac{1}{8} \left(g_n^{i+2,j} \sqrt{A_{n,i}} + g_n^{i-2,j} \sqrt{A'_{n,i}} \right) \left(\frac{1}{k_1+k_3} - \frac{1}{k_2+k_3} \right) \right\} \mathcal{D}_{i,j}^n(\mathcal{O}).
$$
(4.108)

Next, $\mathcal{D}_{i,j}^n(\Omega)$ are eigenfunctions of the following operators,

$$
\mathbf{L}^2 \mathcal{D}_{i,j}^n(\Omega) = n(n+1) \mathcal{D}_{i,j}^n(\Omega),
$$

$$
L_{\hat{w}} \mathcal{D}_{i,j}^n(\Omega) = i \mathcal{D}_{i,j}^n(\Omega),
$$
(4.109)

$$
L_{\pm}^* \mathcal{D}_{i,j}^n(\Omega) = \sqrt{n(n+1) - i(i \pm 1)} \mathcal{D}_{i\pm 1,j}^n(\Omega),
$$

with $\mathbf{L}$ the angular momentum operator, given by Eq. 4.65, $\mathbf{L}^2 = L_{\hat{u}}^2 + L_{\hat{v}}^2 + L_{\hat{w}}^2$ and $L_{\pm} = L_{\hat{u}} \pm \sqrt{-1}L_{\hat{v}}$ (i is already being used). From Eq. 4.109, we can derive

$$
(L_-^*)^2 \mathcal{D}_{i+2,j}^n(\Omega) = \sqrt{A_{n,i}} \mathcal{D}_{i,j}^n(\Omega),
$$
(4.110)

$$
(L_+^*)^2 \mathcal{D}_{i-2,j}^n(\Omega) = \sqrt{A'_{n,i}} \mathcal{D}_{i,j}^n(\Omega).
$$

Inserting these results (Eqs. 4.109 and 4.110) in Eq. 4.108 and resubstituting Eq. 4.102 with $\Omega = \mathcal{O}$ we obtain,

$$
\int d\Omega' \frac{w(\Omega')}{w_0^{0,0}} g(\Omega') = \left(1 + \tfrac{1}{4} \left(\frac{1}{k_1+k_3} + \frac{1}{k_2+k_3} \right) (L_{\hat{w}}^2 - \mathbf{L}^2) \right.
$$

$$
\left. - \tfrac{1}{2} \frac{1}{k_1+k_2} L_{\hat{w}}^2 + \tfrac{1}{8} \left(\frac{1}{k_1+k_3} - \frac{1}{k_2+k_3} \right) (L_+^2 + L_-^2) \right) g(\mathcal{O}). \quad (4.111)
$$

Rearranging a bit and applying the RCL on Eq. 4.111, we obtain the required result

$$
M \left(\int d\Omega' \frac{w(\Omega')}{w_0^{0,0}} g(\Omega') - g(\mathcal{O}) \right) \to -\tfrac{1}{2} \left(\bar{M}_{2,3} L_{\hat{u}}^2 + \bar{M}_{1,3} L_{\hat{v}}^2 + \bar{M}_{1,2} L_{\hat{w}}^2 \right) g(\mathcal{O}),
$$
(4.112)

which is the same as Eq. 4.101.

Part 2

Heteropolymeric Chains

5

BRANCHED HETEROCHAINS

An isotropic-to-nematic (I-N) bifurcation analysis is performed for monodisperse fluids of (very generally) branched heterochains. Heterochains consist of various types of segments. The main result is the derivation of a matrix whose most negative eigenvalue corresponds to the bifurcation density.

5.1. Introduction

Rodlike particles in solution can show liquid crystalline phase behaviour. In many ways, the simplest liquid crystalline phase transition is that between the isotropic (orientationally disordered) and the nematic (orientationally ordered) fluid. In 1949, it was shown by Onsager that model fluids of long impenetrable rods undergo an isotropic-to-nematic (I-N) transition on increasing density [7]. The driving quantity is the average excluded volume of two rods, which is large in the isotropic and smaller in the nematic phase. Onsager wrote down the non-linear integral equation describing the system, in which the excluded volume acts as kernel. It proved impossible to solve the problem exactly in the nematic phase, and Onsager himself solved it approximately by using trial functions [7], a route which was followed later by Straley [83] and Odijk [52]. Others used truncated expansions in Legendre polynomials [84, 60] and in Refs. [59, 85], the original equations of Onsager are numerically solved on a grid using an iteration scheme. An important contribution concerning Onsager's model is that by Kayser and Raveché in 1978 [37]. They observed that the low-symmetry nematic solutions bifurcate from the high-symmetry isotropic solutions. Using the symmetry of the kernel and linearizing around the isotropic solution, they located the bifurcation density and constructed the (initially unstable) nematic branch which connects to the stable nematic solution. A strength of this analysis is that the bifurcation density was obtained in closed form.

Parallel to and following the above efforts of solving the original model of Onsager, there have been investigations to the effect of particle shape, flexibility, bi- and polydispersity, charges on the rods and long-range attractions between rods (see e.g. Refs. [13, 48]). In Refs. [64, 65], Mulder extended the bifurcation analysis of Kayser and Raveché [37] to biaxial particles, showing that for specific particle dimensions a biaxial nematic phase is favored over a uniaxial nematic. (Biaxial objects are not cylindrically symmetric, as opposed to uniaxial objects.) Khokhlov and Semenov (KS) considered a fluid of impenetrable wormlike polymers [32, 33]. The interactions between the polymers were treated much the same as Onsager, but the conformational entropy of these wormlike polymers is very different from the orientational entropy of rigid rods. They

themselves solved the equations using Onsager's trial function and complete numerical solutions were obtained only later by Chen [36]. KS also mention the analytical bifurcation result for wormlike polymers [33].

In previous chapters, we considered chains of cylindrically symmetric rods (Chap. 3) and biaxial rods (Chap. 4). In both cases, we performed bifurcation analysis and in both cases we considered the results in the limit of continuous flexibility, i.e. wormlike chains (Chap. 3, same as KS) and ribbonlike chains (Chap. 4, new). In the present chapter, we extend the I-N bifurcation analysis to a much more general class of monodisperse fluids of chains of cylindrically symmetric rodlike segments. The chains are allowed to be branched and the segments can have various dimensions, hence branched heterochains. It is for the first time that polymers with such a general geometry are considered. We take into account the interactions within the polymer exactly and the interactions between polymers on a mean field level. Our main result will be the derivation of a matrix, depending on model parameters, whose most negative eigenvalue corresponds to the bifurcation density. The elements of the corresponding eigenvector represent the relative degree of order of the segments at the bifurcation. The symmetry of the nematic phase is usually uniaxial and the phase transition first-order. The results of this chapter will be used in the following chapters where we consider specifically main chain and side chain liquid crystalline polymers.

The rest of the chapter is organized as follows. In Sec. 5.2, we present the model (including approximations), the free energy functional and we derive the stationarity equations. A more compact notation is introduced in Sec. 5.3 where we also define operators we need in the following sections. Sec. 5.4 deals with the symmetries of the phases and the segments, the order parameters and the (Legendre) coefficients needed. The bifurcation analysis is the topic of Sec. 5.5 and in the last section we conclude and review the results (Sec. 5.6).

5.2. General Model and Formalism

The system under consideration is a monodisperse fluid of N (possibly) branched chains in a volume V. The chains are discrete and consist of M cylindrically symmetric rod-like segments of R different types τ_p (so $p \in \{1, \cdots, R\}$) with dimensions l_{τ_p} and d_{τ_p} (and $l_{\tau_p} \gg d_{\tau_p}$). Segments on different chains are assumed to be impenetrable to each other, so the excluded volume of two chains is the relevant quantity (see Chap. 3). Every segment is labeled by m (so $m \in \{1, \cdots, M\}$) and its orientation is described by a single unit vector $\hat{\omega}_m$ pointing along the long axis. The conformation of a chain is specified by the orientations of all segments, $\mathbf{\Omega} = (\hat{\omega}_1, \cdots, \hat{\omega}_M)$. Note that the labeling of segments in a branched chain is not straightforward (see Fig. 5.1). A segment is characterized by its label and its type, as this specifies the interactions with other segments both within and outside the chain. However, not to complicate the notation straight away by using everywhere a label as well as a type specification, we will use just the label and assume it implicitly contains the type specification as well. So, suppose segment m is of type τ_p, then we write l_m instead of l_{τ_p} referring to its length. And for the ODF (Eq. 5.8), we write $f_m(\hat{\omega}_m)$ instead of $f_m^{(\tau_p)}(\hat{\omega}_m)$. Only later, we average over all segments of a certain type.
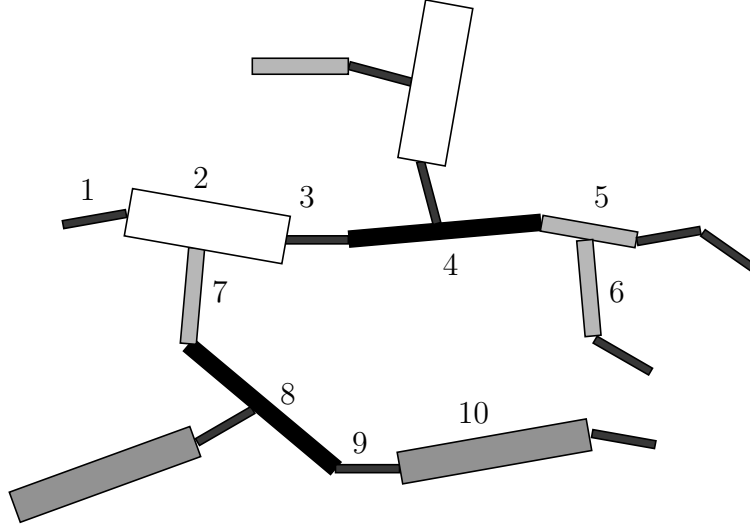
FIGURE 5.1. A branched heterochain of rodlike segments. The example of labeling is added to show that, in case of branched chains, segments with non-consecutive labels can be nearest neighbours (like 2 and 7).

In Chap. 3, we showed that the free energy $\mathcal{F}$ of a monodisperse fluid of hard chains in the second virial approximation and without spatial order is given by

$$\frac{\beta_{\mathrm{B}}\mathcal{F}[f]}{N} = \log\left(\rho\mathcal{V}_{\mathrm{T}}\right) + \int d\mathbf{\Omega} f(\mathbf{\Omega})\left[\log f(\mathbf{\Omega}) - 1\right] + \beta_{\mathrm{B}}\int d\mathbf{\Omega} f(\mathbf{\Omega})U(\mathbf{\Omega})$$
$$+ \tfrac{1}{2}\rho\int d\mathbf{\Omega} d\mathbf{\Omega}' f(\mathbf{\Omega})f(\mathbf{\Omega}')\mathcal{E}(\mathbf{\Omega}, \mathbf{\Omega}'). \tag{5.1}$$

$\beta_{\mathrm{B}} = 1/k_{\mathrm{B}}T$ is the Boltzmann factor, $\rho = N/V$ the number density, $\mathcal{V}_{\mathrm{T}}$ the "thermal volume". The quantity $U(\mathbf{\Omega})$ is the internal energy as a function of the conformation $\mathbf{\Omega}$ and $\mathcal{E}(\mathbf{\Omega}, \mathbf{\Omega}')$ is the volume excluded of two chains with conformations $\mathbf{\Omega}$ and $\mathbf{\Omega}'$. The function $f(\mathbf{\Omega})$ is the conformational distribution function (CDF) and is the normalized probability ($\int d\mathbf{\Omega} f(\mathbf{\Omega}) = 1$) of finding a chain with conformation $\mathbf{\Omega}$. And for the integral representation, we use $\int d\mathbf{\Omega} = \int d\hat{\omega}_1 \cdots d\hat{\omega}_M$.

In thermodynamic equilibrium, the free energy reaches a minimum and the functional is stationary. Therefore, we consider the variation of Eq. 5.1 with respect to the CDF,

$$\frac{\delta}{\delta f(\mathbf{\Omega})}\frac{\beta_{\mathrm{B}}\mathcal{F}}{N} - \beta_{\mathrm{B}}\mu = 0 \tag{5.2}$$

with the chemical potential μ playing the role of Lagrange multiplier needed to enforce normalization. Eliminating μ from Eq. 5.2 yields the stationarity equation,

$$f(\mathbf{\Omega}) = Q^{-1}[f]\exp\left[-\beta_{\mathrm{B}}U(\mathbf{\Omega}) - \rho\int d\mathbf{\Omega}' f(\mathbf{\Omega}')\mathcal{E}(\mathbf{\Omega}, \mathbf{\Omega}')\right] \tag{5.3}$$

in which Q is the factor due to normalization,

$$Q[f] = \int d\mathbf{\Omega}\exp\left[-\beta_{\mathrm{B}}U(\mathbf{\Omega}) - \rho\int d\mathbf{\Omega}' f(\mathbf{\Omega}')\mathcal{E}(\mathbf{\Omega}, \mathbf{\Omega}')\right]. \tag{5.4}$$

We now turn to more details in the description. As in Chap. 3, we approximate the excluded volume $\mathcal{E}(\mathbf{\Omega}, \mathbf{\Omega}')$ between two chains with the sum of their segment-segment excluded volumes,

$$\mathcal{E}(\mathbf{\Omega}, \mathbf{\Omega}') = \sum_{m,m'=1}^{M} \mathcal{E}_{m,m'}(\hat{\omega}_m, \hat{\omega}'_{m'}), \tag{5.5}$$

and allowing for different kinds of segments (differing in length l and width d),

$$\mathcal{E}_{m,m'}(\hat{\omega}_m, \hat{\omega}'_{m'}) = V_{m,m'} \sin \gamma(\hat{\omega}_m, \hat{\omega}'_{m'}) = l_m l_{m'}(d_m + d_{m'}) \sin \gamma(\hat{\omega}_m, \hat{\omega}'_{m'}), \tag{5.6}$$

where $\gamma(\hat{\omega}_m, \hat{\omega}'_{m'})$ is the plane angle between $\hat{\omega}_m$ and $\hat{\omega}'_{m'}$. The dimensions l_m and d_m are the length and width respectively of segment m and the volume $V_{m,m'}$ is defined by Eq. 5.6. Note that the excluded volume between two segments, $\mathcal{E}_{m,m'}$, is uniaxial, as it only depends on a polar angle, $\sin \gamma(\hat{\omega}_m, \hat{\omega}'_{m'}) = \sqrt{1 - (\hat{\omega}_m \cdot \hat{\omega}'_{m'})^2}$. Following Chap. 3, we assume here too that *within* a chain the segments only interact via their nearest neighbours m, m',

$$U(\mathbf{\Omega}) = \sum_{(m,m')} u_{m,m'}(\hat{\omega}_m, \hat{\omega}_{m'}), \tag{5.7}$$

where $\sum_{(m,m')}$ is the sum over all nearest neighbours (m, m') in the chain (with $(m, m') = (m', m)$, so every pair is only counted once). Eq. 5.7 does not take into account interactions within a chain which skip a number of segments (see Chap. 3). Although, we do not further specify $u_{m,m'}$ in this chapter, we assume it is uniaxial $u_{m,m'}(\hat{\omega}_m \cdot \hat{\omega}_{m'})$ as well as symmetric, $u_{m,m'} = u_{m',m}$. This is not necessary for the analysis, but it does apply to all cases we are interested in (see Chaps. 6 and 7).

Inserting these expressions for U and $\mathcal{E}$ in Eq. 5.3 and defining the single-segment orientational distribution function (ODF),

$$f_m(\hat{\omega}_m) = \prod_{k \neq m} d\hat{\omega}_k f(\mathbf{\Omega}), \tag{5.8}$$

yields a set of stationarity equations,

$$f_m(\hat{\omega}_m) = Q^{-1} \int \prod_{k \neq m} d\hat{\omega}_k \prod_{(k,k')} w_{k,k'}(\hat{\omega}_k, \hat{\omega}_{k'}) \prod_{k=1}^{M} \exp[-\beta_{\mathrm{B}} H_k(\hat{\omega}_k)], \tag{5.9}$$

where $\prod_{k \neq m}$ is a product over all k in the chain but the m'th segment. In this equation, the factors $w_{k,k'}(\hat{\omega}_k, \hat{\omega}_{k'}) = \exp[-\beta_{\mathrm{B}} u_{k,k'}(\hat{\omega}_k, \hat{\omega}_{k'})]$ are the flexibility interactions between nearest neighbours, and $H_k(\hat{\omega}_k)$ is the external effective field on the k'th segment depending selfconsistently on the ODF's,

$$\beta_{\mathrm{B}} H_k(\hat{\omega}_k) = \rho \sum_{k'=1}^{M} V_{k,k'} \int d\hat{\omega}' \sin \gamma(\hat{\omega}_k, \hat{\omega}') f_{k'}(\hat{\omega}'). \tag{5.10}$$

5.3. A Change of Notation

In this subsection, we will introduce a more compact notation to formulate the stationarity equations in the previous section. The notation we present is an extension of the one used by Mulder in Ref. [65]. We will first concentrate on Eqs. 5.9 and 5.10. The space of real integrable functions of orientation $\hat{\omega}$ is called $\mathcal{L}_{\hat{\omega}}$. With $g, h \in \mathcal{L}_{\hat{\omega}}$, the inner product in this space is

$$\langle g, h \rangle = \int d\hat{\omega} g(\hat{\omega}) h(\hat{\omega}). \tag{5.11}$$

And every element of $\mathcal{L}_{\hat{\omega}}$ can be interpreted as an linear operator on $\mathcal{L}_{\hat{\omega}}$ as well,

$$g[h](\hat{\omega}) = \int d\hat{\omega}' g(\hat{\omega}' \cdot \hat{\omega}) h(\hat{\omega}'). \tag{5.12}$$

We define an operator for the external field, $\mathcal{E}_{m,m'}$,

$$K_{k,k'}[g](\hat{\omega}) = V_{k,k'} \int d\hat{\omega}' \sin\gamma(\hat{\omega} \cdot \hat{\omega}') g(\hat{\omega}'). \tag{5.13}$$

Writing this even shorter, $K_{k,k'}[g] = K_{k,k'}[g](\hat{\omega})$ and in case of a labeled $\hat{\omega}_{k'}$, $K_{k,k'}[g]_{k'} = K_{k,k'}[g](\hat{\omega}_{k'})$. Similarly, we write $g_k = g_k(\hat{\omega})$ and $g_k|_k = g_k(\hat{\omega}_k)$. In the same way, the operator for the flexibility interaction becomes,

$$w_{k,k'}[g] = \int d\hat{\omega}' \exp[-\beta_{\mathrm{B}} u_{k,k'}(\hat{\omega} \cdot \hat{\omega}')] g(\hat{\omega}'). \tag{5.14}$$

Both $K_{k,k'}$ and $w_{k,k'}$ are again elements of $\mathcal{L}_{\hat{\omega}}$. Note that both are also Hermitian,

$$\langle g, K_{k,k'}[h] \rangle = \langle K_{k,k'}[g], h \rangle. \tag{5.15}$$

Next, we define the operator $\mathcal{W}_m$ acting on functions $G \in \mathcal{L}_{\hat{\omega}}^M$ and mapping them on $\mathcal{L}_{\hat{\omega}}$,

$$\mathcal{W}_m[[G|_{1,\cdots,M}]] = \int \prod_{k=1}^{M} d\hat{\omega}_k \delta(\hat{\omega} - \hat{\omega}_m) \prod_{(k,k')} w_{k,k'}(\hat{\omega}_k \cdot \hat{\omega}_{k'}) G(\hat{\omega}_1, \cdots, \hat{\omega}_M). \tag{5.16}$$

We have used double brackets to distinguish it from operators acting on $\mathcal{L}_{\hat{\omega}}$. Thus, the stationarity equations (Eqs. 5.9 and 5.10) in the new notation are

$$f_m = \frac{\mathcal{W}_m\left[\left[\prod_{k=1}^{M} \exp\left(-\rho \sum_{k'=1}^{M} K_{k,k'}[f_{k'}]_k\right)\right]\right]}{\left\langle 1, \mathcal{W}_m\left[\left[\prod_{k=1}^{M} \exp\left(-\rho \sum_{k'=1}^{M} K_{k,k'}[f_{k'}]_k\right)\right]\right]\right\rangle}. \tag{5.17}$$

In the bifurcation analysis, we will also need the action of $\mathcal{W}_m$ on a function $g \in \mathcal{L}_{\hat{\omega}}$ at segment m; $g|_m$, and even on two functions $g, h \in \mathcal{L}_{\hat{\omega}}$ at different segments m and m'; $g|_m$ and $h|_{m'}$. In the first case, Eq. 5.16 reduces to

$$\mathcal{W}_m[[g|_{m'}]] = \int \prod_{k=1}^{M} d\hat{\omega}_k \delta(\hat{\omega} - \hat{\omega}_m) \prod_{(k,k')} w_{k,k'}(\hat{\omega}_k \cdot \hat{\omega}_{k'}) g(\hat{\omega}_{m'})$$

$$= W_{m,m'}[g], \tag{5.18}$$

which defines the operator $W_{m,m'}$. Clearly, $W_{m,m'}$ is defined as being an operator and therefore not an element of $\mathcal{L}_{\hat{\omega}}$. The branched chains under consideration do not have

loops, i.e. between an arbitrary pair of segments m, m' there exists one and only one non-selfoverlapping path along the chain. We call the collection of all pairs of *nearest neighbour* segments (k, k') between m and m' (which are generally not nearest neighbours) the path $\mathcal{P}_{m,m'}$. For example, in Fig. 5.1, $\mathcal{P}_{6,10} = \{(6,5), (5,4), (4,3), (3,2), (2,7), (7,8), (8,9), (9,10)\}$. As $(k, k') = (k', k)$, notice that $\mathcal{P}_{m,m'} = \mathcal{P}_{m',m}$. So,

$$W_{m,m'}[g] = \left(w_{m,m_{P-1}}[\cdots w_{m_2,m_1}[w_{m_1,m'}[g]]]\right) \left(\prod_{(k,k') \notin \mathcal{P}_{m,m'}} w_{k,k'}[1] \right)$$

$$= \left(\sum_{\substack{i=0 \\ (m_i,m_{i+1}) \in \mathcal{P}_{m,m'}}}^{P-1} \left(w_{m_{i+1},m_i} \right) [g] \right) \left(\prod_{(k,k') \notin \mathcal{P}_{m,m'}} w_{k,k'}[1] \right), \qquad (5.19)$$

where we say that $\mathcal{P}$ has P elements, $m_0 = m'$ and $m_P = m$. The sequence of w_{m_{i+1},m_i}'s is not important, as they commute [1]. Consequently, it holds that $W_{m,m'} = W_{m',m}$ and $W_{m,m'}$ is Hermitian, $\langle g, W_{m,m'}[h] \rangle = \langle W_{m',m}[g], h \rangle = \langle W_{m,m'}[g], h \rangle$. Further, $W_{m,m'}[1] = \prod_{(k,k')} w_{k,k'}[1] = W^{(0)}$ and $W_{m,m}/W^{(0)}$ is the identity operator.

The action of $\mathcal{W}_m$ on two functions at two different segments,

$$\mathcal{W}_m[[g|_{m'}h|_{m''}]] = \int \prod_{k=1}^{M} d\hat{\omega}_k \delta(\hat{\omega} - \hat{\omega}_m) \prod_{(k,k')} w_{k,k'}(\hat{\omega}_k \cdot \hat{\omega}_{k'}) g(\hat{\omega}_{m'}) h(\hat{\omega}_{m''})$$

$$= W_{m,m',m''}[g, h], \qquad (5.20)$$

which defines the operator $W_{m,m',m''}$. Note that the index m', belongs to the argument g and the index m'' to h. Clearly, we have to switch both if we switch one, $W_{m,m',m''}[g, h] = W_{m,m'',m'}[h, g]$. Conveniently, we can decompose $W_{m,m',m''}$ in terms of $W_{m,m'}$'s. There are three different cases (see Fig. 5.2). First, m' and m'' are on different 'sides' of m (i.e. $\bigcap(\mathcal{P}_{m,m'}, \mathcal{P}_{m,m''}) = \emptyset$),

$$W_{m,m',m''}[g, h] = \left(W^{(0)} \right)^{-1} W_{m,m'}[g] W_{m,m''}[h]. \qquad (5.21)$$

Second, m' is between m and m'' (or vice versa) (i.e. $\bigcap(\mathcal{P}_{m,m'}, \mathcal{P}_{m,m''}) = \mathcal{P}_{m,m'}$), then,

$$W_{m,m',m''}[g, h] = \left(W^{(0)} \right)^{-1} W_{m,m'}[g W_{m',m''}[h]]. \qquad (5.22)$$

These previous two occur also for linear chains. The last one is specific for branched chains; m' and m'' are on different branches (with respect to m) (i.e. $\bigcap(\mathcal{P}_{m,m'}, \mathcal{P}_{m,m''}) = \mathcal{P}_{m,\tilde{m}}$, where $\tilde{m}$ is the segment where the two branches join (again, with respect to m)). So,

$$W_{m,m',m''}[g, h] = \left(W^{(0)} \right)^{-2} W_{m,\tilde{m}}[W_{\tilde{m},m'}[g] W_{\tilde{m},m''}[h]]. \qquad (5.23)$$

This segment $\tilde{m}$ has a special role in the last decomposition; it is always a 'joint', i.e. a segment where three or more arms meet. Arriving at this point, however, we see that we can generalize even further; also for the first two cases we can define a $\tilde{m}$. In the first case, $\tilde{m} = m$, and if we use this in Eq. 5.23, we see that it reduces to Eq. 5.21. In the second case, $\tilde{m} = m'$ (or m'') and again, Eq. 5.23 reduces to Eq. 5.22. The conclusion then is

---

[1]In our case, all $w_{k,k'}(\hat{\omega})$ are uniaxially symmetric and that is why they commute.
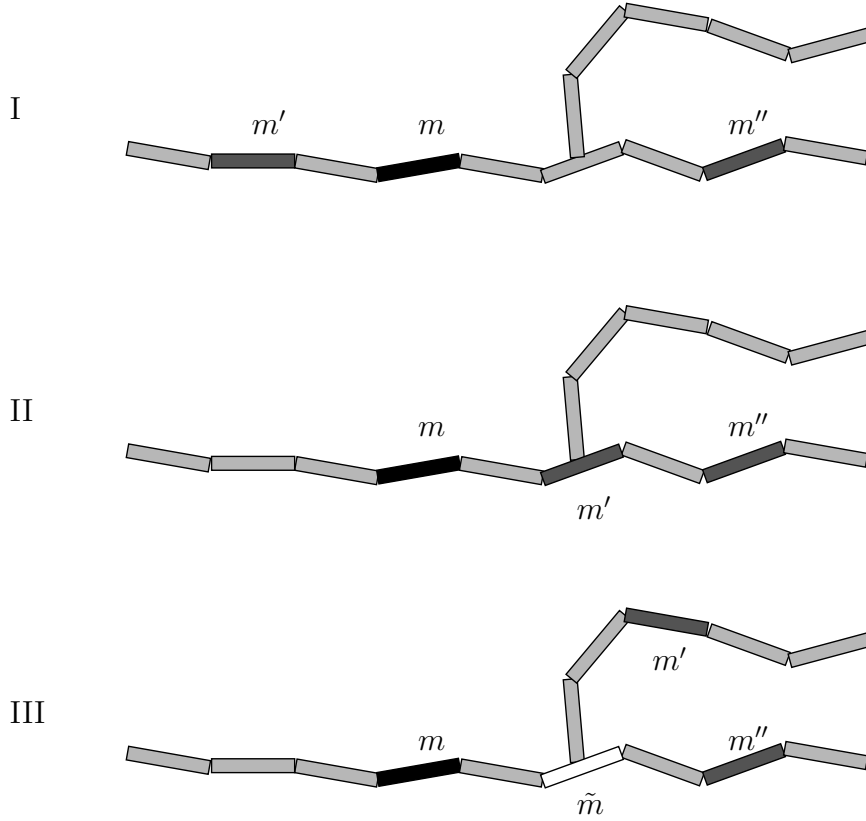
FIGURE 5.2. The three different cases of the operator $W_{m,m',m''}$ (see text). m in between m' and m'' (I), m' in between m and m'' (II) and m, m' and m'', all on different branches, coming together at joint $\tilde{m}$ (III).

that for every triplet m, m', m'' we can find one and only one $\tilde{m}$ for which $W_{m,m',m''}$ is always given by Eq. 5.23. It is straightforward to derive some properties. For instance, $g_1, g_2, g_3 \in \mathcal{L}_{\hat{\omega}}$,

$$\langle g_1, W_{m,m',m''}[g_2, g_3] \rangle = \left(W^{(0)} \right)^{-2} \langle W_{\tilde{m},m}[g_1], W_{\tilde{m},m'}[g_2] W_{\tilde{m},m''}[g_3] \rangle. \tag{5.24}$$

Further, $W_{m,m',m''}[g, 1] = W_{m,m'}[g]$.

5.4. Symmetries, Expansions and Order Parameters

In this section, we analyze what are the possible phases and what order parameters are needed. All segments are uniaxial and therefore they are described by a single unit vector $\hat{\omega}$. As we are considering fluidlike phases, we can have at most orientational ordering with respect to all three lab-fixed axes, $(\hat{x}, \hat{y}, \hat{z})$. One of these axes can be written in terms of the other two, e.g. $\hat{x} = \hat{y} \times \hat{z}$, so that for every segment we need at least two order parameters. A nematic phase with cylindrical symmetry has two equivalent axes, and one order parameter suffices. This nematic is called a uniaxial nematic. In case there is no cylindrical symmetry, there is ordering with respect to all three (or equivalently, two) axes and we are dealing with a biaxial nematic.

Next, we will quantify our statements. The ODF is a function of one unit vector $\hat{\omega} = (\theta, \phi)$, and thus it can be expanded in spherical harmonics,

$$f_m(\hat{\omega}) = \sum_{j=0}^{\infty} \sum_{i=-j}^{j} a_m^{(j,i)} Y_j^i(\hat{\omega}), \tag{5.25}$$

with the coefficients,

$$a_m^{(j,i)} = \langle f_m, Y_j^{i*} \rangle. \tag{5.26}$$

The possible biaxial phases which can occur are assumed to have inversion symmetry (inversion I of the phase does not affect properties) and D_2-symmetry (invariant under the D_2-operations, $D_2 = \{1, R_{\hat{x}}(\pi), R_{\hat{y}}(\pi), R_{\hat{z}}(\pi)\}$, with $R_\sigma(\pi)$ a rotation of π around axis σ). The symmetry group of the phase is then, $D_{2h}(= I \otimes D_2)$. This means that in the expansion 5.25 only terms with even j and i contribute and that $a_m^{(j,i)} = a_m^{(j,-i)}$. Defining $\Delta_{j,i}$-functions,

$$\Delta_{j,i}(\hat{\omega}) = \left(\tfrac{1}{2}\sqrt{2} \right)^{1+\delta_{i,0}} \sqrt{\frac{4\pi}{2j+1}} \left(Y_j^i(\hat{\omega}) + Y_j^{-i}(\hat{\omega}) \right) \tag{5.27}$$

(normalized such that $\int d\hat{\omega} \Delta_{j,i}(\hat{\omega}) \Delta_{j',i'}(\hat{\omega}) = \frac{4\pi}{2j+1} \delta_{j,j'} \delta_{i,i'}$) the ODF-expansion becomes

$$f_m(\hat{\omega}) = \sum_{j=0}^{\infty} \sum_{i=0}^{j} \frac{2j+1}{4\pi} \tilde{a}_m^{(j,i)} \Delta_{j,i}(\hat{\omega}), \tag{5.28}$$

with both i and j even. The coefficients are then given by

$$\tilde{a}_m^{(j,i)} = \langle f_m, \Delta_{j,i} \rangle. \tag{5.29}$$

Due to normalization of f_m, $\tilde{a}_m^{(0,0)} = 1$. In the isotropic phase, all other coefficients are zero, whereas in the nematic phase, these are nonzero. The lowest-order coefficients different in the isotropic and the nematic phases are those with $j = 2$. The $\Delta_{2,i}$-functions are

$$\Delta_{2,0} = \tfrac{1}{2} \left[3(\hat{\omega} \cdot \hat{z})^2 - 1 \right], \tag{5.30}$$

$$\Delta_{2,2} = \tfrac{1}{2}\sqrt{3} \left[(\hat{\omega} \cdot \hat{y})^2 - (\hat{\omega} \cdot \hat{x})^2 \right], \tag{5.31}$$

(they can of course be rewritten as the following relation holds, $(\hat{\omega} \cdot \hat{z})^2 + (\hat{\omega} \cdot \hat{y})^2 + (\hat{\omega} \cdot \hat{x})^2 = 1$) In terms of spherical coordinates they are

$$\Delta_{2,0} = \tfrac{1}{2} \left[3\cos^2\theta - 1 \right], \tag{5.32}$$

$$\Delta_{2,2} = \tfrac{1}{2}\sqrt{3} \left[\cos 2\phi \sin^2\theta \right]. \tag{5.33}$$

The $j = 2$-coefficients of f_m we choose as our order parameters, so

$$S_m = \tilde{a}_m^{(2,0)} = \langle f_m, \Delta_{2,0} \rangle \tag{5.34}$$

$$B_m = \tilde{a}_m^{(2,2)} = \langle f_m, \Delta_{2,2} \rangle. \tag{5.35}$$

S_m is the usual Maier-Saupe order parameter for uniaxial nematics, with $\hat{z}$ the (main) nematic director. $\hat{y}$ defines a second director with respect to which the system can order, i.e. into a biaxial nematic phase. The biaxial order parameter B_m is zero in the isotropic and uniaxial nematic phases and nonzero in the biaxial nematic.

Next, we will also need the expansions of $w_{k,k'}$ and $K_{k,k'}$. Both have uniaxial symmetry, so

$$\begin{pmatrix} w_{k,k'}(\hat{\omega} \cdot \hat{\omega}') \\ K_{k,k'}(\hat{\omega} \cdot \hat{\omega}') \end{pmatrix} = \sum_{j=0}^{\infty} \frac{2j+1}{4\pi} \begin{pmatrix} w_{k,k'}^{(j)} \\ K_{k,k'}^{(j)} \end{pmatrix} P_j(\hat{\omega} \cdot \hat{\omega}'). \tag{5.36}$$

From Eq. 5.13, it is also clear that $K_{k,k'}$ is also symmetric under exchanging $\hat{\omega}$ with $-\hat{\omega}$ (and $\hat{\omega}'$ with $-\hat{\omega}'$), so $K_{k,k'}^{(j)} = 0$ for odd j. Using $P_j(\hat{\omega} \cdot \hat{\omega}') = \sum_{i=-j}^{j} \frac{4\pi}{2j+1} Y_j^i(\hat{\omega}) Y_j^{-i}(\hat{\omega}')$ it follows that

$$P_{j'}[\Delta_{j,i}](\hat{\omega}) = \frac{4\pi}{2j+1} \Delta_{j,i}(\hat{\omega}), \tag{5.37}$$

where we have used $P_{j'}$ as an operator. Consequently,

$$\begin{pmatrix} w_{k,k'} \\ K_{k,k'} \end{pmatrix} [\Delta_{j,i}] = \begin{pmatrix} w_{k,k'}^{(j)} \\ K_{k,k'}^{(j)} \end{pmatrix} \Delta_{j,i}. \tag{5.38}$$

And applying this to Eq. 5.19 we obtain

$$W_{m,m'}[\Delta_{j,i}] = \left(\prod_{\substack{i=0 \\ (m_i, m_{i+1}) \in \mathcal{P}_{m,m'}}}^{P-1} w_{m_{i+1},m_i}^{(j)} \right) \left(\prod_{(k,k') \notin \mathcal{P}_{m,m'}} w_{k,k'}^{(0)} \right) \Delta_{j,i} \tag{5.39}$$

$$= W_{m,m'}^{(j)} \Delta_{j,i},$$

which defines the "coefficients" $W_{m,m'}^{(j)}$ (these are not Legendre coefficients!). From this we see that for our choice of uniaxial $w_{k,k'}$, it does not matter in which direction the path is traveled; all $w_{k,k'}$ commute with each other. Finally, we will need the following inner products

$$\langle \Delta_{j,i}, \Delta_{j',i'} \Delta_{j'',i''} \rangle = 4\pi \left(\tfrac{1}{2}\sqrt{2} \right)^{1-\delta_{0,ii'i''}} \begin{pmatrix} j & j' & j'' \\ i & \tau'i' & \tau''i'' \end{pmatrix} \begin{pmatrix} j & j' & j'' \\ 0 & 0 & 0 \end{pmatrix}, \tag{5.40}$$

in which the round brackets denote the Wigner 3-j symbols. τ' and τ'' are freely chosen from $\{-1, 1\}$ in order to get $i + \tau'i' + \tau''i'' = 0$ and $j + j' + j''$ is even (if these conditions are not fulfilled, $\langle \Delta_{j,i}, \Delta_{j',i'} \Delta_{j'',i''} \rangle = 0$). So, summarizing,

$$\langle \Delta_{j,i}, K_{m,m'}[\Delta_{j',i'}] \rangle = K_{m,m'}^{(j)} \delta_{j,j'} \delta_{i,i'}, \tag{5.41}$$

$$\langle \Delta_{j,i}, W_{m,m'}[\Delta_{j',i'}] \rangle = W_{m,m'}^{(j)} \delta_{j,j'} \delta_{i,i'}, \tag{5.42}$$

and

$$\langle \Delta_{j,i}, W_{m,m',m''}[\Delta_{j',i'}, \Delta_{j'',i''}] \rangle =$$

$$= 4\pi \left(\tfrac{1}{2}\sqrt{2} \right)^{1-\delta_{0,ii'i''}} W_{m,m',m''}^{(j,j',j'')} \begin{pmatrix} j & j' & j'' \\ i & \tau'i' & \tau''i'' \end{pmatrix} \begin{pmatrix} j & j' & j'' \\ 0 & 0 & 0 \end{pmatrix}$$

$$= 4\pi \left(\tfrac{1}{2}\sqrt{2} \right)^{1-\delta_{0,ii'i''}} W_{\tilde{m},m}^{(j)} W_{\tilde{m},m'}^{(j')} W_{\tilde{m},m''}^{(j'')} \begin{pmatrix} j & j' & j'' \\ i & \tau'i' & \tau''i'' \end{pmatrix} \begin{pmatrix} j & j' & j'' \\ 0 & 0 & 0 \end{pmatrix}, \tag{5.43}$$

in which $\tilde{m}$ is the segment corresponding to the triplet m, m', m'' (see between Eqs. 5.23 and 5.24). Here, we have defined the "coefficients" $W^{(j,j',j'')}_{m,m',m''}$. The relevant nonzero 3-j symbols for our analysis are

$$\begin{pmatrix} 2 & 2 & 2 \\ 0 & 0 & 0 \end{pmatrix} = -\begin{pmatrix} 2 & 2 & 2 \\ 0 & 2 & -2 \end{pmatrix} = -\sqrt{\frac{2}{35}}. \tag{5.44}$$

5.5. Bifurcation Analysis

5.5.1. Bifurcation Analysis: Segment Labels. In this subsection, we determine the properties of the point in the phase diagram where a nematic solution branches off the isotropic one; the bifurcation point. At every density ρ, the isotropic distributions ($f_{k,0} = 1/4\pi$) are solutions to the stationarity equations. At low densities these are (meta)stable, whereas at high densities they are unstable. The density at which the isotropic solution changes stability, is called the bifurcation density and a new non-isotropic (nematic) solution appears. In order to find the properties of the bifurcation point, we proceed by constructing solutions which are isotropic with small (infinitesimal) nematic perturbations. The perturbations are characterized by a single (arbitrary) parameter ε and the solutions are expanded in the following way,

$$f_k = f_{k,0} + \varepsilon f_{k,1} + \varepsilon^2 f_{k,2} + \cdots$$
$$\rho = \rho_0 + \varepsilon \rho_1 + \varepsilon^2 \rho_2 + \cdots. \tag{5.45}$$

These expansions are inserted in Eqs. 5.17, and terms of equal order in ε will be equated. We first expand

$$\prod_k \exp\left(-\rho \sum_{k'} K_{k,k'} [f_{k'}]_k\right) =$$
$$\exp\left(-(\rho_0 + \varepsilon\rho_1 + \varepsilon^2\rho_2) \sum_{k,k'} K_{k,k'} [f_{k',0}]_k\right) \left\{ 1 - \varepsilon\rho_0 \sum_{k,k'} K_{k,k'} [f_{k',1}]_k \right.$$
$$\left. -\varepsilon^2\left(\rho_1 \sum_{k,k'} K_{k,k'} [f_{k',1}]_k + \rho_0 \sum_{k,k'} K_{k,k'} [f_{k',2}]_k - \tfrac{1}{2}\rho_0^2\left(\sum_{k,k'} K_{k,k'} [f_{k',1}]_k\right)^2\right)\right\}. \tag{5.46}$$

Now, $f_{k,0} = 1/4\pi$ so the exponential factor in front is a constant. The operation of $\mathcal{W}_m$ on Eqs. 5.46,

$$\mathcal{W}_m\left[\left[\prod_k \exp\left(-\rho \sum_{k'} K_{k,k'} [f_{k'}]_k\right)\right]\right] = \exp\left(-\frac{1}{4\pi}(\rho_0 + \varepsilon\rho_1\right.$$
$$\left. +\varepsilon^2\rho_2) \sum_{k,k'} K_{k,k'} [1]\right)\left\{ W^{(0)} - \varepsilon\rho_0 \sum_k W_{m,k}\left[\sum_{k'} K_{k,k'} [f_{k',1}]\right] + \right.$$

$$-\varepsilon^2 \left(\rho_1 \sum_k W_{m,k} \left[\sum_{k'} K_{k,k'} \left[f_{k',1} \right] \right] + \rho_0 \sum_k W_{m,k} \left[\sum_{k'} K_{k,k'} \left[f_{k',2} \right] \right] \right.$$

$$\left. -\tfrac{1}{2}\rho_0^2 \sum_{k,l} W_{m,k,l} \left[\sum_{k'} K_{k,k'} \left[f_{k',1} \right], \sum_{l'} K_{l,l'} \left[f_{l',1} \right] \right] \right) \right\}. \quad (5.47)$$

Due to the normalization, the exponential prefactor disappears. Further, we have $\langle 1, f_{k,n} \rangle = 0$ for $n > 0$. We now equate the equal orders in ε. The zeroth order is trivial, the first order bifurcation equations are

$$f_{m,1} = -\frac{\rho_0}{4\pi W^{(0)}} \sum_k W_{m,k} \left[\sum_{k'} K_{k,k'} \left[f_{k',1} \right] \right], \quad (5.48)$$

and to second order in ε,

$$f_{m,2} =$$

$$- \left(4\pi W^{(0)} \right)^{-1} \left\{ \rho_0 \sum_k W_{m,k} \left[\sum_{k'} K_{k,k'} \left[f_{k',2} \right] \right] + \rho_1 \sum_k W_{m,k} \left[\sum_{k'} K_{k,k'} \left[f_{k',1} \right] \right] \right.$$

$$- \frac{1}{2}\rho_0^2 \left(\sum_{k,l} W_{m,k,l} \left[\sum_{k'} K_{k,k'} \left[f_{k',1} \right], \sum_{l'} K_{l,l'} \left[f_{l',1} \right] \right] \right.$$

$$\left. \left. - \frac{1}{4\pi} \left\langle 1, \sum_{k,l} W_{m,k,l} \left[\sum_{k'} K_{k,k'} \left[f_{k',1} \right], \sum_{l'} K_{l,l'} \left[f_{l',1} \right] \right] \right\rangle \right) \right\}. \quad (5.49)$$

We concentrate for a moment on the first order bifurcation equation, Eq. 5.48. Both $K_{k,k'}$ and $W_{m,k}$ have such a form that they do not mix the various vectors in solution space; i.e. both of them map $\Delta_{j,i}$ on $\Delta_{j,i}$ for every j, i. And also, the eigenvalues (see Eqs. 5.38) are only dependent on the j-mode. Consequently, $f_{k,1}$ must be a linear combination of harmonics of only a single j,

$$f_{k,1} = \sum_i c_{k,1}^{(j,i)} \Delta_{j,i}, \quad (5.50)$$

where the $c_{k,1}^{(j,i)}$ are coefficients. Then, on the basis of experience and the form of the excluded volume operator (Eq. 5.13, i.e. with a single broad minimum for total alignment of the two particles and no other minima, see Ref. [65]) we expect the system to become unstable first with respect to the $j = 2$-mode [2]. So,

$$f_{k,1} = c_{k,1}^{(2,0)} \Delta_{2,0} + c_{k,1}^{(2,2)} \Delta_{2,2}. \quad (5.51)$$

Substituting this in Eqs. 5.48 and 5.49 and taking the inner product with $\Delta_{2,i}$, we get two equations for the first order (for $i = 0$ and $i = 2$),

$$c_{m,1}^{(2,i)} = -\frac{\rho_0}{4\pi W^{(0)}} \sum_k W_{m,k}^{(2)} \sum_{k'} K_{k,k'}^{(2)} c_{k',1}^{(2,i)}, \quad (5.52)$$

---

[2] In principle, it still matters what form the $w_{k,k'}$ have, but we assume that it does not affect this statement.

and also two for the second order,

$$c_{m,2}^{(2,i)} + \left(4\pi W^{(0)}\right)^{-1} \left\{ \sum_k W_{m,k}^{(2)} \sum_{k'} K_{k,k'}^{(2)} \left(\rho_0 c_{k',2}^{(2,i)} + \rho_1 c_{k',1}^{(2,i)} \right) \right. $$

$$\left. + \frac{1}{2}\rho_0^2 \sum_{k,l} W_{m,k,l}^{(2,2,2)} \sum_{k'} K_{k,k'}^{(2)} \sum_{l'} K_{l,l'}^{(2)} \langle f_{k',1} f_{l',1}, \Delta_{2,i} \rangle \right\} = 0, \quad (5.53)$$

with

$$\langle f_{k',1} f_{l',1}, \Delta_{2,0} \rangle = -4\pi\frac{2}{35} \left(c_{k',1}^{(2,0)} c_{l',1}^{(2,0)} - c_{k',1}^{(2,2)} c_{l',1}^{(2,2)} \right)$$

$$\langle f_{k',1} f_{l',1}, \Delta_{2,2} \rangle = 4\pi\frac{2}{35} \left(c_{k',1}^{(2,0)} c_{l',1}^{(2,2)} + c_{k',1}^{(2,2)} c_{l',1}^{(2,0)} \right).$$

The constant normalization term drops out because its inner product with $\Delta_{2,i}$ is zero. Turning again to the first-order bifurcation equation, Eq. 5.52, we can make one final step on this level. We have obtained two eigenvalue equations, for $i = 0, 2$. However, in both cases the eigenvalue (corresponding to ρ_0) is the same and so is the matrix. Therefore, we conclude that the two problems must be the same and so are the eigenvectors, up to a multiplicative constant, $c_{k',1}^{(2,2)} = \mu c_{k',1}^{(2,0)} = \mu c_{k',1}$, where we drop the superscript from now on. So the two first-order bifurcation equations reduce to one,

$$c_{m,1} = -\frac{\rho_0}{4\pi W^{(0)}} \sum_k W_{m,k}^{(2)} \sum_{k'} K_{k,k'}^{(2)} c_{k',1}. \qquad (5.54)$$

The problem with this linear eigenvalue equation is that it is too big. $c_{m,1}$ is a vector of dimension M which is very large in general. Therefore, in the next subsection, we will average over all segments of a certain type.

5.5.2. Bifurcation Analysis: Type Averages. In this subsection, we will reformulate the bifurcation analysis in terms of the types, where previously, we have done that in terms of segment labels. The reason for this is that the number of types R is typically much smaller than M, reducing the bifurcation equation from a M-dimensional to a R-dimensional problem. With R being 2 in case of main chain polymers (Chap. 6) or 3 in case of side chain polymers (Chap. 7) the bifurcation equation should be tractable.

We first define the average ODF of a certain type,

$$f_{\tau_p}(\hat{\omega}) = \frac{1}{M_{\tau_p}} \sum_{k \in \tau_p} f_k(\hat{\omega}). \qquad (5.55)$$

Consequently, a similar equation holds for the coefficients,

$$c_{\tau_p,n}^{(j,i)} = \frac{1}{M_{\tau_p}} \sum_{k \in \tau_p} c_{k,n}^{(j,i)}. \qquad (5.56)$$

Turning again to the first-order bifurcation equation, Eq. 5.54, we proceed by recognizing that the quantity $K_{k,k'}^{(2)}$ is the same for all $k \in \tau_q$ and $k' \in \tau_{q'}$. Consequently, we can

write

$$\sum_{k'} K^{(2)}_{k,k'} c_{k',1} = \sum_{q'} \sum_{k' \in \tau_{q'}} K^{(2)}_{k,k'} c_{k',1}$$

$$= \frac{1}{M_{\tau_q}} \sum_{q'} M_{\tau_q} M_{\tau_{q'}} K^{(2)}_{k,k'} \frac{1}{M_{\tau_{q'}}} \sum_{k' \in \tau_{q'}} c_{k',1}$$

$$= \frac{1}{M_{\tau_q}} \sum_{q'} K^{(2)}_{\tau_q,\tau_{q'}} c_{\tau_{q'},1} \qquad (5.57)$$

where we have defined $K^{(2)}_{\tau_q,\tau_{q'}} = M_{\tau_q} M_{\tau_{q'}} K^{(2)}_{k,k'}$ for $k \in \tau_q$ and $k' \in \tau_{q'}$. Defining also

$$W^{(2)}_{\tau_p,\tau_{p'}} = \frac{1}{M_{\tau_p} M_{\tau_{p'}}} \sum_{k \in \tau_p} \sum_{k' \in \tau_{p'}} W^{(2)}_{k,k'}, \qquad (5.58)$$

$$W^{(2,2,2)}_{\tau_p,\tau_{p'},\tau_{p''}} = \frac{1}{M_{\tau_p} M_{\tau_{p'}} M_{\tau_{p''}}} \sum_{k \in \tau_p} \sum_{k' \in \tau_{p'}} \sum_{k'' \in \tau_{p''}} W^{(2,2,2)}_{k,k',k''}. \qquad (5.59)$$

we can write for the first-order bifurcation equation (combining Eqs. 5.56, 5.57 and 5.58 with Eq. 5.54),

$$c_{\tau_p,1} = -\frac{\rho_0}{4\pi W^{(0)}} \sum_q W^{(2)}_{\tau_p,\tau_q} \sum_{q'} K^{(2)}_{\tau_q,\tau_{q'}} c_{\tau_{q'},1}, \qquad (5.60)$$

In the same way, Eqs. 5.53 can be written in terms of these 'type-specific' quantities. We give them without further details, for $i = 0$,

$$c^{(2,0)}_{\tau_p,2} - \frac{\rho_1}{\rho_0} c_{\tau_p,1} + \left(4\pi W^{(0)}\right)^{-1} \left\{ \rho_0 \sum_q W^{(2)}_{\tau_p,\tau_q} \sum_{q'} K^{(2)}_{\tau_q,\tau_{q'}} c^{(2,0)}_{\tau_{q'},2} \right.$$

$$\left. -2\pi \frac{2}{35} \rho_0^2 \left(1 - \mu^2\right) \sum_{q,r} W^{(2,2,2)}_{\tau_p,\tau_q,\tau_r} \sum_{q'} K^{(2)}_{\tau_q,\tau_{q'}} c_{\tau_{q'},1} \sum_{r'} K^{(2)}_{\tau_r,\tau_{r'}} c_{\tau_{r'},1} \right\} = 0, \quad (5.61)$$

and for $i = 2$,

$$c^{(2,2)}_{\tau_p,2} - \frac{\rho_1 \mu}{\rho_0} c_{\tau_p,1} + \left(4\pi W^{(0)}\right)^{-1} \left\{ \rho_0 \sum_q W^{(2)}_{\tau_p,\tau_q} \sum_{q'} K^{(2)}_{\tau_q,\tau_{q'}} c^{(2,2)}_{\tau_{q'},2} \right.$$

$$\left. +4\pi \frac{2}{35} \rho_0^2 \mu \sum_{q,r} W^{(2,2,2)}_{\tau_p,\tau_q,\tau_r} \sum_{q'} K^{(2)}_{\tau_q,\tau_{q'}} c_{\tau_{q'},1} \sum_{r'} K^{(2)}_{\tau_r,\tau_{r'}} c_{\tau_{r'},1} \right\} = 0, \quad (5.62)$$

where we have substituted

$$\left\langle f_{\tau_{q'},1} f_{\tau_{r'},1}, \Delta_{2,0} \right\rangle = -4\pi \frac{2}{35} \left(1 - \mu^2\right) c_{\tau_{q'},1} c_{\tau_{r'},1}$$

$$\left\langle f_{\tau_{q'},1} f_{\tau_{r'},1}, \Delta_{2,2} \right\rangle = 4\pi \frac{2}{35} 2\mu c_{\tau_{q'},1} c_{\tau_{r'},1}.$$

We have also used Eq. 5.60 and the fact that $c^{(2,2)}_{\tau_p,1} = \mu c^{(2,0)}_{\tau_p,1} = \mu c_{\tau_p,1}$. This can be expressed more compact in terms of matrices, so the first order equation,

$$\mathbf{c}_1 = -\frac{\rho_0}{4\pi W^{(0)}} \mathbf{W}^{(2)} \cdot \mathbf{K}^{(2)} \cdot \mathbf{c}_1, \tag{5.63}$$

and the second order for $i = 0$,

$$\mathbf{c}_2^{(2,0)} - \frac{\rho_1}{\rho_0} \mathbf{c}_1 + \left(4\pi W^{(0)}\right)^{-1} \left\{ \rho_0 \mathbf{W}^{(2)} \cdot \mathbf{K}^{(2)} \cdot \mathbf{c}_2^{(2,0)} \right.$$
$$\left. -2\pi \frac{2}{35} \rho_0^2 \left(1 - \mu^2\right) \mathbf{W}^{(2,2,2)} : \left(\mathbf{K}^{(2)} \cdot \mathbf{c}_1\right)^2 \right\} = 0, \tag{5.64}$$

and for $i = 2$,

$$\mathbf{c}_2^{(2,2)} - \frac{\rho_1 \mu}{\rho_0} \mathbf{c}_1 + \left(4\pi W^{(0)}\right)^{-1} \left\{ \rho_0 \mathbf{W}^{(2)} \cdot \mathbf{K}^{(2)} \cdot \mathbf{c}_2^{(2,2)} \right.$$
$$\left. +4\pi \frac{2}{35} \rho_0^2 \mu \mathbf{W}^{(2,2,2)} : \left(\mathbf{K}^{(2)} \cdot \mathbf{c}_1\right)^2 \right\} = 0. \tag{5.65}$$

The dot product refers to ordinary matrix multiplication. The notation " : " refers to contraction with respect to two indices, and we have written $\left(\mathbf{K}^{(2)} \cdot \mathbf{c}_1\right)^2$ instead of $\left(\mathbf{K}^{(2)} \cdot \mathbf{c}_1\right) \otimes \left(\mathbf{K}^{(2)} \cdot \mathbf{c}_1\right)$. At this point, we want to emphasize that the bold face symbols refer to the type-specific quantities and consequently have dimensions R (for vectors), $R \times R$ (for matrices) or $R \times R \times R$ (for $\mathbf{W}^{(2,2,2)}$).

Again, we first consider the first-order bifurcation equations. Eq. 5.63 is an $R \times R$ matrix eigenvalue equation where we suppose that R is reasonably small, so it is solvable. The eigenvalues of $(W^{(0)})^{-1}\mathbf{W}^{(2)} \cdot \mathbf{K}^{(2)}$, we call λ_p and the corresponding eigenvectors $\mathbf{v}_p$. We assume that the eigenvalues are labelled in increasing order, i.e. $p = 1$ corresponds to the most negative, and $p = R$ to the most positive one. The physical argument, we then use is that the eigenvalue which corresponds to the lowest (positive) density is selected, i.e. λ_1 and therefore $\mathbf{c}_1 = \mathbf{v}_1$. Consequently,

$$\mathbf{f}_1 = \mathbf{v}_1(\Delta_{2,0} + \mu\Delta_{2,2}), \quad \rho_0 = -\frac{4\pi}{\lambda_1}. \tag{5.66}$$

The coefficient μ has to be obtained from the second order bifurcation equations. The dual eigenvector $\bar{\mathbf{c}}_1$ at the same eigenvalue is generally not the same as $\mathbf{c}_1$ as $(W^{(0)})^{-1}\mathbf{W}^{(2)} \cdot \mathbf{K}^{(2)}$ is not Hermitian. We normalize as follows, $\bar{\mathbf{c}}_1^* \cdot \mathbf{c}_1 = 1$ (the asterisk as superscript refers to the comlex conjugate of the vector).

Turning now to the second order equations, we assume that it is the case that $(W^{(0)})^{-1}\mathbf{W}^{(2)} \cdot \mathbf{K}^{(2)}$ is diagonizable [3]. When the matrix is diagonizable, the set of eigenvectors $\mathbf{v}_p$ form a complete (though generally not orthogonal) basis in R-dimensional space. (In case of Hermitian matrices, an orthogonal set is obtained.) The dual eigenvectors $\mathbf{w}_p$ (or left eigenvectors, as opposed to the normal right eigenvectors) are generally not the same as $\mathbf{v}_p$ (again only in case of Hermitian matrices, $\mathbf{w}_p = \mathbf{v}_p$). An interesting property is that although $\mathbf{v}_p^*$ is not necessarily orthogonal to other $\mathbf{v}_{p'}$, this does hold

---

[3]If a matrix is not diagonalizable, there are eigenvalues with degeneracy greater than the dimension of their corresponding eigenspace, and a Jordan form is the best one can get. We do not consider this case here.

for $\mathbf{w}_p^*$, i.e. $\mathbf{w}_p^* \perp \mathbf{v}_{p'}$ if $\lambda_p \neq \lambda_{p'}$. (In case of degenerate eigenvalues we can construct the (dual) eigenvectors in such a way that the above still holds.) Further, we assume they are normalized in the following way, $\mathbf{w}_p^* \cdot \mathbf{v}_p = 1$ and note that $\bar{\mathbf{c}}_1 = \mathbf{w}_1$. Consequently, we can expand the vectors $\mathbf{c}_2^{(2,i)}$ (for $i = 0, 2$) in terms of the complete set $\mathbf{v}_p$,

$$\mathbf{c}_2^{(2,i)} = \sum_p \alpha_p^{(2,i)} \mathbf{v}_p, \tag{5.67}$$

and the coefficients $\alpha_p^{(2,i)}$,

$$\alpha_p^{(2,i)} = \mathbf{w}_p^* \cdot \mathbf{c}_2^{(2,i)}. \tag{5.68}$$

So,

$$(W^{(0)})^{-1} \mathbf{W}^{(2)} \cdot \mathbf{K}^{(2)} \cdot \mathbf{c}_2^{(2,i)} = \sum_p \lambda_p \alpha_p^{(2,i)} \mathbf{v}_p. \tag{5.69}$$

Taking the inner product of Eqs. 5.64 and 5.65 with $\bar{\mathbf{c}}_1^*$ and remembering that $\rho_0 = -4\pi/\lambda_1$, we then get for $i = 0$,

$$\frac{\rho_1}{\rho_0} + \frac{1}{2}\frac{2}{35}\rho_0^2 \left(1 - \mu^2\right) \left(W^{(0)}\right)^{-1} \left(\bar{\mathbf{c}}_1 \cdot \mathbf{W}^{(2,2,2)} : \left(\mathbf{K}^{(2)} \cdot \mathbf{c}_1\right)^2\right) = 0, \tag{5.70}$$

and for $i = 2$,

$$\frac{\rho_1 \mu}{\rho_0} - \frac{2}{35}\rho_0^2 \mu \left(W^{(0)}\right)^{-1} \left(\bar{\mathbf{c}}_1 \cdot \mathbf{W}^{(2,2,2)} : \left(\mathbf{K}^{(2)} \cdot \mathbf{c}_1\right)^2\right) = 0. \tag{5.71}$$

These are two equations, with two unknown variables, ρ_1 and μ, which can be solved;

$$\mu = 0 \quad \text{or} \quad \mu = \pm\sqrt{3}, \tag{5.72}$$

and

$$\rho_1 = \frac{2}{35}\rho_0^3 \left(W^{(0)}\right)^{-1} \left(\bar{\mathbf{c}}_1 \cdot \mathbf{W}^{(2,2,2)} : \left(\mathbf{K}^{(2)} \cdot \mathbf{c}_1\right)^2\right) \neq 0. \tag{5.73}$$

If $\left(\bar{\mathbf{c}}_1 \cdot \mathbf{W}^{(2,2,2)} : \left(\mathbf{K}^{(2)} \cdot \mathbf{c}_1\right)^2\right) = 0$, then, $\rho_1 = 0$, and μ has to be determined from the next-order bifurcation equations (third), but will generally not be as in Eqs. 5.72. Using Eq. 5.72 in Eqs. 5.64 and 5.65, it follows that the two second order bifurcation equations are also the same (like the first order), hence $\mathbf{c}_2^{(2,2)} = \nu \mathbf{c}_2^{(2,0)} = \nu \mathbf{c}_2$, with ν a prefactor. The other $(R-1)$ (independent) equations (inner products of $\mathbf{w}_p^*$ with Eqs. 5.64 or 5.65) yield the components $\alpha_p^{(2,0)} = \alpha_p$ except for $p = 1$. If needed, the α_1 and ν can be determined from the next order bifurcation equations. When $\rho_1 = 0$, the vectors $\mathbf{c}_2^{(2,0)}$ and $\mathbf{c}_2^{(2,2)}$ will generally be different. Physically, all values of μ in Eqs. 5.72 correspond to a uniaxial nematic phase (substitute μ in Eqs. 5.66). When $\rho_1 = 0$, μ is generally different and the resulting phase is a biaxial nematic which has lower symmetry. We review the results more extensively in the next section.

5.6. Conclusion

As was stated, the eigenvalue λ_1 corresponding to the lowest (positive) density yields the physical solution. The components of the corresponding eigenvector, $\mathbf{c}_1$, represent the relative order of the various types (infinitesimally small at the bifurcation point). However, in principle $\mathbf{c}_1$, as well as $-\mathbf{c}_1$ solve the equations. One sign corresponds to ordering parallel to the nematic director $\hat{n}$ (which is the physical solution) and the other to ordering perpendicular to $\hat{n}$ (which has to be discarded on basis of physical arguments). The sign can be found by realizing that the field (on segments of any type) must have a minimum for $\hat{\omega} = \hat{n}$, and therefore, it must hold that $\sum_{q=1}^{R} K^{(2)}_{\tau_p,\tau_q} \cdot c_{\tau_q,1} \leq 0$ for all p.

The three solutions for μ (Eq. 5.72), all correspond to uniaxial ordering, although with respect to different axes ($\hat{z}$, $\hat{y}$ or $\hat{x}$) (as can be easily checked from Eq. 5.66). In general, the phase transition is first order, because $\rho_1 \neq 0$. When $\rho_1 = 0$, μ has to be determined from the next-order bifurcation equations. In that case, the nematic phase is generally biaxial and the phase transition second order. The latter is only expected to happen, when there are two or more components, preferring different axes of ordering (i.e. chains with joints where two (or more) branches are perpendicularly connected). In case of uniaxial ordering, we can state without loss of generality (choosing the $\hat{z}$ as the nematic director),

$$\mathbf{f}_1 = \mathbf{c}_1 P_2, \quad \rho_0 = -\frac{4\pi}{\lambda_1} \ . \tag{5.74}$$

The eigenvector $\mathbf{c}_1$ yields the relative *average* order of each of the R components. However, different segments of some type, can still have different order, depending on where they are in the chain. For instance, segment k of type τ_p is likely to have a different order than segment k' of type τ_p if its neighbouring segments are different. If we want to know the differences in ordering for segments of the same type τ_p, we need the vector $c_{k,1}$ instead of $c_{\tau_p,1}$. Their relation is given by Eq. 5.56. Then, considering Eq. 5.60, if we do not average over the last label m, we obtain

$$c_{m,1} = -\frac{\rho_0}{4\pi W^{(0)}} \sum_q W^{(2)}_{m,\tau_q} \sum_{q'} K^{(2)}_{\tau_q,\tau_{q'}} c_{\tau_{q'},1}, \tag{5.75}$$

with the $M \times R$-matrix,

$$W^{(2)}_{m,\tau_q} = \frac{1}{M_{\tau_q}} \sum_{k \in \tau_q} W^{(2)}_{m,k}. \tag{5.76}$$

So, when, the (R-dimensional) eigenvector $\mathbf{c}_1$ (with elements $c_{\tau_p,1}$) is obtained from the bifurcation analysis, one can calculate the (M-dimensional) eigenvector $c_{m,1}$ as well. The 'only' extra quantity, we need to know is the matrix $W^{(2)}_{m,\tau_q}$.

In ending this chapter, we want to summarize the results. Using the approach of segmented chains, we have written down the equations for orientational ordering in a monodisperse fluid of (very generally) branched heteropolymers. The segments are hard bodies, and within the polymer, bending interactions between successive segments are included. We have derived the equations describing the system's behaviour at the isotropic-to-nematic bifurcation point. The central quantity is the matrix $(W^{(0)})^{-1}\mathbf{W}^{(2)}$.

$\mathbf{K}^{(2)}$, whose most negative eigenvalue, λ_1, corresponds to the bifurcation density, $\rho_0 = -4\pi/\lambda_1$. The corresponding eigenvector $\mathbf{c}_1$ represents the average order distribution over the various types. The bifurcating order of individual segments can also be computed. The matrix $\mathbf{K}^{(2)}$ is usually quite straightforward to compute, but $(W^{(0)})^{-1}\mathbf{W}^{(2)}$ can be more tedious. In general, the bifurcating phase is uniaxial and the phase transition first order, but in case the quantity $(\bar{\mathbf{c}}_1 \cdot \mathbf{W}^{(2,2,2)} : (\mathbf{K}^{(2)} \cdot \mathbf{c}_1)^2)$ is zero, the phase transition is second order to a biaxial nematic (although, to be sure, the next-order equations need to be solved). These general results are used in the chapters following this one, applied to more specific systems, like main chain and side chain polymers.

6

MAIN CHAIN LC POLYMERS

The isotropic-to-nematic bifurcation analysis is applied to main chain liquid crystalline (LC) polymers. We compute the bifurcation density and the bifurcating order along the polymer as a function of 4 model parameters.

6.1. Introduction

Mesogenic molecules are capable of forming LC (or mesomorphic) phases as a function of temperature or concentration, in which case they are thermotropic or lyotropic, respectively. Incorporating these mesogenic groups in polymers in the right way, they may keep their LC behaviour, like e.g. field orientability and birefringence. From an applied perspective, these 'liquid crystalline polymers' (LCP's) have some additional interesting properties, compared to low-molecular weight LC's. The polymer character may render the material effectively solid, allowing it to be formable into films or fibers without the need to contain it in a cell – chemical cross links may be added to stabilize. The resulting long time constants make these materials interesting for optical data storage. Furthermore, the glass temperature is increased and crystallinity is usually totally suppressed, so the LC state can even be frozen in. Other advantages are the prevention of demixing of the various components and the possibility to incorporate even other kinds of groups (with e.g. fluorescent properties) in the polymers as well. There are roughly two kinds of LCP's containing mesogenic groups; those, where they are located within the polymers, are called main chain LCP's, and those, which have side chains containing them, are referred to as side chain LCP's – although there are also combinations of both. Some books on the structure, properties and applications of LCP's are Refs. [1, 26, 86, 87]. In this chapter, we focus on main chain polymers; side chain LCP's are the subject of the next chapter.

Already in 1923, Vorländer studied the effect of increasing molecular length in melts of benzene rings para linked through ester groups, and noted the increasing transition temperatures [4]. Synthesizing a polymer of these units, poly(p-benzamide), he found that it did not melt but instead it charred, concluding that very long molecules might be liquid crystalline but that practical problems interfere, i.e. unmeltable in this case. In 1956, Robinson reported on the structure and phase equilibria of poly(γ-benzyl-L-glutamate) [22]. These first LCP's were polymers in solution where the stiff main chains themselves acted as LC formers. They were investigated to develop synthetic silk, eventually leading to the development of high-tensile strength fibers like Kevlar [23] – although the importance of their LC nature to these fibers was not fully recognized
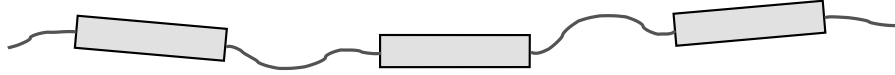
FIGURE 6.1. A few units of a main chain LC polymer.

until the 80's. The successfull introduction of applications based on low-molecular weight LC's, like LC displays, in the 60's and 70's, lead to an exploding interest in LCP's. Substantial progress was made by Jackson and Kuhfuss, who synthesized random copolyesters, thus bringing down the melting temperature considerably [24]. And later, the importance of the spacer concept, first applied in side chain LCP's, made its way to main chain LCP's, allowing the incorporation of real mesogens. At present, all LC phases found for low molecular weight LC's (and more) have been found for LCP's and the field is as large as ever. Some popular topics are chirality and (anti)ferroelectricity in LCP's, elastomers and dendrimers.

Pioneering work in the understanding of LC behavior in rodlike molecules was done by Onsager [7], Flory [8] and Maier and Saupe [9]. However, flexibility of the molecules is a key ingredient in describing LC behavior of polymers. Theories modeling main chain LCP's as wormlike chains, which have flexibility distributed homogeneously along the chain, date mostly from the 80's [33, 34, 52]. Khokhlov and Semenov derived an expression for the conformational entropy of wormlike chains in terms of distribution functions [32, 33]. Warner and coworkers used expansions in spheroidal wave functions [34, 88]. In the beginning of the 90's, some theories for main chain LCP's were formulated using as an ingredient the actual geometry of the molecules, i.e. having stiffer and more flexible parts [89, 90, 91, 92] – although there had been earlier attempts by Khokhlov and coworkers (see Ref. [93] and references therein). Simulations of genuine long polymer systems have not been performed, simply because the systems are too big. There are some reports for shorter molecules, consisting of linked hard spheres [94], somewhat flexible spherocylinders [95] and mesogens separated by spacers [96].

In this chapter, we consider main chain LC polymers consisting of rodlike mesogens and wormlike spacers. These main chain LCP's are described by 4 or, in case they are infinitely long, 3 parameters. We formulate the isotropic-to-nematic (I-N) bifurcation analysis developed in Chap. 5 for this system, so the interaction between two polymers is their mutual excluded volume, and we use the Onsager approximation. The bifurcation analysis takes into account the interactions within the chain in an exact fashion. The results are analytical expressions for the I-N bifurcation density and relative bifurcating order along the chain as a function of model parameters. We compare our results with the Maier-Saupelike theories of Yurasova and coworkers [89, 90, 91] and Wang and Warner [92].
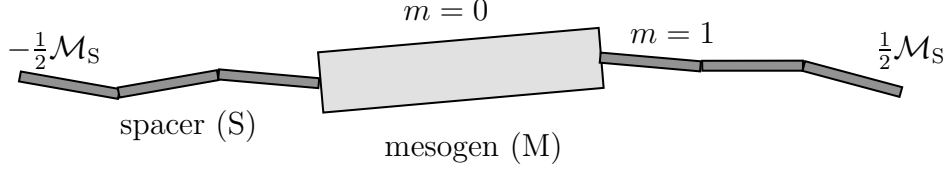
FIGURE 6.2. A unit of a main chain LC polymer.

6.2. Model Parameters

The main chain polymers, we consider, consist of $\mathcal{N}$ repeating units. Every unit consists of a mesogen and a bit of spacer on each side (see Figs. 6.1 and 6.2). We use the segmented-chain approach of the previous chapter. In that language, we have two types of segments, and $R = 2$. The mesogens (type $\tau_2 = M$) have dimensions l_M and d_M and their total number in the polymer is $M_M = \mathcal{N}\mathcal{M}_M = \mathcal{N}$ ($\mathcal{M}_M = 1$ is the number of mesogens in a unit). The number of spacer segments (type $\tau_1 = S$) in one unit is $\mathcal{M}_S$, so their total number is $M_S = \mathcal{N}\mathcal{M}_S$. The spacer segments have dimensions l_S and d_S. Suppose for simplicity that $\mathcal{M}_S$ is even, so every unit consists of $\frac{1}{2}\mathcal{M}_S$ spacer segments, a mesogen segment and again $\frac{1}{2}\mathcal{M}_S$ spacer segments, see Fig. 6.2. The segment label is m (or k) and runs along the chain; $m \in \{1, \cdots, M\}$, with $M = \mathcal{N}(\mathcal{M}_S + 1)$ the total number of segments. Every $(n(\mathcal{M}_S + 1) - \frac{1}{2}\mathcal{M}_S)$'th segment (with n the label of a unit) is a mesogen, all the others are spacer segments. Often, we also use the label m within a unit, so then $m \in \{-\frac{1}{2}\mathcal{M}_S, \cdots, \frac{1}{2}\mathcal{M}_S\}$. It should be clear from the context, what the range of m is.

We recall the excluded volume between two segments m and m' on different polymers is

$$\mathcal{E}_{m,m'}(\hat{\omega}, \hat{\omega}') = l_{\tau_p} l_{\tau_{p'}} (d_{\tau_p} + d_{\tau_{p'}}) |\sin \gamma(\hat{\omega}, \hat{\omega}')|, \tag{6.1}$$

where $m \in \tau_p$ and $m' \in \tau_{p'}$. Between nearest-neighbour segments within a polymer, we use the same potential as in Chap. 3, as it is locally harmonic in case of mutual alignment,

$$u_{m,m+1}(\hat{\omega}, \hat{\omega}') = -J_S \hat{\omega} \cdot \hat{\omega}'. \tag{6.2}$$

We assume this potential between the spacer segments, but, to curb the number of parameters, also between the spacer and the mesogen segments.

In order to loose an extra model parameter, we use (lateron) the wormlike chain limit (WCL) for the spacers. Since Khokhlov and Semenov [33], the wormlike chain concept is quite popular as a model for main chain LC polymers. However, here we assume the mesogens to be liquid crystalline and not so much the wormlike spacers, which act (only) to decouple the mesogens. The WCL for the spacers is given by

$$l_S \to 0, \quad \beta_B J_S \to \infty, \quad \mathcal{M}_S \to \infty, \tag{6.3}$$

with the following combinations remaining constant,

$$P_S = \beta_B J_S l_S \quad \bar{\mathcal{M}}_S = \mathcal{M}_S / \beta_B J_S. \tag{6.4}$$

FIGURE 6.3. The wormlike chain limit

The quantities P_S and $\bar{\mathcal{M}}_S$ are the persistence length of the spacer and the number of persistence lengths in one spacer, respectively. The label becomes continuously as well, $\bar{m} = (m/M)\bar{M}$ (and therefore $m \to \infty$). In general, a bar over a quantity refers to the WCL.

Another way to reduce the number of parameters is by assuming the polymer to be infinitely long. Due to translational symmetry along the chain, every unit is the same as its neighbour (and there are no free end effects). One has to take care to rescale the density as well,

$$\mathcal{N} \to \infty, \quad \rho \to 0 \quad \text{with} \quad \rho\mathcal{N} \quad \text{finite,} \tag{6.5}$$

where, obviously, $\rho\mathcal{N}$ is the unit number density (whereas ρ is the polymer number density). This limit, we call the infinite polymer limit (IPL). We will explicitly state when this limit is used or not (furtheron, we will also investigate the effect of increasing chain lengths).

Using the scale invariance of the system, we define dimensionless quantities to reduce the number of effective parameters even more. The dimensions of the mesogens are the most logical choice to use as a standard, as these are not subject to either the WCL or the IPL, so

$$\tilde{P}_S = P_S/l_M \quad \text{and} \quad \tilde{d}_S = d_S/d_M, \tag{6.6}$$

and the dimensionless unit density

$$\eta = 2l_M^2 d_M \rho\mathcal{N}. \tag{6.7}$$

The main chain polymers in the WCL and using dimensionless quantities are described by 4 or, also using the IPL, 3 model parameters, i.e. $\tilde{P}_S$, $\tilde{d}_S$, $\bar{\mathcal{M}}_S$ and, in case of finite polymer lengths, $\mathcal{N}$. In physical situations, $\tilde{d}_S$ will usually be smaller than one. In fact, we will use frequently the case that $\tilde{d}_S = 0$. It is instructive, because there are no contributions from the SS interactions (there is no excluded volume between two zero-thickness spacers). However, note that the MS excluded volume is not zero, so the zero-thickness spacers still contribute (Eq. 6.1).

The nematic phase in this system of polymers is uniaxial. All components in the polymer favour parallel ordering, and there is no molecular mechanism which can oppose this. Therefore, we need only the uniaxial nematic order parameters, one for every component,

$$S^{(\tau_p)} = \langle f_{\tau_p}, P_2 \rangle \tag{6.8}$$

We are also interested in the order along the polymer,

$$S_m = \langle f_m, P_2 \rangle, \tag{6.9}$$

which is related with Eq. 6.8 through $S^{(\tau_p)} = \frac{1}{M_{\tau_p}} \sum_{m \in \tau_p} S_m$. In the following, as we did just here, we usually write things in the segmented chain approach (with discrete labels etc.) and specifically state when the WCL or the IPL is applied.

6.3. Bifurcation Details

In this section, we evaluate the matrices $\mathbf{K}^{(2)}$ and $\mathbf{W}^{(2)}/W^{(0)}$, which are needed to solve the first-order bifurcation equation (Eq. 5.63). First, we consider the segmented chains, and then, the WCL and the IPL are applied. The results of the bifurcation analysis are the subject of the next section.

To be complete, we give again the bifurcation equation,

$$\mathbf{c} = -\frac{\rho_0}{4\pi W^{(0)}} \mathbf{W}^{(2)} \mathbf{K}^{(2)} \mathbf{c}, \tag{6.10}$$

where the lowest positive value for ρ_0 equals the (physical) bifurcation density ρ_*. The 2 elements of the bifurcating vector $\mathbf{c}_*$ yield the relative bifurcating order of the components. The 2×2-matrix $\mathbf{K}^{(2)}$ is has the following elements (Eqs. 5.13 and 5.36),

$$K_{\tau_p, \tau_{p'}} = s_2 \mathcal{N}^2 \mathcal{M}_{\tau_p} l_{\tau_p} \mathcal{M}_{\tau_{p'}} l_{\tau_{p'}} (d_{\tau_p} + d_{\tau_{p'}}). \tag{6.11}$$

Of course, $\mathcal{M}_M = 1$ and $s_2 = -\pi^2/8$ is the second Legendre coefficient of $|\sin\gamma|$. We normalize $\mathbf{K}^{(2)}$ with respect to its lower right element, $\boldsymbol{\kappa} = (s_2 \mathcal{N}^2 2 l_M^2 d_M)^{-1} \mathbf{K}^{(2)}$. In the WCL, we obtain

$$\bar{\boldsymbol{\kappa}} = \begin{bmatrix} \bar{\mathcal{M}}_S^2 \tilde{P}_S^2 \tilde{d}_S & \bar{\mathcal{M}}_S \tilde{P}_S \frac{1}{2}(1 + \tilde{d}_S) \\ \bar{\mathcal{M}}_S \tilde{P}_S \frac{1}{2}(1 + \tilde{d}_S) & 1 \end{bmatrix}. \tag{6.12}$$

Note that there is no $\mathcal{N}$-dependence in $\bar{\boldsymbol{\kappa}}$.

Next, we caculate the elements of the 2×2-matrix $\mathbf{W}^{(2)}/W^{(0)}$. From Eq. 6.2, we know that all interactions between nearest-neighbour segments are the same. Therefore, between two segments m and m', we get simply (see Eq. 5.39)

$$\frac{W_{m,m'}^{(2)}}{W^{(0)}} = \sigma^{|m-m'|} \tag{6.13}$$

with $\sigma = w^{(2)}/w^{(0)}$. The coefficients $w^{(j)}$ are the jth Legendre coefficients of $w(\cos\theta) = \exp[\beta J_S \hat{\omega} \cdot \hat{\omega}']$, and θ the angle between $\hat{\omega}$ and $\hat{\omega}'$. Consequently, the expression for the elements of $\mathbf{W}^{(2)}/W^{(0)}$ (see Eq. 5.58),

$$\frac{W_{\tau_p, \tau_{p'}}^{(2)}}{W^{(0)}} = \frac{1}{M_{\tau_p} M_{\tau_{p'}}} \sum_{m \in \tau_p} \sum_{m' \in \tau_{p'}} \sigma^{|m-m'|}, \tag{6.14}$$

with both τ_p and $\tau_{p'}$ being either S or M. At this point, we define $\boldsymbol{\alpha} = \mathcal{N} \mathbf{W}^{(2)}/W^{(0)}$, in order to have a compact notation, and also, to rescale it with $\mathcal{N}$ because the elements of

$\mathbf{W}^{(2)}/W^{(0)}$ diverge in the IPL. Consequently, the expressions for the elements of $\boldsymbol{\alpha}$ are

$$\alpha_{S,S} = \frac{\mathcal{N}}{\mathcal{N}^2 \mathcal{M}_S^2} \sum_{m,m'=1}^{\mathcal{N}(\mathcal{M}_S+1)} \sigma^{|m-m'|} - \frac{\alpha_{S,M} + \alpha_{M,S}}{\mathcal{M}_S} - \frac{\alpha_{M,M}}{\mathcal{M}_S^2} \tag{6.15}$$

$$\alpha_{S,M} = \alpha_{M,S} = \frac{\mathcal{N}}{\mathcal{N}^2 \mathcal{M}_S} \sum_{m=1}^{\mathcal{N}(\mathcal{M}_S+1)} \sum_{n=1}^{\mathcal{N}} \sigma^{|m-(n(\mathcal{M}_S+1)-\frac{1}{2}\mathcal{M}_S)|} - \frac{\alpha_{M,M}}{\mathcal{M}_S} \tag{6.16}$$

$$\alpha_{M,M} = \frac{\mathcal{N}}{\mathcal{N}^2} \sum_{n,n'=1}^{\mathcal{N}} \sigma^{|n-n'|(\mathcal{M}_S+1)} \tag{6.17}$$

where we have (partly) expressed the elements in a recurrent fashion. We note that all sums above can be performed analytically. However, we are mainly interested in the results in the WCL and therefore proceed directly. In the WCL, σ becomes (to first order in $1/\beta J$)

$$\sigma = \frac{\int_{-1}^1 dx P_2(x) \exp[\beta J x]}{\int_{-1}^1 dx \exp[\beta J x]} \to 1 - 3(\beta J)^{-1}, \tag{6.18}$$

and therefore

$$\sigma^{\mathcal{M}_S} \to \left(1 - 3(\beta J)^{-1}\right)^{\beta J \bar{\mathcal{M}}_S} = \exp\left[-3\bar{\mathcal{M}}_S\right], \tag{6.19}$$

where we have used $\lim_{n\to\infty}(1+\frac{x}{n})^n = e^x$. As an example, we evaluate the summation in Eq. 6.17 (over n and n'),

$$\frac{1}{\mathcal{N}} \sum_{n,n'=1}^{\mathcal{N}} \sigma^{|n-n'|(\mathcal{M}_S+1)} \to \frac{1}{\mathcal{N}} \sum_{n,n'=1}^{\mathcal{N}} e^{-3\bar{\mathcal{M}}_S|n-n'|}$$

$$= \frac{1 + e^{-3\bar{\mathcal{M}}_S}}{1 - e^{-3\bar{\mathcal{M}}_S}} \left(1 - \frac{2e^{-3\bar{\mathcal{M}}_S}}{\mathcal{N}} \frac{1 - e^{-3\mathcal{N}\bar{\mathcal{M}}_S}}{1 - e^{-6\bar{\mathcal{M}}_S}}\right). \tag{6.20}$$

For the summations over m, we note that these become integrals in the WCL,

$$\frac{1}{\mathcal{N}\mathcal{M}_S} \sum_{m=1}^{\mathcal{N}(\mathcal{M}_S+1)} \to \frac{1}{\mathcal{N}\bar{\mathcal{M}}_S} \int_0^{\mathcal{N}\bar{\mathcal{M}}_S} d\bar{m}, \tag{6.21}$$

and finally, the contributions due to $\alpha_{M,M}$ in Eq. 6.16 and those due to $\alpha_{M,M}$ and $\alpha_{S,M}$ in Eq. 6.15 go to zero in WCL. Skipping the rest of the integral evaluations, we immediately move on to the results, and Eqs. 6.15 to 6.17 become, in the WCL,

$$\bar{\alpha}_{S,S} = \frac{2}{3\bar{\mathcal{M}}_S} \left(1 - \frac{1 - e^{-3\mathcal{N}\bar{\mathcal{M}}_S}}{3\mathcal{N}\bar{\mathcal{M}}_S}\right) \tag{6.22}$$

$$\bar{\alpha}_{S,M} = \bar{\alpha}_{M,S} = \frac{2}{3\bar{\mathcal{M}}_S} \left(1 - \frac{e^{-\frac{3}{2}\bar{\mathcal{M}}_S}}{\mathcal{N}} \frac{1 - e^{-3\mathcal{N}\bar{\mathcal{M}}_S}}{1 - e^{-3\bar{\mathcal{M}}_S}}\right) \tag{6.23}$$

$$\bar{\alpha}_{M,M} = \frac{1 + e^{-3\bar{\mathcal{M}}_S}}{1 - e^{-3\bar{\mathcal{M}}_S}} \left(1 - \frac{2e^{-3\bar{\mathcal{M}}_S}}{\mathcal{N}} \frac{1 - e^{-3\mathcal{N}\bar{\mathcal{M}}_S}}{1 - e^{-6\bar{\mathcal{M}}_S}}\right) \tag{6.24}$$

For infinitely long polymers (IPL), it is clear which terms drop out, and the matrix $\bar{\boldsymbol{\alpha}}$ becomes

$$\bar{\boldsymbol{\alpha}} = \left[\begin{array}{cc} \frac{2}{3\mathcal{M}_S} & \frac{2}{3\mathcal{M}_S} \\ \frac{2}{3\mathcal{M}_S} & \frac{1+e^{-3\mathcal{M}_S}}{1-e^{-3\mathcal{M}_S}} \end{array} \right] \tag{6.25}$$

In terms of these new matrices $\bar{\boldsymbol{\kappa}}$ and $\bar{\boldsymbol{\alpha}}$ the bifurcation equation is

$$\bar{\mathbf{c}} = -\frac{\eta_0 s_2}{4\pi} \bar{\boldsymbol{\alpha}} \bar{\boldsymbol{\kappa}} \bar{\mathbf{c}}. \tag{6.26}$$

As the problem is 2-dimensional, it has solutions

$$-\frac{\eta_0 s_2}{4\pi} = \frac{\pi \eta_0}{32} = 2 \left/ \left(\text{tr}(\bar{\boldsymbol{\alpha}}\bar{\boldsymbol{\kappa}}) \pm \sqrt{\text{tr}^2(\bar{\boldsymbol{\alpha}}\bar{\boldsymbol{\kappa}}) - 4\det(\bar{\boldsymbol{\alpha}}\bar{\boldsymbol{\kappa}})} \right) \right. , \tag{6.27}$$

with tr and det being the trace and determinant of matrices respectively. $\text{tr}(\bar{\boldsymbol{\alpha}}\bar{\boldsymbol{\kappa}})$ is always larger than zero; $\det(\bar{\boldsymbol{\alpha}}\bar{\boldsymbol{\kappa}})$ can be both positive and negative. (It can be checked as well that $\text{tr}^2(\bar{\boldsymbol{\alpha}}\bar{\boldsymbol{\kappa}}) \geq 4\det(\bar{\boldsymbol{\alpha}}\bar{\boldsymbol{\kappa}})$ for this system, so that the eigenvalues are real.) Consequently, the physical bifurcation density is given by

$$\eta_* = \frac{64}{\pi} \left/ \left(\text{tr}(\bar{\boldsymbol{\alpha}}\bar{\boldsymbol{\kappa}}) + \sqrt{\text{tr}^2(\bar{\boldsymbol{\alpha}}\bar{\boldsymbol{\kappa}}) - 4\det(\bar{\boldsymbol{\alpha}}\bar{\boldsymbol{\kappa}})} \right) \right. , \tag{6.28}$$

and, putting the mesogen order to one, $\bar{\mathbf{c}}_* = \left(\begin{array}{c} \bar{c}_{S,*} \\ 1 \end{array} \right)$, we get for the average order of the spacers,

$$\bar{c}_{S,*} = (2(\bar{\boldsymbol{\alpha}}\bar{\boldsymbol{\kappa}})^{(2,1)})^{-1} \left((\bar{\boldsymbol{\alpha}}\bar{\boldsymbol{\kappa}})^{(1,1)} - (\bar{\boldsymbol{\alpha}}\bar{\boldsymbol{\kappa}})^{(2,2)} + \sqrt{\text{tr}^2(\bar{\boldsymbol{\alpha}}\bar{\boldsymbol{\kappa}}) - 4\det(\bar{\boldsymbol{\alpha}}\bar{\boldsymbol{\kappa}})} \right), \tag{6.29}$$

with $(\bar{\boldsymbol{\alpha}}\bar{\boldsymbol{\kappa}})^{(i,j)}$ being the (i,j)'th element of the matrix $\bar{\boldsymbol{\alpha}}\bar{\boldsymbol{\kappa}}$.

The bifurcating order along the polymer, is given by the M-dimensional (primed) vector $\mathbf{c}'$ (see Eqs. 5.75 and 5.76),

$$\mathbf{c}' = -\frac{\rho_0}{4\pi W^{(0)}} \mathbf{W}^{(2)'} \mathbf{K}^{(2)} \mathbf{c}, \tag{6.30}$$

and the (primed) $M \times 2$-matrix $\mathbf{W}^{(2)'}$ is given by

$$\frac{W^{(2)}_{m,\tau_{p'}}{}'}{W^{(0)}} = \frac{1}{M_{\tau_{p'}}} \sum_{m' \in \tau_{p'}} \sigma^{|m-m'|}. \tag{6.31}$$

Also in this case, we define $\boldsymbol{\alpha}' = \mathcal{N} \mathbf{W}^{(2)'}/W^{(0)}$. In the WCL, the discrete segment label m becomes continuous and the elements of $\boldsymbol{\alpha}'$ behave as $\alpha'_{m,\tau_{p'}} \to \bar{\alpha}'_{\tau_p,\tau_{p'}}(\bar{m})$, where $m, \bar{m} \in \tau_p$. So, in the WCL, also $\bar{\boldsymbol{\alpha}}'$ is a 2×2-matrix, differing from $\bar{\boldsymbol{\alpha}}$ that its elements depend on $\bar{m}$. Note that, because $\bar{m} \in \tau_p$, $\bar{\alpha}'_{\tau_p,\tau_{p'}}(\bar{m})$ is not symmetrical. The evaluation of $\bar{\boldsymbol{\alpha}}'$ is similar to that of $\bar{\boldsymbol{\alpha}}$, so we give them without further comment,

$$\bar{\alpha}'_{S,S}(\bar{m}, n) = \frac{1}{3\bar{\mathcal{M}}_S} \left(2 - e^{-3(\bar{m}+(n-\frac{1}{2})\bar{\mathcal{M}}_S)} - e^{-3((\mathcal{N}-n+\frac{1}{2})\bar{\mathcal{M}}_S-\bar{m})} \right) \tag{6.32}$$
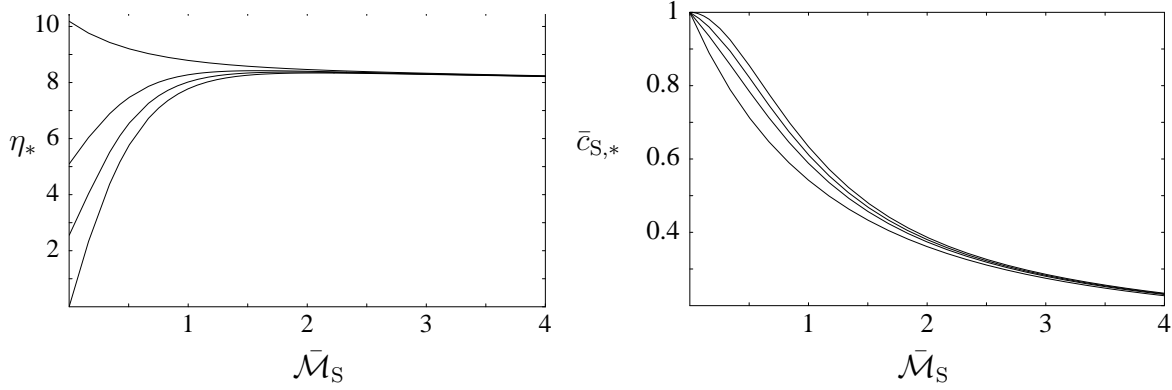
FIGURE 6.4. The I-N bifurcation density (left) and the relative bifurcating order of the spacers (right) as a function of spacer length, $\bar{\mathcal{M}}_\mathrm{S}$, for various values of the polymer length, $\mathcal{N}$. The parameters are $\tilde{P}_\mathrm{S} = 0.3$ and $\tilde{d}_\mathrm{S} = 0$. For the left figure, from the top curve to the bottom, the polymer length is, respectively, $\mathcal{N} = 1$, $\mathcal{N} = 2$, $\mathcal{N} = 4$ and $\mathcal{N} = \infty$. For the right figure, this is the same, except that $\mathcal{N}$ increases from bottom to top. It can be checked that at $\bar{\mathcal{M}}_\mathrm{S} = 0$, $\eta_* = 32/\pi\mathcal{N}$ (the rigid rod result). The average order of the mesogens is set equal to 1.

$$\bar{\alpha}'_{S,M}(\bar{m}, n) = \mathrm{e}^{-3|\bar{m}|} + \mathrm{e}^{-3(\bar{\mathcal{M}}_\mathrm{S}+\bar{m})}\frac{1 - \mathrm{e}^{-3(n-1)\bar{\mathcal{M}}_\mathrm{S}}}{1 - \mathrm{e}^{-3\bar{\mathcal{M}}_\mathrm{S}}}$$

$$+ \mathrm{e}^{-3(\bar{\mathcal{M}}_\mathrm{S}-\bar{m})}\frac{1 - \mathrm{e}^{-3(\mathcal{N}-n)\bar{\mathcal{M}}_\mathrm{S}}}{1 - \mathrm{e}^{-3\bar{\mathcal{M}}_\mathrm{S}}} \quad (6.33)$$

$$\bar{\alpha}'_{M,S}(n) = \frac{1}{3\bar{\mathcal{M}}_\mathrm{S}}\left(2 - \mathrm{e}^{-3(n-\frac{1}{2})\bar{\mathcal{M}}_\mathrm{S}} - \mathrm{e}^{-3(\mathcal{N}-n+\frac{1}{2})\bar{\mathcal{M}}_\mathrm{S}}\right) \quad (6.34)$$

$$\bar{\alpha}'_{M,M}(n) = \frac{1 + \mathrm{e}^{-3\bar{\mathcal{M}}_\mathrm{S}} - \mathrm{e}^{-3n\bar{\mathcal{M}}_\mathrm{S}} - \mathrm{e}^{-3(\mathcal{N}-n+1)\bar{\mathcal{M}}_\mathrm{S}}}{1 - \mathrm{e}^{-3\bar{\mathcal{M}}_\mathrm{S}}} \quad (6.35)$$

In Eqs. 6.32 to 6.35, n denotes the unit-dependence, and therefore, the label $\bar{m}$ stays within the unit, $\bar{m} \in [-\frac{1}{2}\bar{\mathcal{M}}_\mathrm{S}, \frac{1}{2}\bar{\mathcal{M}}_\mathrm{S}]$. In case of infinite polymer lengths, both $\mathcal{N}$ and n (and their difference, $\mathcal{N} - n$) go to infinity, and it is clear which terms in Eqs. 6.32 to 6.35 drop out. In all cases it holds that

$$\bar{\boldsymbol{\alpha}} = \frac{1}{\mathcal{N}\bar{\mathcal{M}}_\mathrm{S}}\sum_{n=1}^{\mathcal{N}}\int_{-\frac{1}{2}\bar{\mathcal{M}}_\mathrm{S}}^{\frac{1}{2}\bar{\mathcal{M}}_\mathrm{S}} d\bar{m}\,\bar{\boldsymbol{\alpha}}'(\bar{m}, n). \quad (6.36)$$

So, having solved the eigenvalue problem, Eq. 6.26, for η_* and $\bar{\mathbf{c}}_*$, one can compute the order along the polymer,

$$\bar{\mathbf{c}}'_* = \begin{pmatrix} \bar{c}'_{\mathrm{S},*}(\bar{m}, n) \\ \bar{c}'_{\mathrm{M},*}(n) \end{pmatrix} = -\frac{\eta_* s_2}{4\pi}\bar{\boldsymbol{\alpha}}'(\bar{m}, n)\bar{\boldsymbol{\kappa}}\bar{\mathbf{c}}_* \quad (6.37)$$

where, again, we emphasize that $\bar{m} \in [-\frac{1}{2}\bar{\mathcal{M}}_\mathrm{S}, \frac{1}{2}\bar{\mathcal{M}}_\mathrm{S}]$ and $n \in \{1, \cdots, \mathcal{N}\}$.

Finally, in ending this section, we want to mention a few limiting cases of our system for which we know the results (at least, on the level of the bifurcation analysis). In case
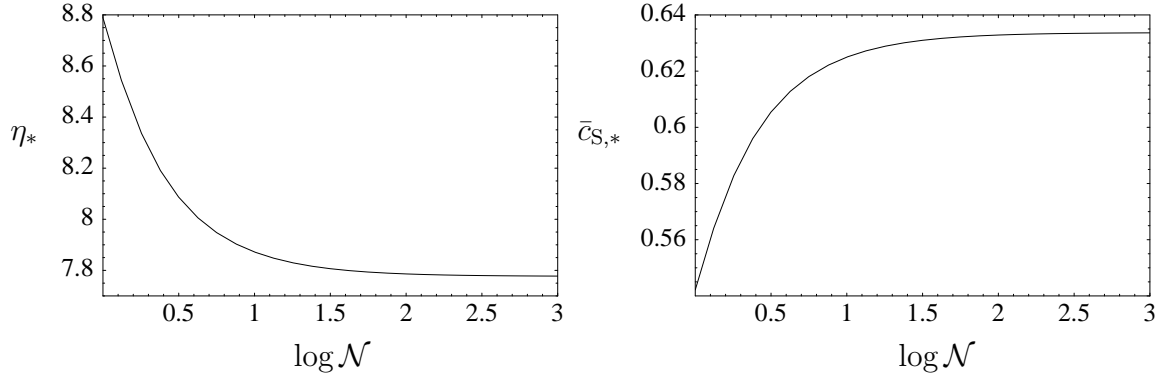
FIGURE 6.5. The dependence of the bifurcation density (left) and the relative bifurcating order of the spacers (right) on the length of the polymer, $\mathcal{N}$. The parameters are $\tilde{P}_\text{S} = 0.3$, $\tilde{d}_\text{S} = 0$. and $\bar{\mathcal{M}}_\text{S} = 1$. The magnitude of the vertical axes depends quite critically on the spacer length $\bar{\mathcal{M}}_\text{S}$ (i.e. much larger for small $\bar{\mathcal{M}}_\text{S}$ and vice versa). The order of the mesogens is set equal to 1.

of zero-length spacers (by putting $\tilde{P}_\text{S} = 0$), the polymers reduce to chains of mesogens, coupled via a zero-size hinge and a coupling constant $\exp(-3\bar{\mathcal{M}}_\text{S})$. Then, the bifurcation density is given by Eq. 3.62 in Chap. 3 in which $\sigma = \exp(-3\bar{\mathcal{M}}_\text{S})$. Another case of zero-length spacers is obtained when $\bar{\mathcal{M}}_\text{S} = 0$, and the polymers reduce (effectively) to long rods of length $\mathcal{N} l_\text{M}$ (i.e. the original Onsager model). Then, the bifurcation density is the result due to Kayser and Raveché, $\eta_* = 32/\pi\mathcal{N}$ [37]. This result, we also mention in the next section, where we plot the dependence of the bifurcation density on the spacer length $\bar{\mathcal{M}}_\text{S}$. The last limiting case is a bit less accessible. The wormlike chain result can be obtained by setting $P_\text{S} \gg l_\text{M}$, or $l_\text{M} \to 0$ (zero-size mesogens). This means, we have to rescale the density η in terms of P_S instead of l_M. Realizing this, also this last result is checked in a straightforward fashion, and the bifurcation density becomes as in Eq. 3.63.

6.4. Bifurcation Results

The analytical results, we have obtained in the previous section, will be plotted and discussed in the present. We investigate the dependence of the bifurcation density and spacer order on some of the model parameters. Usually, we vary the spacer length, $\bar{\mathcal{M}}_\text{S}$, as this is experimentally the most accessible parameter. We also look at the effect of increasing chain length, $\mathcal{N}$. The bifurcating order along the polymer will also be plotted, both for infinitely long chains (where we plot just one unit) and for finite lengths. The other parameters are usually set as follows: $\tilde{P}_\text{S} = 0.3$ and $\tilde{d}_\text{S} = 0$. We don't aim to describe a real system, but just focus on the features of this approach.

In Fig. 6.4 (left), we have plotted the bifurcation density for various values of the polymer length, $\mathcal{N} = \{1, 2, 4, \infty\}$ (from top curve to bottom, respectively). On the right, in Fig. 6.4, we have given the average order of the spacer at bifurcation, for the same values of $\mathcal{N}$, with the difference that $\mathcal{N}$ increases from the bottom curve to the top.
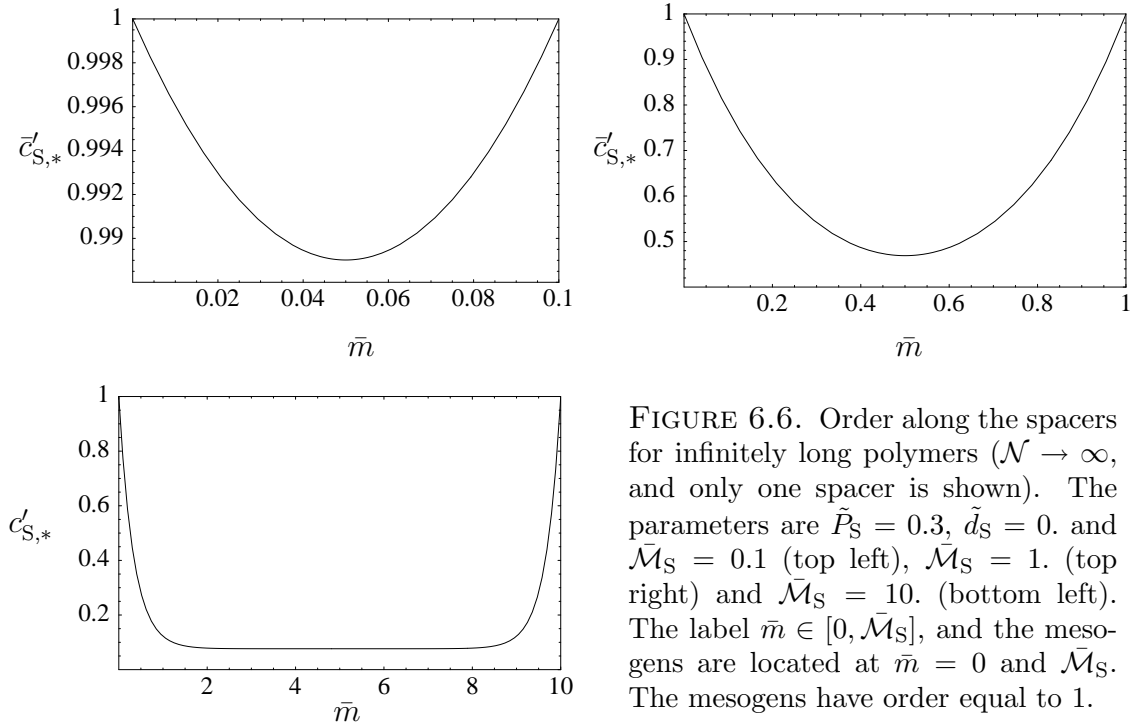
FIGURE 6.6. Order along the spacers for infinitely long polymers ($\mathcal{N} \to \infty$, and only one spacer is shown). The parameters are $\tilde{P}_S = 0.3$, $\tilde{d}_S = 0$. and $\bar{\mathcal{M}}_S = 0.1$ (top left), $\bar{\mathcal{M}}_S = 1$. (top right) and $\bar{\mathcal{M}}_S = 10$. (bottom left). The label $\bar{m} \in [0, \bar{\mathcal{M}}_S]$, and the mesogens are located at $\bar{m} = 0$ and $\bar{\mathcal{M}}_S$. The mesogens have order equal to 1.

When $\bar{\mathcal{M}}_S = 0$, the chain is nothing more than a sequence of $\mathcal{N}$ tightly connected mesogens of length l_M, or equivalently, one long mesogen of length $\mathcal{N}l_M$. Consequently, $\eta_*(\bar{\mathcal{M}}_S = 0) = 32/\pi\mathcal{N}$ and $\bar{c}_{S,*}(\bar{\mathcal{M}}_S = 0) = 1$. Increasing the spacer length, $\bar{\mathcal{M}}_S$, the mesogens become more disconnected from each other, and the bifurcation density goes up. (Except for $\mathcal{N} = 1$, because there is only one mesogen per molecule. Here increasing the spacer length just increases the dimensions of the molecule and as a result the bifurcation density goes down.) When the spacer length roughly exceeds 1 to 3, the mesogens are totally decoupled and there is no $\mathcal{N}$-dependence any more. Going to very large spacer lengths, we are effectively only increasing the dimensions of the molecules and, therefore, $\bar{\mathcal{M}}_S$-dependence of η_* slowly goes down (hardly visible in Fig. 6.4, but this effect is somewhat more pronounced for $\tilde{d} \neq 0$). The average order (Fig. 6.4 (right)) of the spacers decreases with increasing $\bar{\mathcal{M}}_S$, as the mesogen concentration gets diluted more and more and the resulting orientational field (external as well as within the chain) decreases.

In Fig. 6.5, the dependence of the bifurcation density and the spacer order on the length of the polymer is plotted for a single value of $\bar{\mathcal{M}}_S$. At this spacer length ($\bar{\mathcal{M}}_S = 1$), there is still some orientational coupling between the mesogens. Consequently, increasing the chain length decreases the bifurcation density (and increases the spacer order). This effect is much stronger for lower $\bar{\mathcal{M}}_S$ and much weaker for higher $\bar{\mathcal{M}}_S$.

The order along infinitely long polymers is plotted in Fig. 6.6. The upper left (very short spacers) and lower left plots (very long spacers) are extreme cases, the upper right is for spacers of intermediate lengths. Starting with the very long spacers (lower left), we see that the spacer order at the mesogens (at $\bar{m} = 0$) is the same as the mesogen order but then moving away, it 'relaxes' to a plateau. For intermediate lengths, the same happens except that it is hard to identify the relaxed part, as the relaxation tales seem
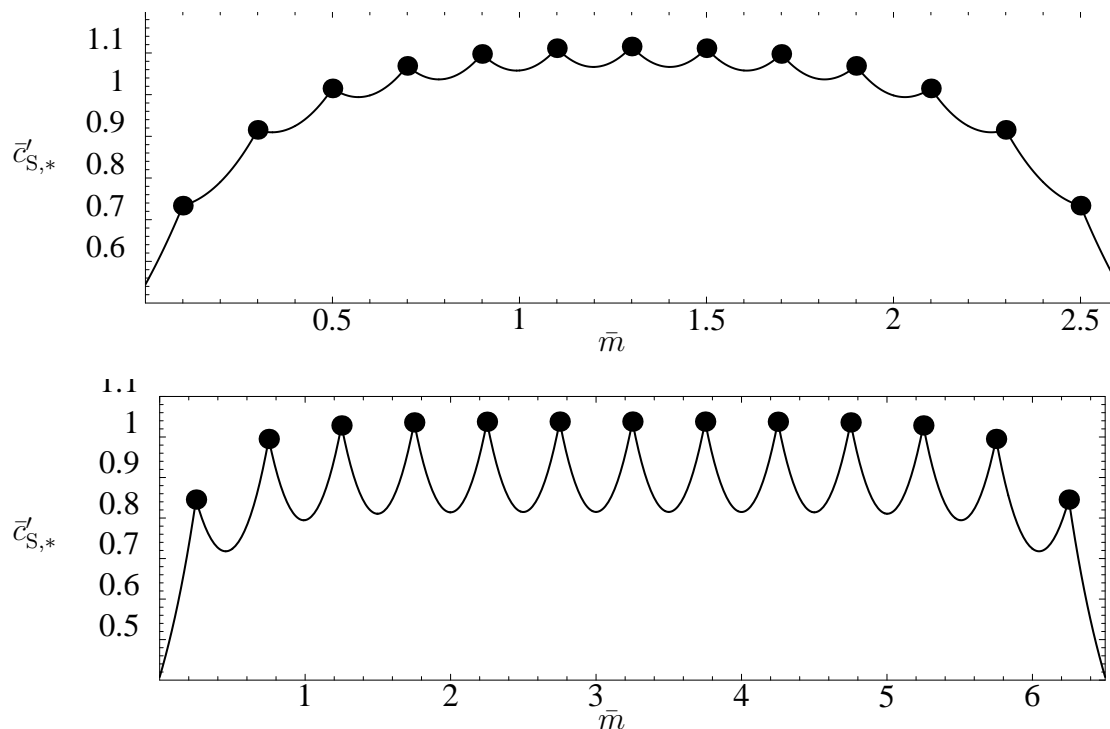
to touch (this is based on the shape and the vertical scale). For small lengths, the shape of the order dependence is the same as for intermediate lengths but the scale is much smaller. In this case the mesogens are so close that the spacers can not relax to their plateau value.

In Fig. 6.7, we have plotted the order along a polymer of $\mathcal{N} = 13$ units. Three different spacer lengths have been used and chosen such that it shows nicely the effect of the finite length of the polymer on the order distribution along it. In general, for linear polymers it is a well-known result that in the nematic phase, the order at the ends is lower than in the middle. In case of the top plot, the spacers are quite short, and the influence of the ends propagates several units (about 5 or 6) to the middle of the chain. As a result the spacers in between are ordered almost equally strong as the mesogens they are connected with. In the middle plot, the spacers are longer, and therefore, the number of units that 'feel' the ends is smaller (2 to 3). Simultaneously, the spacers can keep a more disordered conformation. In the bottom plot, the spacers are again longer and the above effects are even more pronounced.

6.5. Conclusion and Discussion

We have applied the segmented-chain approach, developed in the previous chapter, to the case of main chain LC polymers. The geometry of these polymers is explicitly taken into account; i.e. consisting of mesogenic blocks connected by more flexible spacers. We have applied the wormlike chain limit to the spacers. The resulting model has 3 model parameters (i.e. $\bar{\mathcal{M}}_S$, $\tilde{P}_S$ and $\tilde{d}_S$), for infinitely long polymers or 4 (i.e. plus $\mathcal{N}$), in case of polymers of finite lengths. We have treated the intra-molecular interactions exactly, and using bifurcation analysis, obtained analytical information on the I-N phase transition.
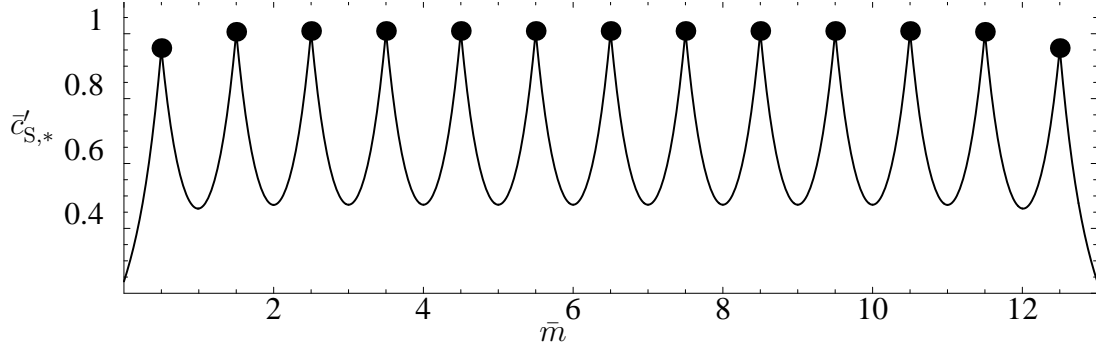
FIGURE 6.7. Order along the chain for a finite-length polymer, $\mathcal{N} = 13$. The black dots are the mesogens and the lines are the spacers. The parameters are $\tilde{P}_S = 0.3$, $\tilde{d}_S = 0.$ and $\bar{\mathcal{M}}_S = 0.2$ (previous page, top), $\bar{\mathcal{M}}_S = 0.5$ (previous page, bottom) and $\bar{\mathcal{M}}_S = 1.$ (here). The label $\bar{m} \in [0, \mathcal{N}\bar{\mathcal{M}}_S]$, the mesogens (black dots) are located at $\bar{m} = (n - \frac{1}{2})\bar{\mathcal{M}}_S$ with $n \in \{1, \cdots, \mathcal{N}\}$ and the average order of the mesogens is 1.

One of the most important results is the dependence of the bifurcation density on the spacer length ($\bar{\mathcal{M}}_S$), which shows a huge increase in density for small spacer lengths, confirming the experimental finding that spacers decouple the mesogens Another nice result is the relative order profile along the (finite-length) polymers.

In three papers by Yurasova et. al. [89, 90, 91], a Maier-Saupe theory (using temperature) is used to describe the same system (although, in Ref. [91], also the mesogens have some flexibility). They use the spherical approximation to analytically compute the partition function for infinitely long polymers and the resulting theory has 4 parameters, which is one more than ours. The reason for these extra parameters is that in case of excluded volumes, the dimensions of the polymer totally fix the interactions, whereas in case of Maier-Saupelike theories, more parameters are needed to fix them. Among other results, they plot the dependence of the transition temperature on spacer length, and find a minimum. This is similar to what we find; i.e. a maximum in the density as a function of spacer length (see Fig. 6.4). In both cases (theirs and ours), the extremum has a steep side, on the small-spacer side, and a shallow one, on the large-spacer side. A somewhat unphysical result they obtain is that for large spacer lengths, the order parameter at the phase transition of the spacers is larger than that of the mesogens. This suggests that, in that case, the spacers are driving the transition and one should pay attention to the physical validity of the theory.

Wang and Warner [92] also use a Maier-Saupe theory with 4 parameters to describe the same system of infinitely long polymers. They write down an exact formulation (concerning the intra-molecular degrees of freedom) of the partition function and then use an expansion in terms of spheroidal wavefunctions of which they keep only the 'ground state' contribution. In the resulting stationarity equations, contributions appear which are due to the fact that the components are embedded in a polymer (in a way, this is a first-order correction to Maier-Saupe mean field theory). Also there, a strong decrease of transition temperature is found for small spacer lengths.

As we do for side chain polymers in the next chapter, it is possible to write down and solve numerically the stationarity equations for main chain polymers in the nematic phase. However, concerning nematic phases, something other than that the ordering becomes gradually stronger with density is not expected, and therefore, we have not performed these calculations. Random copolymers are polymers in which the mesogens and the spacers do not have constant lengths. There are, for instance, two different lengths which they can have, and these alternate in a random fashion along the chain. This can be incorporated in the present theory. However, the interesting effect concerning random copolymers is that they reduce crystalline tendencies and enhance glassy behaviour. This lies far outside the scope of the present approach.

On the other hand, inhomogeneous ordering (i.e. a smectic) is expected to take place at some density. In terms of modeling, however, this is hard to include, as spatial coupling between remote parts of the polymer can not be discarded. We want to make a few more remarks on this. A mixture of thick and thin hard rods tend to demix (even in the isotropic phase) as they have an unfavourable interaction [97]. This demixing tendency of the components might help to stabilize the smectic phase in systems of main chain LC polymers. Although on the other hand, the system has to pay for the reduction of entropy by confining the spacers to inbetween the layers. In experimental situations, where systems of block copolymers show microphase separation, both blocks usually have some flexibility and consist of several (or many more) persistence lengths. In this way, in the microseparated phase, the blocks can still retain a considerable amount of entropy within the microseparated domains. Therefore, it would be very interesting to see how microphase separation emerges in systems of hard wormlike block copolymers (without any other but the steric interactions) and competes with ordinary nematic ordering. Bifurcation analysis may be a useful tool.

7

Side Chain LC Polymers

We study orientational ordering in a fluid of side chain liquid crystalline (LC) polymers. The interchain interactions are considered in a mean field (Onsager) approximation, but the intrachain interactions are described exactly. We find no nematic-to-nematic phase transitions, in contrast with earlier predictions by Warner and coworkers [98, 99].

7.1. Introduction

Side chain LC polymers are polymers with side chains containing mesogenic or LC forming groups. The polymer is referred to as the backbone and the LC forming groups as the mesogens. In Chap. 6, we have given a more extensive introduction to the history and (possible) applications of LC polymers (LCP's) in general. Here, we will only make a few more comments, specific for the case of side chain LCP's. In the 1970's, the field of LC's and LCP's was rapidly growing. However, systematic investigations started only after Ringsdorf, Finkelmann and coworkers, in 1978, recognized that, in order to form LC phases, spacers were needed to decouple the mesogenic groups from the backbones [25, 100, 101]. Before, mesogens were directly linked to the backbone, yielding, apart from a few cases, only glasses with some optical anisotropy. Above the glass transition polymers tend to adopt a coillike conformation, maximizing their entropy. In case of direct linkage, the motions of the mesogens and the backbone are strongly coupled, and the LC tendency of the mesogens has to compete with the coillike tendency of the backbone. Moreover, the mesogens can not freely rotate as they are so tightly connected to the backbone that they experience steric hindrance. Inserting a flexible aliphatic spacer between the mesogens and the backbone solves these problems, decoupling the orientation and (partly) the position of the mesogen from the backbone. The introduction of the spacer concept marked the beginning of the development of many new compounds. Remarkably, the spacer concept found its way to the field of main chain LCP's, only later, where before, predominantly stiff-chain polymers were used [102]. Still, at present, side chain LCP's seem to be more popular than main chain LCP's, which is probably due to the fact that spacers are more effective in the case of side chain LCP's. In side chain LCP's, spacers really decouple the mesogens from the backbone, whereas in main chain LCP's, the mesogens are merely decoupled from each other, but are still embedded in the polymer. Some books on (side chain) LCP's are Refs. [1, 26, 86, 87, 103] and some more recent and more specific reports on the relation
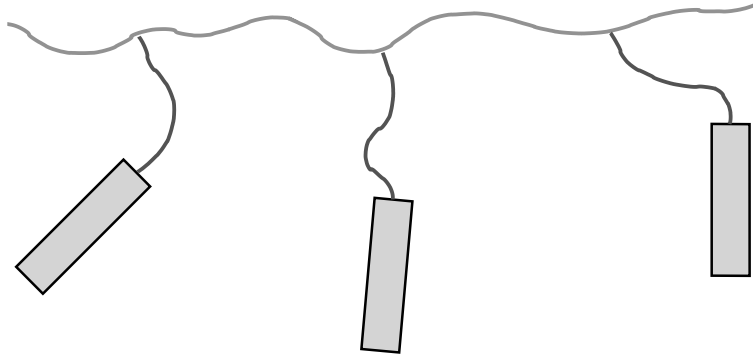
FIGURE 7.1. A few units of a side chain polymer

between molecular structure and LC phase behaviour for some specific compounds are Refs. [30, 104, 105, 106, 107].

There are not many theories for LC ordering in side chain LCP's. Khokhlov and coworkers used a variant of Flory's lattice method [93, 108]. A more serious approach has been taken by Warner and coworkers [98, 99]. They used side chain LCP's consisting of a wormlike backbone with rigid mesogenic groups hinged perpendicularly on it. All interactions between the various components (backbone, side chains) were modeled in a mean field (Maier-Saupe) way and as such, there were only effective fields on the components and no field contributions acting directly within the polymer. The main results were phase diagrams (temperature vs. relative fraction of side chains) featuring three uniaxial nematic phases and first order nematic-to-nematic phase transitions. Biaxial phases have been included as well in Ref. [109]. In Ref. [110], Renz and Warner argue that layer hopping is an essential feature of side chain LCP's in the smectic phase. We are not aware of other molecular statistical theories or simulations relating molecular parameters of side chain LCP's to the bulk LC phase behaviour.

In this chapter, we consider side chain LC polymers consisting of a backbone and, on regular distances, mesogens connected to the backbone via flexible spacers. The backbone is thought to be infinitely long, so we do not have to deal with end effects, and a side chain LCP is described effectively by 6 model parameters. We assume that two polymers interact through their mutual excluded volume, allowing us to use the Onsager approximation. Increasing the density, the mesogens go from the isotropic to a nematic phase. Due to the perpendicular hinge of the spacer to the backbone, a backbone can assume an oblate or a prolate conformation in the nematic phase, depending on the stiffness of the spacer. We use the isotropic-to-nematic (I-N) bifurcation analysis, developed in Chap. 5, for this system. The I-N bifurcation density and bifurcating order along the backbone and spacers are obtained in analytical form. We also calculate numerically the distribution functions on a grid. As a result, we locate the exact phase transition as well as obtain the behaviour of the system for higher densities, in the nematic phase. We find no nematic-to-nematic phase transitions. We compare our results with those of Warner and coworkers [98, 99] and end with an outlook.
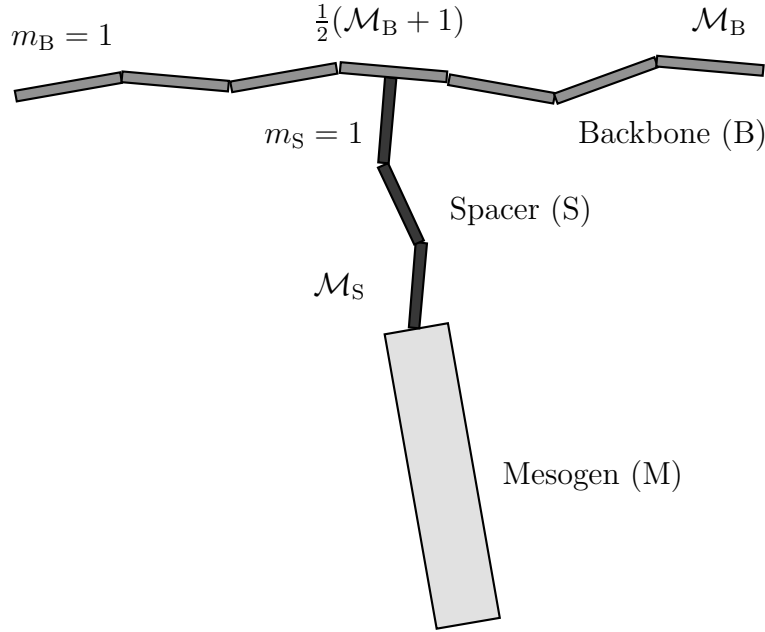
$m_B = 1$ $\frac{1}{2}(\mathcal{M}_B + 1)$ $\mathcal{M}_B$

$m_S = 1$ Backbone (B)

Spacer (S)

$\mathcal{M}_S$

Mesogen (M)

FIGURE 7.2. A unit of a side chain polymer

7.2. General Remarks

7.2.1. Model Parameters. We will assume that the polymers consist of $\mathcal{N}$ repeating units. Every unit consists of a piece of backbone (being $\mathcal{M}_B$ type-B segments), a rather flexible spacer ($\mathcal{M}_S$ type-S segments) and a mesogen (1 type-M segment). For simplicity (although not necessary), we assume that $\mathcal{M}_B$ is odd and that the first segment of the spacer is connected to the middle of the backbone piece, i.e. the $\frac{1}{2}(\mathcal{M}_B + 1)$th segment. See also Figs. 7.1 and 7.2. Note that $M_B = \mathcal{N}\mathcal{M}_B$, $M_S = \mathcal{N}\mathcal{M}_S$ and $M_M = \mathcal{N}$, where the roman M's denote the number of segments in the whole polymer and the gothic $\mathcal{M}$'s the number of segments in a unit. The dimensions of the backbone segments are l_B and d_B, for the spacer segments they are l_S and d_S, and for the mesogens: l_M and d_M. Further, in the language of Chap. 5, the number of different types is $R = 3$, and we put $\{\tau_1, \tau_2, \tau_3\} = \{B, S, M\}$. For the nearest neighbour bending potential we use

$$u_{B,B}(\hat{\omega}, \hat{\omega}') = -J_B \hat{\omega} \cdot \hat{\omega}'$$

$$u_{B,S}(\hat{\omega}, \hat{\omega}') = \begin{cases} 0 & \text{if} \quad \hat{\omega} \cdot \hat{\omega}' = 0 \\ \infty & \text{if} \quad \hat{\omega} \cdot \hat{\omega}' \neq 0 \end{cases}$$

$$u_{S,S}(\hat{\omega}, \hat{\omega}') = -J_S \hat{\omega} \cdot \hat{\omega}' \tag{7.1}$$

$$u_{S,M}(\hat{\omega}, \hat{\omega}') = -J_S \hat{\omega} \cdot \hat{\omega}',$$

with the BS-potential forcing (at least locally) perpendicular orientations of backbone and side chain and thus providing the mechanism for the competition in the nematic ordering of these two components. In order not to introduce many more model parameters, we have chosen to use a rigid form (no bending) for $u_{B,S}$ and to use J_S also for $u_{S,M}$. This will not influence the results. As was stated in Chap. 5, the interactions between segments on different chains are described via their mutual excluded volume, Eq. 5.6.
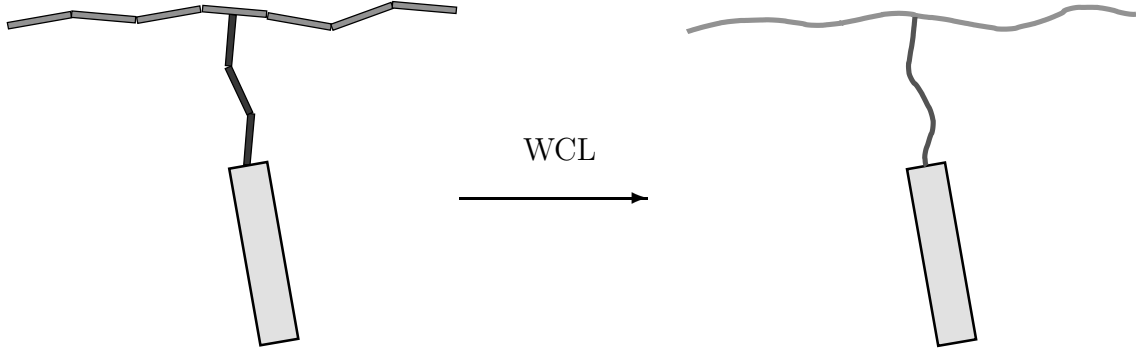
FIGURE 7.3. The wormlike chain limit

Thus, the total number of model parameters we have is 11: the dimensions of the 3 segments (l_B, d_B, l_S, d_S, l_M and d_M), two coupling constants (J_B and J_S), the number of segments in the backbone and the spacer *per unit* ($\mathcal{M}_B$ and $\mathcal{M}_S$) and finally, the number of repeating units ($\mathcal{N}$).

7.2.2. The Wormlike Chain Limit. In order to reduce the number of model parameters we will apply, at some point in the analysis furtheron, the so-called wormlike chain limit (WCL) to the backbone and spacers. Furthermore, since Khokhlov and Semenov [32, 33], the wormlike chain concept (introduced by Kratky and Porod [49]) is widely used to model nematic ordering in somewhat flexible molecules. Going from our system of segmented chains to continuously flexible chains, the WCL can be formulated as follows,

$$
\begin{aligned}
l_B \to 0, & \quad \beta J_B \to \infty, & \mathcal{M}_B \to \infty \\
l_S \to 0, & \quad \beta J_S \to \infty, & \mathcal{M}_S \to \infty
\end{aligned}
\tag{7.2}
$$

where the following products and ratios stay finite,

$$
\begin{aligned}
P_B = \beta J_B l_B & \quad \bar{\mathcal{M}}_B = \mathcal{M}_B/\beta J_B \\
P_S = \beta J_S l_S & \quad \bar{\mathcal{M}}_S = \mathcal{M}_S/\beta J_S
\end{aligned}
\tag{7.3}
$$

The WCL for segmented chains is discussed extensively in Chapter 3. The quantities P_{τ_p} are persistence lengths of type τ_p and $\bar{\mathcal{M}}_{\tau_p}$ the number of persistence lengths in one repeating unit. In general, when quantities appear with a bar over them, they refer to the fact that the WCL has been taken. By applying the WCL to the backbone and the spacers (and making them continuously flexible) we loose two model parameters: $l_B, J_B, \mathcal{M}_B \to P_B, \bar{\mathcal{M}}_B$ and $l_S, J_S, \mathcal{M}_S \to P_S, \bar{\mathcal{M}}_S$. The physical results are expected to stay the same.

7.2.3. Other Considerations. We can proceed simplifying the system (and loosing another model parameter) by assuming the backbone is infinitely long. In this way, every unit finds itself in the 'middle' of the polymer since the influence of the free ends of the backbone is zero. This, we call the infinite backbone limit (IBL),

$$
\mathcal{N} \to \infty \quad \rho \to 0 \quad \text{with} \quad \rho\mathcal{N} \quad \text{finite},
\tag{7.4}
$$

where the density ρ has to go to zero in order to have a finite unit density $\rho\mathcal{N}$. This limit allows us to consider (effectively) only a single unit, as every unit in the chain is
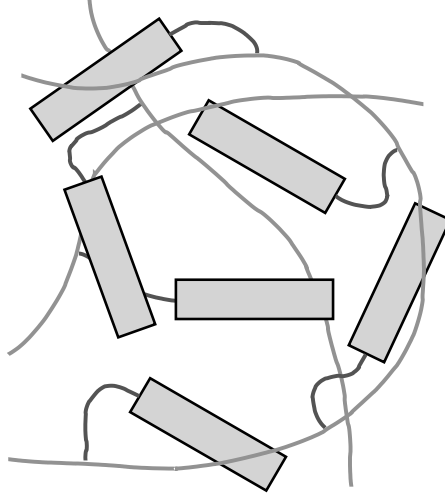
FIGURE 7.4. The isotropic phase

exactly the same as its neighbour. Note, however, although there are no 'free end effects' (and all units are effectively the same), that *within* a unit, the orientational distribution functions (ODF's, see Eq. 5.8) will generally still vary; i.e. we expect $f_{m=1}^{(B)}(\hat{\omega})$ (on the backbone, between two spacer hinges) and $f_{m=\frac{1}{2}(\bar{\mathcal{M}}+1)}^{(B)}(\hat{\omega})$ (on the backbone, on a spacer hinge) to be different in the nematic phase.

Finally, as our system is scale-invariant we can use dimensionless length scales and effectively drop two more parameters. The mesogens are the largest segments (they are the liquid-crystal formers) and are not subject to the WCL, and therefore, we choose to measure the other length scales in units of l_M and d_M. So,

$$\tilde{P}_{\tau_p} = P_{\tau_p}/l_M \quad \text{and} \quad \tilde{d}_{\tau_p} = d_{\tau_p}/l_M \ , \tag{7.5}$$

with $\tau_p \in \{B, S\}$ and the tilde denoting dimensionless quantities. We define a dimensionless unit density, by rescaling as follows

$$\eta = 2l_M^2 d_M \rho \mathcal{N}. \tag{7.6}$$

Using the above two limits and the scale-invariance, we reduce the number of model parameters to 6: $\tilde{P}_B$, $\tilde{d}_B$ and $\bar{\mathcal{M}}_B$ for the backbone, and $\tilde{P}_S$, $\tilde{d}_S$ and $\bar{\mathcal{M}}_S$ for the spacers. Although 6 is still a large number, if we want to explore all of parameter space, it is a significant reduction compared to 11. In practical physical situations, though, it will generally hold that $0 < \tilde{d}_B, \tilde{d}_S < 1$. A case we find instructive and frequently use is obtained by setting $\tilde{d}_B = \tilde{d}_S = 0$ and $\tilde{P}_B = \tilde{P}_S$, leaving only three model parameters. In this case, where backbone and spacers have zero thickness, the BB, BS and SS excluded volumes are zero, but the BM, SM and MM are not. The interesting phases (topic of the next subsection) will still be there.

7.2.4. Nematic Phases and Order Parameters. We restrict ourselves to uniaxial phases. Biaxial nematic phases would be expected in side chain polymers with mesogens in the side chains as well as the backbone. In this last case, the competition (for nematic ordering) between the backbone and the side chains could result in a biaxial
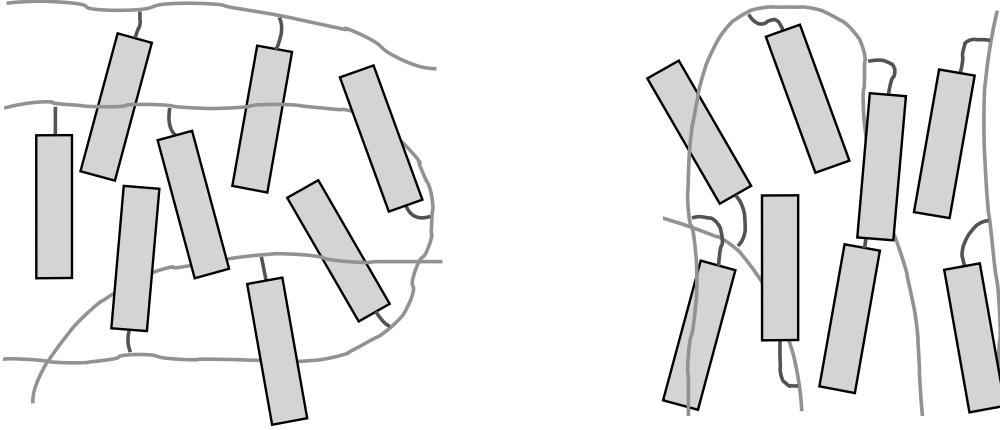
FIGURE 7.5. The oblate and prolate nematic phases

nematic. However, we are considering side chain polymers with only mesogens in the side chains and therefore expect uniaxial nematics. As the side chain polymers consist of three components, we have three order parameters for uniaxial nematics,

$$S^{(\tau_p)} = \langle f_{\tau_p}, P_2 \rangle, \tag{7.7}$$

with $\tau_p \in \{\mathrm{B, S, M}\}$.

At low unit densities η, the side chain polymers are in the isotropic phase and all order parameters are zero, $S^{(\tau_p)} = 0$. On increasing the density, at some point, the mesogens will order with respect to a direction $\hat{n}$, $S^{(\mathrm{M})} > 0$. As a result, the backbone and the spacers (experiencing the orientational field) will order as well. It then depends on the model parameters what happens. In case of short stiff spacers (and small $\bar{\mathcal{M}}_{\mathrm{B}}$ as well), the backbone is forced to orientations perpendicular to $\hat{n}$, hence $S^{(\mathrm{B})} < 0$ and $S^{(\mathrm{S})} > 0$. In case of longer (more flexible) spacers (and/or $\bar{\mathcal{M}}_{\mathrm{B}}$ large), the spacers can bend, and the backbone can order parallel to $\hat{n}$ as well, $S^{(\mathrm{B})}, S^{(\mathrm{S})} > 0$. So, there is a competition between the backbone (which can lower its average excluded volume with the mesogens by organizing parallel) and the spacers (which can lower their average internal energy by assuming a more straight conformation). The nematic phase for which $S^{(\mathrm{M})}, S^{(\mathrm{S})} > 0$ and $S^{(\mathrm{B})} < 0$, we call oblate nematic (ON) (because the backbone has on average an oblate conformation) and to the phase where $S^{(\mathrm{M})}, S^{(\mathrm{S})}, S^{(\mathrm{B})} > 0$, we refer to as prolate nematic (PN). [1] For even higher densities, the excluded volume becomes more and more important, and a system in the ON phase is expected to have a transition to the PN phase.

---

[1]The qualifications oblate and prolate refer to the shape of the backbone coil, and as such to the radius of gyration of the coil in different directions. The connection between the average backbone order parameter, $S^{(\mathrm{B})}$, and the shape of the backbone coil is not a trivial one, and should, in principle, be investigated further. However, there is a rough correspondence between the two, and we proceed bearing this in mind. In Ref. [34], radii of gyration are considered for wormlike chains in Maier-Saupe effective fields.

It has already been mentioned in the previous subsection that, in a nematic phase, the ODF's will generally vary along the backbone and the spacers. For a point on the backbone, it depends wether or not there is the branch of a spacer closeby. And on a spacer, it matters a lot being close to the mesogen (stronger ordered) or to the backbone (weaker ordered). Consequently, we are also interested in the m-dependence of $S^{(B)}$ and $S^{(S)}$,

$$S_m^{(\tau_p)} = \langle f_m, P_2 \rangle \quad \text{with} \quad m \in \tau_p, \tag{7.8}$$

and $\tau_p \in \{B, S\}$.

7.3. Bifurcation Analysis

7.3.1. Technical Details. The first-order bifurcation equation for a system of branched heteropolymers is given by Eq. 5.63. In this subsection, we will solve this equation for the case of side chain polymers. To that end, we proceed by evaluating the matrix elements of $\mathbf{K}^{(2)}$ and $\mathbf{W}^{(2)}/W^{(0)}$. As our side chain polymers consist of 3 components, both $\mathbf{K}^{(2)}$ and $\mathbf{W}^{(2)}/W^{(0)}$ are 3×3-matrices. We start with the segmented chains (using all 11 model parameters) and gradually work our way towards the 6-parameter formulation. We specifically state when we apply the WCL, the IBL or when we start using dimensionless quantities.

For all combinations (p, p'), the excluded volume interactions have the following form (Eq. 5.6),

$$\mathcal{E}_{\tau_p, \tau_{p'}}(\hat{\omega}, \hat{\omega}') = M_{\tau_p} M_{\tau_{p'}} V_{\tau_p, \tau_{p'}} |\sin \gamma(\hat{\omega}, \hat{\omega}')|, \tag{7.9}$$

and therefore (from Eqs 5.13 and 5.36),

$$\begin{aligned} K_{\tau_p, \tau_{p'}}^{(2)} &= s_2 \mathcal{N}^2 \mathcal{M}_{\tau_p} \mathcal{M}_{\tau_{p'}} V_{\tau_p, \tau_{p'}} \\ &= s_2 \mathcal{N}^2 \mathcal{M}_{\tau_p} l_{\tau_p} \mathcal{M}_{\tau_{p'}} l_{\tau_{p'}} (d_{\tau_p} + d_{\tau_{p'}}), \end{aligned} \tag{7.10}$$

with $\mathcal{M}_M = 1$ and $s_2 = -\pi^2/8$ the second Legendre coefficient of $\sin \gamma$. Defining the dimensionless matrix $\boldsymbol{\kappa} = (s_2 \mathcal{N}^2 2 l_M^2 d_M)^{-1} \mathbf{K}^{(2)}$, and applying the WCL, we obtain

$$\begin{aligned} \bar{\kappa}_{\tau_p, \tau_{p'}} &= \bar{\mathcal{M}}_{\tau_p} \tilde{P}_{\tau_p} \bar{\mathcal{M}}_{\tau_{p'}} \tilde{P}_{\tau_{p'}} \tfrac{1}{2} (\tilde{d}_{\tau_p} + \tilde{d}_{\tau_{p'}}), \\ \bar{\kappa}_{\tau_p, M} &= \bar{\kappa}_{M, \tau_p} = \bar{\mathcal{M}}_{\tau_p} \tilde{P}_{\tau_p} \tfrac{1}{2} (1 + \tilde{d}_{\tau_p}), \\ \bar{\kappa}_{M, M} &= 1, \end{aligned} \tag{7.11}$$

with $\tau_p, \tau_{p'} \in \{B, S\}$. There is no $\mathcal{N}$-dependence in κ, so the IBL has no effect.

In order to calculate the matrix elements $W_{\tau_p, \tau_{p'}}^{(2)}/W^{(0)}$ we first define

$$\sigma_{\tau_p, \tau_{p'}} = w_{\tau_p, \tau_{p'}}^{(2)}/w_{\tau_p, \tau_{p'}}^{(0)}, \tag{7.12}$$

where $w_{\tau_p, \tau_{p'}}^{(j)}$ is the jth Legendre coefficient of $w_{\tau_p, \tau_{p'}}(\hat{\omega}) = \exp[-\beta u_{\tau_p, \tau_{p'}}(\hat{\omega})]$. Then, between two segments, m and m' we have (Eq. 5.39)

$$\frac{W_{m,m'}^{(2)}}{W^{(0)}} = \prod_{\substack{(k, k') \in \mathcal{P}_{m,m'} \\ \text{and } k \in \tau_p \ k' \in \tau_{p'}}} \frac{w_{\tau_p, \tau_{p'}}^{(2)}}{w_{\tau_p, \tau_{p'}}^{(0)}} = \prod_{\substack{(k, k') \in \mathcal{P}_{m,m'} \\ \text{and } k \in \tau_p \ k' \in \tau_{p'}}} \sigma_{\tau_p, \tau_{p'}} \tag{7.13}$$

where the product is over all pairs (k, k') which are nearest neighbours lying on the non-selfoverlapping path, $\mathcal{P}_{m,m'}$, between m and m' (see Chap. 5 above Eq. 5.19). The quantity σ depends on the types where k and k' belong to. Then, the matrix elements are (Eq. 5.58)

$$
\begin{aligned}
\frac{W^{(2)}_{\tau_p,\tau_{p'}}}{W^{(0)}} &= \frac{1}{M_{\tau_p} M_{\tau_{p'}}} \sum_{m \in \tau_p} \sum_{m' \in \tau_{p'}} \frac{W^{(2)}_{m,m'}}{W^{(0)}} \\
&= \frac{1}{M_{\tau_p} M_{\tau_{p'}}} \sum_{m \in \tau_p} \sum_{m' \in \tau_{p'}} \prod_{\substack{(k,k') \, \in \, \mathcal{P}_{m,m'} \\ \text{and } \, k \in \tau_p \;\; k' \in \tau_{p'}}} \sigma_{\tau_p,\tau_{p'}}
\end{aligned}
\tag{7.14}
$$

This last formula is basically a recapitulation of section 5. Defining the matrix $\boldsymbol{\alpha} = \mathcal{N} W^{(2)}_{\tau_p,\tau_{p'}}/W^{(0)}$, we can write down the expression for the side chain polymers,

$$
\alpha_{\mathrm{B,B}} = \frac{\mathcal{N}}{M_{\mathrm{B}}^2} \sum_{k,k'=1}^{\mathcal{M}_{\mathrm{B}}} \sigma_{\mathrm{B,B}}^{|k-k'|},
\tag{7.15}
$$

$$
\alpha_{\mathrm{B,S}} = \frac{\mathcal{N}}{M_{\mathrm{B}} M_{\mathrm{S}}} \sum_{n,n'=1}^{\mathcal{N}} \sum_{k=1}^{\mathcal{M}_{\mathrm{B}}} \sum_{k'=1}^{\mathcal{M}_{\mathrm{S}}} \sigma_{\mathrm{B,B}}^{|(n-n')\mathcal{M}_{\mathrm{B}}+k-\frac{1}{2}(\mathcal{M}_{\mathrm{B}}+1)|} \sigma_{\mathrm{B,S}} \sigma_{\mathrm{S,S}}^{k'-1},
\tag{7.16}
$$

$$
\alpha_{\mathrm{B,M}} = \frac{\mathcal{N}}{M_{\mathrm{B}} \mathcal{N}} \sum_{n,n'=1}^{\mathcal{N}} \sum_{k=1}^{\mathcal{M}_{\mathrm{B}}} \sigma_{\mathrm{B,B}}^{|(n-n')\mathcal{M}_{\mathrm{B}}+k-\frac{1}{2}(\mathcal{M}_{\mathrm{B}}+1)|} \sigma_{\mathrm{B,S}} \sigma_{\mathrm{S,S}}^{\mathcal{M}_{\mathrm{S}}-1} \sigma_{\mathrm{S,M}},
\tag{7.17}
$$

$$
\alpha_{\mathrm{S,S}} = \frac{\mathcal{N}}{M_{\mathrm{S}}^2} \left(\mathcal{N} \sum_{k,k'=1}^{\mathcal{M}_{\mathrm{S}}} \sigma_{\mathrm{S,S}}^{|k-k'|} + \sum_{\substack{n,n'=1 \\ n \neq n'}}^{\mathcal{N}} \sum_{k,k'=1}^{\mathcal{M}_{\mathrm{S}}} \sigma_{\mathrm{S,S}}^{k-1} \sigma_{\mathrm{B,S}} \sigma_{\mathrm{B,B}}^{|n-n'|\mathcal{M}_{\mathrm{B}}} \sigma_{\mathrm{B,S}} \sigma_{\mathrm{S,S}}^{k'-1} \right),
\tag{7.18}
$$

$$
\begin{aligned}
\alpha_{\mathrm{S,M}} = \frac{\mathcal{N}}{M_{\mathrm{S}} \mathcal{N}} \Bigg(& \mathcal{N} \sum_{k=1}^{\mathcal{M}_{\mathrm{S}}} \sigma_{\mathrm{S,S}}^{\mathcal{M}_{\mathrm{S}}-k} \sigma_{\mathrm{S,M}} \\
& + \sum_{\substack{n,n'=1 \\ n \neq n'}}^{\mathcal{N}} \sum_{k=1}^{\mathcal{M}_{\mathrm{S}}} \sigma_{\mathrm{S,S}}^{k-1} \sigma_{\mathrm{B,S}} \sigma_{\mathrm{B,B}}^{|n-n'|\mathcal{M}_{\mathrm{B}}} \sigma_{\mathrm{B,S}} \sigma_{\mathrm{S,S}}^{\mathcal{M}_{\mathrm{S}}-1} \sigma_{\mathrm{S,M}} \Bigg),
\end{aligned}
\tag{7.19}
$$

$$
\alpha_{\mathrm{M,M}} = \frac{\mathcal{N}}{\mathcal{N}^2} \left(\mathcal{N} + \sum_{\substack{n,n'=1 \\ n \neq n'}}^{\mathcal{N}} \sigma_{\mathrm{S,M}} \sigma_{\mathrm{S,S}}^{\mathcal{M}_{\mathrm{S}}-1} \sigma_{\mathrm{B,S}} \sigma_{\mathrm{B,B}}^{|n-n'|\mathcal{M}_{\mathrm{B}}} \sigma_{\mathrm{B,S}} \sigma_{\mathrm{S,S}}^{\mathcal{M}_{\mathrm{S}}-1} \sigma_{\mathrm{S,M}} \right).
\tag{7.20}
$$

The matrix $\boldsymbol{\alpha}$ is symmetric, so we have only given the elements above the diagonal. The indices n, n' are used to sum over units, and the indices k, k' are used to sum over

segments within a unit. At this point, we note that all the sums above can be performed analytically. However, we are interested in the WCL and IBL, so we do not bother computing these sums, and proceed directly. The $\sigma_{\tau_p, \tau_{p'}}$'s we need, become in the WCL (to first order),

$$\sigma_{\mathrm{B,B}} = \frac{\int_{-1}^1 dx\, P_2(x) \exp[\beta J_{\mathrm{B}} x]}{\int_{-1}^1 dx \exp[\beta J_{\mathrm{B}} x]} \to 1 - 3\left(\beta J_{\mathrm{B}}\right)^{-1},$$

$$\sigma_{\mathrm{S,S}} \to 1 - 3\left(\beta J_{\mathrm{S}}\right)^{-1},$$

$$\sigma_{\mathrm{B,S}} = \int_{-1}^1 dx\, P_2(x)\delta(x) = -\tfrac{1}{2}, \tag{7.21}$$

$$\sigma_{\mathrm{S,M}} \to 1,$$

where we anticipate that we only need the zeroth order for $\sigma_{\mathrm{S,M}}$. Next, we evaluate (parts of) sums appearing in Eqs. 7.15 to 7.20. First, a power of σ_{τ_p, τ_p} becomes in the WCL,

$$\sigma_{\tau_p, \tau_p}^{\mathcal{M}_{\tau_p}} = \left(1 - 3\left(\beta J_{\tau_p}\right)^{-1}\right)^{\beta J_{\tau_p} \bar{\mathcal{M}}_{\tau_p}} \to \exp\left[-3\bar{\mathcal{M}}_{\tau_p}\right], \tag{7.22}$$

with $\tau_p \in \{B, S\}$ and where we have used $\lim_{n \to \infty}(1 + \frac{x}{n})^n = \exp[x]$. The summation over n and n' becomes

$$\frac{1}{\mathcal{N}} \sum_{\substack{n, n' = 1 \\ n \neq n'}}^{\mathcal{N}} \sigma_{\tau_p, \tau_p}^{\mathcal{M}_{\tau_p}|n - n'|} \to \frac{1}{\mathcal{N}} \sum_{\substack{n, n' = 1 \\ n \neq n'}}^{\mathcal{N}} e^{-3\bar{\mathcal{M}}_{\tau_p}|n - n'|}$$

$$= \frac{2 e^{-3\bar{\mathcal{M}}_{\tau_p}}}{1 - e^{-3\bar{\mathcal{M}}_{\tau_p}}} \left(1 - \frac{1}{\mathcal{N}} \frac{1 - e^{-3\mathcal{N}\bar{\mathcal{M}}_{\tau_p}}}{1 - e^{-3\bar{\mathcal{M}}_{\tau_p}}}\right). \tag{7.23}$$

In the WCL, the backbone and the spacers are continuous, and the summations over k and k' (n.b. not the summations over n and n') have to be replaced by integrations. Roughly, there are two types of integrations ($\bar{k}_{\tau_p} = k/\beta J_{\tau_p}$), i.e.

$$\frac{1}{\mathcal{M}_{\tau_p}} \sum_{k=1}^{\mathcal{M}_{\tau_p}} \sigma_{\tau_p, \tau_p}^k \to \frac{1}{\bar{\mathcal{M}}_{\tau_p}} \int_0^{\bar{\mathcal{M}}_{\tau_p}} d\bar{k}_{\tau_p} e^{-3\bar{k}_{\tau_p}} = \frac{1}{3\bar{\mathcal{M}}_{\tau_p}} \left(1 - e^{-3\bar{\mathcal{M}}_{\tau_p}}\right) \tag{7.24}$$

$$\frac{1}{\mathcal{M}_{\tau_p}^2} \sum_{k,k'=1}^{\mathcal{M}_{\tau_p}} \sigma_{\tau_p, \tau_p}^{|k - k'|} \to \frac{1}{\bar{\mathcal{M}}_{\tau_p}^2} \int_0^{\bar{\mathcal{M}}_{\tau_p}} d\bar{k}_{\tau_p} \int_0^{\bar{\mathcal{M}}_{\tau_p}} d\bar{k}'_{\tau_p} e^{-3|\bar{k}_{\tau_p} - \bar{k}'_{\tau_p}|}$$

$$= \frac{2}{3\bar{\mathcal{M}}_{\tau_p}} \left(1 - \frac{1 - e^{-3\bar{\mathcal{M}}_{\tau_p}}}{3\bar{\mathcal{M}}_{\tau_p}}\right). \tag{7.25}$$

Using these results in Eqs. 7.15 to 7.20, we obtain (in the WCL)

$$\bar{\alpha}_{\mathrm{B,B}} = \frac{2}{3\bar{\mathcal{M}}_{\mathrm{B}}} \left(1 - \frac{1 - e^{-3\mathcal{N}\bar{\mathcal{M}}_{\mathrm{B}}}}{3\mathcal{N}\bar{\mathcal{M}}_{\mathrm{B}}}\right), \tag{7.26}$$

$$\bar{\alpha}_{\mathrm{B,S}} = -\frac{1}{3\bar{\mathcal{M}}_{\mathrm{B}}} \left(\frac{1-\mathrm{e}^{-3\bar{\mathcal{M}}_{\mathrm{S}}}}{3\bar{\mathcal{M}}_{\mathrm{S}}}\right) \left\{1 - \frac{1}{\mathcal{N}}\mathrm{e}^{-\frac{3}{2}\bar{\mathcal{M}}_{\mathrm{B}}}\frac{1-\mathrm{e}^{-3\mathcal{N}\bar{\mathcal{M}}_{\mathrm{B}}}}{1-\mathrm{e}^{-3\bar{\mathcal{M}}_{\mathrm{B}}}}\right\}, \tag{7.27}$$

$$\bar{\alpha}_{\mathrm{B,M}} = -\frac{\mathrm{e}^{-3\bar{\mathcal{M}}_{\mathrm{S}}}}{3\bar{\mathcal{M}}_{\mathrm{B}}} \left\{1 - \frac{1}{\mathcal{N}}\mathrm{e}^{-\frac{3}{2}\bar{\mathcal{M}}_{\mathrm{B}}}\frac{1-\mathrm{e}^{-3\mathcal{N}\bar{\mathcal{M}}_{\mathrm{B}}}}{1-\mathrm{e}^{-3\bar{\mathcal{M}}_{\mathrm{B}}}}\right\}, \tag{7.28}$$

$$\bar{\alpha}_{\mathrm{S,S}} = \frac{2}{3\bar{\mathcal{M}}_{\mathrm{S}}} \left(1 - \frac{1-\mathrm{e}^{-3\bar{\mathcal{M}}_{\mathrm{S}}}}{3\bar{\mathcal{M}}_{\mathrm{S}}}\right) +$$

$$+ \frac{1}{2}\left(\frac{1-\mathrm{e}^{-3\bar{\mathcal{M}}_{\mathrm{S}}}}{3\bar{\mathcal{M}}_{\mathrm{S}}}\right)^2 \frac{\mathrm{e}^{-3\bar{\mathcal{M}}_{\mathrm{B}}}}{1-\mathrm{e}^{-3\bar{\mathcal{M}}_{\mathrm{B}}}} \left(1 - \frac{1}{\mathcal{N}}\frac{1-\mathrm{e}^{-3\mathcal{N}\bar{\mathcal{M}}_{\mathrm{B}}}}{1-\mathrm{e}^{-3\bar{\mathcal{M}}_{\mathrm{B}}}}\right), \tag{7.29}$$

$$\bar{\alpha}_{\mathrm{S,M}} = \frac{1-\mathrm{e}^{-3\bar{\mathcal{M}}_{\mathrm{S}}}}{3\bar{\mathcal{M}}_{\mathrm{S}}} \left\{1 + \frac{1}{2}\mathrm{e}^{-3\bar{\mathcal{M}}_{\mathrm{S}}}\frac{\mathrm{e}^{-3\bar{\mathcal{M}}_{\mathrm{B}}}}{1-\mathrm{e}^{-3\bar{\mathcal{M}}_{\mathrm{B}}}} \left(1 - \frac{1}{\mathcal{N}}\frac{1-\mathrm{e}^{-3\mathcal{N}\bar{\mathcal{M}}_{\mathrm{B}}}}{1-\mathrm{e}^{-3\bar{\mathcal{M}}_{\mathrm{B}}}}\right)\right\} \tag{7.30}$$

$$\bar{\alpha}_{\mathrm{M,M}} = 1 + \frac{1}{2}\mathrm{e}^{-6\bar{\mathcal{M}}_{\mathrm{S}}}\frac{\mathrm{e}^{-3\bar{\mathcal{M}}_{\mathrm{B}}}}{1-\mathrm{e}^{-3\bar{\mathcal{M}}_{\mathrm{B}}}} \left(1 - \frac{1}{\mathcal{N}}\frac{1-\mathrm{e}^{-3\mathcal{N}\bar{\mathcal{M}}_{\mathrm{B}}}}{1-\mathrm{e}^{-3\bar{\mathcal{M}}_{\mathrm{B}}}}\right). \tag{7.31}$$

Applying the IBL, it is clear which terms drop out,

$$\bar{\alpha}_{\mathrm{B,B}} = \frac{2}{3\bar{\mathcal{M}}_{\mathrm{B}}}, \tag{7.32}$$

$$\bar{\alpha}_{\mathrm{B,S}} = -\frac{1}{3\bar{\mathcal{M}}_{\mathrm{B}}} \left(\frac{1-\mathrm{e}^{-3\bar{\mathcal{M}}_{\mathrm{S}}}}{3\bar{\mathcal{M}}_{\mathrm{S}}}\right), \tag{7.33}$$

$$\bar{\alpha}_{\mathrm{B,M}} = -\frac{\mathrm{e}^{-3\bar{\mathcal{M}}_{\mathrm{S}}}}{3\bar{\mathcal{M}}_{\mathrm{B}}}, \tag{7.34}$$

$$\bar{\alpha}_{\mathrm{S,S}} = \frac{2}{3\bar{\mathcal{M}}_{\mathrm{S}}} \left(1 - \frac{1-\mathrm{e}^{-3\bar{\mathcal{M}}_{\mathrm{S}}}}{3\bar{\mathcal{M}}_{\mathrm{S}}}\right) + \frac{1}{2}\left(\frac{1-\mathrm{e}^{-3\bar{\mathcal{M}}_{\mathrm{S}}}}{3\bar{\mathcal{M}}_{\mathrm{S}}}\right)^2 \frac{\mathrm{e}^{-3\bar{\mathcal{M}}_{\mathrm{B}}}}{1-\mathrm{e}^{-3\bar{\mathcal{M}}_{\mathrm{B}}}}, \tag{7.35}$$

$$\bar{\alpha}_{\mathrm{S,M}} = \frac{1-\mathrm{e}^{-3\bar{\mathcal{M}}_{\mathrm{S}}}}{3\bar{\mathcal{M}}_{\mathrm{S}}} \left(1 + \frac{1}{2}\mathrm{e}^{-3\bar{\mathcal{M}}_{\mathrm{S}}}\frac{\mathrm{e}^{-3\bar{\mathcal{M}}_{\mathrm{B}}}}{1-\mathrm{e}^{-3\bar{\mathcal{M}}_{\mathrm{B}}}}\right), \tag{7.36}$$

$$\bar{\alpha}_{\mathrm{M,M}} = 1 + \frac{1}{2}\mathrm{e}^{-6\bar{\mathcal{M}}_{\mathrm{S}}}\frac{\mathrm{e}^{-3\bar{\mathcal{M}}_{\mathrm{B}}}}{1-\mathrm{e}^{-3\bar{\mathcal{M}}_{\mathrm{B}}}}, \tag{7.37}$$

with $\bar{\boldsymbol{\alpha}}$ symmetrical.

In terms of the new matrices, $\bar{\boldsymbol{\kappa}}$ and $\bar{\boldsymbol{\alpha}}$, and the dimensionless unit density, η, the first-order bifurcation equation (Eq. 5.63) becomes

$$\mathbf{c}_1 = -\frac{\eta_0 s_2}{4\pi}\bar{\boldsymbol{\alpha}}\bar{\boldsymbol{\kappa}}\mathbf{c}_1. \tag{7.38}$$

This is a 3×3-matrix eigenvalue problem and therefore soluble. Calling the eigenvalues of the combined matrix $\bar{\boldsymbol{\alpha}}\bar{\boldsymbol{\kappa}}$, λ, then the bifurcation density η_0 is

$$\eta_0 = -4\pi/s_2\lambda = 32/\pi\lambda, \tag{7.39}$$

where the largest positive λ, we call λ_*, corresponds to the smallest (and thus physical; I-N) bifurcation density, η_* [2]. In fact, it is easy to check that $\det(\bar{\boldsymbol{\kappa}}) = 0$, so there are only two nonzero eigenvalues. The eigenvector $\mathbf{c}_*$ corresponding to this λ_* yields relative bifurcating order. Normalizing $\mathbf{c}_*$ such that its third element equals one, $c_{\mathrm{M},*} = 1$, the first two elements equal the average order of the backbone and the spacers in units of that of the mesogens.

In the last part of this subsection, we evaluate the elements of the matrix $\alpha'_{m,\tau_q} = \mathcal{N} W^{(2)}_{m,\tau_q}/W^{(0)}$ (with $m \in \tau_p$), which allows us to calculate the order along the backbone and the spacer (Eqs. 5.75 and 5.76). In the WCL, this matrix behaves as, $\alpha'_{m,\tau_q} \rightarrow \bar{\alpha}'_{\tau_p,\tau_q}(\bar{m}_{\tau_p})$, as the m-dependence becomes continuous. And whereas α'_{m,τ_q} is a $M \times 3$-matrix, $\bar{\alpha}'_{\tau_p,\tau_q}(\bar{m}_{\tau_p})$ is just a 3×3-matrix (with $\bar{m}_{\mathrm{B}}$- and $\bar{m}_{\mathrm{S}}$-dependence though). Note that $\bar{\boldsymbol{\alpha}}'(\bar{m}_{\mathrm{B}}, \bar{m}_{\mathrm{S}})$ (with elements $\bar{\alpha}'_{\tau_p,\tau_q}(\bar{m}_{\tau_p})$) is not symmetrical. The evaluation of $\bar{\alpha}'_{\tau_p,\tau_q}(\bar{m}_{\tau_p})$ runs along the same lines as Eqs. 7.32 to 7.37 and therefore we give them without further comment (in the WCL as well as the IBL),

$$\bar{\alpha}'_{\mathrm{B,B}} = \bar{\alpha}_{\mathrm{B,B}}, \tag{7.40}$$

$$\bar{\alpha}'_{\mathrm{B,S}}(\bar{m}_{\mathrm{B}}) = -\frac{1}{2}\left(\frac{1 - \mathrm{e}^{-3\bar{\mathcal{M}}_{\mathrm{S}}}}{3\bar{\mathcal{M}}_{\mathrm{S}}}\right)\left\{\mathrm{e}^{-3|\bar{m}_{\mathrm{B}} - \frac{1}{2}\bar{\mathcal{M}}_{\mathrm{B}}|} + \right.$$
$$\left. + \left(\mathrm{e}^{3(\bar{m}_{\mathrm{B}} - \frac{1}{2}\bar{\mathcal{M}}_{\mathrm{B}})} + \mathrm{e}^{-3(\bar{m}_{\mathrm{B}} - \frac{1}{2}\bar{\mathcal{M}}_{\mathrm{B}})}\right)\frac{\mathrm{e}^{-3\bar{\mathcal{M}}_{\mathrm{B}}}}{1 - \mathrm{e}^{-3\bar{\mathcal{M}}_{\mathrm{B}}}}\right\}, \tag{7.41}$$

$$\bar{\alpha}'_{\mathrm{B,M}}(\bar{m}_{\mathrm{B}}) = -\frac{1}{2}\mathrm{e}^{-3\bar{\mathcal{M}}_{\mathrm{B}}}\left\{\mathrm{e}^{-3|\bar{m}_{\mathrm{B}} - \frac{1}{2}\bar{M}_{\mathrm{B}}|} + \right.$$
$$\left. + \left(\mathrm{e}^{3(\bar{m}_{\mathrm{B}} - \frac{1}{2}\bar{M}_{\mathrm{B}})} + \mathrm{e}^{-3(\bar{m}_{\mathrm{B}} - \frac{1}{2}\bar{M}_{\mathrm{B}})}\right)\frac{\mathrm{e}^{-3\bar{M}_{\mathrm{B}}}}{1 - \mathrm{e}^{-3\bar{M}_{\mathrm{B}}}}\right\}, \tag{7.42}$$

$$\bar{\alpha}'_{\mathrm{S,B}}(\bar{m}_{\mathrm{S}}) = -\frac{1}{3\bar{\mathcal{M}}_{\mathrm{B}}}\mathrm{e}^{-3\bar{m}_{\mathrm{S}}}, \tag{7.43}$$

$$\bar{\alpha}'_{\mathrm{S,S}}(\bar{m}_{\mathrm{S}}) = \frac{1}{3\bar{\mathcal{M}}_{\mathrm{S}}}\left(2 - \mathrm{e}^{-3\bar{m}_{\mathrm{S}}} - \mathrm{e}^{-3(\bar{\mathcal{M}}_{\mathrm{S}} - \bar{m}_{\mathrm{S}})} + \right.$$
$$\left. + \frac{1}{2}\mathrm{e}^{-3\bar{m}_{\mathrm{S}}}\left(1 - \mathrm{e}^{-3\bar{\mathcal{M}}_{\mathrm{S}}}\right)\frac{\mathrm{e}^{-3\bar{M}_{\mathrm{B}}}}{1 - \mathrm{e}^{-3\bar{M}_{\mathrm{B}}}}\right), \tag{7.44}$$

$$\bar{\alpha}'_{\mathrm{S,M}}(\bar{m}_{\mathrm{S}}) = \mathrm{e}^{-3(\bar{\mathcal{M}}_{\mathrm{S}} - \bar{m}_{\mathrm{S}})} + \frac{1}{2}\mathrm{e}^{-3\bar{\mathcal{M}}_{\mathrm{S}} - 3\bar{m}_{\mathrm{S}}}\frac{\mathrm{e}^{-3\bar{M}_{\mathrm{B}}}}{1 - \mathrm{e}^{-3\bar{M}_{\mathrm{B}}}}, \tag{7.45}$$

$$\bar{\alpha}'_{\mathrm{M,B}} = \bar{\alpha}_{\mathrm{M,B}}, \tag{7.46}$$

$$\bar{\alpha}'_{\mathrm{M,S}} = \bar{\alpha}_{\mathrm{M,S}}, \tag{7.47}$$

$$\bar{\alpha}'_{\mathrm{M,M}} = \bar{\alpha}_{\mathrm{M,M}}. \tag{7.48}$$

---

[2] Note the difference with Chap. 5 where the most *negative* eigenvalue of $(W^{(0)})^{-1}\mathbf{W}^{(2)} \cdot \mathbf{K}^{(2)}$ corresponds to the physical bifurcation density. The reason is that $(W^{(0)})^{-1}\mathbf{W}^{(2)} \cdot \mathbf{K}^{(2)}$ and $\bar{\boldsymbol{\alpha}}\bar{\boldsymbol{\kappa}}$ have opposite sign.

The variables $\bar{m}_B$ and $\bar{m}_S$ are defined within a unit and thus run from 0 to $\bar{\mathcal{M}}_B$ and from 0 to $\bar{\mathcal{M}}_S$ respectively. Obviously, there is no $\bar{m}$-dependence in the $\bar{\alpha}'_{M,\tau_p}$, as there is only one mesogen in a unit. Also, $\bar{\alpha}'_{B,B}$ has no $\bar{m}_B$-dependence, because, the backbone is infinitely long. It can be checked quickly that integrating $\bar{\boldsymbol{\alpha}}'$ over $\bar{m}_B$ and $\bar{m}_S$ yields $\bar{\boldsymbol{\alpha}}$, so,

$$\bar{\boldsymbol{\alpha}} = \frac{1}{\bar{\mathcal{M}}_B \bar{\mathcal{M}}_S} \int_0^{\bar{\mathcal{M}}_B} d\bar{m}_B \int_0^{\bar{\mathcal{M}}_S} d\bar{m}_S \bar{\boldsymbol{\alpha}}'(\bar{m}_B, \bar{m}_S). \tag{7.49}$$

So, having solved the eigenvalue problem, Eq. 7.38, for η_* and $\mathbf{c}_*$, we can calculate the vector $\mathbf{c}'_*(\bar{m}_B, \bar{m}_S)$,

$$\mathbf{c}'_*(\bar{m}_B, \bar{m}_S) = \begin{pmatrix} c'_{B,*}(\bar{m}_B) \\ c'_{S,*}(\bar{m}_S) \\ 1 \end{pmatrix} = -\frac{\eta_* s_2}{4\pi} \bar{\boldsymbol{\alpha}}'(\bar{m}_B, \bar{m}_S) \bar{\boldsymbol{\kappa}} \mathbf{c}_*, \tag{7.50}$$

normalized with $c'_{M,*} = 1$. The component $c'_{B,*}(\bar{m}_B)$ is the order along the backbone, and $c'_{S,*}(\bar{m}_S)$ the order along the spacer (in units of the mesogen order).

7.3.2. Results. In this subsection, we present and discuss the results for the bifurcation analysis for side chain polymers. The subsection consists of three parts. First, we present some results on determining which combination of model parameters yields zero (average) backbone order at bifurcation. Next, we plot some dependences of η_* and $\mathbf{c}_*$ on model parameters and finally, we also plot the order along the backbone and spacer, $\mathbf{c}'_*(\bar{m}_B, \bar{m}_S)$. The model parameters, we usually allow to vary are $\bar{\mathcal{M}}_S$ and sometimes $\bar{\mathcal{M}}_B$ as these parameters are most easily experimentally accessible. The other parameters are usually set as follows: $\tilde{d}_B = \tilde{d}_S = 0$ and $\tilde{P}_B = \tilde{P}_S = 0.3$. We do not aim to describe a 'real' system, but only want to explore the features of this approach.

The combination of model parameters, for which the backbone has zero average order at the bifurcation, can be found with

$$c_{B,*} = 0. \tag{7.51}$$

To analytically solve this equation (containing all 6 parameters), is impossible as it has a transcendental structure, i.e. it is a combination of $e^{-3\bar{\mathcal{M}}_S}$, $\bar{\mathcal{M}}_S$ and powers of them (the same goes for $\bar{\mathcal{M}}_B$). The cause for this is that the backbone as well as the spacers act in two ways; firstly, through the stiffness, they couple orientations on different parts of the chain (yielding factors like $e^{-3\bar{\mathcal{M}}_S}$ and $e^{-3\bar{\mathcal{M}}_B}$), but on the other hand, they also contribute to the external field because they have dimensions themselves (giving factors $\bar{\mathcal{M}}_S$ and $\bar{\mathcal{M}}_B$). It is rather straightforward, however, to construct a numerical scheme to find the roots of Eq. 7.51. (Although, in its simplified form, according to *Mathematica*, Eq. 7.51 covers about two pages.) This, we have done and the results are presented in Fig. 7.6.

We can solve Eq. 7.51, analytically, when we put $\tilde{P}_S = 0$. In this way, the spacer has no dimensions (it does not matter what value $\tilde{d}_S$ has) and does not enter into the external field. As $\bar{\mathcal{M}}_S \neq 0$, this means that the mesogens are directly hinged on the backbone with $e^{-3\bar{\mathcal{M}}_S}$ acting as an orientational coupling parameter (large $\bar{\mathcal{M}}_S$, small coupling and vice versa). Also putting $\tilde{d}_B = 0$, we get a very simple relation between
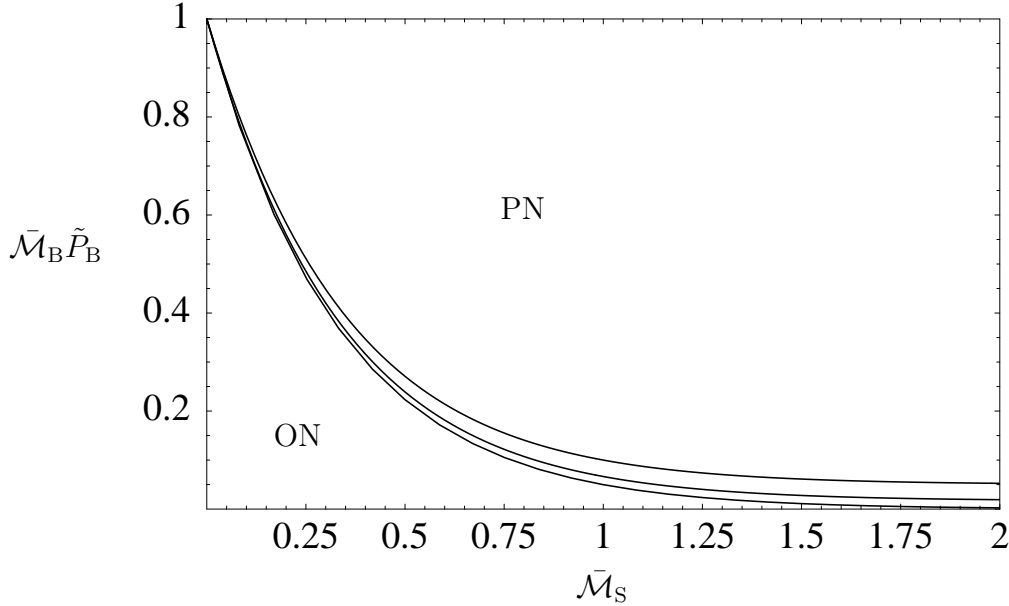
FIGURE 7.6. Combinations of $\bar{\mathcal{M}}_B$ and $\bar{\mathcal{M}}_S$ for which the system has zero backbone order at bifurcation. The parameters are: $\tilde{d}_B = \tilde{d}_S = 0$, $\tilde{P}_B = 0.3$ and $\tilde{P}_S = 0$. (lower curve) $\tilde{P}_S = 0.1$ (middle curve) $\tilde{P}_S = 0.3$ (upper curve). The lower curve is the analytical result, Eq. 7.52 and the other two are obtained by numerically finding the root of Eq. 7.51. For each curve, the system has negative backbone order when $(\bar{\mathcal{M}}_S, \bar{\mathcal{M}}_B)$ is below it, and positive when above.

the remaining parameters,

$$\bar{\mathcal{M}}_B \tilde{P}_B = e^{-3\bar{\mathcal{M}}_S}. \tag{7.52}$$

So basically, when the mesogen-backbone coupling, $e^{-3\bar{\mathcal{M}}_S}$, equals the backbone distance between two spacers, the average backbone order at bifurcation is zero (for these side chain polymers without spacers). If $\bar{\mathcal{M}}_B \tilde{P}_B > 1$, there is no spacer length, $\bar{\mathcal{M}}_S$, for which this order is zero (see Fig. 7.6).

Some general remarks on Fig. 7.6 can be made. For combinations $(\bar{\mathcal{M}}_S, \bar{\mathcal{M}}_B)$ above the curve, the system becomes unstable with respect to the PN phase, and below, with respect to the ON phase. The $(\bar{\mathcal{M}}_S, \bar{\mathcal{M}}_B)$-graph is monotonic decreasing; i.e. when the spacers are longer, the backbone is more decoupled from the mesogen and is therefore more likely to order parallel to the field. And finally, the longer the spacers are, the more important are the associated excluded volume effects, so as $\bar{\mathcal{M}}_S$ increases the deviations from the analytical result, Eq. 7.52, increase as well (and this is again stronger for larger $\tilde{P}_S$, obviously).

In Figs. 7.7(a) to (d), we have plotted the I-N bifurcation density, η_*, (left) and the components of the bifurcating eigenvector, $\mathbf{c}_*$, (right) as a function of the spacer length $\bar{\mathcal{M}}_S$. The four figures correspond to an increasing spacer separation, $\bar{\mathcal{M}}_B = \{0.1, 0.4, 1., 5.\}$. The parameter values are not representative but chosen to obtain some variation in the graphs.

$$(a)$$

$$(b)$$
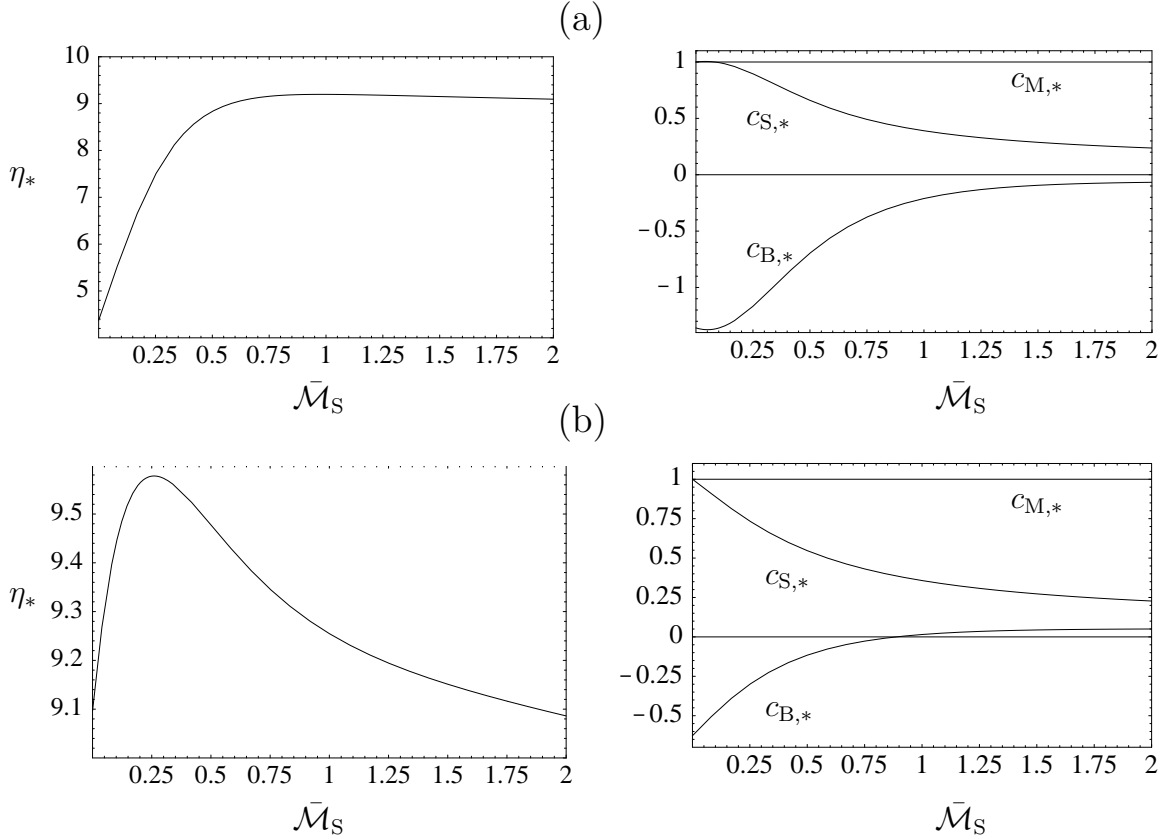
In Fig. 7.7(a), the length of the backbone is very small. Then, for $\bar{\mathcal{M}}_S$ small, a mesogen is strongly coupled to the next mesogens (being so 'close' via spacer and backbone). The I-N transition will therefore be at low densities, due to the rigidity of the molecule. Increasing the spacer length, the mesogens become more disconnected and the transition is postponed to higher densities. At some spacer length, the mesogens are effectively decoupled, and increasing the spacer length further, is just increasing the dimensions of the molecule. This results in decrease of the I-N bifurcation density after passing through a maximum (this effect is better visible in Fig. 7.7(b)). For larger backbone lengths, $\bar{\mathcal{M}}_B$, the mesogens are already disconnected for $\bar{\mathcal{M}}_S = 0$ and the $\bar{\mathcal{M}}_S$-dependence of η_* is monotonically decreasing (Figs. 7.7(c) and (d)).

The $\bar{\mathcal{M}}_S$-dependences of the components of $\mathbf{c}_*$ is roughly the same for all four cases, Figs. 7.7(a) to (d). The normalization is such that $c_{M,*} = 1$ for all parameters. For small $\bar{\mathcal{M}}_S$, the order of the spacers is close to that of the mesogens (because a spacer is very short, all of it is close to a mesogen). The order of the backbone is very low (often negative, corresponding to ON) because the coupling with the mesogen is strong. Increasing the spacer length decouples the backbone and the spacers (on average) from the mesogens, and they can order themselves more with respect to the (infinitesimal) external field. For the spacers, this means that $c_{S,*}$ decreases and for the backbone, $c_{B,*}$ increases (and it passes through zero at some $\bar{\mathcal{M}}_S$, if it was negative).

In Figs. 7.8 and 7.9, we have plotted the bifurcating order along the backbone and spacer, respectively, for various lengths. Again, the parameter values are choses such
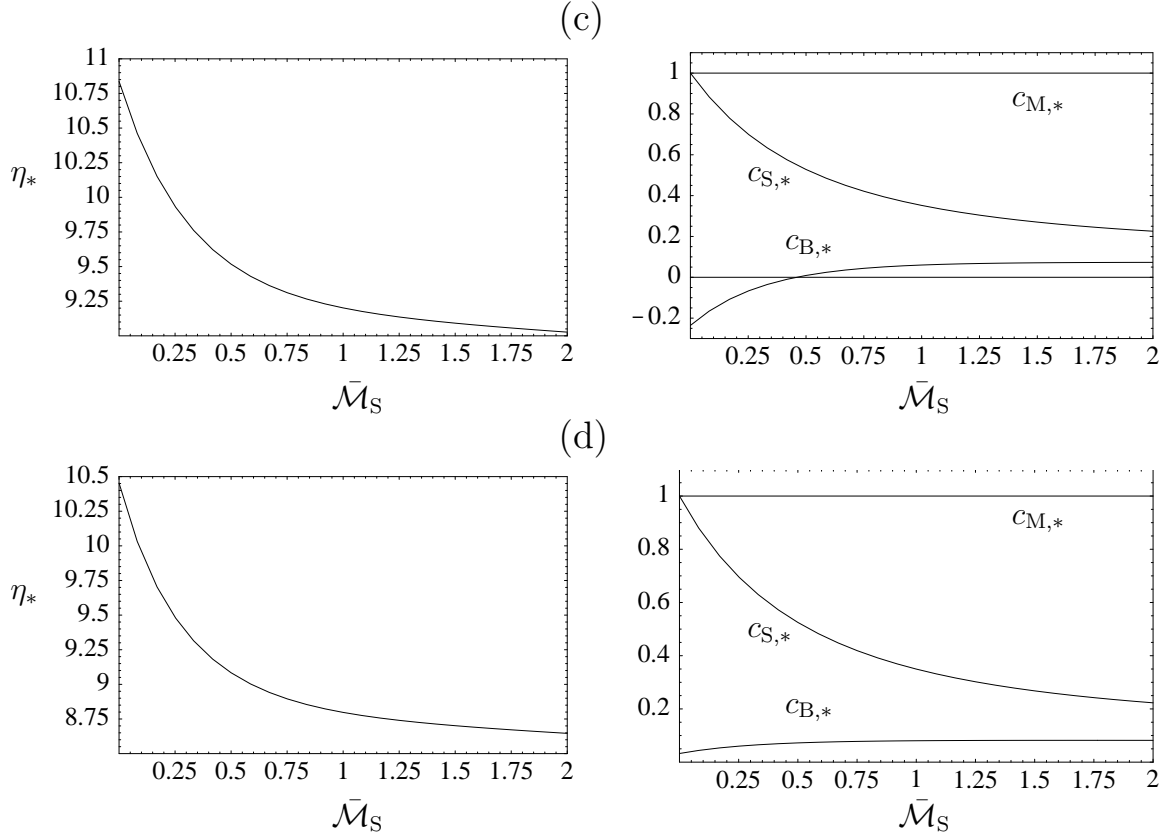
(c)

(d)

FIGURE 7.7. Four pairs of figures (a to d) showing the I-N bifurcation density (left) and the relative order of the components (right) as a function of spacer length, $\bar{\mathcal{M}}_\mathrm{S}$, for various values of the spacer separation, $\bar{\mathcal{M}}_\mathrm{B}$. The parameters are: $\tilde{d}_\mathrm{B} = \tilde{d}_\mathrm{S} = 0$, $\tilde{P}_\mathrm{B} = \tilde{P}_\mathrm{S} = 0.3$ and $\bar{\mathcal{M}}_\mathrm{B} = 0.1$ (a), $\bar{\mathcal{M}}_\mathrm{B} = 0.4$ (b), $\bar{\mathcal{M}}_\mathrm{B} = 1$. (c) and $\bar{\mathcal{M}}_\mathrm{B} = 5$. (d). The order of the backbone ($c_{\mathrm{B},*}$) and the spacers ($c_{\mathrm{S},*}$) is measured in terms of that of the mesogens ($c_{\mathrm{M},*}$) which is set equal to one everywhere. For comparison, the bifurcation density of a gas of free mesogens is $32/\pi \approx 10.186$.

that there is some variation in the graphs and do not correspond to realistic cases. The unit is the bifurcating mesogen order, $c_{\mathrm{M},*} = 1$.

In Fig. 7.8, we have distiguished three cases of different backbones: very short (upper left), very long (lower left) and intermediate (upper right). If the backbone would be completely disconnected from the spacers and mesogens, it would only experience the external field, and would respond by ordering with respect to it. The case which comes closest to this is when the backbone is large (Fig. 7.8, lower left). In this case, the parts of the backbone in between the spacer hinges hardly experience the effects of the spacers, and therefore order as if they were disconnected. The parts where the spacers are connected to, are affected by the spacers and one can see an (exponential) relaxation of the spacer influence on the backbone while going away from the hinge. For shorter backbones, this relaxation is already less pronounced (Fig. 7.8, upper right) and for very short values of $\bar{\mathcal{M}}_\mathrm{B}$ (Fig. 7.8, upper left), there is basically no relaxation (although the
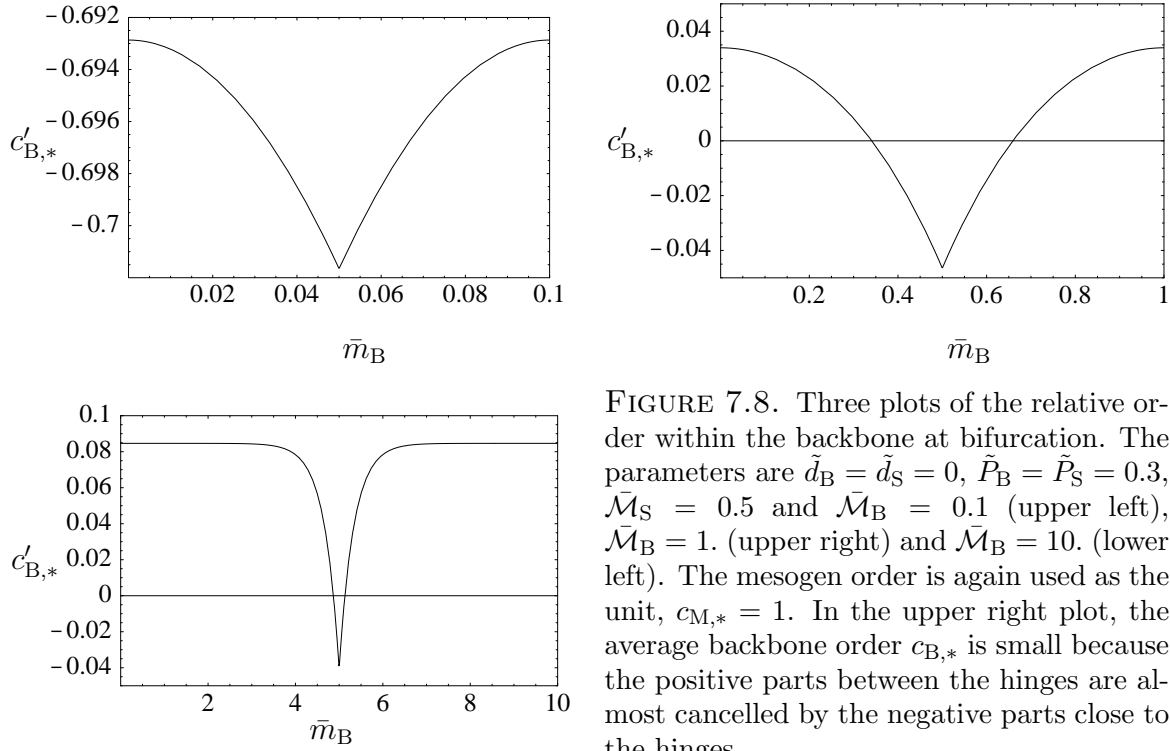
FIGURE 7.8. Three plots of the relative order within the backbone at bifurcation. The parameters are $\tilde{d}_\mathrm{B} = \tilde{d}_\mathrm{S} = 0$, $\tilde{P}_\mathrm{B} = \tilde{P}_\mathrm{S} = 0.3$, $\bar{\mathcal{M}}_\mathrm{S} = 0.5$ and $\bar{\mathcal{M}}_\mathrm{B} = 0.1$ (upper left), $\bar{\mathcal{M}}_\mathrm{B} = 1.$ (upper right) and $\bar{\mathcal{M}}_\mathrm{B} = 10.$ (lower left). The mesogen order is again used as the unit, $c_{\mathrm{M},*} = 1$. In the upper right plot, the average backbone order $c_{\mathrm{B},*}$ is small because the positive parts between the hinges are almost cancelled by the negative parts close to the hinges.

slope is zero halfway between two hinges, but this is due to symmetry). The claim that there is almost no relaxation in the upper left figure of Fig. 7.8 is strengthened by the fact that the vertical scale is much smaller than those of the other two figures. From the upper right figure, it is now clear as well, that an average zero backbone order does not mean that the whole backbone has zero order, but that the negative order of the backbone at the hinges cancels with the positive order of the parts in between the hinges.

In Fig. 7.9, we have again distinguished three cases: long, short and intermediate spacer lengths. For all three cases, the mesogen is attached at $\bar{m}_\mathrm{S} = \bar{\mathcal{M}}_\mathrm{S}$ and therefore, $c'_{\mathrm{S},*}(\bar{\mathcal{M}}_\mathrm{S}) = 1$. The arguments run along the same lines as those for the backbone. Disconnected spacers (disconnected from backbone and mesogens) would only experience the external field and would order with respect to that. Again, this is most clear for long spacer lengths (Fig. 7.9, lower left). The middles of the spacers are effectively disconnected from backbone and mesogens. The ends are strongly affected and going towards the middle, there is a (exponential) relaxation. For shorter spacer lengths, the relaxed part of the spacer disappears (Fig. 7.9, upper graphs).

7.4. Numerical Analysis

7.4.1. Numerical Details. Bifurcation analysis gives only information on quantities at the bifurcation point. However, we are also interested in equilibrium distributions, at high density, far away from the I-N phase transition. Also, the quantities characterizing the actual phase transition (coexistence densities, absolute values of the order parameters) can not be obtained from bifurcation analysis. Consquently, we have
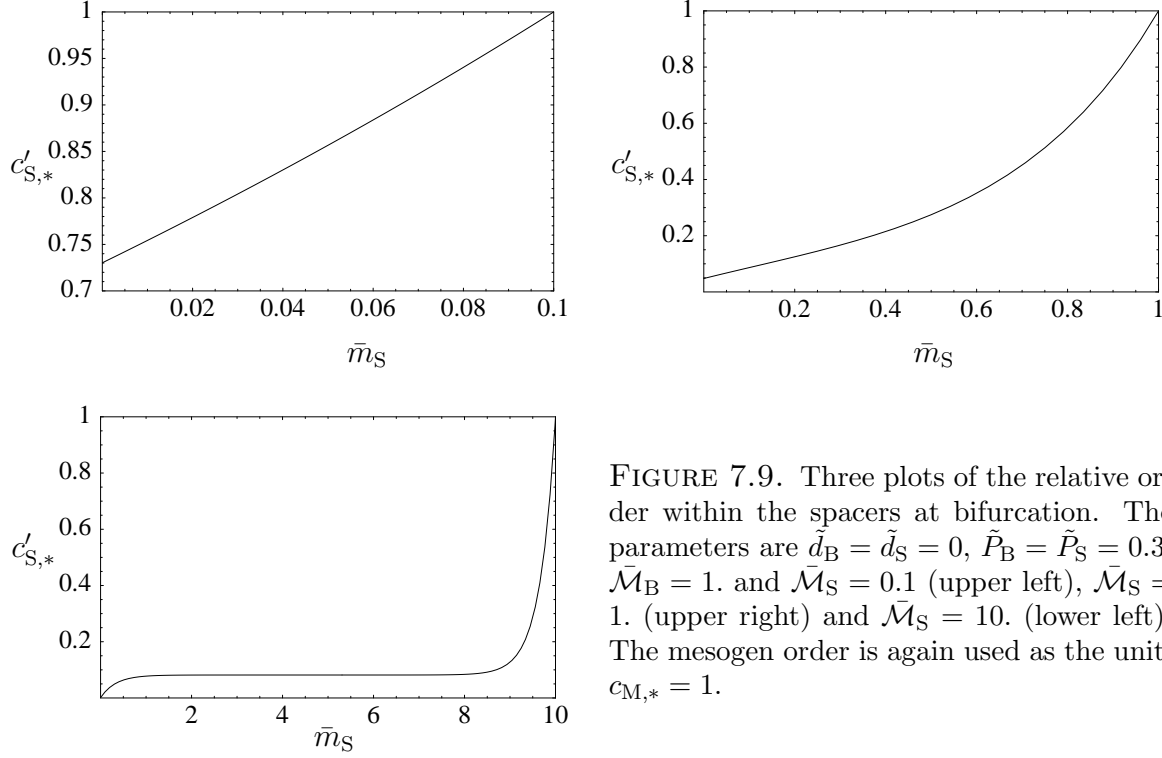
FIGURE 7.9. Three plots of the relative order within the spacers at bifurcation. The parameters are $\tilde{d}_B = \tilde{d}_S = 0$, $\tilde{P}_B = \tilde{P}_S = 0.3$, $\bar{\mathcal{M}}_B = 1$. and $\bar{\mathcal{M}}_S = 0.1$ (upper left), $\bar{\mathcal{M}}_S = 1$. (upper right) and $\bar{\mathcal{M}}_S = 10$. (lower left). The mesogen order is again used as the unit, $c_{M,*} = 1$.

numerically solved the stationarity equations. The numerical analysis is the subject of this subsection, and the results are presented in the next.

The numerical analysis is performed for segmented side chain polymers, as the segment label m is already a discrete parameter (in the WCL, $\bar{m}$ would have to be discretized again). Also, in Chap. 3, we have presented numerical results for segmented linear homochains (not branched and only one type of segment) and for large values of the coupling parameters, $\beta J > 10 - 100$ (and $M > 10$), the results were very similar to the results for wormlike chains. At the end of this subsection, we briefly comment on how we interprete the results for segmented chains, and 'translate' them to the WCL.

Much of the analysis is very similar as the numerical section of Chap. 3. Therefore, in the following, we only list the basic equations, the symmetries and the algorithms, and for more details we refer to Chap. 3. First, we recast the stationarity equations (Eqs. 5.9 and 5.10) in a slightly different form,

$$f_m(\hat{\omega}) = Q^{-1} e^{-\beta \mathcal{H}_m(\hat{\omega})} \prod_{m'} q_{m,m'}(\hat{\omega}) \tag{7.53}$$

with

$$\beta H_m(\hat{\omega}) = \eta \sum_{m'=1}^{M} \frac{V_{m,m'}}{2l_M^2 d_M} \int d\hat{\omega}' \sin \gamma(\hat{\omega}, \hat{\omega}') f_{m'}(\hat{\omega}'), \tag{7.54}$$

$$q_{m,m'}(\hat{\omega}) = \int d\hat{\omega}' w_{m,m'}(\hat{\omega}, \hat{\omega}') e^{-\beta \mathcal{H}_{m'}(\hat{\omega}')} \prod_{m'' \neq m} q_{m',m''}(\hat{\omega}'). \tag{7.55}$$

In this form, one readily sees that the ODF has various contributions: one due to the external field, $\beta\mathcal{H}_m$, and a few more due to the fact that the segment is in a chain and has neighbours with which it is orientationally coupled. The orientational 'field', segment m experiences due to nearest neighbour m' is denoted by $q_{m,m'}(\hat{\omega})$. If m and m' are not nearest neighbours, then $q_{m,m'} = 1$. Most segments have two neighbours, so the product in Eq. 7.54 contains two (relevant) factors. Only a few segments have more or less neighbours (i.e. the mesogens have one and the backbone segments at the hinges have three). The $q_{m,m'}$ on segment m are defined recurrently in Eq. 7.55 in terms of the $q_{m',m''}$ on segment m'. In principle, for every repeating unit of the side chain polymer, there are $2(\mathcal{M}_\mathrm{B} + \mathcal{M}_\mathrm{S} + 1)$ $q_{m,m'}$-functions. However, due to the symmetry of the backbone, $q_{m,m-1} = q_{\mathcal{M}_\mathrm{B}-m+1,\mathcal{M}_\mathrm{B}-m+2}$, the number of $q_{m,m'}$-functions is reduced to $2(\mathcal{M}_\mathrm{S} + 1) + \mathcal{M}_\mathrm{B}$.

The side chain polymers have cylindrical symmetric segments and as we are only considering uniaxial nematic phases, every distribution function (and field) is effectively only a function of a single polar angle, $f_m(\theta)$, $q_{m,m'}(\theta)$ and $\beta\mathcal{H}_m(\theta)$. Azimuthal integrations (over ϕ) can be performed or absorbed in the integration kernel (see Chap. 3). Furthermore, the nematic phases are up-down symmetric, so f_m, $q_{m,m'}$ and $\beta\mathcal{H}_m$ are invariant to $\theta \leftrightarrow \theta - \pi$.

To compute the ODF's, we use an iterative algorithm similar to that of Ref. [59], which we also used in Chap. 3. The iterative loop consists of using the ODF's to calculate the fields, $\beta\mathcal{H}_m$ and $q_{m,m'}$, which are, in turn, used to calculate the ODF's (Eqs. 7.53 to 7.55). Starting from extreme nematic distributions ($f_m(\theta) = \delta(\theta)$), this iteration process converges to the nematic solution (if that exists for the chosen density). We call this loop the f_m-loop. In order to get results consistent with the IBL, we have to evaluate the $2(\mathcal{M}_\mathrm{S} + 1) + \mathcal{M}_\mathrm{B}$ $q_{m,m'}$-functions over and over again (within every single iteration step of the f_m-loop) until their (normalized) θ-dependence does not change anymore. This loop of reevaluating the $q_{m,m'}$-functions, we call the $q_{m,m'}$-loop. Note that the $q_{m,m'}$-loop is located within the f_m-loop [3].

Coexistence values of the densities can be computed by equating the pressures and chemical potentials in the isotropic and nematic phases (or equivalently, finding the common tangents of the free energy in both phases),

$$
\begin{array}{rcl}
P(\eta_\mathrm{nem}) & = & P(\eta_\mathrm{iso}) \\
\mu(\eta_\mathrm{nem}) & = & \mu(\eta_\mathrm{iso})
\end{array} . \tag{7.56}
$$

The free energy can be computed by using the mean field expression,

$$
\frac{\beta\mathcal{F}}{N\mathcal{N}} = -\log\tilde{Q} - \tfrac{1}{2}\eta \sum_{m,m'\in\mathrm{unit}} \frac{V_{m,m'}}{2l_M^2 d_M} \int\int d\hat{\omega}d\hat{\omega}' |\sin\gamma(\hat{\omega},\hat{\omega}')| f_m(\hat{\omega}) f_{m'}(\hat{\omega}'). \tag{7.57}
$$

---

[3]The $q_{m,m'}$-loop refers to the fact that we start with $q_{1,0} = 1$ (the flexibility field on the end of the chain!) Then, we evaluate $q_{2,1}$, next $q_{3,2}$ etc. until we reach $q_{\bar{\mathcal{M}}_\mathrm{B}+1,\bar{\mathcal{M}}_\mathrm{B}}$, which is set equal to $q_{1,0}$ (next unit). Then, the whole thing is done again. This is the $q_{m,m'}$-loop and is performed over and over again until the difference between $q_{1,0}$ and the next $q_{1,0}$ is below some threshold. Then we are in the 'middle' of the polymer.

$\tilde{Q}$ is the partition function of the unit (in the IBL) and in the second part of the right-hand side, the sum is taken over all m, m' in the unit. The most striking in Eq. 7.57 is the absence of the ideal gas term, but this drops out in the IBL; i.e. $(\log \rho)/\mathcal{N}$ goes to zero. The partition function of the unit, $\tilde{Q}$, can be computed by realising that the $q_{m,m'}$-functions are (constrained) partition functions themselves; i.e. $\mathrm{e}^{-\beta\mathcal{H}_m(\hat{\omega})}q_{m,m'}(\hat{\omega})$ is the partition function of the chain starting from m in the direction of m' (and everything beyond m') with the orientation of segment m constrained. Consequently,

$$\log \tilde{Q} = \lim_{\mathrm{IBL}} \left(\log Q^{(\mathcal{N})} - \log Q^{(\mathcal{N}-1)} \right) \tag{7.58}$$

with $Q^{(\mathcal{N})} = \int d\hat{\omega}\mathrm{e}^{-\beta\mathcal{H}_{\mathcal{M}_\mathrm{B}}(\hat{\omega})}q_{\mathcal{M}_\mathrm{B},\mathcal{M}_\mathrm{B}-1}(\hat{\omega})$ the partition function of a polymer with $\mathcal{N}$ units. If we normalize $q_{\mathcal{M}_\mathrm{B},\mathcal{M}_\mathrm{B}-1}$ in such a way that $\int d\hat{\omega}\mathrm{e}^{-\beta\mathcal{H}_{\mathcal{M}_\mathrm{B}}(\hat{\omega})}q_{\mathcal{M}_\mathrm{B},\mathcal{M}_\mathrm{B}-1}(\hat{\omega}) = 1$ (so $Q^{(\mathcal{N}-1)} = 1$), and then use one more step in the $q_{m,m'}$-loop, to compute $q_{\mathcal{M}_\mathrm{B},\mathcal{M}_\mathrm{B}-1}$, we have

$$\log \tilde{Q} = \int d\hat{\omega}\mathrm{e}^{-\beta\mathcal{H}_{\mathcal{M}_\mathrm{B}}(\hat{\omega})}q_{\mathcal{M}_\mathrm{B},\mathcal{M}_\mathrm{B}-1}(\hat{\omega}). \tag{7.59}$$

Knowing this, we can also normalize $q_{\mathcal{M}_\mathrm{B},\mathcal{M}_\mathrm{B}-1}$ every iteration step in the $q_{m,m'}$-loop, so it does not diverge in the IBL (as we do not needs its absolute value anyway).

The pressure and the chemical potential are

$$\beta P(2l_\mathrm{M}^2 d_\mathrm{M}) = \tfrac{1}{2}\eta^2 \sum_{m,m'\in\mathrm{unit}} \frac{V_{m,m'}}{2l_M^2 d_M} \int\int d\hat{\omega}d\hat{\omega}'|\sin\gamma(\hat{\omega},\hat{\omega}')|f_m(\hat{\omega})f_{m'}(\hat{\omega}') \tag{7.60}$$

$$\beta\mu = -\log\tilde{Q}. \tag{7.61}$$

In concluding this subsection, we make a few comments on how to interpret the results for segmented chains in terms of wormlike chains. In Chap. 3, we learned that there are basically two regimes; in the first one, for chains of more than 10 segments, the coupling βJ needed to be 10 or larger in order to get (approximate) wormlike chains. The second regime is when the number of segments is smaller than 10; in that case, for $\beta J = 10$ the segmented character of the chains is too pronounced and we needed to go to higher values of βJ to 'cover' for this. In this chapter (for the backbone and the spacers), we used, as a rule of thumb,

$$\begin{array}{ll} \beta J \approx 10 & \text{if } M \geq 10 \\ \beta J \geq -20M + 210 & \text{if } M < 10 \end{array}. \tag{7.62}$$

The results were found to be satisfying; higher values of βJ showed only a variation on the order of a few percent in the phase diagrams (see next subsection).

7.4.2. Results. There are two regimes for the density, we focus on in this subsection. First, there is the I-N transition which takes place at low densities. We numerically determine the properties of this transition and compare with the bifurcation results. On the other hand, for higher densities, the excluded volume (which scales with the density) becomes more important relative to the internal stiffness of the polymer (which is independent of density). It is expected that this changes the degree of ordering of the various components, both absolutely as well as relatively.

In Fig. 7.10, we have plotted the average order parameters of the three components as a function of density for a side chain polymer with rather short spacers and backbones
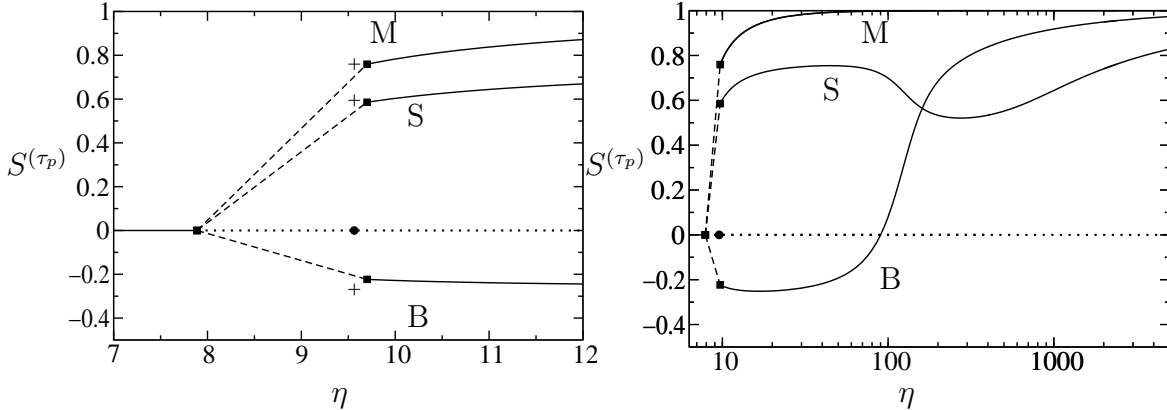
FIGURE 7.10. Order of the components as a function of density on two density scales. The parameters are $\bar{\mathcal{M}}_B = 0.4$, $\bar{\mathcal{M}}_S = 0.2$, $\tilde{P}_B = \tilde{P}_S = 0.3$ and $\tilde{d}_B = \tilde{d}_S = 0$. (where we have used 41 and 21 segments for the backbone and spacer, respectively, with coupling parameters: $\beta J_B = \beta J_S \approx 100$ and dimensions $l_B = l_S \approx 0.003$). Left, the I-N coexistence region, with the filled squares the coexistence points and the filled circle the bifurcation point. The crosses represent the relative order at the bifurcation point, where the bifurcating mesogen order is set equal to the mesogen order at coexistence. Right, the order for larger scales of the density. Note the logarithmic scale of the density.

($\bar{\mathcal{M}}_B = 0.4$ and $\bar{\mathcal{M}}_S = 0.2$). On the left, for small densities; the I-N transition, and on the right the large-density dependence. Also, at five representative values of the density, we have plotted the full order parameter dependence along the spacers and backbone (Fig. 7.11). At the I-N transition, the backbone orders perpendicular to the mesogens, due to the strong coupling via the short spacers (see Fig. 7.11, curves a). Increasing the density, initially, the mesogens order stronger, and due to the short spacers, the backbone is forced even more in the plane perpendicular to the nematic director. In Fig. 7.10 (right), $S^{(B)}$ goes down briefly after the I-N transition and in Fig. 7.11, curve b (left), the order at the hinge has decreased, although, between the hinges the order has increased. With the mesogens ordering, the spacers follow and also $S^{(S)}$ increases strongly (see Fig. 7.11, curve b (right)). On increasing the density further, the excluded volume interactions become more important, and parallel backbone ordering is favored over perpendicular; hence $S^{(B)}$ reaches a minimum and goes up (see Fig. 7.11, curve c and d (left)). At $\eta \approx 90.1$, the *average* order is zero, $S^{(B)} = 0$ (separating ON and PN), and curve c in Fig. 7.11 (left) is the order along the backbone at this density. To allow the backbone to order parallel, the spacers are forced to assume a more bended conformation, resulting in $S^{(S)}$ going down (see Fig. 7.11, curve c and d (right)). Finally, for very high densities stiffness of the components become even less important relative to excluded volume interactions, and as a result, the bending of spacers and backbone becomes more local (closer to the hinge) and the (average) order parameters of the backbone and the spacers ($S^{(S)}$ as well as $S^{(B)}$) go up (see Fig. 7.11, curve e).

The behaviour found in Figs. 7.10 and 7.11 for these specific side chain polymers, is found quite generally for all side chain polymers. There is a low-density regime, dominated by the stiffness of the polymers, and a high-density regime where the excluded
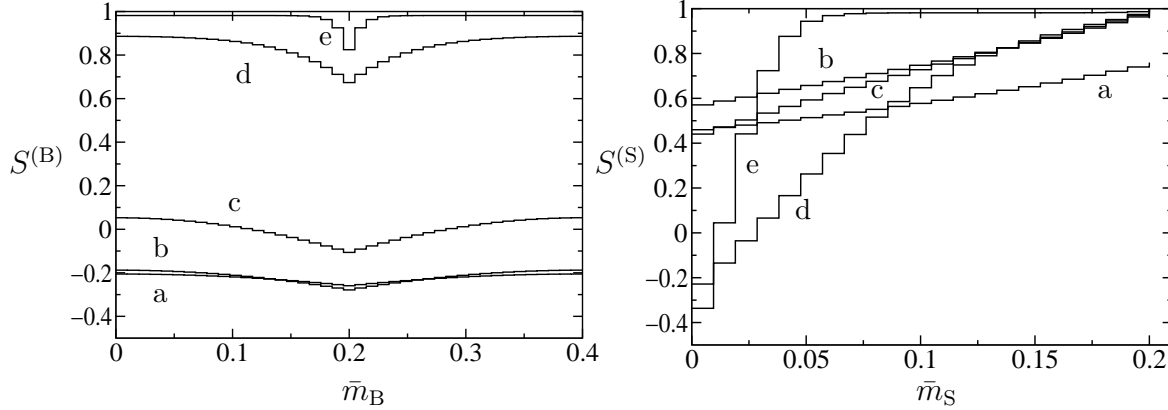
FIGURE 7.11. Order along the backbone (left) and spacer (right) for various densities. The parameters are the same as in Fig. 7.10: $\bar{\mathcal{M}}_B = 0.4$, $\bar{\mathcal{M}}_S = 0.2$, $\tilde{P}_B = \tilde{P}_S = 0.3$ and $\tilde{d}_B = \tilde{d}_S = 0$. (where we have used 41 and 21 segments for the backbone and spacer, respectively, with coupling parameters: $\beta J_B = \beta J_S \approx 100$ and dimensions $l_B = l_S \approx 0.003$). The densities are $\eta = \eta_{nem} \approx 9.7$ (a), $\eta = 40$ (b), $\eta = \eta_{ON-PN} \approx 90.1$ (c), $\eta = 400$ (d) and $\eta = 5000$ (e). Although components are discrete, we have still chosen to use $\bar{m}_B$ and $\bar{m}_S$. Finally, we note that $S^{(S)}(0.2) = S^{(M)}$.

volumes are the most important interactions. In Figs. 7.10 and 7.11, this behaviour is quite pronounced as we have chosen values of the spacer length $\bar{\mathcal{M}}_S$ and spacer separation $\bar{\mathcal{M}}_B$ for which the two regimes are more or less 'separated'. Especially on the spacer, the separated and combined effects of stiffness and excluded volume are well visible (Fig. 7.11). Finally, it has to be noted that this behaviour occurs for different orders of magnitude of the density; the I-N phase transition occurs for densities of the order of 10, the transition from stiffness-dominated to excluded volume-dominated at orders of 100 and the real 'high-density' behaviour only sets in for densities of the order of 1000 (that's why it is so hard to get this all in one plot). However, in most experimental cases, the nematic does not range over more than one order of magnitude of the density (or temperature) and then another phase, usually a smectic, sets in.

To compute the behaviour in Figs. 7.10 and 7.11, we have used a rather good approximation for the wormlike spacers and backbone. From Chap. 3, we know that for values of $\beta J \approx 100$ and $M > 10$ segments, there is effectively no difference in the phase behaviour of segmented and the equivalent wormlike chains. Based on using varying degrees of approximation, we conclude that the expected magnitude of the error is within 1%. Only for very high densities (i.e. Fig. 7.11, curve e), where the discrete character of the components shows, we expect larger deviations.

Fig. 7.12 is the phase diagram, where we have plotted the I-N coexistence densities against the spacer length (left). The bifurcation density follows nicely the nematic coexistence density, and in general, we find that their difference never becomes greater than 5-10%. The point in the phase diagram where the nematic bifurcates with zero backbone order (filled circle) is fairly close to the point where there is zero backbone order at coexistence (where the dotted curve hits the full curve). The analytical result of Eq. 7.52 (filled diamond) is a bit farther away. On the right, the density scale is
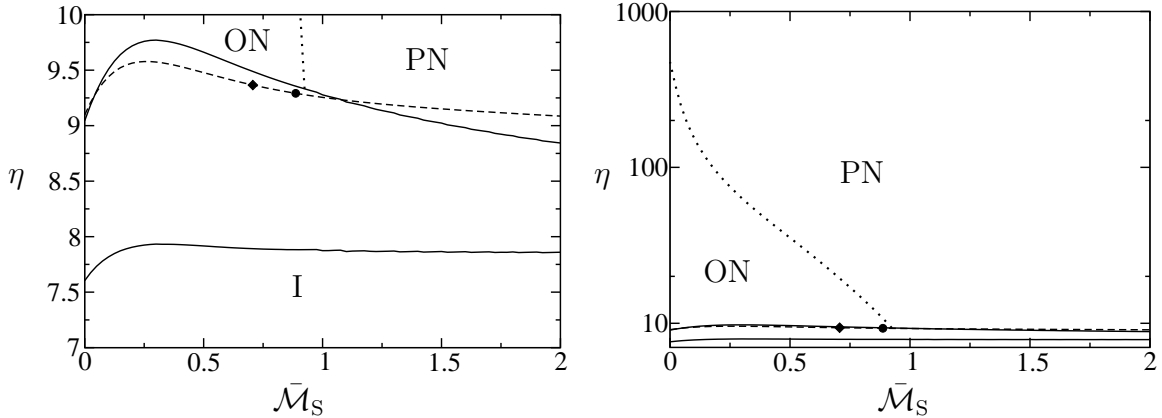
FIGURE 7.12. The phase diagram for side chain polymers; density vs. length of the spacer $\bar{\mathcal{M}}_S$. Both plots are the same, but have different density scales. The parameters are $\bar{\mathcal{M}}_B = 0.4$, $\tilde{P}_B = \tilde{P}_S = 0.3$ and $\tilde{d}_B = \tilde{d}_S = 0$. In determining the discretized parameters, we have used the 'rule of thumb' discussed in the last paragraph of subsection 7.4. Left, the full curves are the I-N coexistence densities, the striped curve is the bifurcation density and the dotted curve is the density where $S^{(B)} = 0$; i.e. the line separating the ON and PN phases. The filled circle is the bifurcation density where $c_{B,*} = 0$ and the filled diamond is the analytical result of Eq. 7.52 (where $\bar{\mathcal{M}}_S = -\frac{1}{3}\ln(\bar{\mathcal{M}}_B \tilde{P}_B) \approx 0.707$). To give an idea, the bifurcation density of a gas of free mesogens is $32/\pi \approx 10.186$. Right, the density scale is larger in order to plot the ON-PN separation curve. Note that this curve does not mark a phase transition between ON and PN.

much larger in order to show the density, where $S^{(B)} = 0$ (separating the ON and PN phases). Here, we state that we found no phase transition between ON and PN. No order parameter (or its derivative) becomes discontinuous at this point. In fact, we have not found any nematic-to-nematic phase transitions in systems of these side chain polymers for any of the model parameters. We come back to this in the next subsection, where we present some arguments why this is so. Finally, in computing Fig. 7.12, we have used the 'rule of thumb', Eq. 7.62, presented in the last paragraph of the previous subsection. This means that for different spacer lengths $\bar{\mathcal{M}}_S$, we have used different parameter values for $\mathcal{M}_S$, βJ_S and l_S. The accuracy is less than what is used for Figs 7.10 and 7.11. Still, comparing it with some checks of higher accuracy, we found a difference of a few percent and on average larger for larger $\bar{\mathcal{M}}_S$. Further, the slight "wiggles" in the coexistence densities for $\bar{\mathcal{M}}_S > 1$ are due to this changing of parameter values.

7.5. Conclusion and Discussion

7.5.1. No Nematic-to-Nematic Phase Transitions. In this subsection, we argue that there are no nematic-to-nematic (N-N) phase transitions in this system of side chain polymers.

Transitions between phases of the same symmetry require a van der Waals-like loop. Such a loop can be located by finding the spinodal points,

$$\frac{\partial P}{\partial \rho} = 0. \tag{7.63}$$

However, as the backbone of the side chain polymers is infinitely long, there is no ideal-gas contribution in the free energy. From Eq. 7.60, it can be easily seen that as a result

$$\frac{\partial P}{\partial \eta} = \tfrac{1}{2}\eta P. \tag{7.64}$$

So, the prescription that the first derivative of the pressure to the density must be zero leads to the prescription that the pressure itself must be zero. From Eq. 7.60, it can be directly seen that this will never happen for nonzero densities (both f_m and $|\sin\gamma|$ are always positive). From these considerations, we conclude that there are no N-N phase transitions.

Moreover, for finite-length backbones, we only expect an additional ideal-gas contribution. And although Eq. 7.64 is no longer valid, the effect of the ideal-gas term will be an additional positive constant (to Eq. 7.64). This would mean that the above argument can be extended to finite-length backbones. The argument also seems to hold for other systems with the same equations, like the main chain LC polymers of the previous chapter.

7.5.2. Comparison with Other Work. In Refs. [98, 99], N-N phase transitions are found in systems of side chain polymers. Warner and coworkers (WWRW) use a Maier-Saupelike theory (using temperature) to describe the interactions between side chain polymers consisting of a wormlike backbone and rigid mesogens hinged onto the backbone on regular distances (no spacers present!). The Maier-Saupe interactions between the components favour parallel ordering of the components. The stiffness interaction between side chains and backbone, via the hinge, is treated on a mean field level (Maier-Saupe) as well, and favours perpendicular ordering. The resulting theory uses 4 model parameters of which one is the effective cross coupling between backbone and side chains (containing both the regular Maier-Saupe external field cotribution and the stiffness contribution via the hinge). WWRW focussed on a general exploration of this model, using universal functions and area rules, to determine the phase behaviour. On decreasing the temperature from the isotropic phase, at some point, one component (say, the side chains) will go into the nematic phase, imposing some kind of order onto the backbone (oblate or prolate, depending on the effective cross coupling). Decreasing the temperature further, the point is reached where the other component (backbone) undergoes a transition as well; i.e. from the weakly ordered (oblate or prolate) nematic to a highly ordered (prolate) nematic. There is a critical point (for some value of the effective cross coupling) associated with this N-N transition and within the model this phenomenon is equivalent to the N-N transition of simple Maier-Saupe rods in a (small) external field. And consequently, this N-N transition is due to the self interaction of the backbones and not due to the cross interaction between backbones and side chains.

In the present theory, as well as that of WWRW, the intermolecular interactions are of the mean-field type; Onsager approximation and Maier-Saupe interactions, respectively. The large difference concerns the stiffness interactions within the polymers, which we take into account in an exact fashion. Also, as an ingredient, we use the actual geometry of the spacers, which couple the orientations of backbone and mesogens through their stiffness, but also act as a component in their own right (i.e. excluding volume for mesogens etc.). The spacer geometry is exactly the reason why our theory has 2 model

parameters more than WWRW. From a global point of view, the results are roughly the same; both theories find the phase sequence I-ON-PN (in case of mesogen ordering, and appropriate model parameters). As was already mentioned, the big difference is that WWRW find N-N phase transitions. The rigorous thermodynamical argument why this not happens in the present model is the proof of the nonexistence of spinodal points in the previous subsection. For the rest, it seems hard to exactly pin down what precise difference between these models causes these differences in phase behaviour, but we list a few possible arguments in the following. The first reason may be the difference in scaling in our theory; the effective field due to the excluded volumes scales with the density and stiffness interactions within the polymer do not depend on density. On increasing the density, the excluded volume interactions become gradually more and more important than the stiffness interactions, allowing the backbone (possibly) to continuously adjust its conformation. Another essential difference between the two theories, is that N-N transition, in case of WWRW, is due to the self interaction of components, while in our model, it is due to the cross interaction. To explain this, in case of side chain ordering, the WWRW-backbones go from oblate to prolate to minimize the backbone-backbone (BB) interaction, where in the present theory the mean field due to the backbone-mesogen (BM) interaction is always larger than the BB one and it is this (cross) interaction which drives the transition.

In conclusion, there are three main differences between the present approach and that of WWRW and which may contribute to the difference in phase behaviour. First, in the WWRW-approach, the intrachain and the extrachain interactions scale in the same way with temperature whereas in our approach they scale differently with the density. Second, in case of our approach, the dimensions of the components totally fix the (excluded volume) interactions. As a result, the BB can never be larger than the BM interactions. In mean field theories, like that of WWRW, these interactions are governed by effective parameters, which can be chosen freely. This might give unphysical results. Third, the fact that we treat the internal degrees of freedom of the polymer in an exact way, does (by itself) not seem to give better results. It does, however, allow us to see how the nematic ordering of the various components (and along them) originates. Finally, we are not aware of (first-order) N-N transitions in experimental LCP systems [102].

7.5.3. Conclusion and Outlook. We analyzed nematic ordering in a monodisperse fluid of side chain LCP's. We took into account the explicit geometry of these polymers (having spacers of nonzero dimensions) and intrachain interactions were considered exactly. Using the results of Chap. 5, we calculated the I-N bifurcation density and bifurcating order of the components (B, S and M). The backbone orders parallel (prolate) or perpendicular (oblate) with respect to the mesogens, depending on the length of the spacers. Numerically, we computed the dependence of the order of the various components on the density. On increasing the density, we found a continuous transition (not a phase transition) from oblate (or weakly prolate) ordering of the backbone to strong prolate ordering. Order along the backbone and spacers has been determined as well, showing nicely the competition between the external (mean) field and intrachain constraints due to stiffness. We have also computed the phase diagram (density vs. spacer length). Our results were compared with the results of Warner and coworkers.

In constructing our theory, we have used the segmented-chain approach, developed in Chap. 3, and there we stated that three kinds of approximations were used. First, we have left out contributions from three polymers interacting simultaneously (second virial approximation), second, two polymers having more than one "interaction site" are not taken into account, and finally, a polymer interacting with itself is also left out (e.g. overlap between different parts of the same chain). As we are considering infinitely long polymers, one could argue that the errors made due to the approximations are not small. However, in the limit of $P_{\mathrm{B}}, P_{\mathrm{S}}, l_{\mathrm{M}} \gg d_{\mathrm{B}}, d_{\mathrm{S}}, d_{\mathrm{M}}$, all three approximations are expected to be very good (Chap. 3). Second, for more realistic ratios of persistence lengths and thicknesses, it is hard to estimate, what is the effect of each of the approximations. Naively, we would say that these 'extra' (double or self-) overlaps are only expected to matter if the segments involved are within a few persistence lengths along the chain (so orientational correlation is not yet lost). In other cases, when these things happen far away from each other, we would only expect a correction to the magnitude of the mean field, and not to its form, and this would mean that the physics would not change. However, we have not investigated this. In this respect, we would like to mention Ref. [111], where some of this is considered for an isolated side chain polymer.

Experimentally, side chain LCP's are famous for forming smectic (Sm) phases. Nematic side chain LCP's must have short spacers, short mesogens and a rather flexible backbone, otherwise they are smectic [1]. An argument due to Finkelmann is that mesogenic monomers which form nematics (usually) form smectics when incorporated in polymers and monomers which are not liquid crystalline yield nematic polymers. This suggests that the smectic phase is expected to interfere with large parts of our phase diagrams, where we computed its nematic behaviour. Also, side chain LCP systems are thought to be able to form biaxial nematic (BN) phases. Obviously, we have not considered either of these phases. It should not be too difficult to perform a bifurcation analysis or even a numerical analysis of the BN (in principle, we can use the same equations). In fact, Warner and coworkers have already performed this in the context of their model [109]. The Sm phase, being much more interesting from an experimental point of view, however, is expected to be more problematic. In the present analysis, there is a central role for the excluded volume, which is a result of integrating out the spatial degrees of freedom. Considering Sm phases, this integration can not be performed and the spatial dependence remains in the distribution funtions. An additional problem is that spatial correlations (unlike orientational correlations) travel much further along the polymer. In the context of the same (Maier-Saupe based) model, Warner and Renz have given an analysis of side chain polymers in the Sm phase, arguing that layer hopping hopping is an essential phenomenon [110].

Bibliography

[1] A. Donald and A. Windle. *Liquid Crystalline Polymers*. Cambridge University Press, 1992.

[2] J. White. *J. Appl. Pol. Sci.: Appl. Pol. Symp.*, 41:3, 1985.

[3] G. Friedel. *Ann. Physique*, 18:273, 1922.

[4] D. Vorländer. *Z. Phys. Chem.*, 105:211, 1923.

[5] S. Fraden. Phase transitions in colloidal suspensions of virus particles. In *Observation, Prediction, and Simulation of Phase Transitions in Complex Fluids*. Kluwer Academic Publishers, 1995.

[6] J. Bernal F. Bawden, N. Pirie and I. Fankuchen. *Nature*, 19:1051, 1936.

[7] L. Onsager. *Ann. N. Y. Acad. Sci.*, 51:627, 1949.

[8] P. J. Flory. *Proc. Roy. Soc. London*, A234:73, 1956.

[9] W. Maier and A. Saupe. *Z. Naturf.*, 14:882, 1959.

[10] R. Zwanzig. *J. Chem. Phys.*, 39:1714, 1963.

[11] J. Vieillard-Baron. *J. Chem. Phys.*, 56:4729, 1972.

[12] D. Frenkel and B. Mulder. *Mol. Phys.*, 55:1171, 1985.

[13] M. P. Allen, G. T. Evans, D. Frenkel, and B. M. Mulder. *Adv. Chem. Phys.*, 86:1, 1993.

[14] P. Bolhuis and D. Frenkel. *J. Chem. Phys.*, 106:666, 1997.

[15] P. Lebwohl and G. Lasher. *Phys. Rev. A*, 6:426, 1972.

[16] G.W. Gray and G.R. Luckhurst, editors. *The Molecular Physics of Liquid Crystals*. Ac. Press, 1979.

[17] G. Vertogen and W. de Jeu. *Thermotropic Liquid Crystals, Fundamentals*. Springer-Verlag, 1987.

[18] S. Chandrasekhar. *Liquid Crystals*. Cambridge University Press, 2nd edition, 1992.

[19] P. G. de Gennes and J. Prost. *The Physics of Liquid Crystals*. Oxford Science Publications, 2nd edition, 1993.

[20] D. Frenkel. Statistical mechanics of liquid crystals. In J. P. Hansen, D. Levesque, and J. Zinn-Justin, editors, *Liquids, Freezing and the Glass Transition*. Elsevier Science Publ. B. V., 1991.

[21] H. Ringsdorf, B. Schlarb, and J. Venzmer. *Angew. Chem. Int. Ed. Engl.*, 27:113, 1988.

[22] C. Robinson. *Trans. Faraday Soc.*, 52:571, 1956.

[23] S. L. Kwolek. Du pont. U. S. Patent 3600350, 1971.

[24] W. J. Jackson and H. F. Kuhfuss. *J. Poly. Sci. Poly. Chem. Ed.*, 14:2043, 1976.

[25] H. Finkelmann, H. Ringsdorf, and J. H. Wendorff. *Makromol. Chem.*, 179:273, 1978.

[26] A. Ciferri, W. R. Krigbaum, and R. B. Meyer, editors. *Polymer Liquid Crystals*. Academic Press, 1982.

[27] V. P. Shibaev and L. Lam, editors. *Liquid Crystalline and Mesomorphic Polymers*. Springer-Verlag, 1994.

[28] N. Boiko, V. Shibaev, B. Ostrovskii, S. Sulyanov, D. Wolff, and J. Springer. *Macromol. Chem. Phys.*, 202:297, 2001.

[29] D. Sentenac, B. Ostrovskii, and W. de Jeu. *Adv. Mater.*, 13:1079, 2001.

[30] B. Ostrovskii, S. Sulyanov, N. Boiko, V. Shibaev, and W. de Jeu. *Eur. Phys. J. E*, 6:277, 2001.

[31] B. Ostrovskii, D. Sentenac, I. Samoilenko, and W. de Jeu. *Eur. Phys. J. E*, 6:287, 2001.

[32] A. R. Khokhlov and A. N. Semenov. *Physica*, 108A:546, 1981.

[33] A. R. Khokhlov and A. N. Semenov. *Physica*, 112A:605, 1982.

[34] M. Warner, J. M. F. Gunn, and A. B. Baumgärtner. *J. Phys. A: Math. Gen.*, 18:3007, 1985.

[35] R. Holyst and P. Oswald. *Macromol. Theory Simul.*, 10:1, 2001.

[36] Z. Y. Chen. *Macromolecules*, 26:3419, 1993.

[37] R. F. Kayser Jr. and H. J. Raveché. *Phys. Rev. A*, 17:2067, 1978.

[38] H. B. Callen. *Thermodynamics and an Introduction to Thermostatistics*. John Wiley and Sons, 2nd edition, 1985.

[39] C. B. P. Finn. *Thermal Physics*. Chapman & Hall, 1986.

[40] M. W. Zemansky. *Heat and Thermodynamics*. McGraw-Hill, 4th edition, 1957.

[41] K. Huang. *Statistical Mechanics*. John Wiley & Sons, 1963.

[42] R. K. Pathria. *Statistical Mechanics*. Pergamon Press, 1972.

[43] J.-P. Hansen and I. R. McDonald. *Theory of Simple Liquids*. Academic Press, 2nd edition, 1986.

[44] B. M. Mulder. Density functional theory. In *Lecture Notes, Han-sûr-Lesse Winter School on Physical Chemistry*, Han-sûr-Lesse, Belgium, feb. 2000.

[45] R. Evans. *Adv. Phys.*, 28:143–200, 1979.

[46] B. M. Mulder. *Phys. Rev. A*, 35:3095, 1987.

[47] B. M. Mulder. Bifurcation analysis of liquid crystal phase transitions. In *Lecture Notes, Advanced NATO Research Workshop Computer Simulation of Liquid Crystals*, Il Ciocco, sept. 1991.

[48] G. J. Vroege and H. N. W. Lekkerkerker. *Rep. Prog. Phys.*, 55:1241, 1992.

[49] O. Kratky and G. Porod. *Recl. Trav. Chim.*, 68:1106, 1949.

[50] P. J. Flory. *Statistical Mechanics of Chain Molecules*. Hanser Publishers, 1989.

[51] A. Yu. Grosberg and A. R. Khokhlov. *Statistical Physics of Macromolecules*. AIP Press, 1994.

[52] Th. Odijk. *Macromolecules*, 19:2313, 1986.

[53] T. Morita. *J. Math. Phys.*, 13:115, 1972.

[54] R. G. Petschek and E. M. Terentjev. *Phys. Rev. A*, 45:930, 1992.

[55] W. Feller. *An Introduction to Probability Theory and Its Applications*. John Wiley and Sons, 3nd edition, 1950.

[56] G. W. Woodbury Jr. *J. Chem. Phys.*, 47:270, 1967.

[57] A. N. Semenov and A. R. Khokhlov. *Sov. Phys. Usp.*, 31:988, 1989.

[58] I. S. Gradshteyn and I. M. Ryzhik. *Table of Integrals, Series, and Products*. Academic Press Inc., 5th edition, 1965.

[59] J. Herzfeld, A. E. Berger, and J. W. Wingate. *Macromolecules*, 17:1718, 1984.

[60] H. N. W. Lekkerkerker, Ph. Coulon, R. v. d. Haegen, and R. Deblieck. *J. Chem. Phys.*, 80:3427, 1984.

[61] M. J. Freiser. *Phys. Rev. Lett.*, 24:1041, 1970.

[62] R. Alben. *Phys. Rev. Lett.*, 30:778, 1973.

[63] J. P. Straley. *Phys. Rev. A*, 10:1881, 1974.

[64] B. M. Mulder. *Liq. Cryst.*, 6:539, 1986.

[65] B. M. Mulder. *Phys. Rev. A*, 39:360, 1989.

[66] M. P. Allen. *Liq. Cryst.*, 8:499, 1990.

[67] S. Sarman. *J. Chem. Phys.*, 104:342, 1996.

[68] L. J. Yu and A. Saupe. *Phys. Rev. Lett.*, 45:1000, 1980.

[69] P. Tolédano and A. M. Figueiredo Neto. *Phys. Rev. Lett.*, 73:2216, 1994.

[70] S. M. Fan, I. D. Fletcher, B. Gündoḡan, N. J. Heaton, G. Kothe, G. R. Luckhurst, and K. Praefcke. *Chem. Phys. Lett.*, 204:517, 1993.

[71] G. R. Luckhurst. *Thin Solid Films*, 393:40, 2001.

[72] J. J. Hunt, R. W. Date, B. A. Timimi, G. R. Luckhurst, and D. W. Bruce. *European Conference on Liquid Crystals 2001 (ECLC2001)*, Halle, Germany, 2001.

[73] F. Hessel, R.-P. Herr, and H. Finkelmann. *Makromol. Chem.*, 188:1597, 1987.

[74] M. Ebert, O. Herrmann-Schönherr, J. H. Wendorff, H. Ringsdorf, and P. Tschirner. *Makromol. Chem., Rapid Commun.*, 9:445, 1988.

[75] R. Alben. *J. Chem. Phys.*, 59:4299, 1973.

[76] A. Stroobants and H. N. W. Lekkerkerker. *J. Chem. Phys.*, 88:3669, 1984.

[77] P. J. Camp, M. P. Allen, P. G. Bolhuis, and D. Frenkel. *J. Chem. Phys.*, 106:9270, 1997.

[78] F. M. van der Kooij and H. N. W. Lekkerkerker. *Phys. Rev. Lett.*, 84:781, 2000.

[79] H. Goldstein. *Classical Mechanics*. Addison Wesley Publ. Co., 2nd edition, 1980.

[80] D. M. Brink and G. R. Satchler. *Angular Momentum*. Oxford University Press, 2nd edition, 1968.

[81] L. D. Landau and E. M. Lifshitz. *Theory of Elasticity*. Pergamon Press, 3rd edition, 1986.

[82] M. Abramowitz and I. A. Stegun. *Handbook of Mathematical Functions*. Dover Publications, Inc., 2nd edition, 1972.

[83] J. P. Straley. *Mol. Cryst. Liq. Cryst.*, 24:7, 1973.

[84] G. Lasher. *J. Chem. Phys.*, 53:4141, 1970.

[85] R. van Roij and B. Mulder. *Europhys. Lett.*, 34:201, 1996.

[86] V. Shibaev and L. Lam, editors. *Liquid Crystalline and Mesomorphic Polymers*. Springer-Verlag, 1994.

[87] C. B. McArdle, editor. *Side Chain Liquid Crystalline Polymers*. Blackie, 1989.

[88] X. J. Wang and M. Warner. *J. Phys. A: Math. Gen.*, 19:2215, 1986.

[89] T. A. Yurasova and A. N. Semenov. *Polymer Science: U. S. S. R.*, 32:223, 1990.

[90] T. A. Yurasova and A. N. Semenov. *Mol. Cryst. Liq. Cryst.*, 199:301, 1991.

[91] T. A. Yurasova and T. C. B. McLeish. *Polymer*, 34:3774, 1993.

[92] X. J. Wang and M. Warner. *Liquid Crystals*, 12:385, 1992.

[93] A. N. Semenov and A. R. Khokhlov. *Sov. Phys. Usp.*, 31:988, 1988.

[94] M. R. Wilson and M. P. Allen. *Mol. Phys.*, 2:277, 1993.

[95] M. Dijkstra and D. Frenkel. *Phys. Rev. E*, 51:5891, 1995.

[96] A. V. Lyulin, M. S. Al-Barwani, M. P. Allen, M. R. Wilson, I. Neelov, and N. K. Allsopp. *Macromolecules*, 31:4626, 1998.

[97] R. P. Sear and G. Jackson. *J. Chem. Phys.*, 103:8684, 1995.

[98] X. Wang and M. Warner. *J. Phys. A: Math. Gen.*, 20:713, 1987.

[99] W. Renz and M. Warner. *Proc. R. Soc. Lond. A*, 417:213, 1988.

[100] H. Finkelmann, H. Ringsdorf, W. Siol, and J. H. Wendorff. *Makromol. Chem.*, 179:829, 1978.

[101] H. Finkelmann, M. Happ, M. Portugal, and H. Ringsdorf. *Makromol. Chem.*, 179:2541, 1978.

[102] W. de Jeu. private communication.

[103] N. A. Platé and V. P. Shibaev. *Comb-Shaped Polymers and Liquid Crystals*. Plenum Press, 1987.

[104] C. T. Imrie, F. E. Karasz, and G. S. Attard. *Macromolecules*, 26:3803, 1993.

[105] A. A. Craig and C. T. Imrie. *J. Polym. Sci., Pt. A: Polym. Chem.*, 34:421, 1996.

[106] F. Hardouin and S. Lecommandoux. *Macromol. Symp.*, 118:207, 1997.

[107] R. P. Nieuwhof, A. T. M. Marcelis, E. J. R. Sudhölter, R. Wursche, and B. Rieger. *Macromol. Chem. Phys.*, 201:2484, 2000.

[108] S. Vasilenko, V. Shibaev, and A. Khokhlov. *Makromol. Chem.*, 186:1951, 1985.

[109] P. Bladon, M. Warner, and H. Liu. *Macromolecules*, 25:4329, 1992.

[110] W. Renz and M. Warner. *Phys. Rev. Lett.*, 56:1268, 1986.

[111] A. Subbotin, M. Saariaho, R. Stepanyan, O. Ikkala, and G. ten Brinke. *Macromolecules*, 33:6168, 2000.

Summary

In this thesis we investigate the influence of molecular flexibility on liquid crystalline phase behaviour. To this end, we develop a segmented chain formalism, which deals with flexibility in a generic way. The segments are hard rodlike bodies and interact as such with the segments of other chains. This interaction is treated in the second virial or Onsager approximation. Within a chain, segments have an orientational coupling with their nearest neighbours, favouring mutual alignment. A limit can be defined to go from segmented to continuously flexible or wormlike chains. We study the nematic phase and the isotropic-to-nematic phase transition. The theoretical tools used are bifurcation and numerical techniques. The intrachain degrees of freedom are taken into account in an exact fashion.

Chap. 1 is the introduction. We discuss some phenomenology and terminology of liquid crystals and liquid crystalline polymers. Also, a brief historical overview is given regarding some experiments, molecular architecture, modelling and simulations. The connection with the work in this thesis is established.

The technical background is the subject of Chap. 2. Some foundations of thermodynamics and statistical mechanics are introduced. Also, we discuss a few more specific topics concerning the thermodynamics of phase transitions and the virial expansion of the free energy, which we need in this thesis. Density functional theory is an alternative formulation of statistical mechanics and able to deal with phase transitions in a natural way. Solutions of lower symmetry often branch off from solutions of higher symmetry when some control parameter is varied. This is called bifurcation and we discuss some properties of the bifurcation point and how it can be located. At the end of the chapter, we discuss two basic models relevant for this thesis; i) the Onsager model for orientational ordering in a fluid of long hard rods and ii) the wormlike chain model for polymers.

The rest of the thesis is divided in two parts. In the first part, polymers consisting of linear associations of a single kind of monomer are considered. These are called (linear) homopolymers and Chaps. 3 and 4 deal with these objects. Polymers consisting of various kinds of segments are called heteropolymers. Heteropolymers are the topic of Part 2 being Chaps. 5 to 7. In this second part, we also include the possibility of branched molecular topologies.

In Chap. 3, we consider chains of cylindrically symmetric rodlike segments. From first principles we build up a density functional formalism. Three approximations are made; we neglect i) interactions between three or more chains simultaneously (Onsager approximation), ii) simultaneous interactions between two chains involving more than one pair of segments and iii) interactions between parts of the same chain which are not nearest neighbours. The resultant density functional description is equivalent to that of a single chain in a self-consistent effective field. The theory of nematic wormlike polymers of Khokhlov and Semenov is obtained as a limiting case [33]. For the segmented chains, we perform bifurcation and numerical analysis. We compare the results to those for

wormlike chains and find a regime for which segmented chains behave approximately as wormlike chains.

Real polymers are never cylindrically symmetric. Therefore in Chap. 4, we study chains consisting of biaxial segments. We perform a bifurcation analysis of the isotropic-to-nematic transition. As for the uniaxial chains, we can define a limit in which the biaxial chains become continuously flexible. This limit we call the ribbonlike chain limit. A ribbonlike chain is characterized by 4 dimensionless model parameters. The stationarity equations and the free energy for ribbonlike chains are derived analogous to Chap. 3. Some interesting aspects of this system are still left to explore; the effect of flexibility on the stability of the biaxial nematic phase might be quite pronounced and a slightly twisted biaxial chain provides a molecular geometry for a cholesteric phase.

The first chapter of Part 2 is Chap. 5. In this chapter, we consider a monodisperse fluid of branched heterochains. We do not specify the molecules and allow for many different types of segments, an unspecified sequence along the chain and an arbitrary degree of branching. We extend the segmented chain formalism to these general objects and perform the isotropic-to-nematic bifurcation analysis. The main result is the derivation of a matrix whose most negative eigenvalue corresponds to the bifurcation density.

The general formalism developed in Chap. 5, is applied to main chain polymers in Chap. 6. Main chain liquid crystalline polymers are linear polymers consisting of rigid mesogens alternating with more flexible spacers. These mesogens are the "liquid crystal formers". Our (finite-length) main chain polymers are described by 4 model parameters. We compute the bifurcation density and bifurcating order along the chain for various spacer lengths. For small spacer lengths the bifurcation density shows a huge increase confirming the experimental finding that spacers decouple the mesogens.

In Chap. 7, we consider side chain liquid crystalline polymers. A side chain polymer consists of a polymer backbone and mesogens which are laterally attached to the backbone via spacers. For infinitely long backbones 6 dimensionless model parameters are needed for these polymers. In the nematic phase the backbone can order parallel to the mesogens (in a prolate conformation) or perpendicular (in an oblate conformation). In the prolate nematic the excluded volume of backbones and mesogens is minimized, but the spacers are on average bent which is an unfavourable conformation. Vice versa, in the oblate nematic the spacers are straight which is more favourable but the backbone-mesogen excluded volume is large. We locate the isotropic-to-nematic transition and compute some properties using the bifurcation analysis of Chap. 5 and a numerical scheme similar to the one used in Chap. 3. The same numerical scheme is also used to compute the nematic behaviour for higher densities. The usual phase sequence upon compression is isotropic - oblate - prolate or directly isotropic - prolate. Moreover we find that the transition between oblate and prolate is not a phase transition in contrast with earlier work by Warner et. al. [98, 99].

Samenvatting

Een proefschrift is over het algemeen het resultaat van vier jaar noeste arbeid, gepropt in boekje van amper 100 tot 150 bladzijden. In die vier jaar heeft de promovendus zich naar het front van de wetenschap gewerkt en daar geprobeerd een klein stapje vooruit te zetten. Deze beeldspraak suggereert al dat een proefschrift hoogst specialistisch en technisch van karakter is. Dit proefschrift is daarop geen uitzondering en omdat de rest van het boekje voor veel mensen onleesbaar is of zo overkomt, neem ik in deze samenvatting de ruimte om wat uit te wijden.

Op school leren we dat er drie verschijningsvormen zijn waarin stoffen voorkomen; vast, vloeibaar en gasvormig. De vaste fase wordt gekenmerkt door het feit een object elastisch vervormbaar. Dus als je ertegenaan duwt zal het een klein beetje vervormen, maar als je ermee stopt, zal het zijn oorspronkelijke vorm weer aannemen. Er is dus een soort van 'herinnering' in het materiaal aanwezig en het kan krachten genereren die de vervorming weer teniet doen. Een vloeistof kan dat niet. Als je een kracht op een vloeistof uitoefent stroomt het in de richting van de kracht. (Als je bijvoorbeeld een emmer water scheef houdt doet de zwaartekracht zijn werk en loopt het water eruit.) Toch zijn er ook overeenkomsten tussen vaste en vloeibare materialen. Gelijke hoeveelheden zijn vaak ongeveer even zwaar; ze hebben ongeveer dezelfde dichtheid. Daarin verschillen gassen weer van de vorige twee. Gassen stromen als vloeistoffen, maar zijn veel ijler.
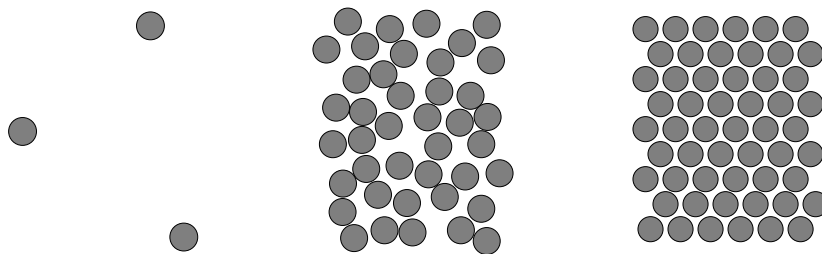

Figuur 8.13. De drie bekende fasen voor bolvormige moleculen die elkaar op korte afstand sterk afstoten en op lange afstanden en licht aantrekken. Links het gas, midden de vloeistof en rechts het kristal.

Natuurlijk stellen schoolboekjes de wereld wat simpeler voor dan die in werkelijkheid is. Het blijkt dat materie is opgebouwd uit moleculen. Moleculen zijn de kleinste deeltjes van een stof die nog steeds de eigenschappen van die stof bezitten. Simpele stoffen zoals argon voldoen aan het bovenstaande profiel en hebben een gasvormige, een vloeibare en een vaste fase (zie Fig. 8.13). Op dit hele kleine niveau zitten de argon atomen netjes op een rooster in geval van de vaste fase, en bewegen ze kriskras door elkaar in de vloeibare fase. De gasvormige fase lijkt op dit niveau op de vloeistof, behalve dan dat de atomen gemiddeld veel verder van elkaar verwijderd zijn. Door de temperatuur of de druk te

veranderen kan een stof van de ene in de andere fase overgaan. Gaan we bijvoorbeeld van hoge naar lage temperatuur, dan komen we voor argon de volgende fase-overgangen tegen; gas - vloeibaar en vloeibaar - vast. Soms ontbreekt de vloeistoffase en vinden we alleen gas - vast.

Argon heeft deze drie fasen omdat de atomen bij benadering bolvormig zijn, ze elkaar sterk afstoten op korte afstanden en elkaar een klein beetje aantrekken op lange afstanden. De meeste stoffen bestaan echter niet uit 'simpele' bolvormige atomen, maar uit moleculen die op hun beurt uit vele atomen kunnen bestaan. Als deze een nogal onbuigzame langwerpige vorm hebben (laten we zeggen staafachtig) dan kunnen er meer fasen voorkomen dan alleen gas, vloeibaar en vast. Namelijk, in de vloeibare toestand bewegen ook deze 'staafjes' kriskras door elkaar, maar nu is het ook belangrijk dat hun richtingen compleet willekeurig zijn. Zowel de posities als de richtingen van de moleculen zijn dus ongeordend. Andersom, in de vaste toestand zitten de staafjes ook hier op een rooster, maar nu moeten ze ook allemaal dezelfde kant opwijzen. De posities en de richtingen van de moleculen zijn dus beiden geordend. Nu kan het gebeuren dat deze moleculen tussen de totaal geordende vaste fase en de totaal ongeordende vloeibare fase, fasen hebben met *gedeeltelijke* ordening. Dit zijn vloeibaar kristallijne fasen. In Fig. 8.14 zijn er een paar getekend voor staafachtige moleculen. De fase waarbij de staafjes ongeveer dezelfde richting opwijzen maar niet op regelmatige afstand van elkaar zitten (en dus nog kriskras door elkaar heen bewegen), heet de nematische fase. De nematische fase is dus eigenlijk een vloeistof met een voorkeursrichting. Om de eerdergenoemde vloeistoffase zonder voorkeursrichting aan te duiden, gebruikt men meestal isotrope fase. Isotroop slaat op het feit dat deze fase er in alle richtingen hetzelfde uitziet. De fase waarin de staafjes ongeveer dezelfde richting opwijzen *en* ook nog in lagen zitten is de smectische fase. Het dient wel benadrukt te worden dat binnen in de smectische lagen de staafjes nog steeds niet op regelmatige afstand van elkaar zitten en kriskras door elkaar bewegen. De smectische fase bestaat dus als het ware uit vloeibare lagen die op elkaar zijn gestapeld.

isotroop   nematisch   smectisch   kristallijn
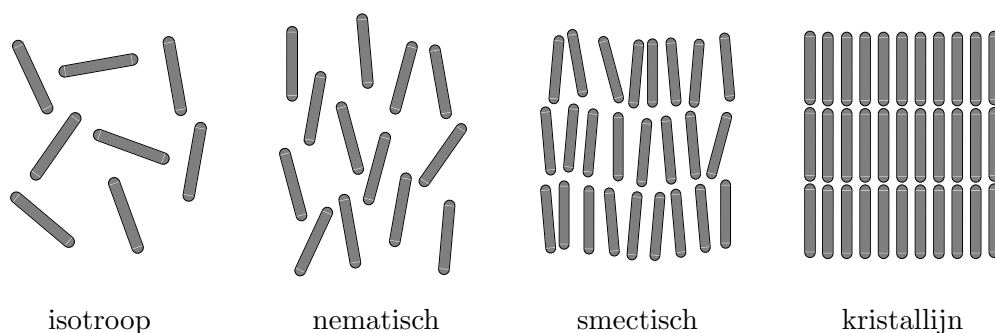
Figuur 8.14. De vloeibaar kristallijne fasen voor staafjes. Links de isotrope vloeistoffase en rechts het kristal. Daartussenin vinden we de nematische fase en de smectische fase.

Het drijvende principe achter deze vloeibaar kristallijne ordening is de 'langwerpige' interactie die deze moleculen met elkaar hebben. Als je bijvoorbeeld lucifers in een luciferdoosje doet, kun je in het begin de lucifers nog op alle mogelijke manieren kwijt. Het maakt dan niet uit of ze toevallig haaks op elkaar liggen of niet. Als je echter doorgaat

met het vullen van het doosje, kom je op een punt dat deze willekeurige stapeling te veel ruimte inneemt. Er passen veel meer lucifers in het doosje als je ze netjes parallel aan elkaar legt. Eenzelfde soort proces zorgt ook voor de vloeibaar kristallijne ordening. Een verschil is dat moleculen altijd bewegen, en op een bepaald moment zelf 'ontdekken' dat parallelle ordening voordeliger is.

Een interessante eigenschap die vloeibaar kristallijne fasen hebben is dat licht in verschillende richtingen in verschillende mate wordt doorgelaten. Dat komt door de voorkeursrichting die deze fasen hebben. Van deze eigenschap wordt gebruik gemaakt in beeldschermen die zijn gebaseerd op vloeibare kristallen (LCD's, liquid crystal displays). Iedereen kent wel de horloges of rekenmachines met de zwarte cijfers op de grijsachtige achtergrond. In de traditionele LCD's zit een dun plakje van een gedraaide nematische fase tussen twee speciale glasplaatjes (polarisatoren). Er wordt licht op geschenen en deze gedraaide nematische fase draait de 'trillingsrichting' van het licht en de glasplaten laten het licht door. Dit is de grijsachtige achtergrond. Door een electrisch veld over het plakje te zetten verandert de voorkeursrichting van het vloeibare kristal. De trillingsrichting van het licht wordt niet meer gedraaid en de glasplaatjes laten het licht niet meer door. Dit zijn de zwarte cijfers. Een voorbeeld van een molecuul dat vloeibaar kristallijne fasen bezit is getekend in Fig. 1.3 in hoofdstuk 1. Overigens gaat dit proefschrift niet over enigerlei toepassingen, maar enkel over systemen die vanuit fundamenteel wetenschappelijk oogpunt interessant zijn.

Sinds de jaren zeventig is het ook mogelijk om de vloeibaar kristallijne groepen in polymeermoleculen op te nemen. Polymeren zijn erg lange ketens van atomen (het kunnen er duizenden zijn). Deze 'vloeibaar kristallijne polymeren' combineren de eigenschappen van vloeibare kristallen en polymeren. Ze hebben nog steeds de vloeibaar kristallijne fasen maar polymeren zijn mechanisch sterker en ook makkelijk verwerkbaar (je kunt er bijvoorbeeld plastic van maken). Deze combinatie maken vloeibaar kristallijne polymeren erg interessant voor industriële toepassingen en er wordt dan ook veel onderzoek naar gedaan. Een schematische voorstelling van twee soorten vloeibaar kristallijne polymeren zijn gegeven in Fig. 8.15. De dikkere stukken heten mesogenen en stellen de vloeibaar kristallijne groepen voor. De dunnere flexibele stukken zijn de polymeergedeelten. Ruwweg zijn er twee soorten; polymeren met groepen in de hoofdketen en polymeren die zijketens hebben waar ze in zitten.
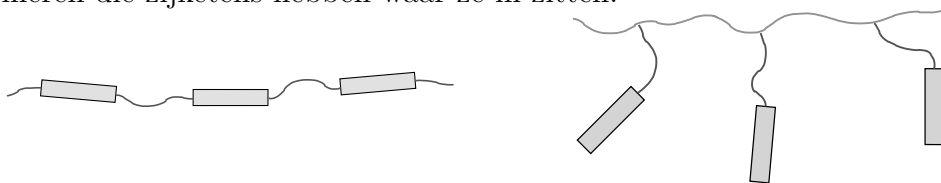

FIGUUR 8.15. Twee schematische voorbeelden van vloeibaar kristallijne polymeren. Slechts een paar herhalende 'eenheden' zijn getekend. Links de hoofdketenpolymeren en rechts de zijketenpolymeren.

Er bestaan een aantal theorieën voor vloeibaar kristallijne ordening van staafachtige moleculen. Deze spitsen zich grotendeels toe op de nematische fase en de overgang van de isotrope naar de nematische fase omdat dit het makkelijkst te beschrijven is. In sommige gevallen worden deze moleculen gemodelleerd als onbuigzame staafjes die vloeibaar kristallijne fase-overgangen hebben door het luciferprincipe van drie alinea's

eerder. Vloeibaar kristallijne polymeermoleculen zijn lange flexibele objecten waar op bepaalde punten wat dikkere stijve stukken in zitten die de vloeibaar kristallijne fasen veroorzaken (zie Fig. 8.15). Hier voldoen die staafachtige modellen dus niet meer, omdat de flexibiliteit een essentieel onderdeel is van het systeem. Modellen voor deze laatste systemen nemen de hoofdketens veelal als flexibele wormachtige objecten (rechts in Fig. 8.16, de wormachtige keten is een bekend model in de polymeerfysica). De vloeibaar kristallijne ordening wordt dan veroorzaakt door 'effectieve' segmenten (een stuk van de keten dat gemiddeld redelijk recht is), die als staafjes fungeren. Sommige modellen gaan nog een stapje verder en houden zelfs rekening met de expliciete geometrie van de moleculen (dus welke stukken dik, dun, stijf of minder stijf zijn). In dit laatste geval, echter, worden de directe verbindingen binnen het polymeer niet meer exact meegenomen, maar als een 'gemiddeld veld' dat op de verschillende componenten werkt; een behoorlijk sterke benadering.

De titel van dit proefschrift is "Flexibele Theorieën voor Flexibele Moleculen". En zoals al gezegd gaat het over vloeibaar kristallijne polymeren, waarbij de buigzaamheid of flexibiliteit een niet te verwaarlozen effect heeft op het fasegedrag. Het formalisme, dat geïntroduceerd wordt, houdt rekening met de de geometrie van de polymeren maar ook de bijdragen van binnen het polymeer kunnen ermee exact worden uitgerekend. Dit formalisme kan gemakkelijk aangepast worden voor de verschillende soorten polymeren (bijvoorbeeld de twee in Fig. 8.15). In die zin zijn deze theorieën dus plooibaar of flexibel te noemen en dit verklaart de keuze voor deze titel. In het laatste stuk van deze samenvatting bespreek ik de hoofdstukken kort een voor een.

Hoofdstuk 1 is de inleiding en daar wordt een kort overzicht gegeven van wat eigenschappen van vloeibare kristallen en vloeibaar kristallijne polymeren. Er worden wat historische achtergronden, experimenten, theorieën en simulaties besproken en de context van het werk in dit proefschrift wordt er weergegeven. Hoofdstuk 2 behandelt de technische achtergrond voor dit proefschrift. Dit zijn redelijk bekende resultaten en worden hier even netjes op een rijtje gezet. De rest van het proefschrift is in twee gedeelten gesplitst. Hoofdstukken 3 and 4 gaan over polymeren die uit één soort onderdeel bestaan; homopolymeren. En in hoofdstukken 5 tot en met 7 mogen de onderdelen van verschillende soorten en maten zijn. Hier mogen de ketens ook vertakt zijn.
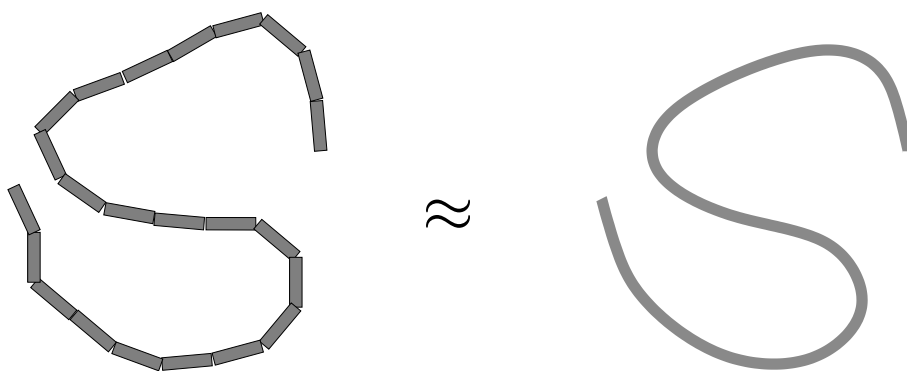

FIGUUR 8.16. Een gesegmenteerde keten lijkt bij vele kleine sterk gekoppelde segmenten veel op een wormachtige keten

Hoofdstuk 3 gaat over ketens die uit segmenten bestaan. Deze segmenten worden gemodelleerd als harde staafjes. Binnen in een keten zijn twee opeenvolgende segmenten gekoppeld met hun richtingen. Deze koppeling is zo dat het voordeliger is voor twee buurstaafjes om ongeveer dezelfde richting op te wijzen en minder voordelig om erg verschillende richtingen te hebben. Het kost dus moeite om deze ketens te buigen. Voor deze gesegmenteerde ketens wordt een formalisme met een stevige theoretische fundering opgeschreven. Er kan precies geïdentificeerd worden waar wat voor benaderingen nodig zijn. Deze gesegmenteerde ketens hebben voor lage dichtheid een isotrope fase, en voor hogere dichtheid een nematische fase. Deze fase-overgang wordt gelocaliseerd met behulp van theoretische technieken. Als deze gesegmenteerde ketens beschouwd worden in het geval dat deze zijn opgebouwd uit heel veel kleine korte staafjes die sterk gekoppeld zijn met hun buren lijken de gesegmenteerde ketens erg op wormachtige ketens (zie Fig. 8.16). Zoals al gezegd zijn dez wormachtige ketens een bekend model voor polymeren.

De benadering van hoofdstuk 3 wordt in hoofdstuk 4 uitgebreid. Hier worden de segmenten niet als staafjes maar als plaatjes gemodelleerd. Plaatjes zijn veel gecompliceerder omdat deze meer 'vrijheidsgraden' hebben. Voor staafjes voldoet het namelijk om één richting te specificeren, terwijl je voor plaatjes twee richtingen nodig hebt. Ketens van deze plaatjes kunnen ook op meer verschillende manieren vervormen. Er zijn namelijk twee verschillende manieren van buiging en je kunt de keten ook verdraaien (torderen).

Hoofdstuk 5 is een erg technisch hoofdstuk waar het formalisme van hoofdstuk 3 wordt uitgebreid voor polymeren die uit willekeurig veel verschillende soorten staafjes kunnen bestaan (dik of dun en lang of kort) en die staafjes mogen elke willekeurige volgorde in de keten hebben. Verder mag de keten vertakt zijn en ook hier worden geen specifieke eisen aan gesteld. De resultaten van dit hoofdstuk worden gebruikt in de volgende twee.

Hoofdstuk 6 gaat over hoofdketenpolymeren (links in Fig.8.15). In de nematische fase zijn de richtingen van de mesogenen (de dikke stukken) sterk geordend terwijl de flexibele verbindingsstukken nog een behoorlijke graad van ongeordendheid vertonen. De fase-overgang wordt gelocaliseerd en ook wordt de afhankelijkheid van de lengte van het verbindingsstuk berekend. Ook de relatieve orde langs het polymeer wordt uitgerekend en dit levert mooie plaatjes op (zie Figuren 6.7).
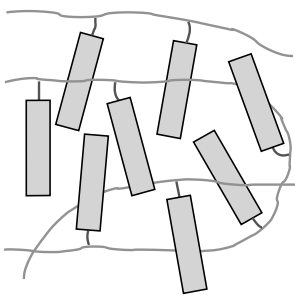
FIGUUR 8.17. De twee situaties voor de nematische fase van zijketenpolymeren. Links richten de hoofdketens zich haaks op de mesogenen en rechts parallel.
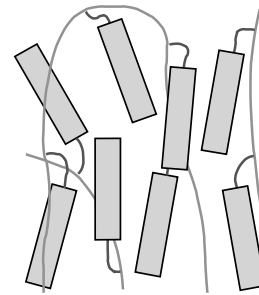
In het laatste hoofdstuk worden de zijketenpolymeren beschouwd (rechts in Fig. 8.15). Bij deze moleculen vormt het polymeer een soort van ruggegraat waaraan zijketens hangen. In deze zijketens zitten de mesogenen en die zijn weer met zo'n verbindingsstukje aan de hoofdketen verbonden. Het interessante van deze moleculen is dat

er een competitie kan ontstaan tussen de verschillende componenten. In de nematische fase zijn de mesogenen weer sterk geordend. Met de hoofdketen kunnen dan twee dingen gebeuren. Als het verbindingsstukje heel kort is zal het over het algemeen niet zo flexibel zijn en dat betekent dat de hoofdketen gemiddeld haaks staat op de mesogenen. Als het verbindingsstukje lang is, is het wat flexibeler en zal het kunnen buigen zodat de hoofdketens zich parallel aan de mesogenen kunnen richten (dit is voordeliger volgens het luciferprincipe). Deze twee situaties zijn schematisch weergegeven in Fig. 8.17. Afhankelijk dus van de lengte van het verbindingsstukje zal het systeen dus voor parallelle of loodrechte hoofdketens kiezen. Hierbij dient te worden opgemerkt dat voor hoge dichtheden de parallelle situatie altijd wint omdat het luciferprincipe belangrijker wordt bij hogere dichtheden. Andere onderzoekers hebben een fase-overgang gevonden van de loodrechte hoofdketens naar de parallelle. In dit proefschrift wordt echter een heel gelijkmatige overgang gevonden. De reden is dat die andere onderzoekers een simpeler model hanteerden dat deze fase-overgang toeliet.

Nawoord

Op deze plaats wil ik een paar mensen bedanken die direct of indirect hebben bijgedragen tot dit proefschrift. Allereerst mijn begeleider en op de valreep ook promotor Bela Mulder. Bela heeft een stijl van wetenschap beoefenen waarbij de natuurkundige neiging tot conceptueel denken hand in hand gaat met een wiskundig strenge benadering. Deze stijl spreekt mij zeer aan. Zijn enthousiasme en didactische kwaliteiten hebben mij zeer gemotiveerd en geholpen de afgelopen viereneenhalf jaar. Ik ben Bela ook als persoon zeer gaan waarderen en ik dank hem voor het vertrouwen dat hij in mij heeft gehouden, ook toen het even wat minder ging.

Daan Frenkel wil ik bedanken voor het feit dat hij mijn promotor wilde zijn. Zijn interesse tijdens de werkbesprekingen heb ik als zeer prikkelend ervaren. Verder bedank ik hem voor het mede scheppen van het onderzoeksklimaat in onze groepen waarbij hoogwaardige wetenschap en een ontspannen sociale omgang ongehinderd samengaan.

In de lente van 2000 heb ik met veel plezier twee maanden doorgebracht in Cleveland aan Case Western Reserve University. Hiervoor wil ik Philip Taylor en zijn groep bedanken. De stimulerende werkbesprekingen die we daar hadden over uiteenlopende onderwerpen hebben me geholpen in het zelfstandig leren inslaan van nieuw richtingen.

De werksfeer op Amolf en meer specifiek in onze (inmiddels zeer grote) koffiegroep is geweldig. Veel collega's hebben me geholpen met mijn (computer)problemen, nooit zelfingenomen en altijd vrijblijvend, zodat ik nooit een aarzeling voelde mijn (soms domme) vragen te stellen. De goede sfeer werd bevestigd en versterkt door het kwartiertje darten dat we gedurende drie jaar deden, 's middags na de lunch in 'Villa Frenkelhof'. Niet zelden stonden we met meer dan tien mensen in het kleine keukentje en vlogen de darts ons om de oren. Ieder nieuw groepslid kon binnen twee weken volwaardig mee in het spelletje 'Killer', waarin de zwakkeren het vaak wonnen van de sterkeren. Buiten werktijd werd er vaak iets georganiseerd; 's avonds samen eten, een spelletje bij iemand thuis, naar de film of gewoon naar de kroeg. Ook denk ik met plezier terug aan de conferenties in Lunteren waar we met velen naartoe gingen. Verder zorgden het zaalvoetbal en de personeelsvereniging voor wat afleiding van de wetenschap.

Bastiaan de Geeter bedank ik voor zijn steun en interesse. Met nagenoeg dagelijkse e-mailtjes en zeer regelmatige bezoekjes hielden we elkaar op de hoogte en hielpen we elkaar door incidentele dipjes heen. Sander Pronk kwam ongeveer tegelijk met mij op Amolf en ik heb het gevoel dat onze (wetenschappelijke) volwassenwording ongeveer gelijk op ging. Ook bedank ik Bastiaan en Sander omdat ze mijn paranimfen willen zijn.

Tot slot bedank ik mijn ouders omdat ze een rustpunt zijn waar ik altijd op kan terugvallen. En Céline ben ik veel verschuldigd voor haar steun, de dingen die ze me heeft geleerd en de prachtige omslag die ze heeft gemaakt.

Curriculum Vitae

Op 7 maart 1974 werd ik geboren in Lichtenvoorde. In juni 1992 behaalde ik het VWO diploma en in augustus van dat jaar begon ik met de studie Technische Natuurkunde aan de Universiteit Twente. Het doctoraalexamen werd afgelegd in maart 1997 en het afstudeerproject betrof een studie naar het 'Feynman Checkerboard Model', een pad-integraalbeschrijving voor de ééndimensionale Diracvergelijking, onder leiding van prof. dr. F. W. Wiegel. Sinds mei 1997 ben ik als onderzoeker in opleiding verbonden aan het FOM-Instituut voor Atoom- en Molecuulfysica. Het onderzoek werd uitgevoerd onder begeleiding van prof. dr. B. M. Mulder en staat beschreven in dit proefschrift. Tijdens deze periode ben ik gedurende twee maanden te gast geweest bij prof. dr. P. L. Taylor aan Case Western Reserve University in Cleveland, Ohio in de Verenigde Staten.